issn 0065-3713

INSTITUT D'AERONOMIE SPATIALE DE BELGIQUE

3 · Avenue Circulaire
B · 1180 BRUXELLES

AERONOMICA ACTA

A - N° 360 - 1991

DEVELOPMENT STUDY OF IMPROVED MODELS OF THE EARTH'S RADIATION ENVIRONMENT

by

JOSEPH LEMAIRE IASB
MICHEL ROTH IASB
JACQUES WISEMBERG IASB
POL DOMANGE IASB
DOMINIQUE FONTEYN BIRA
JEAN MICHEL LESCEUX IASB
GERARD LOH IASB/STI

GEORGES FERRANTE MATRA-ESPACE
CHRISTIAN GARRES MATRA-ESPACE
JACQUES BORDES MATRA-ESPACE

SUSAN McKENNA-LAWLOR STI

JIM I. VETTE JIV Assoc

BELGISCH INSTITUUT VOOR RUIMTE-AERONOMIE

3 · Ringlaan
B · 1180 BRUSSEL

PREFACE

The monograph entitled "DEVELOPMENT OF IMPROVED MODELS OF THE EARTH'S RADIATION ENVIRONMENT" is the final report of a study achieved by a team formed by members of the Institut d'Aéronomie Spatiale de Belgique (Brussels), Matra-Espace (Toulouse), Space Technology Ireland (Dublin). It is the result of a fruitful collaboration of all the TREND team members, including Jim VETTE, and several other consultants which are cited and acknowledged in the monograph itself.

This study has been performed for ESA. The ESA Technical Manager was Dr. Eamonn DALY (WMA/ESTEC); this project has been managed by Joseph LEMAIRE at the Institut d'Aéronomie Spatiale de Belgique.

AVANT-PROPOS

La monographie intitulée "DEVELOPMENT OF IMPROVED MODELS OF THE EARTH'S RADIATION ENVIRONMENT" est le rapport final d'une étude réalisée par un groupe formé de membres de l'Institut d'Aéronomie Spatiale de Belgique (Bruxelles), de Matra-Espace (Toulouse) et de Space Technology Ireland (Dublin). Il est le résultat d'une collaboration fructueuse entre tous les membres du groupe TREND, y compris Jim VETTE, et de plusieurs autres consultants qui sont cités et remerciés dans la monographie.

Cette étude a été réalisée pour l'ESA. Le manager technique de l'ESA était le Dr. Eamonn DALY (WMA/ESTEC). Ce projet a été dirigé par Joseph LEMAIRE à l'Institut d'Aéronomie Spatiale de Belgique.

VOORWORD

De verhandeling getiteld "DEVELOPMENT OF IMPROVED MODELS OF THE EARTH'S RADIATION ENVIRONMENT" is het eindverslag van een studiegroep waaraan deelnamen leden van het BIRA (Brussel), Matra-Espace (Toulouse), Space Technology Ireland (Dublin). Het is het resultaat van een vruchtbare samenwerking tussen alle TREND medewerkers, Jim VETTE inbegrepen, en van verschillende andere raadgevers, die in deze verhandeling genoemd en bedankt worden.

Deze studie werd voor ESA uitgevoerd. De technische manager voor ESA was de heer Dr. Eamonn DALY (WMA/ESTEC), dit project werd door Joseph LEMAIRE van het BIRA bestuurd.

VORWORT

Die Monographie "DEVELOPMENT OF IMPROVED MODELS OF THE EARTH'S RADIATION ENVIRONMENT" betitelt, ist der Schlussbericht einer Studiegruppe bestehend aus Mitglieder von BIRA (Brussel), von Matra-Espace (Toulouse) und Space Technology Ireland (Dubin). Er ist das Resultat einer fruchtbaren Zusammenarbeit zwischen alle Mitarbeitern der TREND Gruppe, Jim VETTE, einbegriffen, und von mehreren anderen Beratern die in dieser Monographie genannt und bedankt sind.

Die Studie wurde für ESA durchgeführt. Der technische Manager für ESA war Herr Doktor Eamonn DALY (WMA/ESTEC); dieses Projekt wurde von Joseph LEMAIRE von BIRA geleitet.

Summary

The radiation environment models of the Earth have been reviewed and reevaluated. Several limitations of the earlier Earth's radiation models and of the way they have been used in the past for dose predictions along orbits of future spacecraft are identified and discussed in this report produced by the TREND study team.

A new Solar Proton Events statistical model has been documented and implemented in the UNIRAD software used by ESA for expected dose calculations. Two sets of trapped electron flux measurements from LANL and IUE satellites have been analysed and compared to the existing NASA model predictions. These new data analysis confirm that the existing models predict in general too high radiation fluxes and therefore too high radiation doses. This leads aerospace engineers to build too thick and heavy shields to protect high sensitive electronic components or space habitacles for manned spacefights. The TREND study has shown the urgent need for continued updating of space environment models. Recommendations and directions for future developments in modelling the radiation environment of the Earth have been given in this Final Report of TREND.

Résumé

Les modèles de l'environnement radioactif de la Terre ont été revus et réévalués. Ce rapport, réalisé par le groupe d'étude TREND, identifie et discute la manière avec laquelle ces modèles ont été utilisés dans le passé en vue de prédire les doses radiatives le long des orbites des futurs satellites. Certaines limitations de ces modèles ont ainsi été mis en évidence.

Un nouveau modèle statistique des événements avec protons solaires a été documenté et implanté dans le code UNIRAD utilisé par l'ESA dans le calcul des doses prévues. Deux mesures de flux d'électrons piégés provenant des satellites LANL et IUE ont été analysées et comparées aux prédictions des modèles actuels de la NASA. Ces nouvelles analyses de données confirment le fait que les modèles actuels prédisent en général des flux radiatifs trop élevés et dès lors des doses trop importantes. Ces prédictions poussent les ingénieurs à construire des boucliers trop épais et trop lourds dans le but de protéger les composants électroniques très sensibles ou les habitacles spatiaux destinés aux vols habités. L'étude du groupe TREND a mis en évidence le besoin urgent d'une ré-évaluation constante des modèles de l'environnement spatial. Ce rapport final fournit une liste de recommandations pour les développement futurs de la modélisation de l'environnement de la Terre.

Samenvatting

De modellen over het aardse radioaktieve milieu werden herzien en herschat. Dit verslag, door de studiegroep TREND uitgevoerd, identificeert en bespreekt de manier waarop, in 't verleden, deze modellen gebruikt werden om de radioactieve dosissen langs de loopbaan van de toekomstige satellieten, te voorzien. Daardoor werden enkele beperkingen van deze modellen vastgesteld.

Een nieuw statistisch model van de evenementen met zonne protons werd gedocumenteerd en in het software van UNIRAD ingevoerd, welk door ESA gebruikt wordt voor de berekeningen van de verwachte dosissen. Twee metingeenheden van betrapt elektronstromen, vanuit de satellieten LANL ern IUE, werden onderzocht en met de bestaande verwachtingen van de NASA modellen vergeleken. Deze nieuwe data ontleding bevestigt het feit, dat de bestaande modellen, in 't algemeen, te hoge radioaktieve stromen voorzien en, dus ook, te hoge radioektieve dosissen. Daardoor bouwen de ingenieurs te zware en dikke schilden om de uiterst gevoelig elektronische bestanddelen, ofwel de ruimtehut van de bemande ruimte-vaartuigen, te beschermen. De TREND studie heeft getoond dat, er een dringend gebruik is, aan een voortdurende evaluatie van de ruimtemilieu modellen. Dit laatste TREND verslag geeft een aantal aanbevelingen en krachtlijnen wat de toekomstige modelisatie van het radioaktieve aardse-milieu betreft.

Zusammenfassung

Die Modelle in Beziehung mit der radioaktiven Umwelt der Erde wurden durchgesehen und verbessert. Dieser Bericht, von der Studiengruppe TREND hergestellt, identifiziert und bespricht die Weise wobei diese Modelle in der Vergangenheit gebraucht worden sind, um die radioaktiven Dosen an der Umlaufbahn der zukünftigen Satellieten entlang, vorauszusagen.

So hat man gewissen Beschränkungen der Modelle festgestellt. Ein neues statistisches Modell der Ereignisse mit Solarprotons wurde bewiesen und im software von UNIRAD hereingeführt und wird von ESA gebraucht zur Berechnungen der Schätzung von radioaktiven Dosen. Zwei Messerung-einheiten von erwischten Elektronströme, aus den Satelliten LANL und IUE wurden untersucht und mit den Voraussagen über die heutigen Modellen verglichen. Diese neuen Data-Analysen, befestigen, dass die heutigen Modelle, im allgemeine, zu starke radioaktive Strömen voraussagen und deswegen auch zu starke Dosen. Diese Vorhersagen haben zur Folge, dass die Ingenieure zu schwere und dicke Schilde bauen, um die höchst-empflindliche elektronischen Komponenten im bewohnten Raum oder im bewohnten Raumfahrtzeugen zu schützen. Die Studie der TREND Gruppe hat es deutlich gemacht, dass man einen dringenden Bedarf an einer ständigen Schätzung der Weltraummodelle hat. Dieser Schlussbericht gibt eine Reihe Ermahnungen und Anweisungen, was die zukünftige Entwicklung der Modelisation der radioaktiven Erdenraum betrifft.

INSTITUT D'AERONOMIE SPATIALE DE BELGIQUE

DEVELOPMENT OF IMPROVED MODELS OF THE EARTH'S RADIATION ENVIRONMENT

(ESTEC/Contract No. 8011/88/NL/MAC)

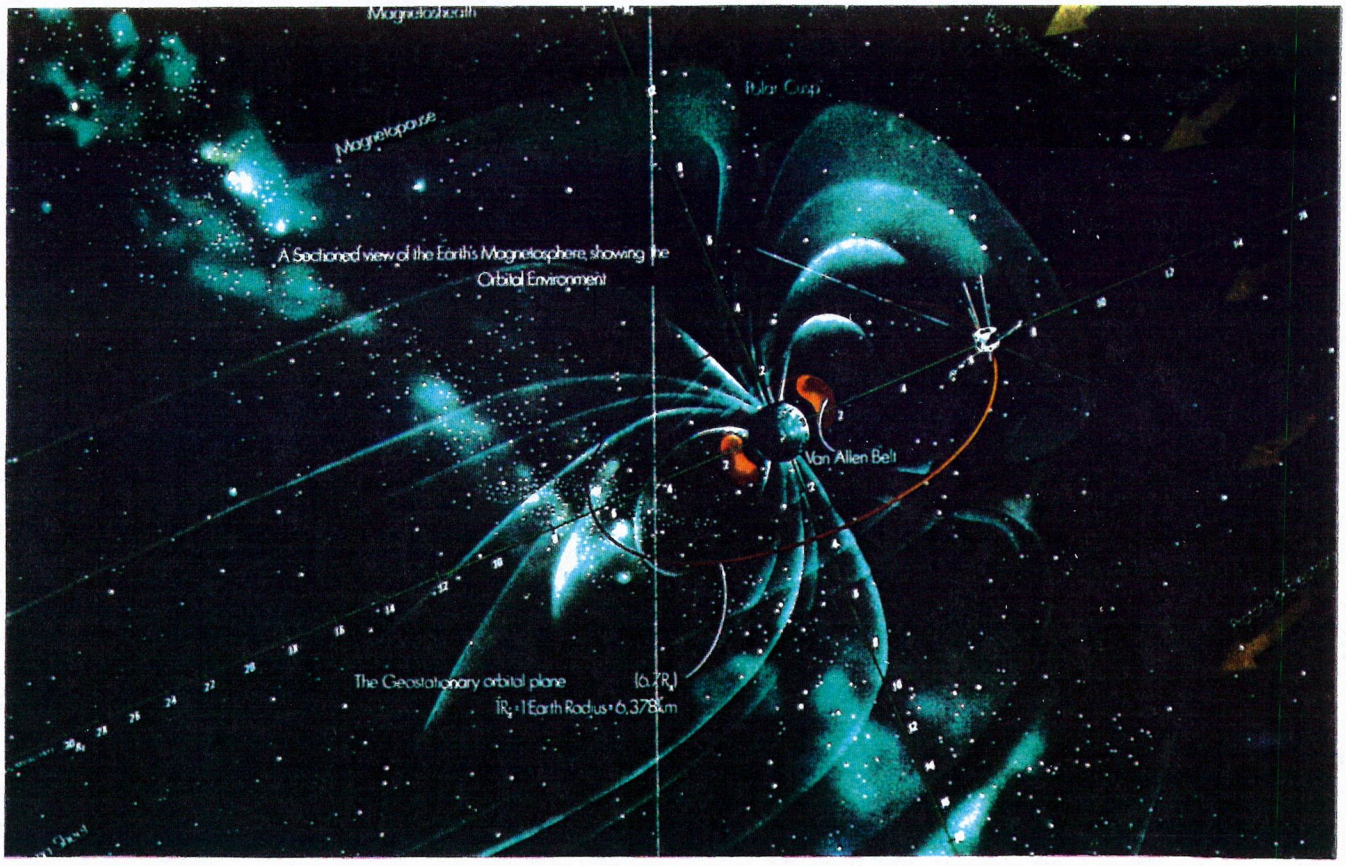

FINAL REPORT

S T I (Ireland)

MATRA ESPACE

J.I. VETTE (USA)

TREND

DEVELOPMENT STUDY OF IMPROVED MODELS OF THE EARTH'S RADIATION ENVIRONMENT

(ESTEC CONTRACT 9011/88/NL/ MAC)

FINAL REPORT

TEAMS MEMBERS OF TREND

JOSEPH LEMAIRE	IASB
MICHEL ROTH	IASB
JACQUES WISEMBERG	IASB
POL DOMANGE	IASB
DOMINIQUE FONTEYN	BIRA
JEAN MICHEL LESCEUX	IASB
GERARD LOH	IASB/STI
GEORGES FERRANTE	MATRA-ESPACE
CHRISTIAN GARRES	MATRA-ESPACE
JACQUES BORDES	MATRA-ESPACE
SUSAN McKENNA-LAWLOR	STI
JIM I. VETTE	JIV Assoc

ESA TECHNICAL MANAGER

EAMONN DALY ESEC/WMA

ISSUED AND PRINTED AT IASB

25 SEPTEMBER 1990

FOREWORD

This Final Report contains the main results obtained and recommendations made by the TREND team during the study "Development of improved models of the Earth's radiation environment". This study has started 1 February 1989 under ESA contract ESTEC/8011/88/NL/MAC.

TREND was initiated and funded by ESA under the ESTEC/CONTRACT 8011/88/NL/MAC. Significant investments have also been made in this project by MATRA-ESPACE (Toulouse), by SPACE TECHNOLOGY IRELAND (STI) (Dublin), by the INSTITUT d'AERONOMIE SPATIALE de BELGIQUE (IASB) (Brussels) and by JIV ASSOCIATES (Virginia) consulted for the whole duration of this study. Invited scientists have participated to TREND's progress meetings in Dublin, in Toulouse, in Noordwijk, and Brussels. The advise obtained from them and support provided by their Laboratory or Organisation is deeply acknowledged by TREND.

The TREND team is formed by

Joseph LEMAIRE from the Institut d'Aeronomie Spatiale de Belgique (IASB), has been the project manager of TREND. He has contributed to the description and evaluation of magnetic field models and transformation to B and L (or other) coordinate systems. He also contributed to the recommendations for future flight requirements and modelling activities.

Michel ROTH (IASB) described and evaluated the different probabilistic solar proton event models,and prepared the software design requirements necessary for the implementation of an alternative (new) solar flare proton event model proposed by Feynman et al. . Michel ROTH described and documented the existing methods and software

subroutines used in UNIRAD to compute the flux reduction due to 'geomagnetic cut-off'.

Jacques WISEMBERG (IASB) studied physical processes involved in the interaction between the Earth's radiation environment and Earth's atmosphere. He has also implemented and studied Hassitt's FORTRAN code, which was kindly provided to TREND by Carl McIlwain.

Dominique FONTEYN (IASB) implemented and tested the new models for the external magnetic field by TSYGANENKO (1987, 1989).

Pol DOMANGE (IASB) developed and tested the new software BLXTRA which now permits computation of values of B and L for any combination of internal and external magnetic field models. Local time dependence and Kp dependence of the external magnetic field which have been added.

The IASB team has also been assisted part time by very efficiently by Leo FEDULLO and Jacques BARTHELEMY, as programmers.

Georges FERRANTE head of the system division at MATRA-ESPACE, has advised and lead the important data processing and model coding activities

Jacques BORDE from MATRA contributed also to the tasks described in the previous paragraph, but he has been mainly in charge of developing the codes needed to read and process the satellite data used by TREND to improve existing models for the region of geostationary orbit. He compared also the mapping of satellite flux measurements obtained with and without an external magnetic field model. He developed finally a series of new graphical tools

Christian GARRES from MATRA has been involved in the implementation, coding and testing of the new solar flare

proton event model of Feynman et al. model; he also integrated this model and BLXTRA into the former TREP software package; he implemented the programs to determine the local time variations and standard deviations of the omnidirectional flux of trapped particles.

Gerard LOH (STI/IASB) supported the data processing tasks at MATRA. In close contact with JIV ASSOCIATES he developed a set of codes to read and process the IUE tapes.

Susan McKENNA-LAWLOR, head of SPACE TECHNOLOGY (Ireland) Ltd (STI) has been responsible for identifying spacecraft missions, instruments, and data sets relevant to this study. Data formats and their availability were identified. Also, future orbital missions of ESA with potential capability for monitoring the Earth's radiation environment were investigated.

Jim VETTE, president of JIV ASSOCIATES, has advised the TREND team during the project. He contributed in so many respects that it would be too long to mention them all. Because of his expertise in the area of modelling the Earth's trapped radiation environment, he contributed mainly to the description and evaluation of the trapped particle models in chapter 4 of TREND's TECHNICAL NOTES 1 and 2. He also helped STI and IASB in preparing part of TN 3 and 6. His stimulating advice and action as TREND's 'ambassador' beyond the Atlantic, has been crucial for the project, and is acknowledged by all.

TREND's project started 1 February 1989 for a duration of 15 months. Time and financial limitations necessarily restricted what could be attempted in this project. However, TREND made considerable progress in analysing environment modelling problems, identifying solutions and beginning the data analysis tasks which is a long term effort which needs continuity, motivation and perseverance. Collecting satellite data sets, shipping them over the Atlantic, processing them and analysing them often needs

more than 15 months of time. Doing this for more than one data set with totally different tape formats and physical contents made this task of TREND even more difficult and challenging.

During the course of this study a number of interesting extensions of this work have been identified by TREND.

TREND was lead to focus its efforts in analysis data covering limited regions of B-L space but nevertheless important ones : i.e. (1) near geostationnary orbit where LANL data offer an excellent coverage, and (2) in the range of intermediate L-values with IUE data which required completely new data processing software. TREND identified a number of other satellite data sets (e.g. DMSP data) which would have covered other regions of the B-L space (e.g. the low-altitude region).

Identification of problems

Other important contributions of TREND are contained in TECHNICAL NOTE 2 : serious needs for revisiting from a basic and novel point of view the mapping methods of the trapped radiation environment at the low-altitude edge of radiation belts. Indeed, this is the region where future ESA manned spacecraft will orbit, and, where Columbus and the Space Station will operate for a considerable amount of time.

In TECHNICAL NOTE 6 we identified a series of needs for future ESA missions and identified flight data requirements. The results of this analysis is that "minimally intrusive" monitors (detectors of energetic particles) should be flown almost routinely, on all types of missions.

The better we will be able to sample and to model the crowded region of space, the better will be the use made of resources of launching rockets and spacecraft. Indeed, the more uncertain aerospace engineers are, the heavier must be the shielding they will have to lift into orbit to protect man and microelectronic devices. Therefore the relatively minor cost of radiation environment studies can result in substantial project cost-saving and performance improvements.

Outline of this Final Report

After a first chapter containing an over all presentation of the scope, objectives and background we describe the evaluation of current models in chapter 2. The software and data requirements & developments are summarized in chapter 3. The data analysis and modelling results form the chapter 4. Chapters 5 and 6 contain respectively future flight requirements and the conclusions of TREND.

Acknowledgments

During this study the ESA study manager, Eamonn DALY has followed TRENDS's model development and data analysis progress. His experience, time and collaboration has been greatly appreciated by TREND's team members. We benefited also from Cecil TRANQUILLE's experience who processed ISEE data.

Carl McILWAIN, Susan GUSSENHOVEN, and Andrei KONRADI participated in the TREND progress meetings where they presented their activities, in the area of Earth's radiation environment modelling and data processing. Their

advice and contributions have enlighten and strenghten the work of TREND. We expect to continue cooperation and coordinate future activities with them in the future. We are also grateful to Joe KING, from NSSDC for his support in transferring data to TREND or ESTEC via SPAN or tape. In this respect our tanks are also extended to Howard LECKNER for his interaction with JIV Associates and TREND. R. POST transfered LANL and IUE data from NSSDC very quickly and efficiently. Dan BAKER has guided TREND's steps to Tom CAYTON at Los Alamos National Laboratory, who is currently in charge of the processed LANL data. TREND's team is thankful to them all for their cooperation.

Joe KING transmitted the IUE data available at NSSDC to TREND via Jim VETTE. Ralph POST made the IUE data available on SPAN. Without this important input much less would have been achieved. Both are heartly thanked for their collaboration to the TREND project.

We acknowledge also the Director of Institut d'Aéronomie Spatiale de Belgique, Dr. Marcel ACKERMAN, who gave full support to this study and its realisation. Dr. J.M.LESCEUX, J. BARTHELEMY, A.SIMON, L. FEDULLO and the administrative staff at IASB have provided a most efficient help to the project manager of TREND. They are all deeply acknowledged for their cooperation.

The scientific, technical and administrative staff of IASB, MATRA-ESPACE, and of SPACE TECHNOLOGY IRELAND Ltd have also contributed to make this project a sucessful and most rewarding one.

TABLE OF CONTENT

1. GENERAL OVERVIEW AND BACKGROUND FOR TREND

1.1 Introduction

Radiation damage in outer space is one of the problems confronting any mission in orbit above the protective shield formed by the Earth's atmosphere. The radiation environment above is quite complex, varying by orders of magnitudes both with altitude and time. It effects sensitive microelectronic devices and the operation requirements for manned missions.

In this study it is proposed

- to evaluate existing models of the Earth's radiation environment,
- to identify their limitations, and to outline requirements for future generation of environmental models;
- to identify the relevant particle measurements which are available to improve existing Earth's radiation environment models,
- to analyse some of these data and contribute a new step to long term modelling efforts which started at NSSDC/WDC-A-R&S in the 60's ;
- to make recommendation for future flight measurements and monitoring of the Earth's radiation environment.

1.2 Radiation effects and hazards

Space missions are heavily impacted by the trapped energetic particles and solar energetic particles in a number of ways. Electric charging of spacecraft surfaces occurs as a result of hot plasma with energies of the order of 20 keV. Such a plasma injected from the geomagnetic tail

during moderate and large magnetic storms, can produce surface discharges that result in spurious operation or damage to a high altitude spacecraft.

Energetic protons and electrons produce spurious signals in detection sensors. Particle induced backgrounds present complications in the form of saturation masking of true signals, increased dead time and requirements for increased signal processing. Energetic particles, through the deposition of energy in matter, can produce spurious signals in any sensors : Cerenkov radiation in optical sensors, photocathode noise in photomultipliers, direct energy deposits in solid-state detectors, e.g. CCD, HgCdTe Infrared sensors...

Relativistic electrons with energies larger than 500 keV embedded within dielectrics, produce electric potentials in excess of the breakdown potential of the material. This results in discharges that act as spurious signals or can damage sensitive components like solar cells, electronic systems. The radiation dose effects which are observed at all altitudes limit the operational life of these components.

In some orbits, the transient heat additional input due to enhanced energetic particle population can exceed 5 W/m^2. For ultra-low-temperature IR sensors, such as on the Infra-Red Astronomy Satellite IRAS, this additional heat load must be considered in the design of the spacecraft and in the management of this mission.

The effect of the radiation environment on man in space is another important reason to study and model as carefully as feasible the distribution of energetic particles beyond 150 km altitude, at all latitudes and at all longitudes. The biological hazards are a strong inducement to invest in continous monitoring of the Earth's radiation environment, and modelling of its short term evolution like during geomagnetic storms and solar flare

events, as well as over long term periods, like the solar activity cycle.

The feasibility of conducting extended manned space missions is based on an adequate understanding of the biological risks and on providing the adequate protection to reduce the risks to acceptable levels. This implies proper software tools to predict the proton and electron fluxes, and, by consequence the expected radiation doses for the future ESA's manned space missions.

The requirement of shielding the astronauts from the earth radiation environment impact heavily on the weight, cost and operation of manned missions. Therefore, a correct evaluation of this environment is essential to reduce both their costs and risks.

Because the cost of a radiation-hardened microelectronic device is much greater than its non-hardened equivalent, a good estimate of the expected radiation environment is required in order to insure that radiation-hardened devices are used when and where needed and not elsewhere. Thus, space system designers require long-range predictions of the energetic particle environment.

1.3 Background of TREND's study

TREND stands for TERRESTRIAL RADIATION ENVIRONMENT DEVELOPMENTS. But TREND has also been concerned with the re-evaluation of the non-trapped solar flare particles penetrating the Earth's magnetosphere and atmosphere during Solar Proton Events. In order to determine the radiation doses that a satellite will experience during its future mission a series of software programs are needed.

1.3.1 Tools available and their links

The tools which were available to TREND when this study was started on 1 February 1989, are part of UNIRAD. The VMS-FORTRAN codes of all main programmes and subroutines used in UNIRAD were provided to TREND by E.J. Daly (ESTEC/WMA).

Software used for transformation of geographic or geodetic coordinate systems into geomagnetic B and L coordinates (SHELLG,BLINE) , TREP (including access routines), KINGFL, Models AE8,AP8 etc... were also provided by E.J. Daly . Additional software tools were also provided to this study team by C.E.McIlwain (UCSD/CASS, La Jolla) and N. Tsyganenko (Univ. of Leningrad).

On top of the experience of the TREND team members and consultants the large number of scientific papers, reviews and books which have been consulted should be considered as the main tools available. Some of these bibliographical references are quoted in this final report, but a more comprehensive list can be found in the series of six technical notes prepared by TREND.

The UNIRAD architecture is shown in fig.1-1. The UNIRAD software tools available can be divided into several interlinked packages:

- the SAPRE package generates a given number geodetic coordinates of points along the orbit of a spacecraft whose orbital elements are given as input in a NAMELIST file. These geodetic positions are stored in an interface file for use as inputs to the SHELLG chain of programs.

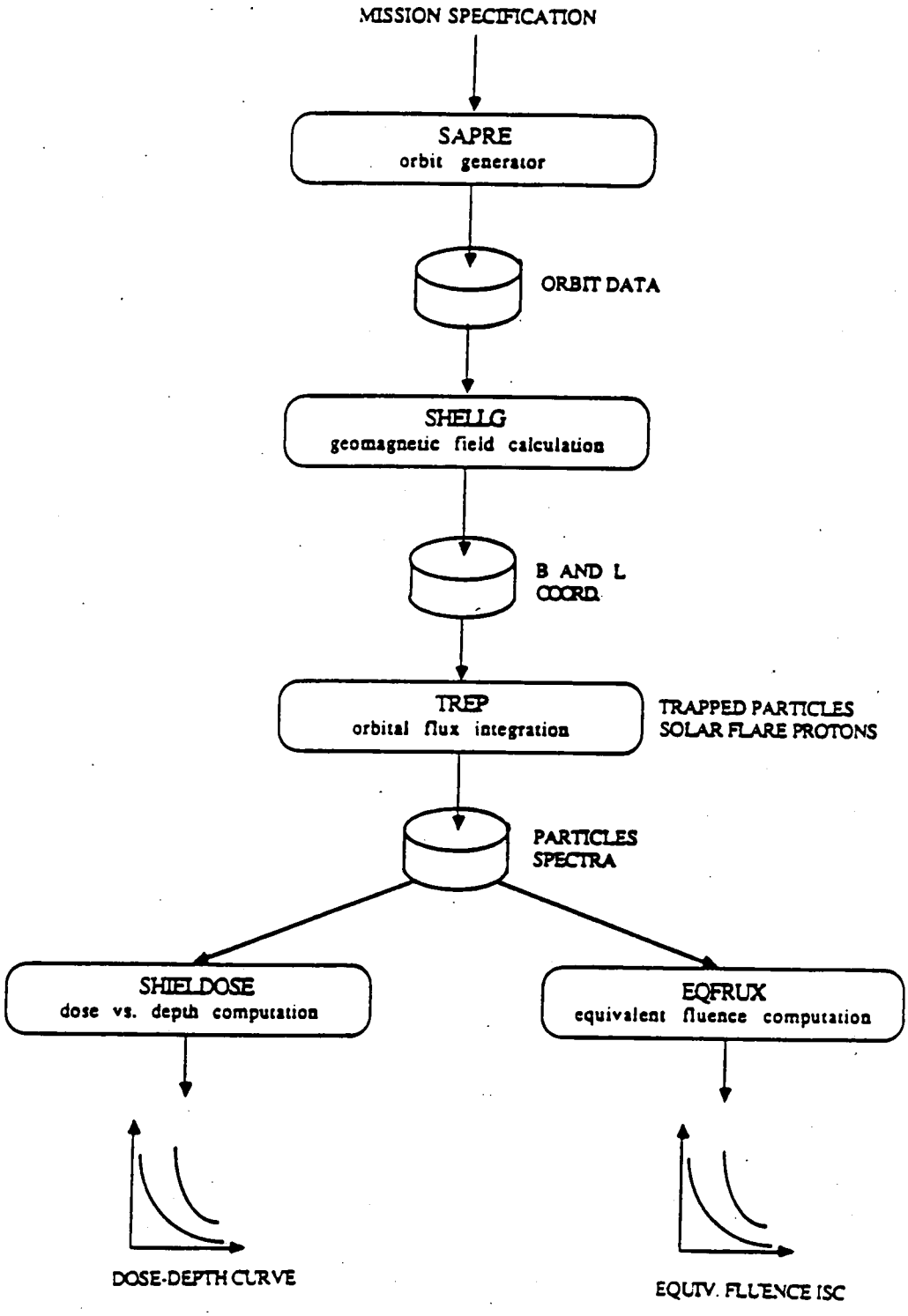

Fig.1-1. Block diagram of the UNIRAD software package.

- SHELLG computes the magnetic coordinates for each of these points. To do so a magnetic field model needs to be chosen. This choice is determined by giving in the NAMELIST file an identification number corresponding to the harmonic expansion adopted to describe the magnetic field distribution. Note that because of the secular variation of the geomagnetic field an epoch (BLTIME) must also be given as an additional input. In UNIRAD only internal magnetic field models were implemented so far, and some of the key internal magnetic field (e.g. IGRF-85 or J&C-60) were missing. The outputs of SHELLG are the values of B and L for all points along the orbit. These outputs are then stored in the interface file which includes the inputs for the next chain of programs: TREP.

- The third chain is TREP which calculates the expected omnidirectional flux of electrons and protons for each orbital point determined by the B and L values. These fluxes are calculated for a series of energy intervals fixed in the NAMELIST file. In addition to the integral flux, above a fixed energy threshold TREP computes also the differential flux. Furthermore, TREP integrates also these differential energy and integral energy fluxes over the whole duration of the space mission, in order to obtain the fluences. All these outputs are then stored in another interface file which is then used for instance by the SHIELDOSE program designed to compute radiation doses predicted behind a shield of a given shape and thickness, of Aluminium, Silicon, H_2O or S_iO_2 (see fig. 1-1).

TREP uses empirical models for the trapped particles. The latest NASA models are used i.e. AE8 and AP8 models. There are different versions (MIN and MAX) for solar minimum and solar maximum conditions. These models are stored as data in matrix form as functions of B, L and Energy. Furthermore, KINGFL, the probabilistic model of King is used in TREP to predict the expected number of

solar flares and their contribution to the total fluences for the total length of a space mission. Since the expected annual number of ordinary and anomalously large solar flares proton events is larger during solar active years than near the sunspot minimum, there is an additional input parameter that needs to be given to TREP: it is the number of years a space mission will spend during the active period of a solar cycle. Note that the KINGFL program will also predict a lower frequency of ordinary flares for solar minimum.

It can be seen that the UNIRAD is already a complex package of software of many different subroutines codes, which unfortunately were not (or sometimes only partially) documented.

1.3.2 Problems arising in radiation dose predictions

1.3.2.1 Secular variations of the geomagnetic field

A well publicized problem arising in radiation flux prediction was pointed out by McCormack (1986) and discussed by Konradi, Hardy and Atwell (1987). As a consequence of secular evolution of the internal components of the geomagnetic field the low-altitude trapped radiation fluxes predicted for the year 2000, increases dramatically when calculated using currently developed methods which are implemented in UNIRAD.

1.3.2.2 Comparisons of dose measurements and model predictions

A second series of problems arose from recent comparisons of actual dose measurements and the predicted dose values based on AE8 and AP8 empirical models. Gussenhoven et al.(1987) report short term dose

measurements made at low altitudes with the Defense Meteorological Satellite Proram (DMSP) F7 satellite which carried dosimeters (840 km; LEO orbit). Inner radiation belt protons, outer radiation belt electrons and solar flares observations were presented for the period 1984 to 1985. These measurements were compared to predictions of the NASA models AE8 and AP8. The NASA model values for proton dose in the South Atlantic Anomaly (SAA) are approximately 50 % higher than the DMSP average values for a thickness of 0.55 gm/cm^2 Aluminium shielding. Furthermore, the NASA outer zone electron model prediction values are found too high by an average factor of 6. Their reliability for short term predictions was also questionned by the AFGL group.

Pruett (1980) measured radiation dose in the DMSP/F1 orbit for one year: April 1977 to April 1978, a period following solar minimum. His dose measurements showed that near solar minimum the NASA models values were also too high i.e. too conservative.

On the other hand Baker et al.(1986) and Vampola (1988) add the concern that the NASA models understate the very energetic electron flux (E > 2 MeV) in the outer zone. This may especially be the case during the current solar cycle which is a 'robust' one. Indeed, AE8 includes solar-cycle effects based on nominal solar activity observed in the 60's.

1.3.2.3 Local time and dynamic effects

Another major concern is that observations at high altitude indicate that the radiation belts respond to geomagnetic activity; but current models give time averaged flux values. Although, comprehensive dynamical models are still beyond grasp, complementary models providing the standard deviation of the observed flux values would be a significant improvement, already.

It was also felt that ignoring average local time variations and shell splitting at geosynchronous was a limitation of currently used AE8 and AP8 models (Daly,1989). Note, however that implementation of the LT variation corresponding to the AE4 model in UNIRAD, goes some way to rectifying this deficiency in UNIRAD (Tranquille, personnal communication 1989).

This is a list of major problems which arose in the recent years concerning the radiation flux models. Although, the issues mentioned above are not the only ones, they certainly contributed to stimulate the Development Study of Improved Models of the Earth's Radiation Environment which is described in this final report and in the six technical notes issued by TREND.

1.3.3 Current and future related activities

The initial momentum imparted to the study of the Van Allen belt particles trapped into the magnetosphere lasted almost a decade from 1961 to 1970. For various reasons this effort has gradually declined in favor of investigations concerning particles with energies lower than 100 keV. Indeed, it is these particle populations that contribute mostly to determine the dynamics of the magnetosphere.

However, a renewed interest for the harder corpuscular radiation environment is now under way, both in the US and within ESA which supports the present TREND study. The reasons for this have been outlined above. We note below a number of related activities.

CRRES - The Combined Release and Radiation Effects Satellite (CRRES) is in line with this renewed efforts going on in the US. This satellite mission will perform

chemical releases and will measure the Earth's radiation environment, including its effects on spacecraft components. It is a joint US Air force/NASA program. The CRRES program supports, among other experiments, the AFGL Space Radiation Effects Program (SPACERAD). The SPACERAD program is a comprehensive space and ground-test program to:

- measure radiation-induced single event upsets (SEU) and total dose degradation of state-of-the-art microelectronic devices in a known space environment;
- update the static models of the radiation belts and develop the first dynamic models of the high energy particle populations in near-Earth environment, among many other component related laboratory studies.

During the SPACERAD portion of the misson, the CRRES satellite will have a low inclination , highly elliptical (400 km to 36 000 km) orbit that will traverse the most intense radiation regions of the inner and outer radiation belts. The goal of the three-year mission is to obtain a statistically significant data set for the empirical analyses.

It is expected that following the launch of CRRES in 1990, a large analysis and modelling effort will begin. ESA should remain "in-touch" with this new trend.

NSSDC/WDC-A-R&S - Although the modelling effort of the radiation environment has been slowed down until the CRRES mission, there is still a continuing interest at NSSDC; the SPAN network system which is managed at NSSDC is important for all current and future modelling activities. NSSDC, Joe King, D.M. Sawyer, and D.Bilitza indicated that they plan be becoming more active again in the area of Earth radiation environment modelling after CRRES data will become available.

GSFC (Greenbelt, Md) - D.S. Stern designs new empirical models for the external magnetic field of the Earth as well as alternative transformation methods to be useful in mapping the contribution of the external magnetic field (see Stern, 1985, 1987, 1990).

JSC (Houston-Texas) - At NASA/Johnson Space Center (JSC) A. Konradi and colleagues specialize in several areas in which further work on models needs to be done.
- Conversion of omnidirectional fluxes stored in current empirical models to time averaged pitch angle distributions.
- Introduction of the east-west asymmetry.
- Development of a scheme for treating secular decay of the Earth's magnetic dipole.
- Development of a method to account for the altitude dependence of the particle fluxes as a function of the phase and magnitude of the solar cycle including the delay times involving the depletion and re-population of low altitude energetic inner belt protons.
- PHIDE detector - protons and heavy ion detector experiment for shuttle and space station.

AFGL - At the Air Force Geophysical Laboratory there has been in the recent years a strong emphasis to investigate the distribution of energetic trapped and non-trapped (solar flare) protons and electrons, using the data collected over many years with the DMSP satellite at low altitude (840 km) and on a high inclination orbit. Several important papers based on these data have been published by M.S.Gussenhoven et al.(1985, 1987, 1988), Mullen et al. (1987).

The study of solar proton events is also a standing interest of Smart and Shea at AFGL who published recently a comprehensive review on this topic (Smart and Shea, 1989). As already mentioned, AFGL is deeply involved with the CRRES mission.

NOAA/SEL - Space Environment Laboratory (Boulder), Ron Zwickl, H. Sauer and W. Wagner are responsible for GOES and NOAA satellite data and processing them. They have plans for data products in this area.

NOAA/NGDC - (Boulder) is the place where NOAA and GOES data are currently archived.

Aerospace Corporation (Los Angeles) - A long standing and continued interest for the earth radiation environment has been maintained since the early 60's. Pruett (1980) from Aerospace Corporation compared DMSP and NTS-2 dosimeter measurements with AE8 and AP8 model predictions. Blake, Paulikas, Schulz, and Vampola contributed importantly to the study of the earth radiation environment during the last three decades. In this respect, see the recent paper by Vampola (1989). They are also involved with CRRES.

LANL - The Los Alamos National Laboratory has contributed in the recent years a series of papers on relativistic electrons observed in the outer zone, and on their possible Jovian origin (Baker et al., 1979, 1987, 1989).The energetic particle measurements made with the LANL satellites contributed tremendously to the area, and provided a unique set of observations to TREND.

JPL - At Jet Propusion Lab. (Pasadena), J.Feynman and colleagues became interested in the statistical distribution of solar proton events over the three last solar cycles. They proposed recently a new probabilistic model to replace the earlier NASA model of King (1974).

CASS (UCSD- La Jolla) - At the Center for Astrophysics and Space Science, Carl McIlwain responsible for the B-L coordinate system maintains interest in coordinate systems more suitable for mapping the low altitude distribution of the radiation fluxes. Walter Fillius is a Co-I on one of the CRRES energetic particle experiments.

MSFC - John Watts and co-workers are concerned with the East-West asymmetry problem on Space Station Freedom (SSF). John Watt is also chairman of the SSF Ionizing Radiation Working Group. The group has also studied radiation environment measured on shuttle and performed Cosmic Ray Studies by balloon.

MDAC (Huntington Beach) - At McDonnell Douglas Astronautics Corporation, K.A. Pfitzer is also working in an area closely related to the Earth's radiation environment. He showed recently that the atmospheric density is an important parameter for interpolating the trapped radiation dose at times other than solar maximum or solar minimum when standard NASA models are available (MIN and MAX models).

ESA - Spacecraft designers in Europe rely fully on the NASA environmental models for predictions of the radiation risks of future mission. In this respect Europeans have been consumers of AE8 and AP8 trapped radiation models, more than developers of new or updated models of their own. Although still rather limited in Europe and within ESA, the interest for Earth's radiation environment model development is growing especially at the Mathematics and Software Division of ESTEC. This is confirmed by the present TREND study.

Furthermore, a survey of medium energy electrons at high altitude based on ISEE-1 satellite data has been undertaken and presented by Daly and Tranquille (1989). This analysis provides an overview of electrons fluxes in the energy range 22-1200 keV, as a function of geomagnetic coordinates and local time, for observations collected between November 1977 and September 1979. These observations also show significant differences with the AE8 model, confirming the need for updating the existing Earth's radiation environment models.

OBSERVATOIRE DE PARIS - MEUDON. - Solar activity and solar proton events have been studied here for several decades.

MSSL - At Mullard Space Science Laboratory, University College London, there is a current interest for the Earth's radiation environment. Data from the SEM instruments on METEOSAT have been analyzed in this respect at MSSL. In particular there has been continuing interest in the anomalies seen on METEOSAT and their correlation with the space environment. Two instruments were flown

(1) on METEOSAT F2, there was a spacescraft charging monitor which measured electrons between 50 eV and 20 keV. Although surface charging was detected, there was no correlation with anomalies, which led to the suggestion of flying a higher energy detector on P2.
(2) On METEOSAT P2, launched June 1988, a 30-300 keV electron instrument was flown. The major result from this was that in the first year of operation a correlation was found between detector flux and the anomalies on the spacecraft. Analysis of these data are continuing at MSSL.

RAE - is interested in radiation modelling and measurements .

USSR - Beside the important external magnetic field model development carried out by N.A.Tsyganenko at the University of Leningrad, we are not well informed of other research, modelling or monitoring activities taking place currently in the USSR.

This list of places where activities related to Earth's radiation environment modelling or monitoring activities are currently underway may not be exhaustive. It summarises, however, information we were aware of at the time this FINAL REPORT was prepared (August 1990). We

apologize if some other groups active in this area have been overlooked. It would be useful if these groups could react, and inform TREND of their current activities in this field of application.

1.4 The scope & objectives of this study

The objectives of this contract are:

- to provide reliable information on the validity or ortherwise of current Earth's radiation environment models;

- to define the recent terrestrial radiation environment and investigate discrepencies between models and measurements;

- to identify and develop computer-based methods for modelling the Earth's energetic particle environment for ESA's radiation environment analyses;

- to provide updated computer-based models and associated software tools which can be applied in these analyses;

- to identify requirements for future modelling and data acquisition.

Models of both magnetospheric trapped energetic particle flux and solar flare energetic particle fluxes have been considered at all stages in this study.

These objectives have been met by TREND as far as resources allowed. The results of this study have been reported in TREND's technical note 1 to 6. The main achievements are summarized in this final report. The workload has been divided into seven work packages whose description is given below.

1.4.1 Work Package 1 - Evaluation of Current Models

The current models of trapped particle (AE8,AP8) and solar flare particle fluxes ('King model') has been critically evaluated. This includes evaluation of model functional descriptions, physical assumptions, effects of secular variations in the geomagnetic field and correlations with available flight data, especially over the last solar cycle. Items considered include dependence on energy,B,L, pitch-angle, local time and geomagnetic and solar activity. Reasons for discrepancies between models and measurements have been given. Future requirements for models, considering ESA's space programs, have been identified. Technical note 1 has been produced on this work.

1.4.2 Work Package 2 - Model Formalism

Existing modelling methods have been evaluated with regard to the physical processes included and excluded, implicitly or explicitly. Potential alternative model formalisms, have been identified and defined. Recommendations for better methods have been made. Technical note 2 has been produced on this work.

1.4.3 Work Package 3 - Identification and Acquisition of Useable Satellite Data

Sources of existing radiation environment data which are potentially useable in establishing environment models of the type identified in work package 2, along with data availability and data access methods have been identified. The data have been characterized with respect to species, energy, spatial, directional and temporal coverage. Technical note 3 has been produced on this work. It provides detailed descriptions of the data and instrumentations.

1.4.4 Work Package 4 - Data Analysis

Taking into account the results of packages 1, 2 and 3, the data analysis requirements have been proposed. Satellite data have been processed to remove unnecessary data and produce appropriate averages. Plots and summary data files have been produced.

Appropriate data analysis algorithms and data organisations schemes have been defined and implemented. Consideration has been given to temporal, spatial, directional and spectral features of the data and to the characteristics of the instrumentation used in their acquisition. Averaging, binning and fitting have been performed, yielding plots and further reduced summaries. Other analyses and data presentation have been produced where these were found to be useful. Technical note 4 has been produced on this work. The software developed during execution of this work package will be delivered to ESTEC at the end of this contract.

1.4.5 Work Package 5 - Production of New Models and Tools

Taking into account the results of packages 1,2,3 and 4, appropriate method of incorporating the reduced satellite data into new models have been defined and proposed.

New tables of the Earth's radiation environment near geostationary orbit have been obtained. The associated tools for model and processed-data access have been developed. Technical note 5 has been produced on this work. The software developed during execution of this work package will be delivered to ESTEC at the term of this study.

1.4.6 Work Package 6 - Definition of Flight Measurement Requirements

On the basis of the preceding work, data coverage inadequacies in species, energy, spatial, directional or temporal terms, have been identified and where necessary, recommendations have been made for remedying the situation made. Technical note 6 has been produced on this work.

1.4.7 Work Package 7 - Conclusions and Recommendations

Conclusions have been drawn from the work, summarizing the work performed and results produced, and identifying problem areas. Recommendations have been made for tackling the problems and for future work in this area. These conclusions and recommendations form part of this final report which is a synthesis of the principal results of the contract.

2. EVALUATION OF CURRENT AND NEW MODELS

2.1 Brief description of the radiation environment

What is this environment formed of, and, what are the sources of the main components of the damaging corpuscular radiation under concern in this study? Chapter 4 in TN1 contains a detailed description of this environment. See also Chapter 3 in TN6 as well as the comprehensive review by Vampola (1989), Smart and Shea (1989). Only a brief outline is given here.

Energetic particles come from the Sun. There are charged particles trapped into the geomagnetic field. Some of the latter ones are a consequence of local diffusion and acceleration processes of magnetospheric particles, but the more energetic ones are 'debris' of Cosmic Ray Albedo Neutron Decay.

Fig.2-1 shows typical energy integral fluxes of these different populations of charged particles which are observed in the magnetosphere.

2.1.1 Particles coming from the Sun

The Sun emits continously charged particles forming the solar wind supersonic flow. But in addition to this relatively low energy (10-200 eV) and dense plasma (5-10 cm^{-3}), the Sun emits from time to time, at the occasion of large solar flare eruptions, robust showers of protons and relativistic electrons travelling between the Sun and Earth at almost the speed of light for the most energetics ones. These particles which have energies larger than 0.5 MeV (for the electrons), penetrate most easily the Earth's

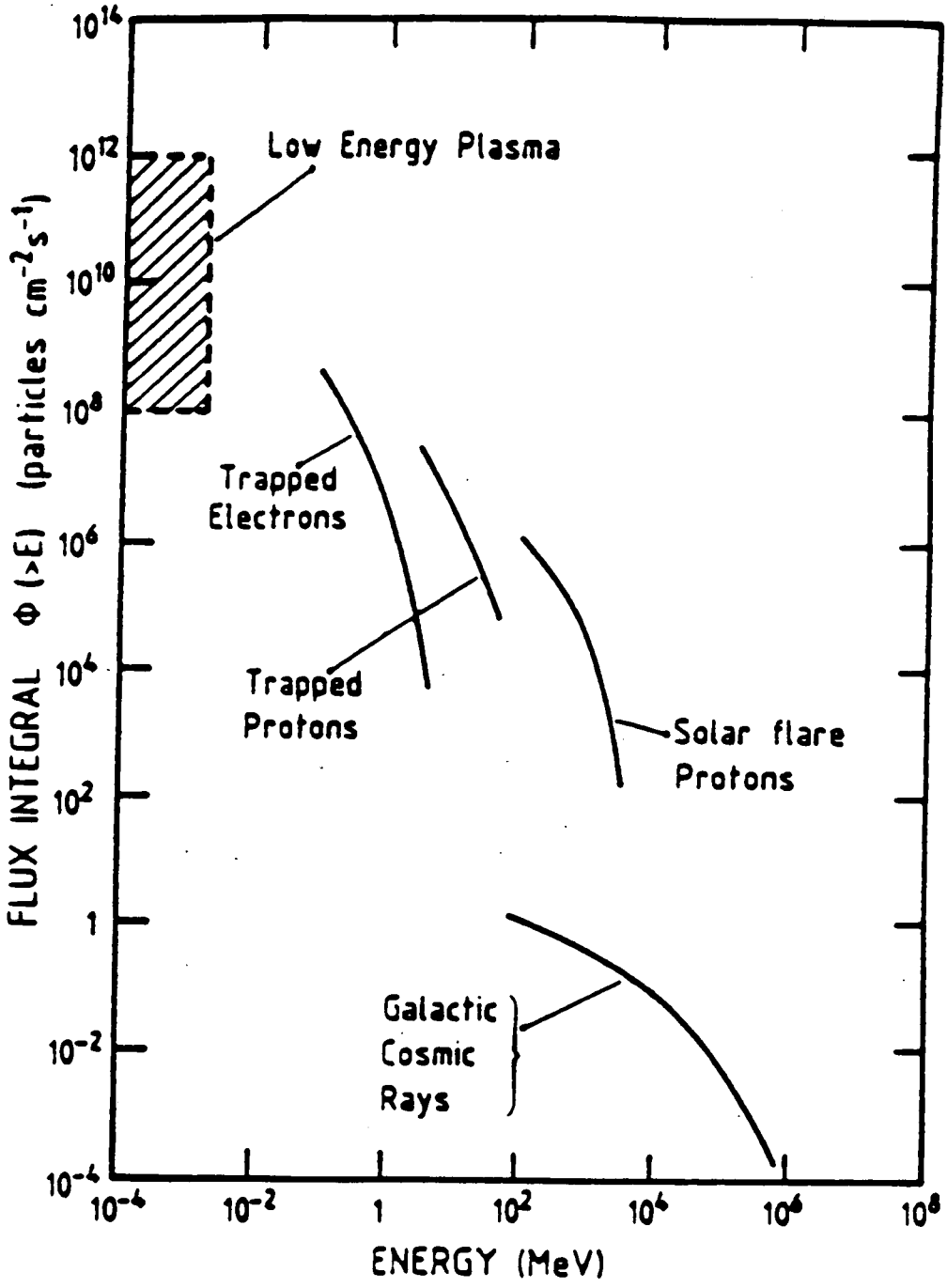

Fig.2-1. Typical energy integral flux of the different populations of charged particles in the Earth magnetosphere (after Blake and Paulikas, 1970).

upper atmosphere above the polar caps, where the geomagnetic field line distribution allows easier access into the magnetosphere.

2.1.1.1 Geomagnetic cut-off

The Earth's dipole magnetic field filters charged particles according to their 'magnetic rigidity' (: momentum/charge). For each point along the orbit of a spacecraft, and, for each direction, there exists a magnetic rigidity below which ions cannot arrive from outside the magnetosphere.

Störmer (1930) showed that the cutoff rigidity at the Earth's surface is given by :

$$R_S = \frac{M}{r^2} [1 - (1 - \cos\gamma \cos^3\lambda)^{1/2}]^2 / [\cos\gamma \cos\lambda]^2 \qquad (2.1)$$

for positively charged particles, where

M = normalized dipole moment of the Earth ($M \simeq 60$)

R_S = magnetic rigidity in GeV/ec

r = radial distance from the dipole centre in earth radii

λ = latitude in offset dipole coordinates and,

γ = the angle from which the particle arrives with respect to local east in offset dipole coordinates.

The magnetic rigidity, R, is related to the particle energy by :

$$E = (M_o^2 + R^2Z^2/A^2)^{\frac{1}{2}} - M_o \qquad (2.2)$$

where E is the kinetic energy in GeV/c (1 GeV/c = 1000 MeV/c),

R is the magnetic rigidity in GeV/ec

A is the particle's mass in amu

Z is the particle's charge and

M_o = 0.931 GeV

As can be seen from Störmer equation (2.1), R_s depends strongly on the geomagnetic latitude. This means that the geomagnetic cutoff will vary drastically around the orbit of a spacecraft, especially at high inclinations.

From equation (2.1), it can be deduced that the magnetic rigidity of a positive particle that circles the Earth in the equatorial plane ($\lambda = 0°; \gamma = 0°$), at the distance r from the centre of the dipole has the critical value (R_c).

$$R_c = \frac{M}{r^2} \qquad (2.3)$$

The value of R_c depends on the magnetic moment of the Earth and on the distance r of the point of observation from the Earth's magnetic centre. This distance is different for different measurements, both because observations may be carried out at different altitudes above sea level and because, on account of the eccentricity of magnetic dipole, r is not a constant at the Earth's

surface. Thus, the value of R_C is not exactly the same for all point of observations. However, Rc is never very far from the round number

$$R_C = 6 \times 10^{10} \text{ volts} \qquad (2.4)$$

which corresponds to $r = 6.36 \times 10^8$ cm (the mean radius of the solid Earth is 6.37×10^8 cm).

For vertical direction ($\gamma = 90°$), (2.1) reduces to

$$R_S = \frac{M}{4r^2} \cos^4 \lambda \qquad (2.5)$$

In figure 2.2, the values of R_S/R_C corresponding to the vertical direction (zenith angle = 0°, $\gamma = 90°$), to the direction of 45° to the zenith toward the west ($\gamma = 135°$) and to the direction at 45° to the zenith toward the east ($\gamma = 45°$) are plotted against geomagnetic latitude.

Notice that the separation between the cutoff momenta corresponding to directions on opposite sides of the meridian plane increases with decreasing geomagnetic latitude.

Equation (2.1) shows that the Earth's magnetic field produces two major effects on the intensity distribution of cosmic rays, a latitude effect and an east-west effect.

The cutoff rigidity in the vertical direction as well as in any direction specified by given values of the zenith angle and the azimuthal angle, increases steadily with decreasing geomagnetic latitude. Thus, as one proceeds from the poles toward the equator, particles of greater and greater rigidity are removed by the Earth's magnetic field, and the total flux of primary cosmic rays incident upon the top of the atmosphere decreases.

For a given point of observation and for a given zenith angle, the cutoff rigidity is a function of the azimuth that has a maximum in the eastern direction and a minimum in the western direction for positively charged particles, and the other way around for negatively charged particles. Thus, primary particles of a given sign will reach to the top of the atmosphere with an asymmetric intensity distribution relative to the meridian plane, positive particles arriving with greater abundance from the western part of the sky and negative particles from the eastern part.

The 'cut-off geomagnetic rigidity' increases as the latitude decreases. It is maximum at the geomagnetic equator. The resulting gradual reduction of flux of solar particles at lower geomagnetic latitudes is called the called 'geomagnetic cut-off'.

For routine "engineering-level" evaluation of the geomagnetic shielding of flare protons, some guidance may be provided. The geomagnetic shielding can be computed on the basis of the trajectory in B, L space. The (r, λ) coordinates can be computed from B and L according to the method of Roberts (1964) which provides a convenient scheme to accomplish the inverse transformation of the system of equations :

$$B = B_o(4 - 3\cos^2\lambda)^{\frac{1}{2}} / \cos^6\lambda \qquad (2.7)$$

$$r = L\cos^2\lambda \qquad (2.8)$$

$$\text{where } B_o = M/L^3 \qquad (2.9)$$

The constant M is given by McIlwain (1961): M = 0.311653 Gauss (Earth radii)^3.

From equation (2.8), it can be seen that for vertical arrival, equation (2.5) simplifies to :

$$R_S = \frac{M}{4L^2} \qquad (2.10)$$

Smart and Shea (1967) have shown that McIlwain's L coordinate (McIlwain, 1961) is highly correlated with the effective vertical cutoff rigidity

$$R_S = 15.96\ L^{-2.005} \qquad (2.11)$$

is obtained using the Shea et al. (1965a,1965b) trajectory-derived cutoff values. Equation (2.11) can be used for estimates of vertical cosmic-ray cutoff rigidities on or above the Earth's surface, with the exception of points near the cosmic-ray equator.

However, detailed calculations of the cutoff are available from Shea and Smart (1975). Adams et al. (1983) have calculated a transmission function that modulates the radiation environment in the interplanetary medium to obtain the orbit-averaged radiation environment at any spacecraft in a circular orbit. The procedure used to obtain this transmission function is similar to the one reported by Heinrich and Spill (1979). Some thought must be given to its use on solar flare spectra because the flare particle intensity changes on a time scale comparable to or shorter than an orbital period (Adams et al., 1981). Also the geomagnetic cutoff is suppressed to some extent during a flare.

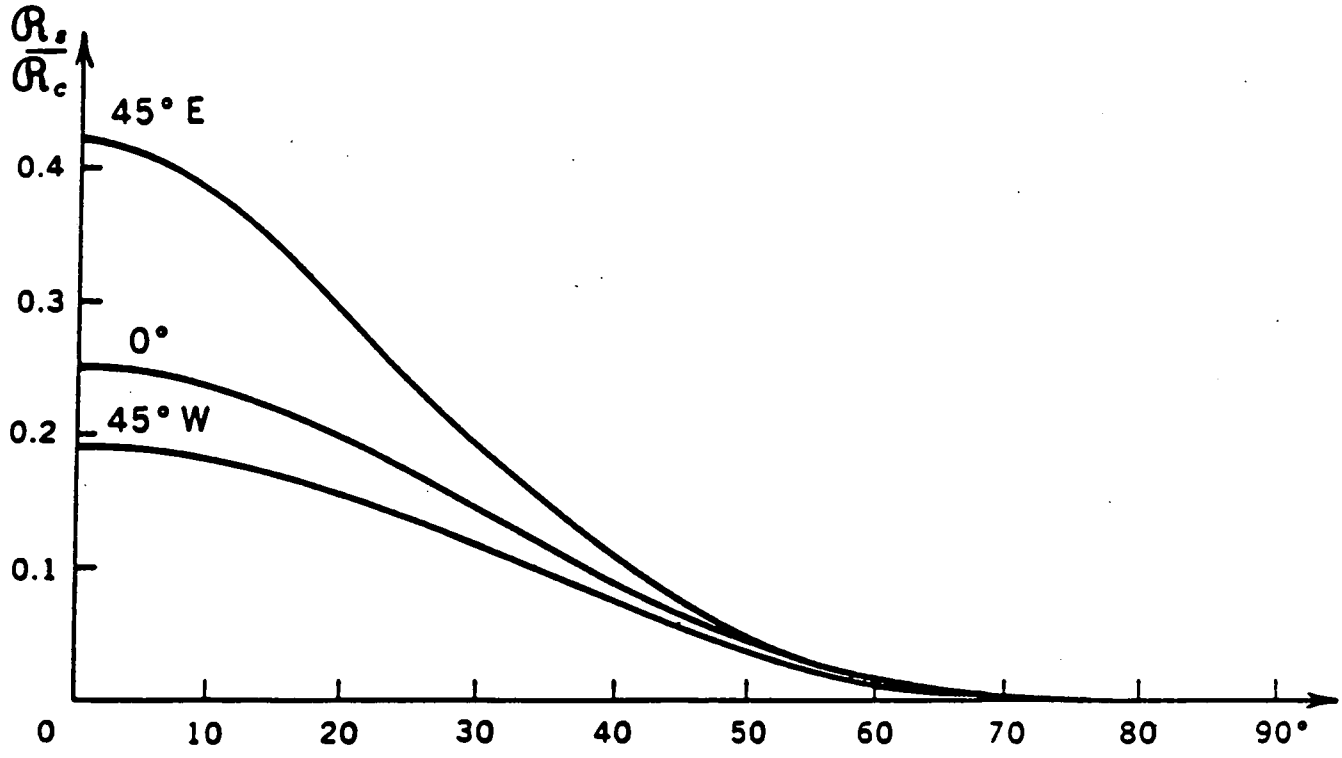

Fig.2-2. R_S/R_e vs. λ for the vertical (0°), for a direction at 45° to the vertical toward the west (45° W), and for a direction at 45° to the vertical toward the east (positive particles). (From Rossi, B. and Olbert, S. ,1970).

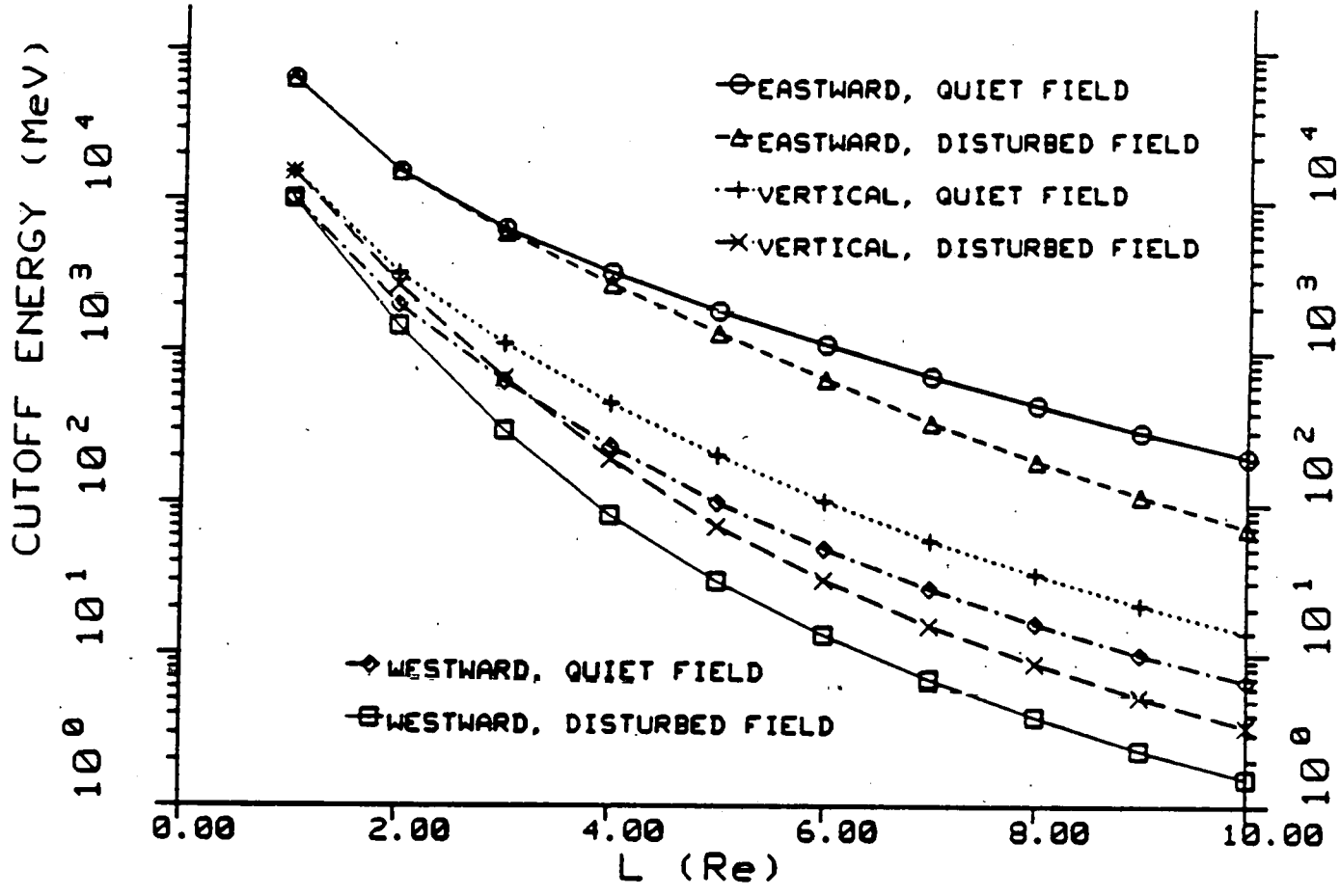

Fig.2-3. Geomagnetic shielding : proton arrival at the geomagnetic equator from different directions under quiet and disturbed geomagnetic conditions.(From Daly, E.J., 1988).

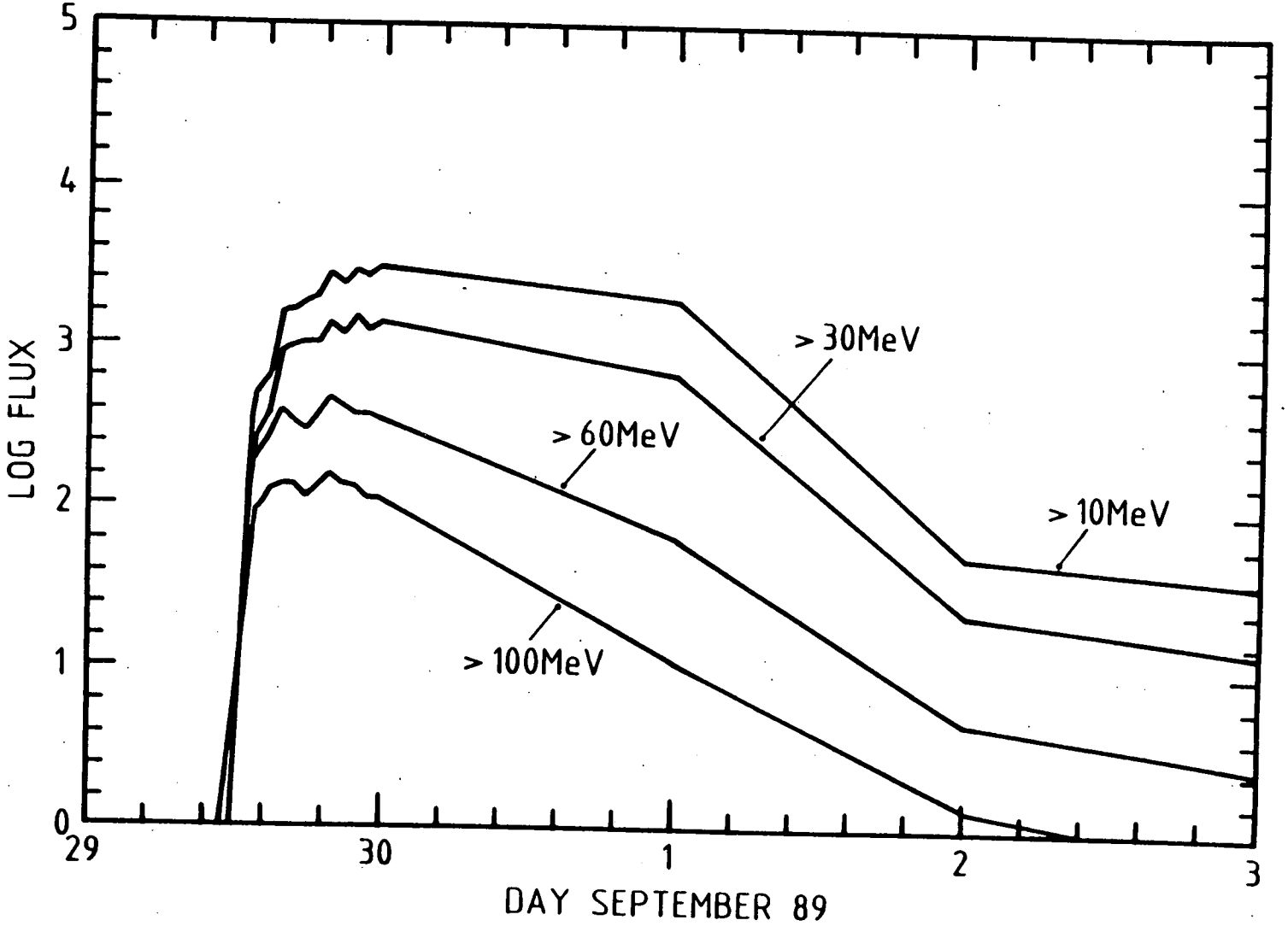

Fig.2-4. Integral flux above different energy thresholds for solar flare protons observed 29 september 1989.

Adams et al. (1981) recommend that the geomagnetic cutoff during a flare, RF, be computed from the "quiet time" cutoff Ro using :

$$\Delta R/R_O = 0.54 \exp (- P_O/2.9) \qquad (2.12)$$

and $R_F = R_O - \Delta R$ (2.13)

where R_F, R_O and ΔR are in GeV/ec.

The effects of the arrival direction (using a dipole field) and magnetospheric state (using equations (2.12) and (2.13)) on proton cutoff energy have been computed by Daly (1988). Typical results are shown in figure 2.3 for proton arrival at the geomagnetic equator from different directions under quiet and disturbed geomagnetic conditions. From this figure, it can be seen that the vertical cutoff model excludes protons of E < 200 MeV from L < 5, in a quiet magnetosphere. This corresponds to the geomagnetic cutoff suggested by Stassinopoulos and King (1974) who reported a model having total cutoff at L = 5. This model is adequate for most cases and is included in TREP (Daly, 1988). However, an arrival-direction-dependent model for flare proton cutoffs throughout B,L space can also be used by TREP if required.

Beyond the uncertainty in the cutoff itself, other sources of error are the darkness of the penumbral shadow and the size assumed for the umbral shadow. At satellite altitude, the Earth's shadow should be taken as shrinking with altitude according to the following equation (Adams et al., 1981) :

$$\text{Omega} = 2\pi \{1 - [(R_e + h)^2 - Re^2]^{\frac{1}{2}} / (R_e + h) \} \qquad (2.14)$$

where "Omega" is the portion of the geometric factor that is occulted at altitude (h) and R_e is the Earth's radius.

As reported by Adams et al. (1981), the uncertainty in the actual value of the geomagnetic cutoff may be 50 percent at low cutoffs during a magnetic storm. This translates into only a ± 50 percent error in the flux, and since this condition is transient, it is only important for solar flares. The flux uncertainty during a solar flare is >>50 percent.

More details about the geomagnetic cut-off and the method used in UNIRAD to compute the resulting flux reduction are given in Chapter 6 of TREND's TECHNICAL NOTES 1. The code used in UNIRAD to calculate the reduction factor due to geomagnetic cut-off is called EXPFAC. Since it has not been changed by TREND, there is reason to discuss this code in this final report.

2.1.1.2 Effects of solar flare protons

Solar proton events produce dramatic geophysical effects in the high latitude ionosphere, e.g. Polar Cap Absorption (PCA) of high-frequency radio waves. The precipitation of solar protons in the polar cap ionosphere enhances the ionization density and changes the electromagnetic propagation characteristics of the medium. These unpredictable showers of solar cosmic-ray particles can be detrimentral for man, for scientific instrumentation, electronic components flown in high latitude or high altitude orbits

A more detailed description of the damages produced by these particles on material and sensitive satellite component has been given in TN6 (Requirements and Recommendations for future flights). A resume of this contribution prepared by TREND can also be found in chapter 5 of this final report.

2.1.1.3 Flux and fluence

Figure 2-4 shows the flux of protons observed with GOES-7 at geostationary orbit (36 000 km altitude) during the solar proton event of 29 September 1989, respectively for energies larger than 10 MeV, 30 MeV, 60 MeV and 100 MeV. The flux per square centimeter integrated over the time duration of the event (3 days) is called 'fluence' of the solar proton event. For this particular event the fluences have been 415×10^7 , 175×10^7 , 38×10^7 and 12×10^7 protons/cm^2, respectively for energies above 10 MeV, 30 MeV, 60 MeV and 100 MeV. More important and therefore more dangerous solar proton events have been observed in 1989 and earlier. One of the largest event ever observed was that of August 1972; its fluence was twice as large as that of 29 September 1989. This event is often taken as reference. It is one of the few 'anomalously large' (AL) solar proton events recorded in the last 33 years.

2.1.1.4 Probability of occurence of solar proton events

The probability of occurence of solar events with a fluence exceeding a given threshold (e.g. 10^9 protons/cm^2) for the whole duration of a space mission is of key importance for the safety of the orbiting instrumentation. The small number of solar proton events during the last 33 years of observations severely limits statistical analyses and can hardly satisfy spacecraft engineers requiring a reliability with 90% confidence level factors. The practice of dividing the available data into solar cycle groups further limits the statistics, and the results are open to a variety of interpretations (Smart and Shea, 1989).

2.1.1.5 King's probabilistic model

Based on observations for the 20th solar cycle (which contained 24 ordinary (OR) solar flare events and only one AL event), King (1974) developped the first probabilistic model which is still in use today. This model has become a standard against which other work is currently compared. This model, also called the 1975 NASA model, predicts the probabilty of exceeding a given fluence for a given mission scenario (Stassinopoulos, 1975).

A detailed description of King's model and of the Burrell's statistics on which it is based has been given in TREND's Technical notes 1 (chapter 5). Since this is standard material we will not repeat it in this final report.

King's solar fluence model is currently implemented in UNIRAD where the subroutine KINGFL computes the expected fluences (FLUEFL in cm^{-2}) for ordinary and anomalously large solar flares, as a function of the length of the mission (TFLARE in years). A confidence level (FLPROB in percent), is an input corresponding to the probability for getting an actual number of flares which is less or equal to the calculated value. But FLPROB can also be an output parameter when the numbers of ordinary flares (NOR) and of anomalously large events (NAL) are supplied as input parameter in the $STEP section of the namelist file UNIRNML. A detailed analysis of this subroutine and of the results it provides can be found in TN2 (chapter 5).

In the past years this model has been criticised as being too limited and not truly representative of the current cycle 22 which looks to be rather similar in amplitude to cycle 19 (Chenette, and Dietrich, 1984; Feynman et al., 1988).

2.1.1.6 Feynman et al.'s model

A new statistical model has recently been proposed by Feynman et al. (1988); see also Feynman and Gabriel (1989). Based on a larger sample of solar proton events spread over solar cycles 19, 20 and 21, they conclude that there is no need for separating statistics for AL events and OR events. Indeed, all fluence data combine to form a continous log-normal distribution. Furthermore, most of these events cluster within a period of 7 years around the date of maximum sunspot number. A short outline of this new model is given in Appendix H. A more detailed one can be found in TREND's TN1 (chapter 5.3).

Note however that this new distribution of solar proton events differs sharply from that reported by Goswani et al. (1988). There is not yet general consensus on what is the most realistic interpretation. More data from more solar cycle need to be collected to settle this important debate.

Although not definitive, the probabilistic model of Feynman et al. (1988), appears to be an interesting alternative and a valuable one. Its implementation by TREND in the UNIRAD software as an alternative to the earlier model has been described in TN 2 and 4. In Chapter 4 of this FINAL REPORT, there will be more about this issue and the FORTRAN code FEYNFL developed by TREND.

2.1.2 Particles trapped in the geomagnetic field

2.1.2.1 Sources

In addition to the solar energetic component (sometimes called solar cosmic rays events) the magnetosphere is filled with trapped charged particles of all energies. The origin of the most energetic ones is not yet fully understood, although it is established that some

are the result of the CRAND process. The CRAND or Cosmic Ray Albedo Neutron Decay is the main source of protons above 10 MeV and electrons above 1-2 MeV in the inner zone. Magnetospheric acceleration and diffusion are producing the more abundant protons in the range 0.5-5 MeV, as well as for the electrons of the outer zone. Baker et al. (1981,1989) considered that part of the relativistic electrons flux observed at geostationary altitude could be of Jovian origin.

2.1.2.2 Charged Particle motion in the geomagnetic field.

When an electrically charged particle is injected into the geomagnetic field with an initial velocity at a certain angle with the field vector, it will follow a helicoidal trajectory about and along a magnetic field line (provided its energy does not exceed the energy threshold for trapping). When it spirals towards a region of higher field intensity, the particle experiences an induced electric field that accelerates its circular or 'cyclotron' motion transverse to the field line. Since the total energy of a particle cannot change in a static magnetic field, the increase in transverse kinetic energy must occur at the expense of a corresponding "slow-down" of the motion parallel to the field line. A point may eventually be reached at which all the parallel kinetic energy has been converted into transverse energy and the particle reverses its parallel motion and spirals back into the opposite direction (see Fig. 2.5). In the geomagnetic field, a charged particle can bounce back and forth between two such 'mirror' points lying on opposite sides of the geomagnetic equator.

In addition to this bounce motion, the fact that the field is not uniform and that field lines are curved causes the particle to drift in longitude around the of earth (see Fig. 2.6); electrons drift eastward and

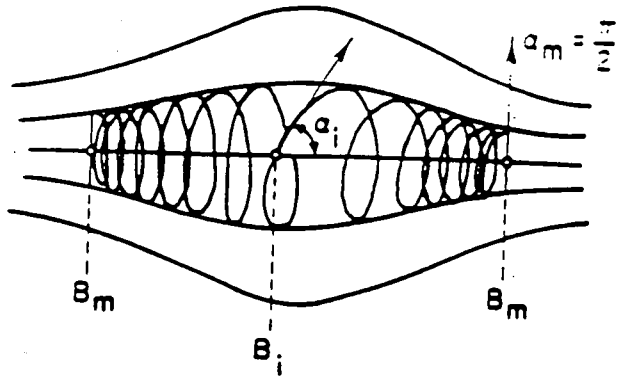

Fig.2-5. Helicoidal trajectory of a trapped particle; pitch angle and mirror points are shown.

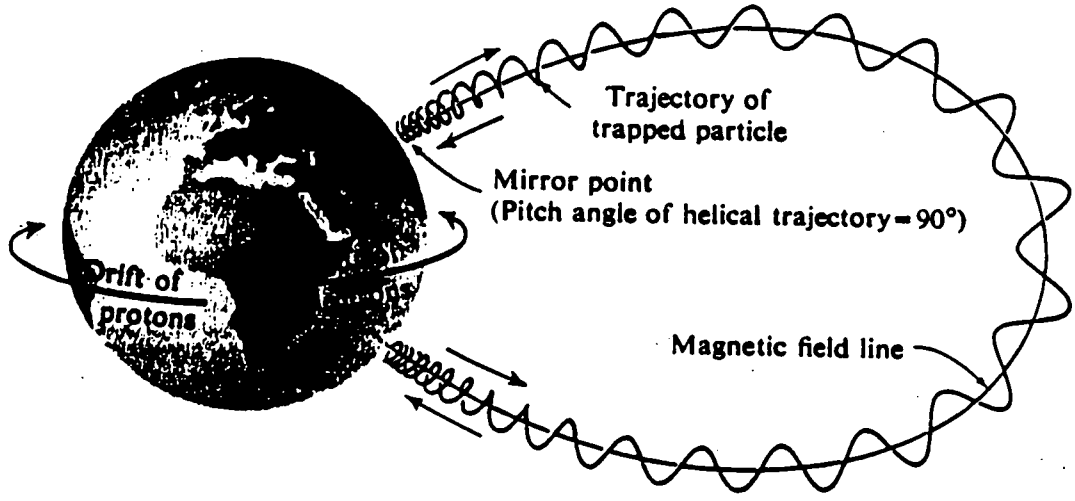

Fig.2-6. Motion of a charged particle in a dipole magnetic field.

protons drift westwards. As a consequence, a charged particle can remain trapped in the geomagnetic field within a fixed drift-shell for a very long time. All these drifting charged particles form the Van Allen radiation belts.

As mentioned above, the motion of a particle trapped in a magnetic field is a combination of three periodicities each one with a characteristic time scale : (1) cyclotron motion around a field line, (2) bounce motion along a field line between two mirror points, and (3) azimuthal drift motion along a 'shell' of field lines around the earth. Associated with each one of these motions are three adiabatic invariants (Northrop, 1963):

(i) the magnetic moment

$$M = p_{\perp}^2 / 2m_oB \qquad (2.15)$$

where $p_{\perp}$ is the particle's momentum component perpendicular to the field line, B is the field intensity, and m_o is the particle's rest mass. This first adiabatic invariant of motion is used to determine the value of magnetic field intensity at the position of the mirror points.

(ii) the second invariant of motion

$$J = \oint p_{\parallel} \, ds \qquad (2.16)$$

is the integral of the parallel component of the momentum along the field line arc length, s, in a full bounce cycle between the two mirror points.
This second adiabatic invariant of motion is proportional to the 'field integral I' sometimes used as a coordinate to map trapped particle fluxes

(iii) the magnetic flux U encompassed by a closed drift

shell:

$$\Phi = \iint ABds \qquad (2.17)$$

where A is the area inside the drift shell.
This third invariant has been used by some authors to introduce a generalized L*-shell parameter which should be conserved in the case of slow secular variations.

These three adiabatic moments are related to three action variables associated with the three action angles defining the phases of the periodic gyration, bounce and drift motions.

The frequencies associated with these three cyclic motions are illustrated in Fig.2.7 for equatorially mirroring protons and electrons as a function of kinetic energy and equatorial distance in the Earth's dipole (L) (Schulz and Lanzerotti, 1974). It can be seen from Fig.2.7 that for a proton of 1 MeV at an equatorial distance of 2 R_E the gyration, bounce and drift frequencies are respectively about 60 Hz, 0.4 Hz and 0.7 mHz; for an electron of the same energy at the same place in the equatorial plane one gets respectively 40 kHz, 5 Hz and 0.5 mHz.

2.1.2.3 Magnetic Field Intensity and Line of Force in a Centred Dipole.

In a pure dipole magnetic field distribution the field intensity in polar coordinates r, θ and φ is given by

$$\mathbf{B} = - B_E \, (2\, \mathbf{e}_r \cos\theta + \mathbf{e}_z \sin\theta) \left(\frac{R_E}{r}\right)^3 \qquad (2.18)$$

where R_E is the radius of the Earth (R_E=6371 km) and B_E is the equatorial magnitude of B at r = R_E (B_E=0.31 Gauss).

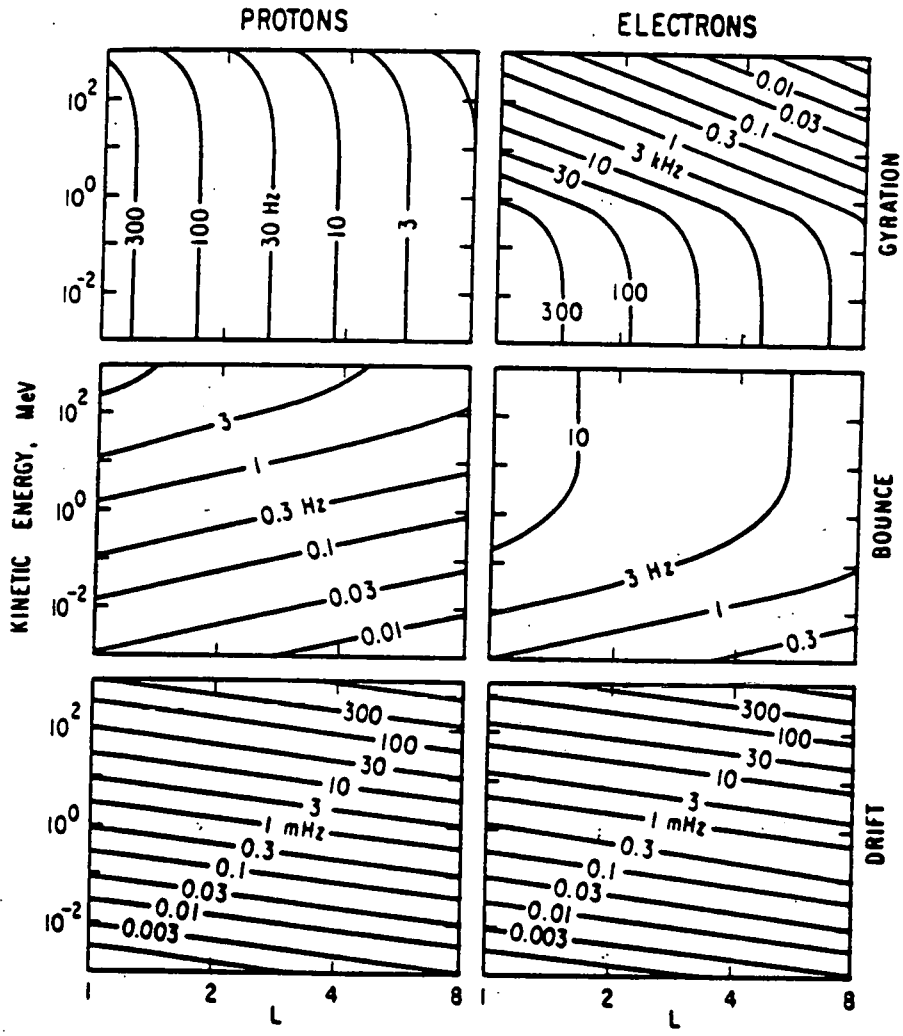

Fig.2-7. Contours of constant adiabatic giration, bounce, and drift frequency for equatorially mirroring particles in a dipole field. Adiabatic approximation fails in the upper right-hand corners (E ≈ 1GeV, L ≈ 8) (from Schulz and Lanzerotti, 1974).

A field line intersects the equatorial plane at a distance r_o from the origin. The equation of this field line is :

$$r = r_o \sin^2\theta \qquad (2.19)$$

The element of arc along the field line is therefore

$$ds = ro\ (1 + 3\cos^2\theta)^{\frac{1}{2}}\sin\theta\ \ d\theta$$

and from this expression follows the value given by

$$S = 2\ r_o\ [1+ 1/2\ 3^{\frac{1}{2}}\ \ln(2 + 3^{\frac{1}{2}})] \approx 3.7603\ r_o \qquad (2.20)$$

for the total length, S, of the field line.

The dipole magnetic field distribution (2.18) can be generated as the curl of the magnetic vector potential, A

$$\mathbf{A} = - B_E\ \mathbf{e}_z\ \frac{R_E^3}{r^2}\sin\theta \qquad (2.21)$$

or as the gradient of the magnetic scalar potential, V

$$V = -B_E\ \frac{R_E^3}{r^2}\cos\theta \qquad (2.22)$$

2.1.2.4 Mirror Points: Value of Bm.

Using conservation of the first adiabatic invariant (2.15) and the conservation of the momentum p ($p^2=p_\perp^2+p_\parallel^2$), where $p_\parallel$ is the component of momentum

parallel to B ($p_\parallel = p \cos\alpha$, where α is the pitch angle), the magnetic field intensity, B_m, at the mirror point can be determined as a function of the equatorial pitch angle α_o or $\alpha(s)$ at any other location along the magnetic field line by

$$B_m = \frac{B(s)}{\sin^2\alpha(s)} = \frac{B_o}{\sin^2\alpha_o} = \frac{B_i}{\sin^2\alpha_i} \qquad (2.23)$$

Indeed at the mirror points where $p_\parallel = o$, the pitch angle α_m becomes equal to 90°. The minimum value of the pitch angle is obtained where B is minimum, i.e. in the magnetic equatorial plane, where $B = B_o$.

2.1.2.5 L-parameter: Bounce Period

The magnetic field intensity B (see eq.2.18) is given by

$$B = \frac{B_E R_E^3}{r^3} (1 + 3\cos^2\theta)^{\frac{1}{2}}/\sin^6\theta \qquad (2.24)$$

The equatorial magnetic field intensity for a dipole field line crossing the equatorial plane at r_o is defined as

$$B_o = B_E R_E^3 / r^3 \qquad (2.25)$$

It has become common practice to label dipole magnetic field lines by L, the radial distance where they cross the equatorial plane (expressed in units of Earth' radii by $L=R_E/r_o$). In an ideal case of a dipole magnetic field model this dimensionless parameter L coincides exactly with

McIlwain's L-parameter defined by

$$L = (B_E / B_o)^{1/3} \tag{2.26}$$

It should, however, be pointed out that in the case of non-dipole magnetic field distributions McIlwain's L-parameter does not identify in a unique manner a magnetic field line. According to McIlwain's original interpretation L should be used with B_m (from eq.2.23) as a new coordinate to label (mirror) points in space instead of I; McIlwain (1961) determined a mathematical method to calculate L(Bm,I) for any non-dipole magnetic field model.
To avoid a common misuse and misinterpretation of McIlwain's L-parameter, it is therefore important to remember that, in general, L varies from one (mirror) point to the other along a real magnetic field line, although this variation is less than 1% in the inner magnetosphere. It is only for the pure dipole case that $L(B_m,I)$ is the same for all (mirror) points along a given magnetic field line!

The bounce motion of a particle's guiding centre along an equipotential field line has a period

$$\tau_b = \oint \frac{ds}{v_\parallel} = \left(\frac{m}{p}\right) \oint (1 - B/B_m)^{-\frac{1}{2}}\, ds \tag{2.27}$$

where the integral is evaluated along the guiding field line (2.18).

The bounce period, τ_b, is then represented as

$$\tau_b = (4\ m\ L\ R_E / p)\ T(y) \tag{2.28}$$

where

$$T(y) = \int_{\theta_m}^{90^\circ} \frac{\sin\theta \ (1 + 3\cos^2\theta)^{\frac{1}{2}} d\theta}{(1 - y^2 \ (1 + 3\cos^2\theta)^{\frac{1}{2}} / \sin^6\theta)^{\frac{1}{2}}} \qquad (2.29)$$

where θm is the colatitude of the mirror point where $B=B_m$ and where $y=\sin \alpha_o$ is determined by eqs.(2.23) and (2.24)

$$y^2 = \sin^2\alpha_o = B_o/B_m = (1 + 3 \cos^2\theta_m)^{-\frac{1}{2}} \sin^6\theta_m \qquad (2.30)$$

For $o<y<1$, exact evaluation of (2.15) in terms of elementary functions of y is impossible, but exact values can be determined numerically. These exact values are given in Table 2.1. A very good approximation of T(y) has been obtained by (Lencheck et al., 1961) and is given by :

$$T(y) \approx T(o) - \frac{1}{2} [T(o) - T(1)](y + y^{\frac{1}{2}}) \qquad (2.31)$$

with

$T(o) \approx 1.3802$

$T(1) \approx 0.7405$

$[T(o) - T(1)]^{\frac{1}{2}} \approx 0.3198$

The approximate values of T(y) are also given in Table 2.1; at worst this estimate deviates from the exact function T(y) by less than 1%.

2.1.2.6 Second Invariant J: Azimuthal Drift Frequency.

The second invariant J, as defined by eq.(2.16), can be approximated by means of

$$J = 2 \ p \ L \ R_E \ Y(y) \qquad (2.32)$$

where

θ_m	$y^{1/2}$	$\sin^{-1} y$	Exact T	Approx T	Exact Y	Approx Y
0°	0.00000	0.00°	1.380	1.380	2.760	2.760
1°	0.00194	0.00°	1.380	1.380	2.760	2.758
5°	0.02165	0.03°	1.376	1.373	2.741	2.730
10°	0.06102	0.21°	1.366	1.359	2.682	2.6633
15°	0.1114	0.71°	1.350	1.341	2.587	2.565
20°	0.1701	1.66°	1.327	1.316	2.457	2.434
25°	0.2352	3.17°	1.298	1.287	2.296	2.275
30°	0.3051	5.34°	1.264	1.253	2.109	2.091
35°	0.3785	8.23°	1.224	1.213	1.901	1.886
40°	0.4539	11.89°	1.179	1.169	1.678	1.666
45°	0.5303	16.33°	1.129	1.121	1.446	1.437
50°	0.6062	21.56°	1.076	1.069	1.211	1.205
55°	0.6804	27.58°	1.020	1.014	0.9793	0.9761
60°	0.7515	34.38°	0.963	0.959	0.7577	0.7562
65°	0.8178	41.97°	0.906	0.905	0.5521	0.5517
70°	0.8773	50.32°	0.854	0.853	0.3693	0.3692
74°	0.9186	57.54°	0.816	0.816	0.2438	0.2438
78°	0.9528	65.20°	0.784	0.785	0.1408	0.1408
82°	0.9785	73.23°	0.760	0.761	0.06386	0.06387
86°	0.9945	81.54°	0.745	0.746	0.01617	0.01617
90°	1.0000	90.00°	0.740	0.740	0.00000	0.00000

Table 2-1 Functions of Bounce Motions in Dipole Field.

$$Y(y) = 2 \int_{\theta_m}^{90^\circ} \frac{\sin\theta \quad (1 + 3\cos^2\theta)^{\frac{1}{2}} d\theta}{[1 - y^2(1 + 3\cos^2\theta)^{\frac{1}{2}}/\sin^6\theta]^{-\frac{1}{2}}} \qquad (2.33)$$

Schulz and Lanzerotti (1974) give an approximation for Y(y) which is better than 1% of the numerically computed values for the whole range of y-values. The exact and approximate values of Y(y) are given in Table 2.1.

The azimuthal drift frequency, Ωd, of a particle of charge, q, and rest mass, mo, with an equatorial pitch angle ao=sin-1y at the radial distance LRE is given by

$$\Omega_d/2\pi = -(3L/2p\gamma)(\gamma^2 - 1)(c/R_E)^2(m_oc/qB_E)[D(y)/T(y)] \qquad (2.34)$$

where

$$D(y) = T(y)/2 - Y(y)/12 \qquad (2.35)$$

This drift frequency is given in Fig.2.7 as a function of L and of the relativistic kinetic energy

$$E = m_oc^2(\gamma - 1) \qquad (2.36)$$

where

$$\gamma^2 = 1 + (p/m_oc^2) = (m/m_o)^2$$

2.1.2.7 Third Invariant

Finally, it can be shown that in the case of a pure dipole the third adiabatic invariant (magnetic field

defined by eq.2.4) is related to the value of L by

$$\Phi = \frac{2pR_E^2 B_E}{L} \qquad (2.37)$$

The inverse relation has been used by Roederer (1970) to assign to each trapped particle a unique and adiabatically invariant L*-shell parameter even in a distorted magnetic field.

This generalized L*-shell parameter, is a 'true invariant' of motion characterizing a drift shell, indeed it is derived from the third adiabatic invariant U. However, the value of L* is difficult to compute for a non-dipole magnetic field model. Although we will indicate later how Roederer (1970) has derived an expression of L* in the rather simple case of a uniformly compressed dipole magnetic field, the calculation of the L*-shell parameter is generally beyond grasp in more complicated B-field distributions. Therefore, it appears that the usage of such a generalized L*-shell parameter is not likely to supersede the usage of McIlwain's L-parameter, although the latter is not strictly constant along non-dipole magnetic field lines .

2.1.2.8 Bm and I Invariants.

When the magnetic field is constant in time, the first two invariants M and J suffice to determine the particle's motion. Moreover, in this case since the particle's kinetic energy is conserved, instead of the energy-dependent quantities M and J, other purely field-geometric quantities can be used. These equivalent invariants are the magnetic field intensity at the mirror point Bm given by eq.(2.23) and the definite integral

$$I = \int (1 - B(s)/B_m)^{\frac{1}{2}} ds = J/2p \qquad (2.38)$$

defined between the two conjugate mirror points; J is given by eq.(2.16) and by (2.32-33) in the special case of a dipole magnetic field model. Note that $I=L\ R_E\ Y(y)$ where Y(y) is defined by eq.(2.33) and given in Table 2.1.

Both Bm and I can be expressed either as a function of spatial coordinates or as a function of a particle's position and pitch angle α_o when it traverses the equatorial surface. The equatorial surface is defined by the locus of all points where B is minimum along the field lines. In the latter case, the relationship between the mirror point field value B_m and the magnetic field intensity B_o at the field line's equatorial (minimum B) point is given by eq.(2.23).

Like J, the integral I cannot be expressed in analytical, closed form, not even for a dipole field. In the case of a pure dipole only numerical values of J and I can be obtained from Table 2.1. However, for particles mirroring close to the equatorial surface (pitch angles near 90°), an analytical approximation can be found even for a non-dipole magnetic field (Roederer,1970).

2.1.2.9 Maximum Trapping Energies.

Charged particles with energies larger than the Maximum Trapping Energy have a gyroradius or radius of curvature larger than the characteristic scale length of the geomagnetic field, H_B, where H_B can be defined as $B/|\text{grad } \mathbf{B}|$. It can be shown that in the equatorial region, H_B is of the order of r/3 where r is the radial distance of the point considered. The gyroradius of a particle is defined as $R_C=m\ v_\perp /ZeB$, where Ze is the electric charge of the particle and $v_\perp$ its velocity perpendicular to the local magnetic field, **B**.

The radius of curvature of cosmic ray particles with energies above 1 GeV/c is larger than the radius of the

Earth and therefore violates the trapping conditions which are often called the 'Alfvèn conditions'. But Cosmic Rays of low energies do not have access to the inner magnetosphere. Indeed there are forbidden Stormer regions which cannot be accessed by particles of certain energies arriving from outside the magnetosphere. A cosmic ray particle must in fact possess a certain magnetic rigidity to reach a given point in the magnetosphere from a given direction. Regions in the outer magnetosphere and over the magnetic poles can be reached for much lower magnetic rigidities than those required to penetrate over the geomagnetic equator. In general, for each point in the magnetosphere and for each direction, there exists a magnetic rigidity below which cosmic rays cannot penetrate. This is called the geomagnetic cut-off (see section 2.1.1.1).

Particles created by Cosmic Ray Neutron Albedo or accelerated by betatron effect inside the forbidden Stormer regions and which have a magnetic rigidity less than a given threshold, will remain trapped and contribute to the Van Allen Belt particles. The maximun energy threshold for trapping, W, depends of course on the radial distance (r_e) as well as on the mass to charge ratio of the particles considered. Fig.2.8 gives the values of W as a function of re (and, conversely r_e as a function of W) for different ion species.

The maximum trapping distance, re, for a given energy, W, displayed in Fig.2.8 corresponds to $R_C/H_B=0.05$ (Lemaire, 1963). Below this maximum trapping distance and below the maximum trapping energy, the 'Alfvèn conditions' are satisfied and the motion of charged particles can be considered to be a superposition of three elementary motions: gyromotion, bounce between two mirror points and azimuthal drift.

It has been pointed out by Schulz and Lanzerotti

(1974) that the time scales for gyration, bounce and drift are respectively separated by a factor of order $\epsilon = \langle mv/ZeS \rangle$, where S is the length of an arc along a field line given by eq.(2.20). The condition $|\epsilon| << 1$ is required for performing the separation of the motion into the three distinct components. This condition imposes the requirement that the gyroradius be much smaller than the length of the guiding field line. This threshold is analogous to that discussed above (i.e. $R_C/H_B << 1$): it leads to similar values for maximum trapping energy evaluation. For particle magnetically confined to the equatorial plane of a dipole field at a radial distance
L R_E, ϵ is given by:

$$\epsilon \approx \beta \, L^2 \, (mc^2 \, / \, 216 \, Z \, GeV)$$

where β is equal to v/c. The limit $|\epsilon| << 1$ required for radiation-belt particles is therefore satisfied by particles up to approximatively $10{,}000/L^2$ MeV for protons, alpha particles and other light ions, as well as relativistic electrons.

2.1.3 McIlwain L-parameter.

2.1.3.1 Why Bm.L instead I.Bm.

Particle fluxes are usually measured at different positions and at different instants in time. Hence, it is necessary to distinguish between spatial and temporal effects. The first thing to do is to single out "equivalent" measurements. This can be done on the basis of Liouville's relation: if we place a directional detector on different points P, Q, R... of a particle shell (Fig.2.9)

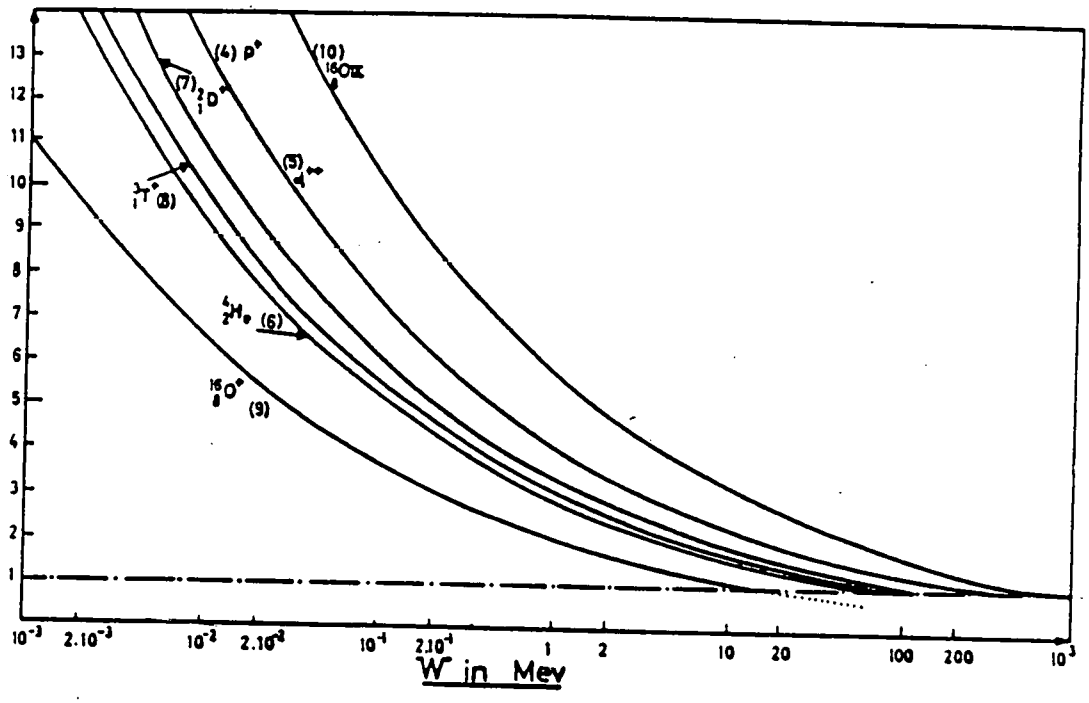

Fig.2-8. Maximum trapping equatorial distances (in Earth's radii) versus maximum trapping energy (from Lemaire, 1963).

looking in the directions of the respective local pitch angles α_P, α_Q, α_R... of the particles in question, we would be measuring the same particle population. In other words, measurements performed on a drift shell with an ideal directional detector pointing in the direction of the local shell-particle pitch angle, are equivalent.

In the absence of external forces, a given direction n at a given point r defines a pair of I,Bm values corresponding to a particle that moves through that point in that given direction. This means that the directional flux can be converted into a function of the shell parameters I and B_m only:

$$j = j(I, B_m, E, t).$$

In the I, B_m coordinate system, the flux j is independent of the longitude φ, unlike in any geographical coordinate system. Of course, instead of I, B_m one could equally well choose any pair of independent functions of I and B_m.

McIlwain's L-parameter is precisely such a function of I and B_m which may be used instead of I to label mirror points or drift shells. In the next section we show how this function $L(I, B_m)$ has been determined for the case of a pure dipole. The meaning of $L(I, B_m)$ for the case of a non-dipole magnetic field distribution will also be re-emphasized in the next section.

2.1.3.2 Relation between L, I and Bm

In the ideal case of a pure centred dipole magnetic field distribution, McIlwain (1961) has determined the relation between L and the shell parameters I and B_m . Obviously, $L=L(I, B_m)$, must be a unique function of I and B_m.

The solution of $L(I,B_m) \approx$ const tells us how one of the I, B_m variables varies at the expense of the other along a dipole field line and, as a matter of fact, along the whole drift shell surface.

Using eqs.(2.38), (2.32) and (2.34) for a pure dipole one obtains

$$I = L\, R_E\, Y(y) \tag{2.39}$$

where Y(y) is the integral (2.33) whose value is given in Table 2.1 as a function of $y=(B_E/L^3B_m)^{\frac{1}{3}}$. Cubing, then multiplying eq.(2.39) by B_mL^3/B_E, and, finally inverting the formula obtained, one gets the formal expression:

$$\frac{L^3B_m}{B_E} = F\left(\frac{I^3B_m}{B_ER_E^3}\right) \tag{2.40}$$

where F represents a function which is not analytic, but can be approximated numerically as shown below.

Thus in a pure dipole field, there exists a function F of B_m and I which determines the value of L uniquely. This relation defines the parameter L or L_d (where the subscript d stands for "dipole") as a function of the pair I,B_m. McIlwain (1961) has deduced the values of F (i.e.:L^3B_m/B_E) as a function of X defined by

22 $$X = \ln(I^3B_m/B_ER_E^3)$$
(2.41)

In Table 2.2 the coefficients a_n are given to calculate the value of

$$Y = \ln(L^3 B_m/B_E - 1) \simeq \sum_{n=o}^{9} a_n x^m \qquad (2.42)$$

which is then used to calculate F or $L^3 B_m/B_E$. In other words to determine L from a pair of values I, B_m one must first calculate X; depending on the value of X one uses, the values of an given in Table 2.2 and the series (2.43) to compute the value of Y and finally the value of L.

Conversely, the coefficients b_n given in Table 2.2., can be used to calculate the value of X from any known value of Y (i.e. the value of I, knowing the value of L and B_m) by using the following series:

$$X \simeq \sum_{n=o}^{9} b_n Y^n \qquad (2.43)$$

Hilton (1971) has found a simpler empirically deduced relationship for $L^3 B_m/B^E$ in the case of a pure dipole:

$$\frac{L^3 B_m}{B_E} \simeq 1 + 1.350474\ g^{1/3} + 0.465380\ g^{2/3} + 0.047546\ g \qquad (2.44)$$

with $$g = I^3 B_m/R_E{}^3 B_E \qquad (2.45)$$

For a given pair of I and B_m the value of g can be calculated by (2.45); the value of L is then easy to compute from (2.44).

Table 2-2

Coefficients a_n for Different Ranges of X

	$X < -22.$	$-22. < X < -3.$	$-3. < X < 3.$	$3. < X < 11.7$	$11.7 < X < 23.$	$X > 23.$
a_0	3.0062102×10^{-1}	6.2337691×10^{-1}	6.228644×10^{-1}	6.222355×10^{-1}	2.0007187	−3.0460681
a_1	3.33338×10^{-1}	4.3432642×10^{-1}	4.3352788×10^{-1}	4.3510529×10^{-1}	$-1.8461796 \times 10^{-1}$	1.
a_2	0	1.5017245×10^{-2}	1.4492441×10^{-2}	1.2817956×10^{-2}	1.2038224×10^{-1}	0
a_3	0	1.3714667×10^{-3}	1.1784234×10^{-3}	2.1680398×10^{-3}	$-6.7310339 \times 10^{-3}$	0
a_4	0	8.2711096×10^{-5}	3.8379917×10^{-5}	$-3.2077032 \times 10^{-4}$	2.170224×10^{-4}	0
a_5	0	3.2916354×10^{-6}	$-3.3408822 \times 10^{-6}$	7.9451313×10^{-5}	$-3.8049276 \times 10^{-6}$	0
a_6	0	8.1048663×10^{-8}	$-5.3977642 \times 10^{-7}$	$-1.2531932 \times 10^{-5}$	2.8212095×10^{-8}	0
a_7	0	1.0066362×10^{-9}	$-2.1997983 \times 10^{-8}$	9.9766148×10^{-7}	0	0
a_8	0	$8.3232531 \times 10^{-13}$	2.3028767×10^{-9}	-3.958306×10^{-8}	0	0
a_9	0	$-8.1537735 \times 10^{-14}$	$2.6047023 \times 10^{-10}$	$6.3271665 \times 10^{-10}$	0	0
E	2.0×10^{-4}	1.0×10^{-6}	7.0×10^{-8}	6.0×10^{-7}	1.2×10^{-5}	5.0×10^{-4}

E = Maximum error in Y.

Coefficients b_n for Different Ranges of Y

	$Y < -7.$	$-7. < Y < -.7$	$-.7 < Y < 2.$	$2. < Y < 8.5$	$8.5 < Y < 20.$	$Y > 20.$
b_0	$-9.0176314 \times 10^{-1}$	−1.5035469	−1.5035665	−1.4921674	−1.3415203	3.0460681
b_1	2.999966	2.516886	2.5166432	2.4799708	2.5733781	1.
b_2	0	$-1.5473094 \times 10^{-1}$	$-1.5579012 \times 10^{-1}$	$-1.0499454 \times 10^{-1}$	-2.747596×10^{-1}	0
b_3	0	-1.482533×10^{-2}	$-1.6991733 \times 10^{-2}$	$-5.6314931 \times 10^{-2}$	2.9961512×10^{-2}	0
b_4	0	5.7665822×10^{-3}	3.3726437×10^{-3}	2.16412×10^{-2}	$-2.1911161 \times 10^{-3}$	0
b_5	0	2.5165553×10^{-3}	9.4374468×10^{-4}	$-3.9980282 \times 10^{-3}$	1.0870528×10^{-4}	0
b_6	0	4.6975588×10^{-4}	$-1.6048742 \times 10^{-4}$	4.5340102×10^{-4}	$-3.5717807 \times 10^{-6}$	0
b_7	0	4.9336212×10^{-5}	$-5.7606054 \times 10^{-5}$	$-3.2040569 \times 10^{-5}$	7.2957464×10^{-8}	0
b_8	0	2.8332675×10^{-6}	1.6653982×10^{-5}	1.3002586×10^{-6}	$-8.0754426 \times 10^{-10}$	0
b_9	0	6.9447496×10^{-8}	$-1.1144463 \times 10^{-6}$	$-2.3206968 \times 10^{-8}$	$3.3797513 \times 10^{-12}$	0
E	5.0×10^{-4}	5.4×10^{-6}	5.2×10^{-7}	1.5×10^{-6}	1.1×10^{-5}	5.0×10^{-4}

E = Maximum error in X.

This procedure formulated by Hilton is therefore more straightforward than that originally based on the eqs.(2.41) to (2.43) and on the coefficients given in Table 2.2. The error obtained in using Hilton's approximation (2.44) to determine McIlwain's L-parameter is less than 0.01%.

Notice that Hilton's approximation (2.44) of eq.(2.39) represents the relation between I and B_m along a dipole field line (or dipole drift shell). Non-dipole field geometries would yield a different functional relationship between I and B_m along a given field line. Furthermore, in an asymmetric field the relation between I and B_m along a field line will be longitude dependent for a given drift shell.

It is, however, always possible, even in any non-dipole magnetic field model to compute the value of Bm corresponding to any geographical point, P, in space; similarly it is also possible to compute the corresponding value of I, by numerically integrating (2.38) along the non-dipole magnetic field line, between the two conjuguate mirror points. This pair of I and Bm coordinates are to some extent equivalent to the geographical coordinates of point P, or of the ring of mirror points passing through P. The pair of coordinates I, B_m can equally well be used to characterize (i.e. to label) a drift shell formed by the arcs of the non-dipole magnetic field lines located between the two conjugate rings of 'mirror points', like that which is illustrated in Fig.2.9. McIlwain's procedure consists to label these non-dipole drift shells with the parameter L, which is determined from I and B_m by using the function F corresponding to a pure dipole (i.e. the formal mathematical expression (2.40) or its Hilton's approximation (2.44)).

It may be pointed out here, that in McIlwain's original derivation of F, the value B_E was assigned the value of 0.311653 Gauss; this value corresponded to the magnetic dipole moment at Epoch 1960 in the GSFC interim magnetic field model of Jensen and Cain (1962). It has been argued that it might be more reasonable to compute McIlwain's L-parameter using the value of B_E from the best available field model for the corresponding Epoch of the measurements (Schulz and Lanzerotti, 1974, p 24.). The reason for such a claim was that because of the small secular decrease in the Earth's dipole magnetic moment, M, not only did B_E decrease but the equatorial radii of all drift shells decrease slightly as a consequence of the betatron effect. Many theoreticians have become sensitive to this issue, and have searched for 'truly invariant' shell parameters like the generalized L* parameter introduced by Roederer (1970).

The alternative procedure to compute L with B_E changing from one Epoch to the other, instead of being fixed to 0.311653 Gauss, appears to have more practical disadvantages than it has significant advantages. In fact, McIlwain (1989,personal communication) has shown that an overestimation of B_E or M by a factor 1-e would result in a relative underestimation for L of e/3, at most. At Epoch 1985 the value of the B_E was 0.30438 Gauss while the value of 0.311653 Gauss is used in eqs.(2.44) and (2.45); this implies that e=(0.311653-0.30438)/0.311653=0.023337=2.3%; consequently the values of L calculated with the true value of BE differs by less than 0.8% from that calculated with McIlwain's standard value. This is a quite small difference compared to other uncertainties associated to any choice of a particular B-field model as well as to the flux measurements themselve.

Therefore, we share the opinion that changing constantly the value of B_E in eqs.(2.44) and (2.45) from one set of measurements to the other would lead to more confusion than it would resolve problems. Changing BE would be alike to constantly changing the unit of length of a ruler to measure distances at different Epochs! This can certainly be done as long as each PI explicitely informs the community as to which value of B_E he has used to compute the B,L coordinates of his instrument..; but since an L-parameter should only be regarded as a 'LABEL' (or a coordinate) to identify a geographical point or a drift shell, it seems reasonable to keep using the same value of B_E (i.e. the unit of length) all the time.

To conclude this section, we wish to emphasize that it is essential to realize that it is only for a pure dipole that L characterizes a given magnetic field line. In a non-dipole field the actual field lines are not characterized by a single L-parameter. Indeed, each point along a particular non-dipole field line is characterized by a different pair of B_m and I values and consequently, a different pair of B_m,L values. However, it has been shown by McIlwain (1961) that the variation of L for points along geomagnetic lines computed from a standard IGRF field model is less than 1 % in the inner magnetosphere.

2.1.3.3 (B,L) Space Description

The coordinates B_m and L, generally called (B,L) coordinates, are known to order inner-zone particle fluxes satisfactorily during magnetically quiet periods.

The "B-L space" for particle flux mapping in a dipole field has a "physical" region (Fig.2.10) bounded by the equatorial field $B_o(L)$ and the surface field $B_E(L)$ given by :

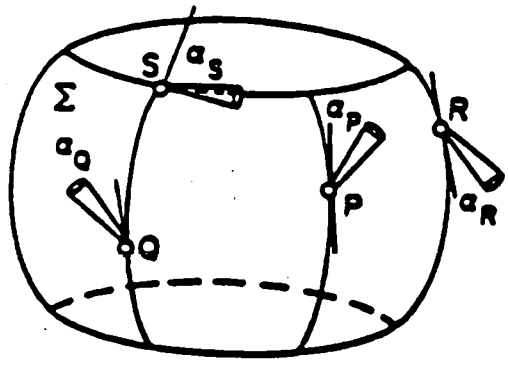

Fig.2-9. Drift shell and pitch angle of a particle
(after Roederer, 1970).

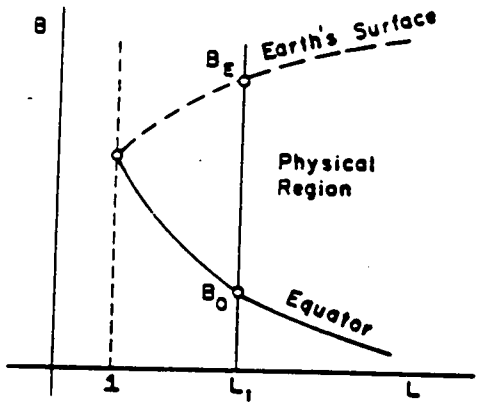

Fig.2-10. B-L space (after Roederer, 1970).

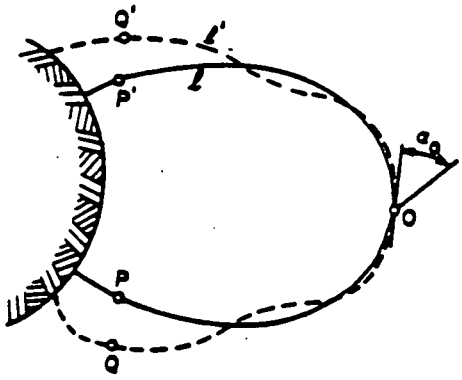

Fig.2-11. Dipole and non-dipole magnetic field lines
(after Roederer, 1970).

$$B_O(L) = \frac{0.311}{L^3} \quad \text{(Gauss)} \qquad (2.46)$$

$$B_E(L) = 0.311\ (4-3/L)^{\frac{1}{2}} \quad \text{(Gauss)} \qquad (2.47)$$

All points of a given dipole drift shell map into a vertical line in B-L space. A given B-L (or B-I) ring maps into a point.

Unfortunately, the Earth's magnetic field is not exactly that of a pure dipole. Within $r<4R_e$, where contributions from external sources can be neglected, higher order multipole terms, related to the uneven geological structure of the Earth's crust and to asymmetries of the magnetization of the Earth's deep interior, play an appreciable role. The multipole terms give field contributions which decrease more rapidly with distance than the dipole field . The field distortion caused by them is thus greater near the surface than further out in space. Let us imagine that we can switch the higher order multipoles on and off at will. If we start with a pure dipole field, the field line going through the equatorial point 0 is 1 (Fig.2.11). Now we turn on all higher multipoles. Say that the field line through the same point 0 (which might not be a minimum-B point any more) looks like the broken curve 1'.

It will differ only very little from unity near the equator, but may depart considerably from one near the Earth. The field intensity at 0 may have changed, but only by a very small amount.

A particle injected with a given pitch angle α_o at 0 along the dipole field line, 1, mirrors at points P, P' where the field intensity is $B_m=B_o/\sin^2\alpha_o$ (2.23). Its I value will be given by eq.(2.25). The same particle, injected with the same pitch angle along the field line 1'

with all multipoles turned on, will mirror at the pair Q,Q′ quite different from P,P′ - but where the field intensity is practically the same :

$$B_Q \approx B_P = B_m = \frac{B_o}{\sin^2 \alpha_o} \qquad (2.48)$$

Since the mirror points Q,Q′ are at positions quite different from P,P′, one might expect the I value (2.24) to be quite different, too. Yet numerical computations by McIlwain (1961) show that this is not the case:

$$\int_Q^{Q'} \left[1 - \frac{B(s)}{B_m} \right]^{\frac{1}{2}} ds \approx \int_P^{P'} \left[1 - \frac{B(s)}{B_m} \right]^{\frac{1}{2}} ds.$$

real field line dipole field line (2.49)

i.e. I(real field line) ≈ I(dipole field line).

The reason for this near-equality is that the integrant $(1-B(s)/B_m)^{\frac{1}{2}}$ contributes mainly in the equatorial region, where the multipole effect is considerably attenuated. Towards the mirror points, where the field distortion becomes more and more noticeable, the integrant decreases towards zero.

The situation is quite different with the bounce period of the half-bounce path length whose integrant contains the same function, but in the denominator. Its main role now is played in the region near the mirror points, causing the bounce period and the bounce path to differ appreciably from the dipole case.

Relations (2.48) and (2.49) have the following consequences :

(i) The functional relationship between I and B_m along a field line in the real geomagnetic field (excluding external sources) is nearly the same as in the dipole case (2.40).

(ii) The L-value defined through the dipole relation (2.40) (but computed using real field value calculations of I and B_m) will be nearly the same along a given field line in the real field and on the whole shell defined by particles mirroring on that field line. This is called "McIlwain's L value". Drift shells are frequently called L-shells in the literature.

(iii) All particles initially mirroring on a common field line will mirror on nearly coincident field lines at all other longitudes, generating a common drift shell (negligible shell splitting).

The fact that L is a "good" parameter with which to label a particle shell in the inner magnetosphere makes L and Bm a good pair of variables for particle flux mapping. Furthermore, in view of negligible shell splitting within about 4 Re the omnidirectional flux does make sense as a physical quantity describing particle distributions and can thus be mapped in B-L space. Fig. 2.12a shows an example of trapped particle flux mapping in (B,L) space. The recipe for omnidirectional flux mapping in the inner magnetosphere is as follows :

(i) place an omnidirectional detector at a given position r_p;

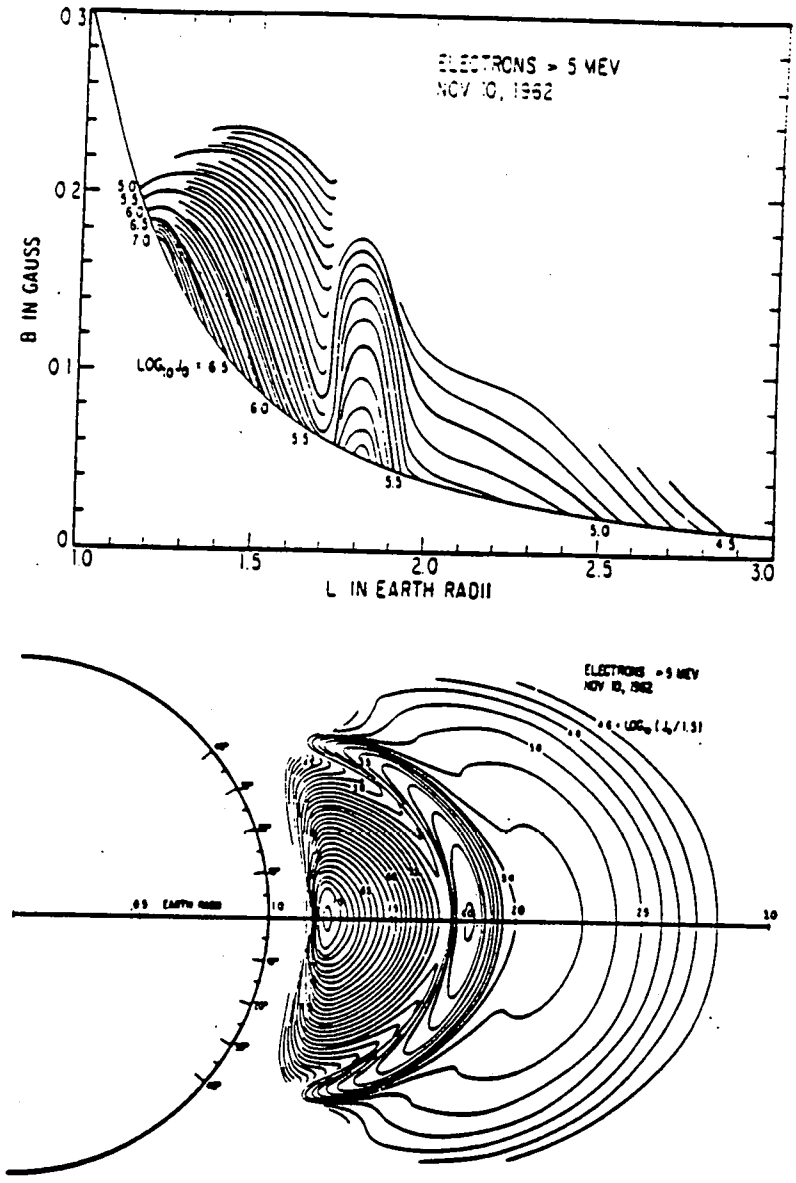

Fig.2-12. Contours of constant intensity of electrons of energies larger than 5 MeV plotted in B-L coordinates (upper graph) and R-k coordinates (lower graph) (from McIlwain, 1966). The electrons in the region around L = 1.4 are those injected by the July 9, 1962 high altitude nuclear explosion (Starfish); the peak in the region L = 1.75 to 2.0 region was presumably injected by Soviet high altitude tests in October - November 1962.

(ii) determine the I and B_m values at that point (i.e. the I, B_m values of a particle mirroring there) using the best available magnetic field model;

(iii) find L through relations (2.40), (2.42) or (2.44);

(iv) repeat for other points r (for instance, the trajectory of a satellite);

(v) plot (by means of interpolation) isointensity contours (J=const curves) in (B_m,L) coordinates (Figs.2.10 and 2.12a), for all measurements taken during a given interval of time (during which it is assumed that conditions have remained constant). In this way, the three-dimensional radiation belts can be mapped in a two-dimensional B-L space. Note that to do so, it is necessary to use a model for the geomagnetic field in addition to the experimental measurements.

It should be pointed out that this procedure can be used in the outer magnetosphere beyond r=4 R_E where external currents become important. In fact, it is mathematically well defined for any dipole or non-dipole magnetic field model. The main difference is that in the inner magnetosphere L does not change significantly along a magnetic field lines while in the outer magnetosphere this is not true: furthermore the equatorial distance of a field line passing through a point whose coordinates are (B,L) can then be quite different from L R_E.

2.1.4 (B/B_o,L), (R,λ) and (α,β) coordinate systems.

Another popular pair of invariant coordinates has been defined by Vette and his colleagues at NSSDC who made ample use of B/B_o instead of B in the AE8 and AP8 models. B_o is here the minimun equatorial magnetic field intensity along the field line passing across the point of observation.

This relative magnetic field intensity variable has practical advantages for plotting purposes. The equatorial regions correspond to $B/B_o=1$, while the low altitudes points are spread near $B/B_o=(4-3/L)^{\frac{1}{3}}$.

There is however a common weakness in using B or B/B_o in the atmospheric cut-off region. Indeed, there the flux varies very rapidly with altitude. Unfortunately, an altitude variation of $\Delta h=100$ km corresponds to a relative change in B or B/B_o of only 0.2%. As a consequence, to obtain a more detailed mapping of trapped radiation flux along low altitude orbits, one should probably introduce another more appropriate coordinate other than B or B/B_o for the low altitude regions.

Daly (personal communication, 1989) suggested to use $(B-B_o)/(B-B_a)$ where $B_a=B_a(\rho)$ is the atmospheric limiting B (cut-off) and $\rho(h)$ is the appropriate atmospheric density.

The Hassitt shell density scale height recently proposed by McIlwain (personal communication, 1989) is another promising variable to map low altitude trapped radiation fluxes.

Northrop (1963) and Stern (1976) have introduced Euler potentials as magnetic coordinates that are useful in many theoretical problems. They use two paramaters, α and β, which specify a line of force and are therefore constant on that line. These parameters are chosen such that the vector potential is

$$\mathbf{A} = \alpha \nabla \beta$$

and the magnetic field is given by

$$\mathbf{B} = \nabla \alpha \times \nabla \beta.$$

In a dipole field these parameters are

$$\beta = \varphi$$

which is the magnetic longitude, and

$$\alpha = M \sin^2 \theta / r.$$

These (α,β) coordinates are useful because they are canonical. As a result, it has often been used to study two-dimensional diffusion in the outer radiation belt (Schulz and Lanzerotti, 1974). Furthermore Stern (1987) has shown how 'streched transformations' can be applied to the Euler potential to describe distorted dipole field lines.

However, since the Euler potentials for non-dipole fields are difficult to determine, these curvilinear coordinates have never been used to represent the detailed Earth's multipole internal field distribution, nor any complex external source field like that in Tsyganenko's B-field model.

Another invariant coordinates system is that defined by R and λ solutions of

$$R = L \cos^2\lambda \tag{2.50}$$

$$B = \frac{B_E}{R^3} \left[4 - \frac{3R}{L} \right]^{\frac{1}{2}} \tag{2.51}$$

where λ is a generalized magnetic latitude.

This (R,λ) system gives a dipole-like representation. Flux mapping in R-λ space is equivalent to a polar coordinate mapping in one meridian.

For low altitude observations, the (R,λ) system is sometimes a less convenient representation of data than the (B,L) map since it tends to spread out and emphasize data near the magnetic equator. But for near geosynchronous

observations it can be more appropriate.

Using R=1 in eq.(2.50), we get a special magnetic latitude called the Invariant Latitude which is defined by

$$\cos^2\Lambda = \frac{1}{L} \qquad (2.52)$$

This value of K which is uniquely related to McIlwain's L-parameter has been widely used as a coordinate to describe processes involving particles mirroring at very high latitudes (auroral processes, polar ionosphere, conjugate photoelectron precipitation, etc.) where this latitude K is better than the dipole magnetic latitude.

Notice however, that R=1 does not correspond exactly to the Earth's surface, due to the effect of higher order terms in the internal field expansion.
The correct computation of Λ (and of R) at a given point on the surface or in space requires the knowledge of both B and L at that point and the subsequent numerical solution eqs.(2.50) and (2.51).

Fig.2.12a and b show an example of trapped particle flux mapping : isointensity contours of electrons of energy 5 Mev are plotted in B-L (upper graph) and in R-λ coordinates (lower graph). Most of the electrons shown in Fig.2.12a and b have been artificially injected by U.S. and U.S.S.R. high altitude nuclear bomb tests (see flux peaks around $L \approx 1.4$ and 1.8, respectively).

2.1.5 South Atlantic Anomaly

A good way of showing the distorting effect of the high multipole terms on particle drift shells is, to determine mirror point trajectories, (i.e. curves of constant I and B_m or L and B_m values). Fig.2.13 displays a plot of mirror point altitude versus longitude, for a

series of L and B_m pairs. Notice how these traces (corresponding drift shells) approach the Earth in the Southern Hemisphere in a longitude region located over the Atlantic Ocean. This represents the so-called "South Atlantic Anomaly", where radiation belt particles have the greatest probability of interaction with the Earth's atmosphere. As a result of secular variations, the location of this SAMA slowly shifts toward the west.

2.1.6 Problems associated with B,L or R, coordinate systems.

There is a fundamental reason why particles originally on one magnetic field line will drift onto different field lines at other longitudes. The integral invariant I is defined in terms of a particle mirror point and therefore exists only for particles mirrored at the point of observation. If a particle flux is measured with an omnidirectional instrument, this flux includes particles mirroring at the observation point and also other particles mirroring below. The omnidirectional flux contains particles of various values of I, but we lump them together with one value of I. It is not surprising, therefore, that they separate and move to different field lines at other longitudes. There is no reason for them to stay together as they drift. If this is the case, then a shell of lines of force defined by a value of L, where L is uniquely related to I, can only approximate the location of particles originally on one field line.

In analysing data from directional particle detectors, one makes an exact representation. One can plot the particles mirror point density or the perpendicular flux, $j_\perp$, in (I, B_m) or (B_m, L) space. There is no fundamental inaccuracy in this system as there is one with omnidirectional flux mapping in these same systems of coordinates. Directional flux data from different

longitudes can be combined exactly here.

The usefulness of the (B,L) coordinates lies in that it can be visualized easily in terms of a dipole field and is accurate enough to combine omnidirectional data for global modelling purposes. It is completely adequate for presenting directional data. The success of McIlwain's L-parameter lies in the fact that in the inner magnetosphere, L does not vary much for particles mirroring at different points on one field line. In the outer magnetosphere this is no more the case. Nevertheless, it can still be used with B_m to label or identify points in space and drift shells whether they are degenerated or not due to 'shell splitting'.

The largest basic inaccuracy occurs when the (B,L) coordinates are used to map <u>omnidirectional flux measurements</u> in the outer magnetosphere for L>4-5. But there are also other reasons why more general coordinates would be welcome for future trapped radiation modelling.

(i) It is known that for low-altitude electrons, there are variations in flux on a (B,L) ring at different longitudes (Imhof and Smith, 1963). The reason is that substantial changes take place for these particles in less than one revolution around the Earth. Therefore, the data at different longitudes cannot be organized accurately into one single set of data. When combining data in longitude, one implicitly assumes that the particles 'live' a long time and make many revolutions. When electrons drift eastward down into the South Atlantic Magnetic Anomaly, the low-altitude particles are lost. As the remaining move up and out of this region, new particles are scattered down into the vacant lost cone which had just be depopulated. The variation of flux with longitude due to the SAMA has been named the <u>windshield-wiper effect</u>. One promising way of approaching this issue may be that pioneered by Hassitt (1965a,b).

(ii) The Earth's magnetic field is distorted by the solar wind dynamic pressure. This produces local time dependent asymmetries in the field in the outer magnetosphere at large L-values. The location of flux contours is known to be dependent on local time. There are ample examples of this local time effect in the well documented SCATHA ENVIRONMENTAL ATLAS (Mullen and Gussenhoven, 1983).

(iii) Furthermore, the solar wind's dynamic pressure changes the outer boundary conditions at the magnetopause almost continuously . This induces time dependent B-field variations as well as impulsive injections of low energy particles into the magnetosphere. Such perturbations of the outer magnetosphere often produce rapid variations in the particle flux, betatron energization and radial motion of drift shells. The time scale of these variations is sometimes so short that the third adiabatic invariant is no more conserved. Many examples of such catastrophic time changes can be found in the literature (see McIlwain 1966, or Hess 1968 for a review). Note that the amplitude and random occurrence of these catastrophic events cannot be described in the theoretical framework of slow diffusion processes like those studied in Schulz and Lanzerotti (1974) or more recently by Chiu et al. (1988). While these diffusion processes are certainly important during prolonged quiet geomagnetic conditions (i.e. during the rare periods when the solar wind dynamic pressure does not vary significantly for one or two days), quasi-stationary diffusion mechanisms are, however, completely overwhelmed by the onset of a magnetospheric substorm or geomagnetic storm events.

To handle such time dependent situations, a new coordinate system would be welcome! Another attractive possibility mentioned by McIlwain (personal communication, 1989) would be to use Dst dependent magnetic fields and electric fields to compute the radial drifts of particles.

But so far, such a more appropriate coordinate system nor such time dependent magnetic field and electric field models do not exist unfortunately.

2.1.7 L - Shell Splitting.

Let us assume a particle that starts at a given longitude φ, circling around a given field line and mirroring at a value B_m. The integral (2.38) computed along the field line between the two mirror points has a value I. This means that when drifting through any other longitude, for example 180° away, this particle will bounce along a field line that passes through the intersection of the corresponding I=const and B_m=const surfaces (see Fig 2.13b). Now take a particle which starts on the same initial field line but mirrors at a lower value $B_m' < B_m$. Its integral I' will also be smaller, I'<I. After a 180° longitudinal drift, this second particle will be travelling along a field line that passes through the intersection of the surfaces I'=const and B_m'=const. Only in the case of perfect azimuthal symmetry (as in the pure dipole) will these surfaces intersect exactly on the same field line as that of the first particle, and thus be coincident. This is called <u>shell degeneracy</u>. In the general case, particles starting on the same field line at a given longitude will populate different shells, according to their initial equatorial pitch angles. This effect is called <u>shell splitting.</u>

Fig 2.13c shows how particles, starting on a common line in the noon meridian, do indeed drift on different shells which intersect the midnight meridian along different field lines. The dots represent the particle' mirror points. Curves giving the position of mirror points for constant equatorial pitch angles are traced for

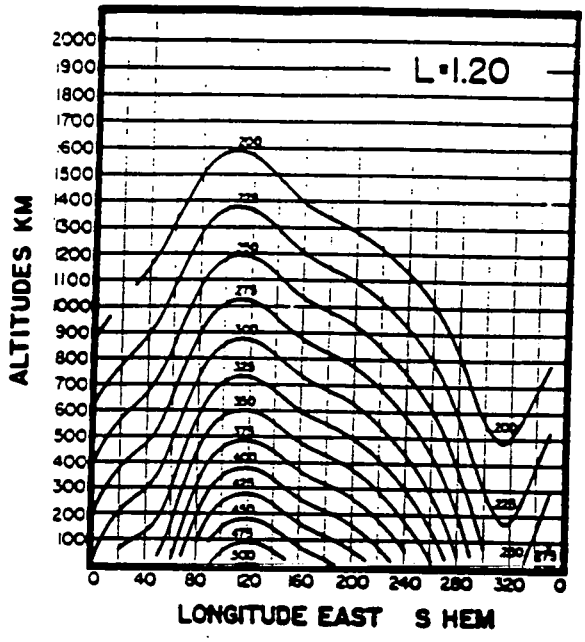

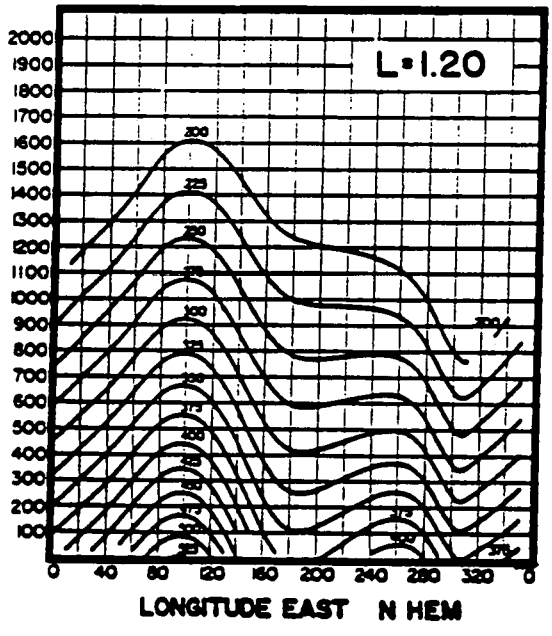

Fig.2-13a. Mirror point altitudes in the southern and northern hemispheres, for the l = 1.20 shell and B_m values (shown in each curve in Gauss) (after Roederer, 1970). Notice their closest approach to the Earth in the Southern hemisphere around 320ø : East longitude (corresponding to the South Atlantic Magnetic Anomaly).

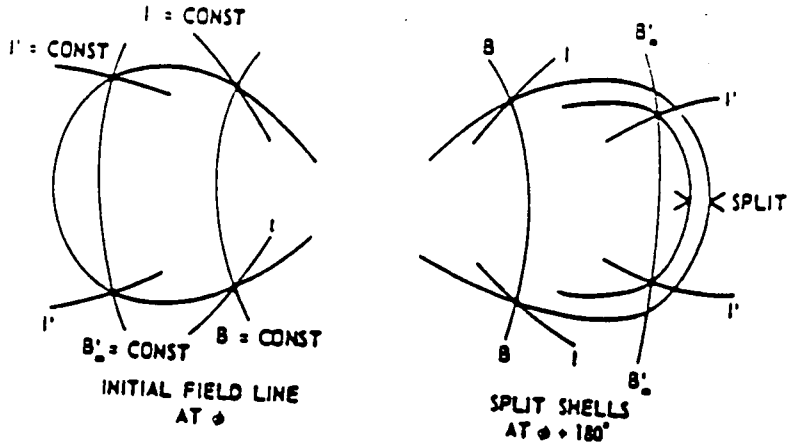

Fig.2-13b. Constant B and constant I contours.

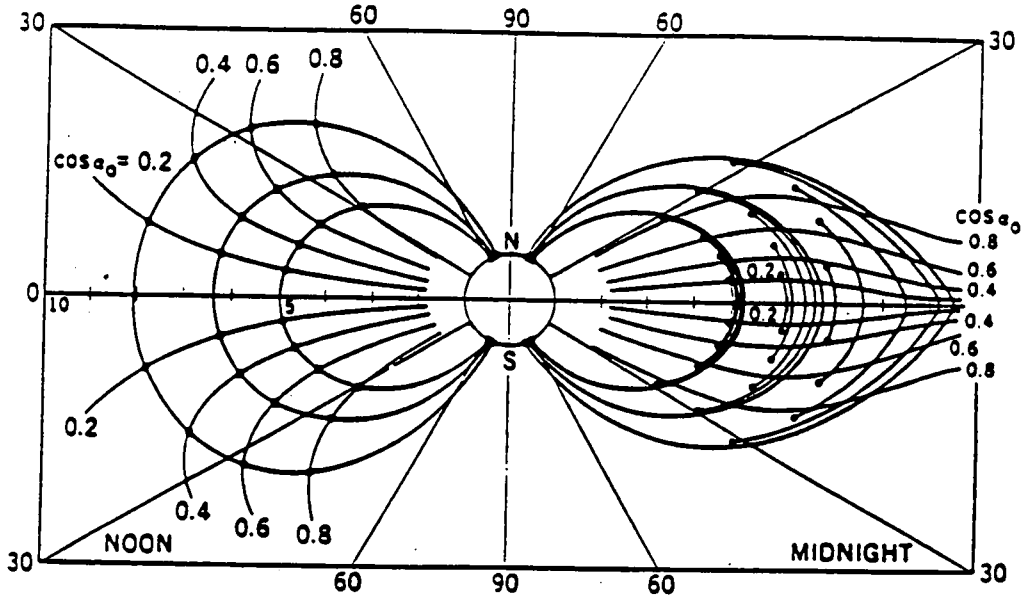

Fig.2-13c. Computed shell splitting for particles starting on common field lines in the noon meridian. Dots represent particles mirror points. Curves giving the position of mirror points for constant equatorial pitch angle a_0 are shown (from Roederer, 1972).

comparison. Notice the change (decrease) in equatorial pitch angle for the same particle when it drifts from noon to midnight.

Notice that, as equatorial pitch angles increase, shell splitting is directed radially inward for particles starting on a common field line at noon, and radially outward for particles starting on the same field line at midnight. Furthermore, shell splitting is maximum for particles mirroring close to the equator.

2.1.8 The case of time dependent fields

When the magnetic field is time dependent, further complications arise. If the time variations are slow (as compared to the particle's drift period), adiabatic theory can still be used, but conservation of the field-geometric quantities I and B_m breaks down. Since the energy of a particle is now no longer conserved, one must go back to the use of the three adiabatic invariants M, J and Φ . Actually, one still may combine the conservation of M and J into the conservation of the field-geometric quantity (Kaufmann, 1965)

$$K = I(B_m)^{\frac{1}{2}} = \text{const} \qquad (2.53)$$

Expressing the magnetic moment at the particle's mirror point, we have

$$M = \frac{p^2}{2m_o B_m} \quad \text{or} \quad \frac{p^2}{B_m} = \text{const} \qquad (2.54)$$

which, with the conservation of the third invariant

$$\Phi = \oint_{\text{shell}} A.dx = \text{const} \qquad (2.55)$$

(in which A is the vector potential and dx is the element of equatorial contour of the particle's drift shell) completes the three relations that govern the slowly time-dependent case. In fact, eqs.(2.57) and (2.59) determine the evolution of a particle's drift shell, whereas (2.58) is used to find the particle's instantaneous energy (Roederer, 1970).

2.1.9 Secular variation of the Earth dipole

Using equation (2.50) written as

$$\frac{L^3 B_m}{M_d} = F\left(\frac{I^3 B_m}{M_d}\right) \qquad (2.56)$$

where M_d is the dipole magnetic moment introduced in McIlwain's (1961) paper : $M_d = B_E \cdot R_E^3 = 0.311653$ gauss R_E^3, one determines the L parameter associated with a pair of I, B_m values calculated for the "real" (model) geomagnetic field. Although the values of I and B_m are computed using a model of the actual magnetic field distribution, the function F(g) remains that corresponding to the dipole field. In Hilton's (1971) form, $g = I^3 B_m / M_d$ is computed from the real field but the constants in (2.44) retain the values calculated for the dipole. From this derivation it appears that L is a function of I and B_m.

The relationship between the flux invariant and L for the dipole field is given by (2.23) or equivalently

$$\Phi = 2pM/L \qquad (2.57)$$

It has been recognized for hundreds of years that the geomagnetic field has secular variations. The effects of this variation on the inner zone protons was made by Schulz and Paulikas (1972a). It was pointed out there that Φ was conserved because of the slow change in the field relative

to the drift period. Taking the derivative of equation (2.57) Schulz and Paulikas obtained

$$\frac{d}{dt} \ln L = \frac{d}{dt} \ln M \approx \frac{-1}{1933 \text{ yr}} \qquad (2.58)$$

They also noted that the conservation of the first two adiabatic invariants (2.15) and (2.16) implies that the drift shell contraction occurs at constant equatorial pitch angle (or mirror latitude).

Consider first a dipole field at two different epoches t_1 and t where the magnetic moments are M_1 and M. Using the conservation of the three adiabatic invariants during the secular change one obtains:

$$L = L_1 \, M/M_1 \sim M \quad \text{(from 2.57)} \qquad (2.59)$$

$$B_m \sim M^{-2} \qquad (2.60)$$

$$p \sim B_m^{-\frac{1}{2}} \sim M^{-1} \quad \text{(from 2.60)} \qquad (2.61)$$

$$I \sim p^{-1} \sim M \quad \text{(from 2.38)} \qquad (2.62)$$

$$g = I^3 B_m / M_d \sim M \qquad (2.63)$$

The equation (2.63) shows that the argument of F in (2.56) is not an invariant when M changes. Consequently, the value of $L^3 B_m/M_d$ varies according to eqs.(2.40), (2.44) or (2.56). The result is a non linear variation of L as a function of M. When M decreases, g decreases as M and from eq (2.44) it results that $L^3 B_m/M_d$ decreases also. For particles mirroring at the equator I = 0, g = 0 and $L \sim M^{2/3}$; for $I \neq 0$, L decreases with M even more rapidly than $M^{2/3}$. Note that the non-linear variation of L versus M is different from that predicted by the conservation of the

third invariant (2.57) according to which we should have L~M (eq. 2.59).

This inconsistency pointed out to us by Vette (personal communication, 1989) disappears when in eq.(2.42), and in the definition of g when the actual moment M is used, instead of M_d. Indeed, in this case

$$g = I^3 B_m / M \sim M^0 = \text{const.}$$

and the value of F(g) is independent of M. Consequently,

$$L^3 \sim M B_m^{-1} \sim M^3 \quad \text{and} \quad L \sim M \tag{2.64}$$

in accordance with eq.(2.45) deduced from the conservation of the third adiabatic invariant.

Therefore, by replacing M_d in the UNIRAD package with the actual geomagnetic moment, M, at the Epoch of observations, we could resolve the inconsistency mentioned above. But we have argued above that the slight improvement in doing so would be outweighted by the inconvenience of losing other more significant advantages, like the uniqueness of the definition of McIlwain's L-parameter.

Note that not only the dipole moment terms of the internal geomagnetic field experience a secular variations, but the quadrupole and octupole terms also change with Epoch. The secular changes of these higher order moments cannot be avoided by replacing M_d by M in the expression (2.56) defining $L(B_m,I)$; as a consequence of the secular variation of these higher order terms, the value of I and B_m does not vary exactly as given for the case of a pure dipole by eqs.(2.62) and (2.60) respectively. Therefore, even if $L(B_m,I)$ were to be computed with a variable M instead of M_d=0.311653 Gauss, the secular variations due to the higher order moments would not be accounted for, and L would not change as expected from the conservation of the

third invariant i.e. according to eq.(2.59).

2.1.10 Extrapolation of trapped radiation fluxes for year 2000.

It has been pointed out by McCormack (1986) and by Konradi and Hardy (1987) that, as a consequence of the secular evolution of the geomagnetic field, the low-altitude trapped radiation fluxes predicted for the year 2000 increase dramatically when calculated using currently developed methods which are implemented in the UNIRAD software package. This is clearly illustrated in Figs 2.14a and 2.14b taken from Daly (1989).

These figures show the orbit-averaged integral fluxes of protons (and electrons) above 100 MeV (and above 2 MeV for the electrons Fig. 2.14b). These fluxes increase dramatically at low altitudes when the B/B_o-L coordinates are calculated using the IGRF models appropriate to different epoches. The AP8 and AE8 trapped radiations models are used by Daly (1989) to determine the omnidirectional fluxes for the calculated pair of B/B_o-L values along 13-circular orbits passing through the South Atlantic Magnetic Anomaly (SAMA) (inclination of the orbit : 28,5°).

The open circle at epoch 1960, corresponds to the result obtained with the NASA/GSFC/1960 geomagnetic field model of Jensen and Cain (1960) and using McIlwain's value of the Earth's dipole (M_d = 0.311653 gauss R_E^3) to compute L from eq.(2.60). The other curves labelled "IGRF-1980 with McIlwain's M", correspond to the series of International Geomagnetic Reference Fields Models extrapolated from Epoch 1980 up to the year 2000 and back to the year 1960; the rate of change of the coefficients g^m_n and h^m_n given by IAGA for the spherical harmonic expansion of the Earth's magnetic field is taken into account.

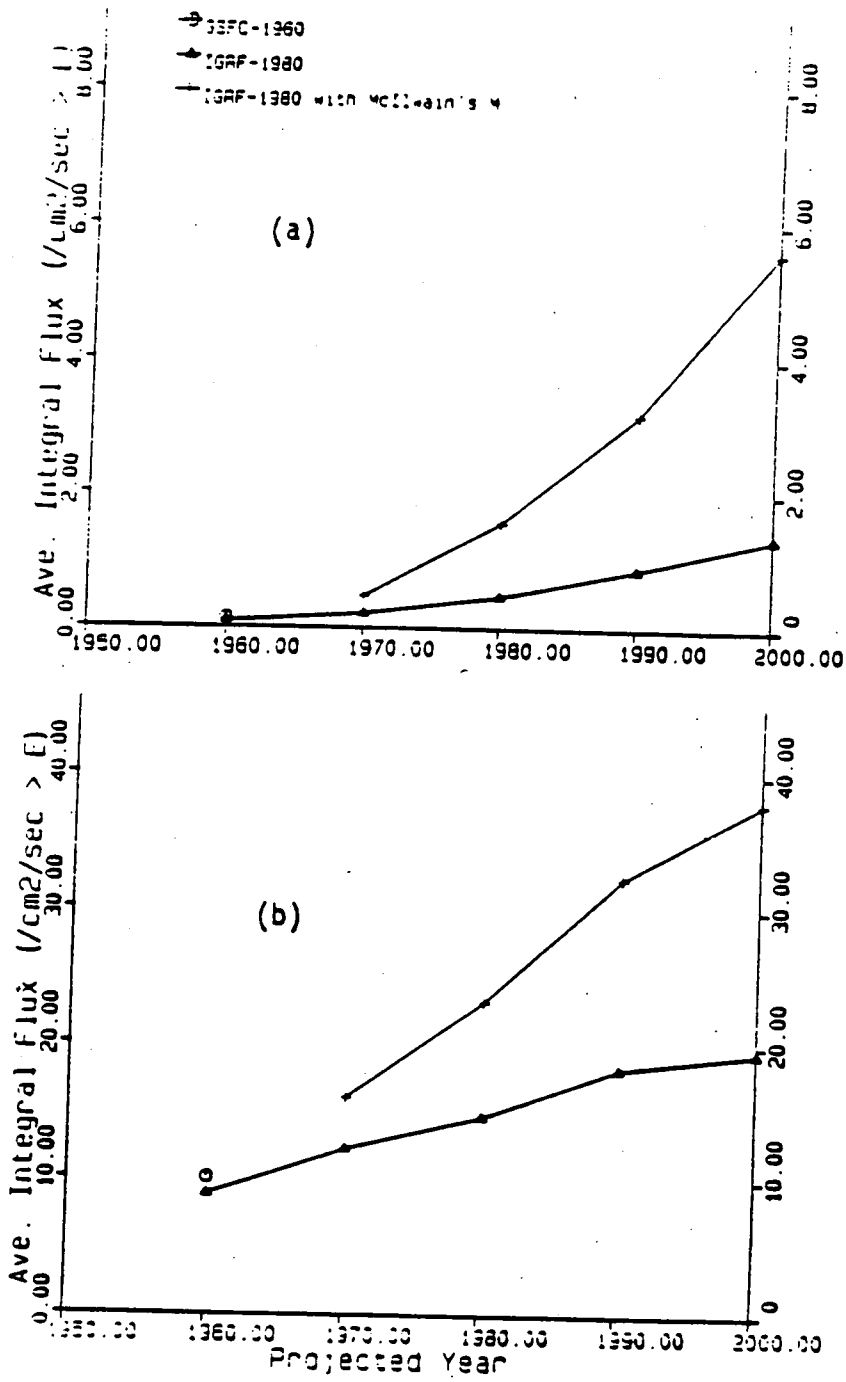

Fig.2-14a. Secular variation of predicted orbit - averaged Integral Flux if Electrons with energies larger then 100 MeV in LEO; a) for 13 circular orbits with an inclination of 28.5° and altitude of 300 km; b) the same orbits but at an altitude of 500 km (after Daly,1989). Different geomagnetic field models are used to compute the B/B_O, L coordinates at different epochs.

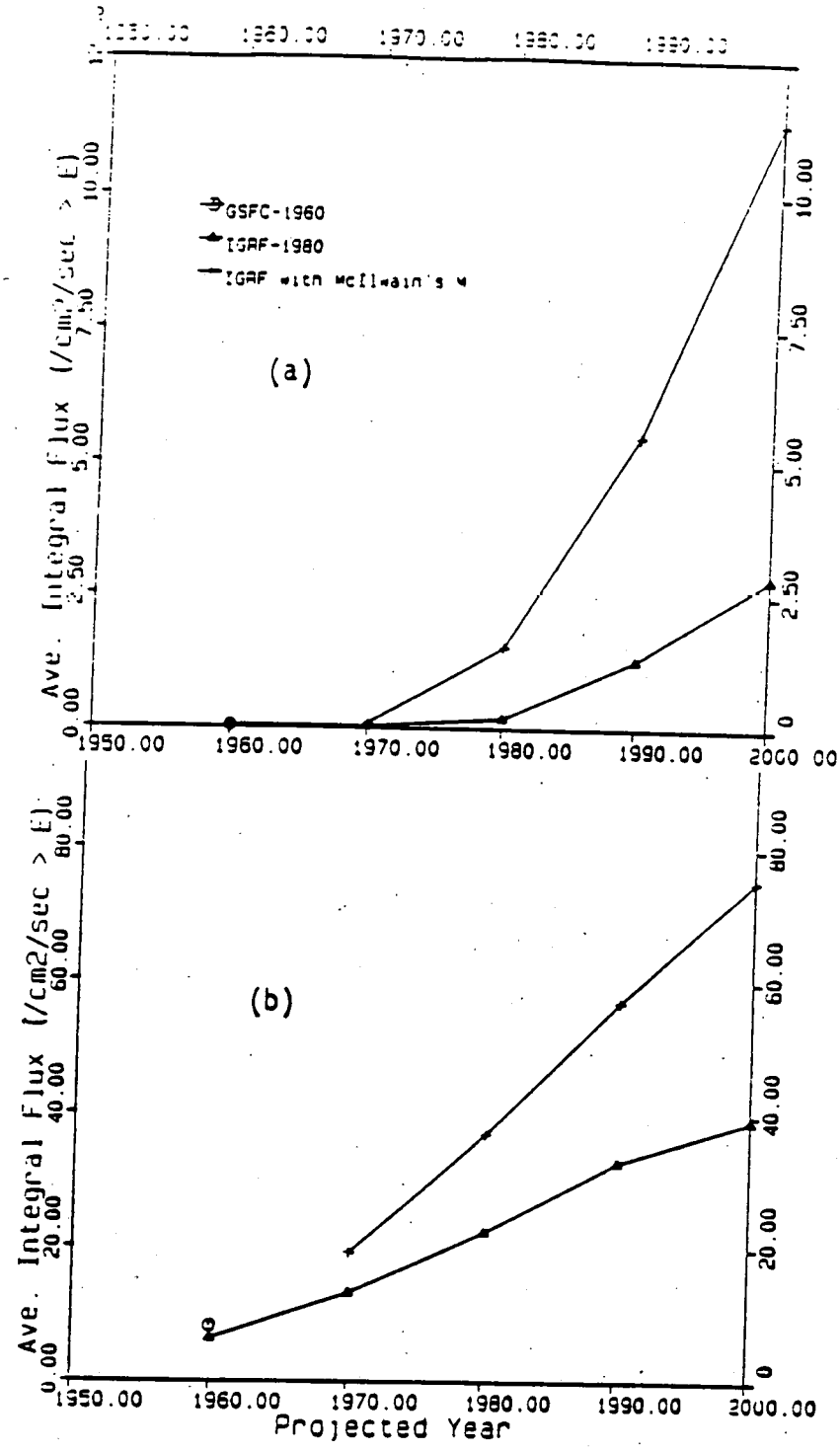

Fig.2-14b. Secular variation of predicted orbit - averaged Integral Flux if Electrons with energies larger then 2 MeV in LEO; a) for 13 circular orbits with an inclination of 28.5° and altitude of 300 km; b) the same orbits but at an altitude of 500 km (after Daly,1989). Different geomagnetic field models are used to compute the B/B_O, L coordinates at different epoch.

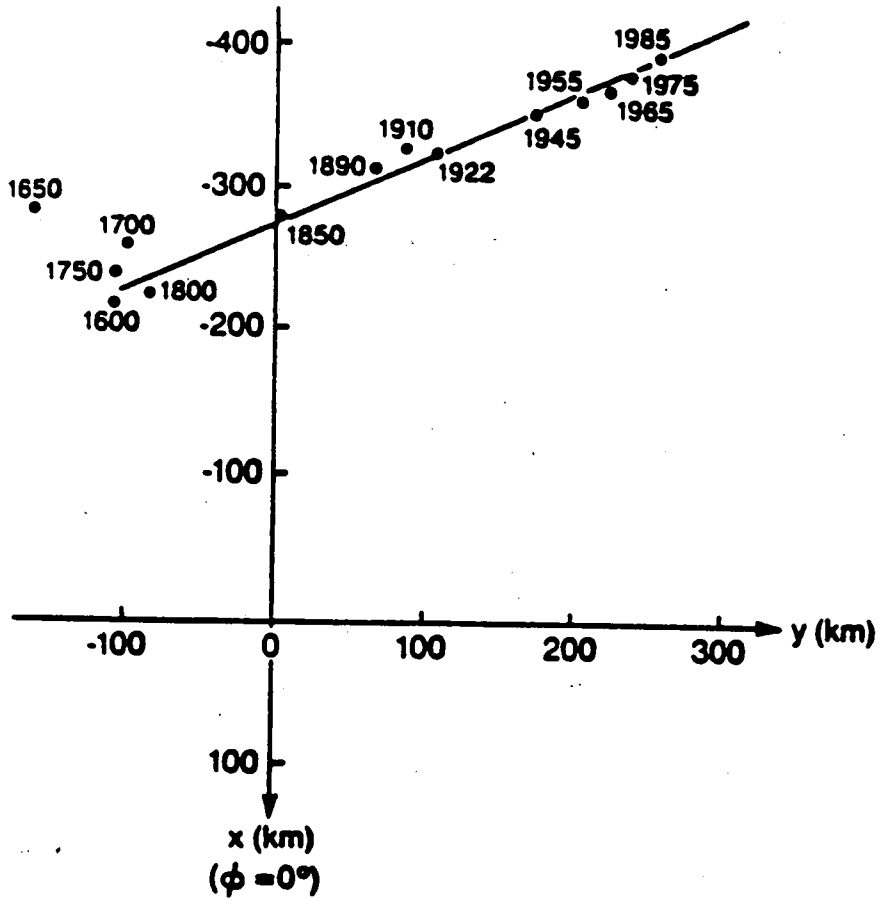

Fig.2-15. Variation of the projection of the eccentric dipole position on the geographical equatorial plave during the interval 1600-1985.

The curves labelled "IGRF-1980" are obtained the same way, but instead of using M_d in (2.56) or (2.44), Daly (1989) has used the actual magnetic moment M corresponding to the appropriate epoch : i.e.

$$M = R_E^3 \left[(g^0_1)^2 + (g^1_1)^2 + (h^1_1)^2 \right]^{\frac{1}{2}} \qquad (2.65)$$

It can be seen from (2.24) and (2.25) that in both cases the low altitude fluxes of protons and electrons increases drastically and most dramatically at lowest altitude. This effect had been pointed out earlier by Konradi et al. (1987).

When the actual magnetic moment (2.65) is used instead of McIlwain's M_d "standard value", the secular increase of intensity is less dramatic, however. This later conclusion is not inconsistent with that deduced from our earlier discussion on the variation of L when M decreases. Indeed, when one assumes that $M_d = 0.311653$ Gauss R_E^3 (corresponding to "IGRF-1980 with McIlwain's M"), L decreases with M approximately as $M^{2/3}$. On the other hand if we assume $M_d = M$ (corresponding to IGRF 1980 with the actual magnetic moment in eqs (2.40) or (2.44)), L is proportional to M (i.e. it decreases faster with M than in the previous case). This implies that the L values computed for a point at a given geographical altitude (let's say for the year 2000), will be lower when M_d is replaced by the actual M in eqs (2.40) or (2.44) than if M_d is used in these same equations. Since the trapped radiation flux increases rapidly with L at low altitude, one can expect that the flux intensity is lower in the case when $M_d = M$, than in the case when McIlwain's standard value is used. The numerical results obtained by Daly (1989) show that the fluxes obtained for an "IGRF model with McIlwain's M" are indeed higher than all others for $M_d = M$.

Note, however, that the overall increase of the fluxes as a function of Epoch (i.e. with decreasing dipole moment) cannot be explained from the secular variation of the dipole component only. Indeed, (i) particles experience a betatron energization when M decreases, and (ii) higher multipole terms in the IGRF spherical harmonic expansion, which account for the South Atlantic Magnetic Anomaly and for the eccentric displacement of the Earth's dipole , also experience significant secular variations which ought to be taken into account.

In the previous section it is mentioned that the secular variation of the quadrupole terms in this expansion cause a slow variation of the position of the magnetic centre (Stern, 1971, Fraser-Smith, 1987). The centre of the dipole is receding from the Earth's centre at a rate larger than 2 km/year.

Fig.2.15 shows the secular variation of the projection of the eccentric dipole position on the geographic equatorial plane during the interval 1600-1985. This "eccentricity" displacement necessarily leads to an additional increase in the averaged radiation intensity along circular low altitude orbits. Indeed, particle shells are gradually dipping deeper into the atmosphere over the South Atlantic.

The gradual secular decrease of the octupole term (3,0) of about 3.6 nT/year, contributes also to enhance the effect of the secular decrease of the main dipole moment on the inner-belt protons (Schulz and Paulikas, 1972,a).

Therefore, we infer that it is not only the secular variation of the dipole term which determines the rapid increase of the predicted fluxes in Figs 2.14a and 2.14b; the secular variations of quadrupole and octupole terms also contribute significant change to the actual geomagnetic field distribution (Fraser-Smith ,1987).

More importantly, to obtain a more realistic low altitude flux for the year 2000 or beyond, the effects of atmospheric cut-off should be taken properly into account in future modelling efforts. In this respect it could be mentioned that Hassitt (1966,1967,1968), in a series of papers and reports provided recently to us by C.E.McIlwain (personal communication, April 1989), made a number of interesting suggestions. His pioneering work ought to be developed to be incorporated in future UNIRAD software packages.

2.1.11 Atmospheric control; East-West Effect.

As already stated above, the inner edge of the Radiation Belts is clearly controlled by the Earth's atmosphere. The product $<\rho>J$ of the omnidirection flux, J and the local time averaged atmospheric density, is nearly a constant for low altitudes. This empirical result is an important feature that should be investigated more thoroughly in future model developments of the low altitude radiation environment. The early attempts along these lines ought to be pursed.

Heckman and Nakano (1963) found another effect related to atmospheric control. At an altitude of about 400 km, trapped protons are encountered in the region of the South Atlantic Anomaly. In analysing the tracks in the emulsions they found that 2.3 times as many protons of E > 57 MeV entered their instrument from the West than from the East.

The explanation of this is that in this region the protons moving from west to east, j_E, have their guiding centers above the satellite while the protons moving from east to west, j_W ,have the guiding centers below the satellite in regions of larger atmospheric density. Considering that the proton flux is inversely proportional to the atmospheric density at the guiding center, the east-

west ratio is given by

$$j_E / j_W = \exp(2 R_C \cos I / H)$$

where I is the dip angle of the field line, H the atmospheric density and R_C the gyroradius. At low altitudes, R_C for 50 MeV protons is indeed of the order of the density scale height (i.e. H = 50-60 km).

Although in existing models of trapped radiation belts, this East-West Effect is not explicitly included, it would be desirable to incorporate this effect in future models for the directional flux of low-altitude radiation environment. However, for the time being it is not obvious yet how this goal is to be achieved.

2.2 GEOMAGNETIC FIEL MODELS

2.2.1 The Internal Geomagnetic Field.

It has been customary to express the magnetic field as the gradient of a scalar potential $V(r,\theta,\phi)$, where r,θ, and ϕ are the geographic spherical coordinates of the point in question (radius vector, north colatitude, and longitude east of Greenwich, respectively). Taking into account that to a first approximation the Earth's magnetic field is that of a dipole, the function V is conveniently expressed as an orthogonal expansion

$$V(r,\theta,\phi) = R_E \sum_{n=1} \sum_{m=o}^{m=n} \left(\frac{R_E}{r}\right)^{n+1} \left(g_n^m \cos m\phi + h_n^m \sin m\phi\right) P_n^m(\theta) \qquad (2.66)$$

R_E is the mean radius of the Earth (6371 km); $P_n^m(\theta)$ are the associated Legendre functions, conveniently normalized (e.g. see. Matsuhita and Campbell (1967); Table 2.3 gives these functions for $n \leq 3$).

g_n^m and h_n^m are parameters whose values must be determined experimentally; they are slowly time dependent (secular variation) (e.g. Cain and Cain, 1971; Fraser-Smith, 1987). These values are given in Table 2.4 for Epoch 1965 for $n \leq 3$). The most widely used expansion for the geomagnetic field in the early Radiation Belt models was that of Jensen and Cain (1962) using data for Epoch 1960.

The index n (order of multipolarity) governs the 'strength' of the radial dependence (decay) of the corresponding terms in relation (2.66) as well as the periodicity (or multiplicity) of the θ dependence . The

	$n = 1$	$n = 2$	$n = 3$
$m = 0$	$\cos\theta$	$\frac{1}{2}(3\cos^2\theta - 1)$	$\frac{1}{2}\cos\theta(5\cos^2\theta - 3)$
$m = 1$	$\sin\theta$	$(3)^{1/2}\sin\theta\cos\theta$	$\frac{(6)^{1/2}}{4}\sin\theta(5\cos^2\theta - 1)$
$m = 2$	...	$\frac{(3)^{1/2}}{2}\sin^2\theta$	$\frac{(15)^{1/2}}{2}\cos\theta\sin^2\theta$
$m = 3$	...	...	$\frac{(10)^{1/2}}{4}\sin^3\theta$

Table 2-3 Assiociated Legendre Functions, Schmidt Normalised

n	m	g_n^m	h_n^m
1	0	−0.30333	0
1	1	−0.02117	0.05759
2	0	−0.01660	0
2	1	0.02997	−0.02002
2	2	0.01561	0.00119
3	0	0.01299	0
3	1	−0.02043	−0.00397
3	2	0.01289	0.00240
3	3	0.00847	−0.00167

Table 2-4 Coefficients of the Field Expansion 2-66 corresponding to IGRF 1965 (values in Gauss)

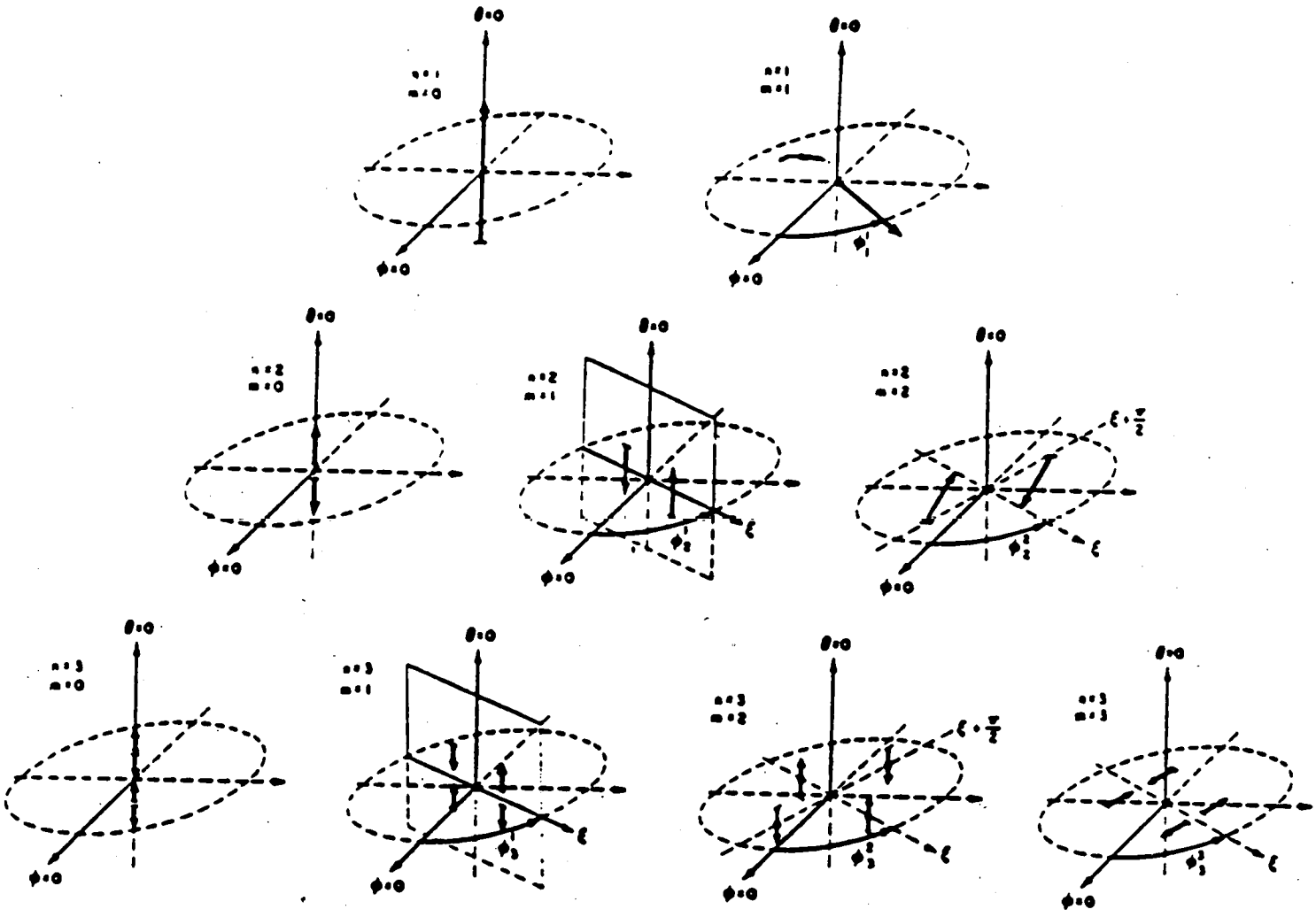

Fig.2-16. Equivalent dipole distributions corresponding to each (n,m) term in the geomagnetic potential expansion 2-67. The multipole moments are proportional to the coefficients c^m_n given by 2-68 and the phase angles shown are given by 2-69.

	m	n	1945	1950	1955	1960	1965	1970	1975	1980	1985	SV
g	0	1	-30634	-30571	-30507	-30411	-30334	-30220	-30100	-29992	-29877	23.2
g	1	1	-2240	-2241	-2134	-2162	-2119	-2068	-2013	-1956	-1903	10.0
h	1	1	5806	5807	5796	5780	5776	5737	5675	5604	5497	-24.5
g	0	2	-1215	-1330	-1432	-1546	-1662	-1781	-1902	-1997	-2073	-13.7
g	1	2	2972	2978	2995	3007	2997	3000	3010	3027	3045	3.4
h	1	2	-1700	-1813	-1896	-1948	-2016	-2047	-2067	-2129	-2191	-11.5
g	2	2	1588	1579	1567	1572	1594	1611	1632	1663	1691	7.0
h	2	2	497	388	263	209	114	25	-68	-200	-309	-20.2
g	0	3	1274	1293	1308	1307	1297	1287	1276	1281	1300	5.1
g	1	3	-1833	-1878	-1955	-1987	-2038	-2091	-2144	-2180	-2208	-4.6
h	1	3	-512	-485	-487	-421	-404	-366	-333	-336	-312	5.3
g	2	3	1225	1271	1293	1288	1292	1278	1260	1251	1244	-0.6
h	2	3	185	228	235	230	240	251	262	271	284	2.3
g	3	3	926	890	897	879	856	838	830	833	835	0.1
h	3	3	-5	-67	-73	-130	-165	-196	-223	-252	-296	-10.8
g	0	4	980	975	964	962	957	952	946	938	937	0.1
g	1	4	771	795	794	804	804	800	791	782	780	-0.6
h	1	4	155	171	167	150	148	167	191	212	233	3.8
g	2	4	544	532	510	492	479	461	438	398	363	-7.8
h	2	4	-280	-306	-275	-272	-269	-266	-265	-257	-250	2.2
g	3	4	-408	-402	-392	-392	-390	-395	-405	-419	-426	-1.4
h	3	4	-68	-51	-44	1	13	26	39	53	68	2.5
g	4	4	300	310	292	267	252	234	216	199	169	-6.8
h	4	4	-158	-184	-249	-254	-269	-279	-288	-297	-298	0.9
g	0	5	-286	-255	-232	-236	-219	-216	-218	-218	-215	1.3
g	1	5	341	353	360	358	358	359	356	357	356	0.1
h	1	5	-14	-8	14	12	19	26	31	46	47	0.1
g	2	5	207	201	237	229	254	262	264	261	253	-1.5
h	2	5	80	101	111	121	128	139	148	150	148	-0.2
g	3	5	-25	-3	-13	-34	-31	-42	-59	-74	-94	-3.2
h	3	5	-65	-95	-90	-115	-126	-139	-152	-151	-155	-0.1
g	4	5	-156	-160	-176	-153	-157	-160	-159	-162	-161	0.1
h	4	5	-114	-100	-111	-108	-97	-91	-83	-78	-75	0.6
g	5	5	-88	-76	-68	-64	-62	-56	-49	-48	-48	-0.1
h	5	5	83	73	77	83	81	83	88	92	95	0.0
g	0	6	68	57	47	47	45	43	45	48	52	1.4
g	1	6	67	50	57	56	61	64	66	66	65	-0.3
h	1	6	9	-1	-7	-13	-11	-12	-13	-15	-16	-0.4
g	2	6	6	15	4	-3	8	15	28	42	50	1.7
h	2	6	118	100	101	106	100	100	99	93	90	-1.1
g	3	6	-244	-261	-250	-241	-228	-212	-198	-192	-186	0.6
h	3	6	18	52	46	55	68	72	75	71	69	-0.8
g	4	6	-12	8	12	3	4	2	1	4	4	0.0
h	4	6	-9	-7	-16	-26	-32	-37	-41	-43	-50	-2.3
g	5	6	14	8	13	4	1	3	6	14	17	0.9
h	5	6	-12	-17	-6	-10	-8	-6	-4	-2	-4	-0.5
g	6	6	-100	-108	-105	-108	-111	-112	-111	-108	-102	1.2
h	6	6	-42	-21	-21	-16	-7	1	11	17	20	-0.1
g	0	7	72	67	80	72	75	72	71	72	75	0.2
g	1	7	-61	-48	-66	-52	-57	-57	-56	-59	-61	-0.6
h	1	7	-42	-44	-52	-53	-61	-70	-77	-82	-82	0.2
g	2	7	6	-3	2	4	4	1	1	2	2	-0.5
h	2	7	-39	-18	-37	-25	-27	-27	-26	-27	-26	1.0
g	3	7	6	16	4	11	13	14	16	21	24	0.8
h	3	7	2	-6	6	-8	-2	-4	-5	-5	-1	1.1
g	4	7	-44	-38	-46	-20	-26	-22	-14	-12	-6	1.0
h	4	7	-1	-8	-1	3	6	8	10	16	23	1.9
g	5	7	-2	1	-15	-4	-6	-2	0	1	4	0.4
h	5	7	25	32	29	28	26	23	22	18	17	0.3
g	6	7	18	9	8	15	13	13	12	11	9	-0.5
h	6	7	-19	-18	-20	-16	-23	-23	-23	-23	-21	0.2
g	7	7	27	11	14	6	1	-2	-5	-2	0	-0.1
h	7	7	-23	-22	-12	-18	-12	-11	-12	-10	-6	0.9
g	0	8	15	16	5	6	13	14	14	18	21	0.7

Table 2-5 Coefficients of the Field Expansion 2-66 corresponding to IGFR 1985 (in nT) and of the Predictive Secular Variation for 1985-1990, in nT/year (after IAGA bulletin,1986).

	m	n	1945	1950	1955	1960	1965	1970	1975	1980	1985	SV
g	1	8	5	4	17	4	5	6	6	6	6	0.0
h	1	8	-7	2	12	7	7	7	6	7	7	0.1
g	2	8	-12	-8	-3	-3	-4	-2	-1	0	0	0.3
h	2	8	9	-2	1	-16	-12	-15	-16	-18	-21	-1.0
g	3	8	-21	-31	-30	-13	-14	-13	-12	-11	-11	0.4
h	3	8	0	-3	10	5	9	6	4	4	5	0.1
g	4	8	18	15	14	-5	0	-3	-8	-7	-9	-0.3
h	4	8	-13	-7	-20	-19	-16	-17	-19	-22	-25	-0.8
g	5	8	16	8	27	10	8	5	4	4	2	-0.3
h	5	8	5	6	5	5	4	6	6	9	11	0.2
g	6	8	-14	-17	-15	-6	-1	0	0	3	4	0.1
h	6	8	26	27	34	23	24	21	18	16	12	-0.8
g	7	8	1	7	1	15	11	11	10	6	4	-0.5
h	7	8	1	-6	4	-2	-3	-6	-10	-13	-16	-0.1
g	8	8	10	13	12	5	4	3	1	-1	-6	-0.8
h	8	8	-19	-22	-19	-18	-17	-16	-17	-15	-10	1.3
g	0	9				13	8	8	7	5	5	
g	1	9				5	10	10	10	10	10	
h	1	9				-22	-22	-21	-21	-21	-21	
g	2	9				4	2	2	2	1	1	
h	2	9				14	15	16	16	16	16	
g	3	9				-12	-13	-12	-12	-12	-12	
h	3	9				5	7	6	7	9	9	
g	4	9				14	10	10	10	9	9	
h	4	9				-5	-4	-4	-4	-5	-5	
g	5	9				5	-1	-1	-1	-3	-3	
h	5	9				0	-5	-5	-5	-6	-6	
g	6	9				-2	-1	0	-1	-1	-1	
h	6	9				11	10	10	10	9	9	
g	7	9				0	5	3	4	7	7	
h	7	9				10	10	11	11	10	10	
g	8	9				0	1	1	1	2	2	
h	8	9				2	-4	-2	-3	-6	-6	
g	9	9				-1	-2	-1	-2	-5	-5	
h	9	9				-2	1	1	1	2	2	
g	0	10				-5	-2	-3	-3	-4	-4	
g	1	10				-2	-3	-3	-3	-4	-4	
h	1	10				3	2	1	1	1	1	
g	2	10				0	2	2	2	2	2	
h	2	10				0	1	1	1	0	0	
g	3	10				-5	-5	-5	-5	-5	-5	
h	3	10				4	2	3	3	3	3	
g	4	10				-2	-2	-1	-2	-2	-2	
h	4	10				3	6	4	4	6	6	
g	5	10				8	4	6	5	5	5	
h	5	10				-4	-4	-4	-4	-4	-4	
g	6	10				3	4	4	4	3	3	
h	6	10				-2	0	0	-1	0	0	
g	7	10				0	0	1	1	1	1	
h	7	10				-3	-2	-1	-1	-1	-1	
g	8	10				1	2	0	0	2	2	
h	8	10				5	3	3	3	4	4	
g	9	10				0	2	3	3	3	3	
h	9	10				3	0	1	1	0	0	
g	10	10				-1	0	-1	-1	0	0	
h	10	10				-3	-6	-4	-5	-6	-6	

Table 2-5 (continued)

n	m	g_n^m	h_n^m	$\dot{g}_n^m$	$\dot{h}_n^m$
1	0	−0.30953	0	0.00016	
1	1	0	0	...	
2	0	−0.00618	0	−0.00020	
2	1	0.02997	0.02255	0.00018	0.00002
2	2	−0.01875	0.00481	0.00007	0.00009
3	0	0.00906	0	−0.00002	...
3	1	−0.01238	−0.01758	−0.00005	−0.00010
3	2	−0.01052	0.01170	−0.00001	0.00001
3	3	−0.00546	−0.00485	0.00001	0.00006

Table 2-6 Field Expansion Coefficients (in Gauss) in the Geomagnetic Coordinate System and their Secular Variation (in Gauss/year), Epoch 1985.

n	m	G_n^m	H_n^m
1	0	−0.30953	0
1	1	0	0
2	0	0	0
2	1	0	0
2	2	−0.01875	0.00481
3	0	0.00688	0
3	1	−0.01263	−0.01896
3	2	−0.00929	0.01441
3	3	−0.00888	−0.00627

Table 2-7 Fiels Expansion Coefficients (in Gauss) in the Eccentric Dipole Coordinate System, transformed from Table 2-6.

index m determines the longitudinal periodicity. The expansion (2.66) only accounts for internal sources of the magnetic field. In later sections, we shall consider the effect of external sources.

Another, probably more physical but less common form of expressing V is the following :

$$V(r,\theta,\phi) = R_E \sum_{n=1}^{} \sum_{m=o}^{m=n} \left(\frac{R_E}{r}\right)^{n+1} c_n^m \cos(m(\phi - \phi_{nm}) \; P_n^m(\theta) \qquad (2.67)$$

with

$$c_n^m = +[(g_n^m)^2 + (h_n^m)^2]^{\frac{1}{2}} \; ; \quad c_n^o = g_n^o \qquad (2.68)$$

$$\phi_n^m = \frac{1}{m} \arctan \frac{h_n^m}{g_n^m} = \frac{1}{m} \arcsin \frac{h_n^m}{c_n^m} \qquad (2.69)$$

ϕ_n^m represents phase angles (with respect to the reference ϕ=0) and c_n^m is a measure of the 'total strength' of each term of the order (n,m). Notice that, according to the second equality in eq.(2.68), the actual quadrant in which ϕ_n^m lies is determined by the sign of h_n^m.

The values of the harmonic or multipole expansion and their secular variation are given in Table 2.5 for Epoch 1985 (IAGA bulletin, 1986).

Roederer (1972) has given a helpful intuitive interpretation of the different terms in the expansions (2.66) and (2.67). This is illustrated in Fig 2.16. Let us first recall that the magnetic field of any spatially confined current distribution can be simulated by an equivalent distribution of elementary 'point dipole' currents clustered around the origin. Each one of the terms

in expansion (2.67) can be thought of as originating in an equivalent distribution of point dipoles at the origin.

The case n=1 represents the contribution from the main dipole directed downward in the real case, owing to the negative sign of g_1^0 All other terms can be considered as perturbations of the main dipole field, particularly when we move away from the Earth's surface ($r>R_E$). For all cases shown in Figure (2.16), one must keep in mind that 'distance between dipoles $d\to 0$, dipole moment $p\to\infty$, maintaining pd=finite~Q (n=2); pd^2=finite~0 (n=3); etc. The values of these equivalent multipole moments Q, 0, etc. are proportional, respectively to the c_n^m coefficients in (2.67). Their spatial orientation is determined by the corresponding phase angles ϕ^m_n, as shown in Figure 2.16.

i) Dipole terms (n=1).

We will first ignore all coefficients in expansion (2.66) and (2.67) except those corresponding to n=1. The m = 0 term represents the field of a dipole oriented along the Earth's rotational axis, of moment g_1^0 . The negative value of g_1^0 in Tables 2.4 and 2.5 indicates that this dipole component is oriented N-S.

The (1,1) terms represent a dipole lying in the $\theta=\pi/2$ plane (the geographic equator), of moment $c_1^1=[(g_1^1)^2+(h_1^1)^2]^{\frac{1}{2}}$ directed along $\phi_1^1=\arctan(h_1^1/g_1^1)=\arcsin(h_1^1/c_1^1)$. For the coefficients in Table (2.4), one obtains $\phi_1^1=110.2^\circ$.

The full n=1 case is thus identified with that of a single, Earth-centered but tilted dipole. The absolute tilt angle θ_o (angle with the Earth's rotation axis) is given by $\theta_o = \arctan(c_1^1/g_1^0)=11.4^\circ$ for the coefficients in Table 2.4. The line defined by this Earth-centered dipole vector is called the geomagnetic axis. Since the dipole vector is directed southward along this axis, yet most of the geophysicists live in the northern hemisphere, they have

preferred to use the geographic longitude ϕ_o of the northern Earth intersection of the geomagnetic axis to define the azimuthal direction of the latter. Thus $\phi_o=\phi_1^1+180°=290.2°$ east geographic longitude. The meridian defined by ϕ_o is called the magnetic meridian.

The (1,1) term can be 'transformed away' by a suitable change of the frame of reference. Indeed, a rotation of the $\theta=0$ axis until it is oriented parallel to the geomagnetic axis (with a convenient choice of the reference longitude) yields a new coordinate system r', θ', ϕ' in which there is no main dipole component in the $\theta'=\pi/2$ plane, i.e., in which the coefficients $c_1^{1'}=g_1^{1'}=h_1^{1'}=0$ and $g_1^{o'}=g_1^o/|g_1^o|[(g_1^o)^2+(g_1^1)^2+h_1^1)^2]^{\frac{1}{2}}=-0.30954$ Gauss (Epoch 1965).

This is the system of geomagnetic coordinates, the 'natural' frame of reference to be used to describe internal-field-controlled physical processes for which the centered-dipole approximation is sufficient. Many magnetospheric processes occurring at a radial distance between 2 and 4-5 R_E can be suitably described in these coordinates. Since we shall frequently be using the absolute value of $g_1^{o'}$, we introduce

$$B_E = -g_1^{o'} = + 0.30954 \text{ Gauss} \qquad (2.70)$$

Note that because of the definition of $g_1^{o'}$ given above, B_E or the related Magnetic dipole value M depends on all three coefficients g_1^o, g_1^1 and h_1^1 given in Table 2.4 or 2.5. In the geomagnetic coordinates system (rotated with respect to the geographic one) the two last coefficients $g_1^{1'}$ and $h_1^{1'}$ have become equal to zero (see Table 2.6).

The $\theta=0$ axis is defined by the magnetic axis northward from the centre of the Earth, and the reference $\phi'=0$ is taken as the one containing the geographic south

pole. This reference meridian thus coincides with the above defined magnetic meridian, of geographic longitude ϕ_o. The $\theta'=\pi/2$ plane is the geomagnetic equator. The geomagnetic and the geographic equators intersect along a line of geographic coordinates $\phi_i=20.2^\circ$ $(+180^\circ)$. The associated coordinate transformations are discussed in an article by Russell (1971).

When we switch to the geomagnetic frame of reference, all higher multipole coefficients g_n^m, h_n^m (or c_n^m, ϕ_n^m) will suffer a change. Table 2.6 (from Stern, 1971) shows their new values, for $n\leq 3$. Since all coefficients in expansions (2.66) and (2.67) are slowly time dependent (secular variation), the system of geomagnetic coordinates is in itself slowly time dependent. Stern (1971) has given expressions for the secular variation of θ_o and ϕ_o (see also Frazer-Smith, 1987).

Particles injected at an equatorial point with 90° pitch angle ($\alpha_{oi}=90^\circ$) will drift along a contour of constant magnetic field intensity $B_o=B_{oi}$ which in this $n=1$ case lies in the geomagnetic equator and is a circle. The relationship between its radius and the equatorial B value is

$$r_o = \left(\frac{B_E}{B_o}\right)^{1/3} \qquad (2.71)$$

where B_E is the main dipole coefficient (2.70).

If the particle is injected at the same equatorial point with a pitch angle different from 90°, it will generate a drift shell whose equatorial intersection is still in the same circle. This is a direct consequence of the cylindrical symmetry pertinent to this case. The drift shell is thus independent of α_{oi}. All particles mirroring on a given field line in a dipole field will populate the

same drift shell, irrespective of their initial pitch angles (shell degeneracy).

A particle shell in a dipole field can be characterized or labelled with the value r_o of the radius of its equatorial trace. The other determining parameter of a trapped particle could be either the value of its mirror point B_m, its equatorial pitch angle α_o, or any other given function thereof. The dimensionless quantity $L = (r_o/R_E)$ is 'McIlwain's L value'.

For near-equatorial particles L is related to the adiabatic invariants I and B_m by the approximate relationship

$$L = \left(\frac{B_E}{B_m}\right)^{1/3} + \frac{(2)^{\frac{1}{2}}}{\pi}\,\frac{I}{R_E} \quad \text{for} \quad \frac{I}{R_E} \ll 1 \qquad (2.72)$$

This expression is easy to interpret physically. For a given mirror-point field intensity B_m, as we increase the I value of a tr2pped particle, the corresponding field line (or drift shell) moves radially outward.

Relationship (2.72) is an approximation valid for $\mu^2_o = \cos^2\alpha_o \ll 1$. For the full range $0 \le \mu_o \le 1$, the function $L = L(I, B_m)$ is more complicated.

The secular variation of the main dipole coefficient B_E (at present a gradual decrease in magnitude of about 0.016 Gauss per century), has an important effect on the ultra stable energetic protons trapped at low-L drift shells (Heckman and Lindstrom, 1972; Schulz and Paulikas, 1972a). The protons whose characteristic lifetimes are of the order of centuries, will be subject to a secular change of drift-shell position and energy. Indeed conservation of the third invariant Φ, which in the dipole field is related to L by eq.(2.43), requires that the L parameter of a given particle decreases as B_E decreases.

ii) Quadrupole terms (n=2).

In the geomagnetic system of coordinates the coefficients are $g_n^{m'}$ and $h_n^{m'}$ and since $g_1^{1'} = h1^{1'} = 0$, we ignore case (1,1) of Figure 2.16. In this section we consider the effects of the quadrupole terms n=2. Notice in Figure 2.16 the equivalent pairs of dipoles corresponding to the terms labelled (2.0), (2.1) and (2.2). In the m=1, 2 cases the phase angles $\phi_2^{1'}$, $\phi_2^{2'}$ determine the orientation of the equivalent dipole pairs, as shown.

The influence of the (2,0) and (2,1) terms can be analyzed very easily on the basis of this picture. Indeed, it is possible to cancel their effects by conveniently displacing the position of the main dipole away from the Earth's centre (i.e., by effecting a translation of the coordinate system). In particular, it can be shown that a translation parallel to the main dipole axis (z axis) by an amount Δz_o changes the g_2^o coefficient to $G_2^o = g_2^{o'} - 2(\Delta z_o / R_E) g_1^{o'}$ (Bernard et al., 1969). Hence choosing $\Delta z_o = (1/2)\, R_E g_2^o / g_1^o$ leads to $G_2^o = 0$, i.e., cancellation of the (2,0) term. On the other hand, a translation $\Delta \xi_o$ perpendicular to the main dipole axis along ξ_1 axis changes the $c_2^1 = [(g_2^{1'})^2 + (h_2^{1'})^2]^{\frac{1}{2}}$ coefficient to $C_2^1 = c_2^{1'} - (3)^{\frac{1}{2}} (\Delta n_o / R_E) g_1^{o'}$. Hence choosing $\Delta \xi_o = [(1/3)^{\frac{1}{2}}] R_E (c_2^{1'} / g_1^{o'})$ leads to $C_2^1 = 0$.

It should be pointed out that the value of the eccentric displacement depends on all the quadrupole coefficient g_2^m and h_2^m (see Frazer-Smith 1987); but since some of these coefficients become equal to zero, in the geomagnetic frame of reference, Δz_o and $\Delta \xi_o$ are fully determined by $g_2^{o'}$, $g_2^{1'}$ and $h_2^{1'}$ only (see Table 2.6)

Notice that this displacement must be taken in the direction ξ^1, given by the phase angle $\phi_2^1 = \arctan(h_2^1 / g_2^1) = \arcsin(h_2^1 / c_2^1)$ (see Figure 2.16). For the coefficients of Table 2.6, the values are $\Delta z_o = 63.6$ km northward of the Earth's centre along the magnetic

axis, and $\Delta\xi_o$=445.4 km perpendicular to the magnetic axis in the direction $\phi_2^{1\prime}$=217° geomagnetic longitude. The point with these coordinates is called the magnetic centre.

The new frame of reference can be called the eccentric-dipole coordinate system r^*, θ^*, ϕ^*. Its origin coincides with the magnetic centre; its θ^*=0 axis and ϕ^*=0 meridian are oriented parallel to the magnetic axis and to the geomagnetic reference meridian, respectively. (In practice one can set $\phi^*=\phi'$. In general, for r>3-4 R_E, the eccentric-dipole coordinates practically coincide with the geomagnetic coordinates). Secular variation, of course, makes all the corresponding transformation parameters slowly time dependent .

In the eccentric-dipole system, the values of the geomagnetic field expansion coefficients will have changed again (Bernard et al., 1969). Table 2.7 shows their new values for n≤3. We denote the transformed coefficients by capital letters G_n^m, H_n^m, C_n^m. By definition, $G_1^1=H_1^1=G_2^o=G_2^1=H_2^1=0$ in this coordinate system. Notice by comparison with Table 2.6 that the remaining quadrupole coefficients G_2^2, H_2^2 stay unchanged in this transformation. On the other hand, it should be pointed out that even if all higher multipole coefficients had originally been zero, the displacement transformation into the eccentric system would introduce non-zero values for all m=0, 1 higher multipoles (Bernard et al., 1969).

To summarize, we can interpret the first-order effect of the (2,0) and (2,1) terms as that of a parallel displacement of the position of the main dipole away from the centre of the Earth. The eccentric-dipole system is the 'natural' frame of reference to be used in the description of purely field-controlled processes occurring near the Earth for which the dipole-type field approximation is a sufficiently good one. But even for the study of higher-order effects, this is the natural frame to start with.

The displacement of the main dipole has important consequences for particles trapped at low altitudes. Neglecting the effect of the (2,2) term as well as that of the higher multipoles, these particles will still behave as prescribed for a dipole field, but as viewed from the Earth's surface (or from an Earth-centered frame of reference), their drift shells appear displaced, with a closest approach over an area east of the Atlantic coast of South America .

Figure 2.17 shows the (highly exaggerated) situation in the $\phi^*=\phi_2{}^1$' plane (geographic longitudes 147° and -33°), which contains the centre of the Earth and the displaced dipole. In the area of closest approach (-33°), trapped particles have their deepest penetration into the atmosphere,suffering a maximum of pitch angle scattering and energy loss. This has been called the 'South American' or 'Brazilian' anomaly of the radiation belt (Vernov et al., 1962) and contributes to an important longitudinal asymmetry in the low-altitude edge of the trapped-electron distribution (Williams and Kohl, 1965; Imhof and Smith, 1966; Roederer et al., 1967). Trapped protons that enter the dense atmosphere in that area are simply eliminated. For higher L values, the effect of the eccentric displacement gradually decreases. For L>2 it may be safely ignored (except for particles mirroring very close to the Earth's surface.)

The secular change of the expansion coefficients causes a slow variation of the position of the magnetic centre. By using the values computed by Stern (1971), one finds that the magnetic centre suffers a westward drift and that it is receding from the Earth's centre at a rate between 2 and 3 km/yr (Schulz and Paulikas, 1972b; Fraser-Smith, 1987). This latter fact means that the 'eccentricity' of the main dipole is increasing with time. Particle shells are thus gradually dipping deeper into the atmosphere, over the South Atlantic. This contributes to

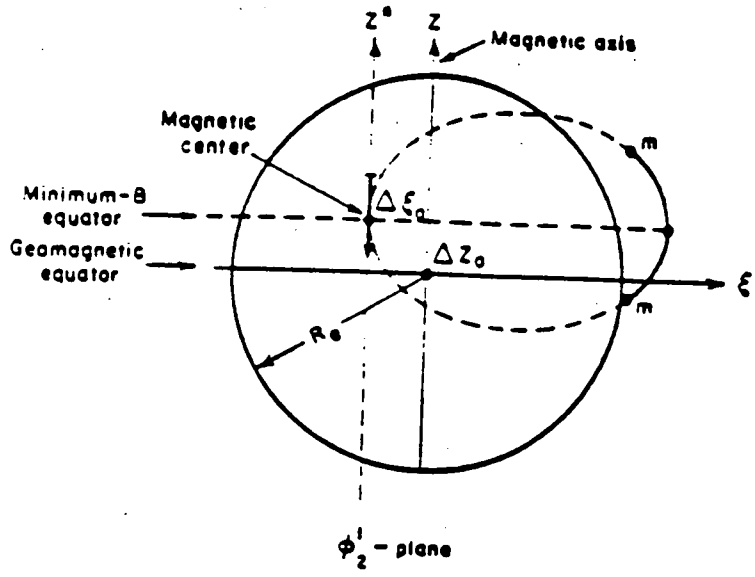

Fig.2-17. Shematic view (highly exaggerated scale) of the eccentric dipole position and its effect on a trapped particle shell (after Roederer, 1972).

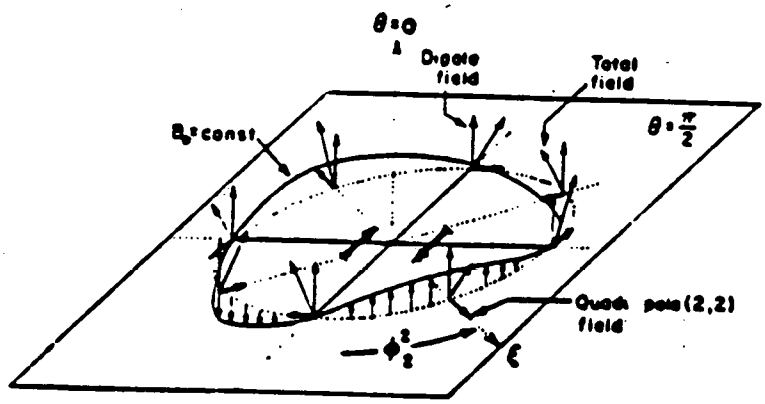

Fig.2-18. Shematic view of the effect of the (2,2) quadrupole term on the drift contour of an equatorial particle (after Roederer, 1972).

enhancement of the effect of the secular decrease of the main dipole. Part of the enhanced flux variation shown in Fig 2.14 due to secular geomagnetic field changes are due to this effect.

The very stable population of energetic protons is continuously eroded away by the atmosphere at its lower edge, in the South Atlantic Magnetic Anomaly (SAMA). This loss is compensated by the secular inward displacement and energization of 'fresh' protons injected (mainly by albedo neutron decay) at higher L shells. The electron precipitation rate due to pitch-angle scattering is so large that secular effects can be neglected for these latter particles.

Finally, we will consider the (2,2) case (Fig.2.16). Since the equivalent pair of dipoles lies in a plane perpendicular to the main dipole, there is no way of 'transforming away' the (2,2) terms. According to Tables 2.6 and 2.7, the corresponding (2,2) coefficients have remained totally unaffected by the transformation from geomagnetic to eccentric dipole coordinates.

Let us consider the effect of the (2,2) terms in the absence of higher multipoles. The equivalent pair of dipoles produces a magnetic field whose geometry in the $\theta^*=(\pi/2)$ plane is sketched in Fig.2.18. At points on that plane, the (2,2) quadrupole field is always perpendicular to that of the main dipole; the resulting total field thus suffers a first-order distortion in direction, but only a second-order distortion in magnitude (Fig.2.18).

The drift contours of 90° pitch angles particles, which at all times must be perpendicular to **B**, will not lie in the $\theta^*= \pi/2)$ plane anymore . Though still remaining equidistant from the origin to first order (because B is modulated only to second order along r^*=const path), they will wiggle up and down with respect to the $\theta^*=\pi/2$ plane with a period of 180° (see Fig.2.18).

In general, all equatorial minimum-B points, defined by $\mathbf{B}.\nabla B=0$ (Schulz, 1971) will lie on a 'potato-chip-shaped' surface. Mirror point rings will suffer a similar distortion because of the (2,2) term. One of the maximum positive elevations on this surface occurs at 12.8° geographic longitude, over the African continent, and not too far from the South Atlantic Magnetic Anomaly (-33° geographic longitude). The effect of the (2,2) term is thus to enhance the effect on trapped particles of the eccentric displacement Δz_o (Figure 2.17) and to extend it farther east (and north), bringing their southern mirror points even farther down in the atmosphere over the South Atlantic and also over the South African continent. This additional effect also contributes to explain the secular flux variation displayed in Fig.2.14.

To the first order in C_2^2/B_E, particles injected with different pitch angles on the same field line will drift along the same shell. Indeed, it can be shown (Roederer et al., 1972) that the quantity $\partial^2 B/\partial s^2$, governing shell splitting (i.e., the pitch-angle dependence of drift shells), is equal to that of a dipole field and hence independent of longitude, to the order of C_2^2/B_E.

McIlwain's L parameter thus retains the same properties as in a pure dipole field (to the first order), except that the points of constant L (drift-shell field lines) will suffer a N-S distortion with a 180° longitudinal period.

In summary, the principal first-order effect of the (2,2) quadrupole is to deform the equatorial surface and hence to deform the shape of trapped-particle drift shells in the N-S direction, without, deforming their equatorial distance to the magnetic centre and without introducing shell splitting.

(iii) Octupole terms (n=3).

According to Figure 2.16, there are four possible equivalent dipole pair configurations corresponding to n=3. The (3,1) and (3,3) terms can be disposed of fairly quickly. It can be shown that by computing the components of **B** that their field perturbations lie in the $\theta^*=\pi/2$ surface, causing a longitude dependent tilt of the total field, but with only a second-order variation of its intensity. Hence, except for a different azimuthal periodicity and phase, their effects are analogous to that of the (2,2) quadrupole warping the equatorial surface and constant-B drift contours, yet keeping them equidistant to the magnetic centre and causing no shell splitting, to first order.

Let us next consider the effects of the azimuthally symmetric case (3,0) in the absence of all other multipoles except the main dipole. On the $\theta^*=\pi/2$ plane, the corresponding field perturbation is perpendicular to that plane. The plane $\theta^*=\pi/2$ thus also represents the equatorial surface. The equatorial field intensity B_o is given by

$$B_o = B_E \left(\frac{R_E}{r_o^*}\right)^3 \left(1 + \frac{3}{2}\frac{G_3^o}{B_E}\left(\frac{R_E}{r_o^*}\right)^2\right) \qquad (2.73)$$

Since according to Table 2.7 $G_3^o>0$, the resulting field on and near the equatorial surface is subjected to a compression of radially decreasing magnitude. A constant-B drift contour corresponding to a 90° pitch angle particle is a concentric circle in the $\theta^*=\pi/2$ plane. For particles mirroring on the equator, the equation of the drift contour is

$$r_o^* = R_E L \left(1 + \frac{1}{2}\frac{G_3^o}{B_E} L^{-2}\right) \qquad (2.74)$$

where

$$L = \left(\frac{B_E}{B_O}\right)^{1/3} \qquad (2.75)$$

is McIlwain's L value (2.72) for particles mirroring at an equatorial point (I=0), where the field intensity is B_O. The (3,0) term is azimuthally symmetric; hence it cannot lead to shell splitting.

It follows from eq.(2.74) that McIlwain's L value will no longer represent the exact distance from the magnetic centre to the equatorial point of a field line. Since $1/2\ G_3^O/B_E=0.011$, according to Table 2.7, an equatorially mirroring particle corresponding to a given L value will drift on a circular contour that lies farther away from the magnetic centre than in the case of a pure dipole field. Moreover, contrarily to what happens in a pure dipole field, the value of L will vary along a given field line.

Roederer (1970) has shown that as a result of the (3,0) term perturbation, the L value will decrease slightly as one moves away from the equator along a field line. Conversely, constant-L surfaces (or lines, in a given meridian) do not represent drift shells (or field lines) any more . In spite of all these small perturbations L does not lose its value as an invariant parameter to describe trapped-particle fluxes.

Finally, it is interesting to note that the secular variation of G_3^O is a gradual decrease (of about 3.6 nT/year). This will contribute even further to enhance the effect of the secular decrease of the main dipole moment on inner-belt protons (inward displacement) illustrated in Fig.2.14. Interestingly enough, it can be shown (Schulz and Paulikas, 1972a) that there is no

particle energization associated with the gradual decrease of G_3^o (the condition ϕ = const yields to secularly contracting drift shells that happen to preserve their equatorial B value).

In summary, the (3,0) octupole term in the geomagnetic field expansion is responsible for an azimuthally symmetric compression of the field on and near the equatorial surface with no shell splitting. McIlwain's L value no longer correctly represents the distance to the equatorial point of a field line; it falls short by a value that can be determined from (2.72).

The most 'interesting' term from a particle-trapping point of view is the (3,2) octupole. Figure 2.19 schematically shows the corresponding field perturbation. The equatorial surface coincides with the $\theta^*=(\pi/2)$ plane, and the resulting field appears compressed or expanded in alternating longitudinal sectors. The magnetic-field intensity on the equatorial surface is given by

$$B = B_E \left(\frac{R_E}{r_o^*}\right)^3 \left[1 - \frac{(15)^{\frac{1}{2}}}{2} \frac{C_3^2}{B_E} \left(\frac{R_E}{r_o^*}\right)^2 \cos 2(\phi^*_o - \phi_3^{*2})\right] \tag{2.76}$$

with

$$C_3^2 = [(G_3^2)^2 + (H_3^2)^2]^{\frac{1}{2}} = 0.01714 \text{ Gauss}$$

$$\phi_3^{*2} = (1/2) \arctan \frac{H_3^2}{G_3^2} = (1/2) \arcsin \frac{H_3^2}{C_3^2} = 60.2^\circ$$

The equation of the drift contour of an equatorial particle corresponding to a given L value (2.75) is therefore

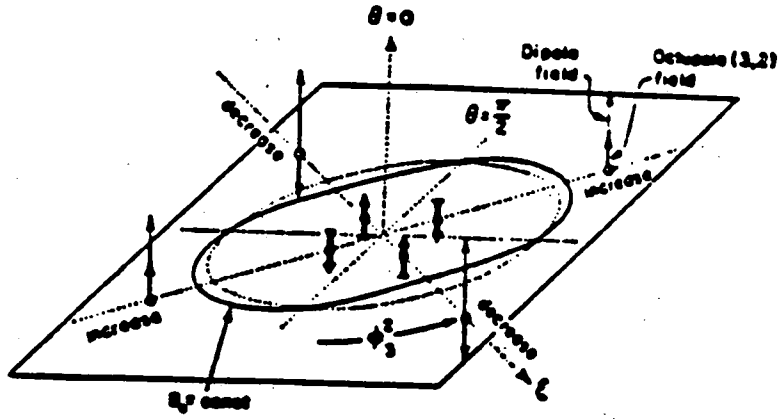

Fig.2-19. Shematic view of the effect of the (3-2) octupole term on the drift contour of an equatorial particle (after Roederer, 1972).

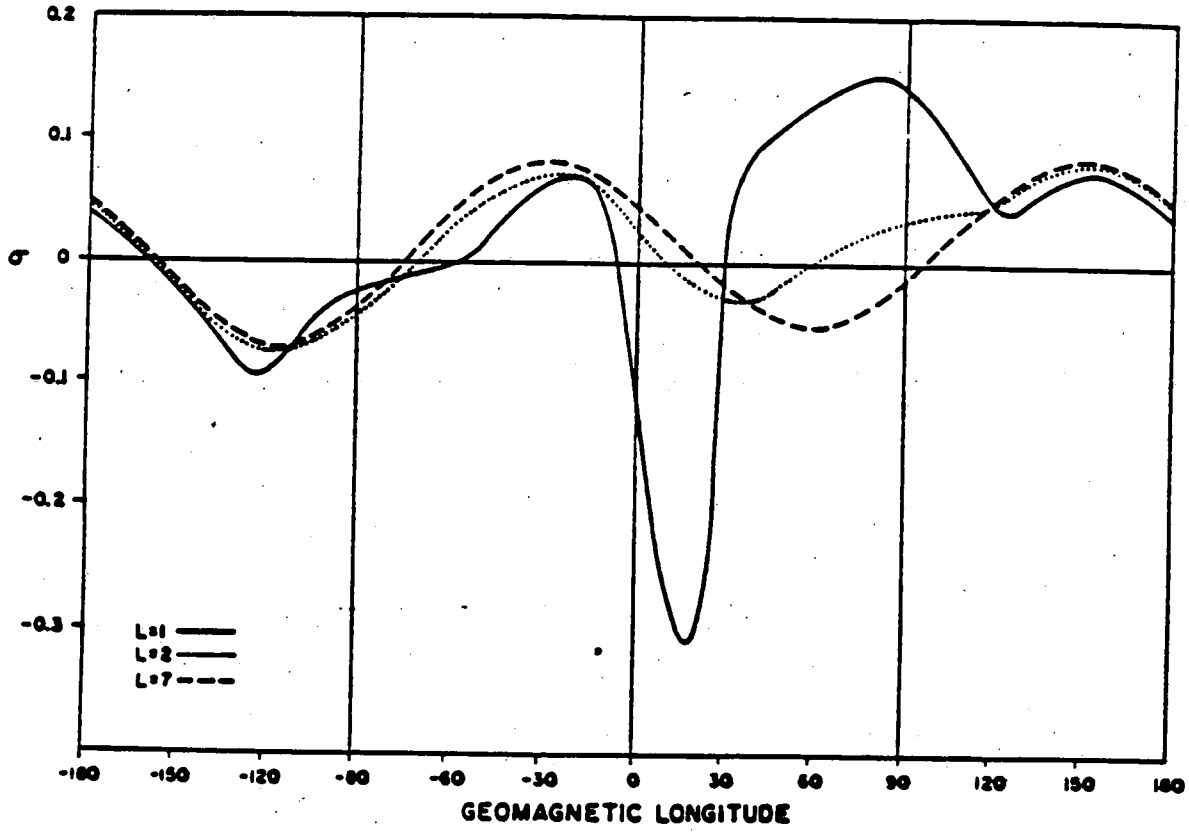

Fig.2-20. Dependence with geomagnetic longitude of the parameter r for different L values. r is a measure of the effect if static field perturbations on trapped particles. Notice the two anomalies at low L values, at longitudes corresponding to the South Atlantic and South Africa (after Roederer et al.,1972).

$$r^*_o = R_E L \left[1 - \frac{(15)^{\frac{1}{2}}}{6} \frac{C_3{}^2}{BE} L^{-2} \cos 2(\phi^*_o - \phi^{*2}_3)\right] \qquad (2.77)$$

The equation is that of a slightly eccentric ellipse with its axes oriented along $\phi_3{}^{*2}$ and $\phi_3{}^{*2}+(\pi/2)$ (Fig.2.19). McIlwain's L value again does not represent the distance to the equatorial point of a field line when the dipole is perturbed by a (3,2) octupole.

Since The quantity $\partial^2 B/\partial s^2$ is dependent on $\phi_o{}^*$, we now will have shell splitting. The (3,2) octupole term is thus the first term in the multipole expansions (2.66) or (2.67) to cause first-order shell splitting. It has been shown by Roederer et al.(1972) that the second-order shell splitting caused by the (2,2) quadrupole, though having the same L dependence and nearly the same phase, is an order of magnitude smaller than that of the (3,2) term.

Roederer (1972) has shown that the maximum possible radial displacement of a particle whose mirror point is scattered from, say, the equatorial value B_{oi} to B_m is given by

$$|\Delta r_{max}{}^*| = \frac{23(15)^{\frac{1}{2}}}{54} \frac{R_E}{L} \frac{C_3{}^2}{B_E} \left(1 - \frac{B_{oi}}{B_m}\right) \qquad (2.78)$$

For L=1.25, B_{oi}=0.1578 Gauss and B_m=0.2345 Gauss (values corresponding to a L,B_m ring dipping to 125-km altitude in the South Atlantic anomaly), we obtain $\Delta r_{max}{}^*$=152 km. This is an appreciable amount when compared to the atmospheric scale height (33km) at these altitudes.

According to Roederer et al.(1972), the octupole (3,2)

term drift shell splitting may contribute to the observed increase toward low L values of the radial diffusion coefficient of trapped electrons (Newkirk and Walt, 1968; Farley, 1969). Indeed, pitch-angle scattering will be accompanied by radial diffusion whenever there is a shell splitting (i.e. whenever a change in pitch angle causes a change in particle shell (Roederer, 1968)). The considerable enhancement of atmospheric Coulomb scattering of electrons toward lower L shells, in association with an increase of octupole shell splitting eq.(2.78), may thus contribute to an upturn of the radial diffusion of electrons as they approach the lower edge of the radiation belt.

Finally, the (3,2) term also causes a variation of L along field lines. Roederer (1972) has shown that the variation of L along a field line is given by

$$\left(\frac{\partial L}{\partial B_m}\right)_{fl} = \frac{2(15)^{\frac{1}{2}}}{27} \frac{C^2{}_3}{B_E} L^2 \cos 2(\phi_o{}^* - \phi_3{}^{*2}) =$$

$$= 0.0513\ L^2 \cos 2(\phi_o{}^* - \phi_3{}^{*2}) \qquad (2.79)$$

The longitudinal amplitude of this variation is an order of magnitude larger than the corresponding (3,0) effect . There are two sectors in which $\partial L/\partial B_m|_{fl}$ is positive ($105.2^\circ \leq \phi \leq 195.2^\circ$ and $285.2^\circ \leq \phi^* \leq 15.2^\circ$); it is negative otherwise.

iv. Higher multipole terms (n≥4)

1. If n + m is even, the equatorial surface is warped (with longitudinal periodicity of order m); a particle drift shell is accordingly distorted along a N-S direction, but its equatorial trace still remains equidistant from the magnetic centre (to the first order in the corresponding expansion coefficient), and there is shell degeneracy.

2. If n + m is odd, the equatorial surface coincides with the $\theta^*=(\pi/2)$ plane, particle drift shells have N-S symmetry but are distorted radially (with longitudinal periodicity of order m), and shell splitting to the first order occurs.

There is no point in analyzing each higher term individually. It is the collective action of all higher-order terms that really counts. A convenient and comprehensive way of examining the collective effect on trapped-particle shell distortion is to compute the quantity $\partial^2 B/\partial s^2$ along the drift contour of an equatorial particle (constant-B contour). Figure 2.20 shows numerically computed results (Roederer et al., 1972) for L=1, 2 and 7, with L defined by eq.(2.75). Actually, what is represented in Figure 2.20 is the quantity

$$\sigma = L^2 \left(\frac{\partial^2 B/\partial s^2}{\partial^2 B/\partial s^2|_{dipole}} - 1 \right) \qquad (2.80)$$

For L=7, the curve indicates that only the octupole (3,2) effect remains in action at that distance. (Naturally, at such a high L value, neglecting external sources leads to a very unrealistic field description).

At L=2, an appreciable deviation appears at longitudes corresponding to the African continent, and at L=1 there is in addition a large distortion over the South Atlantic. One calls these deviations the 'true' South African and South Atlantic (or Brazilian) Magnetic Anomalies, respectively. The South Atlantic anomaly is narrower in longitude and decays faster than the South African anomaly as one moves out radially. It can be shown (mainly from phase angle $\phi_n{}^{*m}$ considerations in the eccentric-dipole coordinate system) that the main terms responsible for these anomalies are (in order of importance) (5,4) and (4,3) for the South African anomaly

and (6,5) and (4,3) for the South American anomaly. It should come as no surprise that these 'true anomalies' lie near places where particle shells have their closest approach to the Earth's surface, and that at the opposite longitude the higher-multipole field perturbations are at a minimum.

Figure 2.20 interpreted in combination with expression (2.53) shows that shell splitting still remains fairly small for the 'full' internal-field expansion and that the octupole (3,2) term provides the main contribution, except for the two longitude intervals in the anomalies, at low L values.

As regards the radial distortion of drift shells, one finds essentially the same result : the octupole (3,2) term provides the main effect (elliptical deformation), except for two extra 'bumps' at low L, one inward (over the South Atlantic) and the other outward (over south Africa). The inward bump contributes even further to enhancement of the lowering of mirror points over the South Atlantic. Roederer et al. (1972) show that all these effects are strongly correlated in phase with equatorial surface distortions caused by the even n+m terms of expansion (2.56) or (2.57).

2.2.2 The External Geomagnetic Field.

The internal multipoles can be neglected beyond L≈3-4. In that region of space, even the centered dipole is a satisfactory approximation of the internal field. What complicates the picture beyond L≈4 is the effect of external currents. We do not have a good, trustworthy representation of the resulting field perturbations, as we do have for the internal field. Actually, we may never have one, because of complicated time variations that are present practically at all times.

One can identify three main current systems in the undisturbed outer magnetosphere, a current system on the magnetospheric boundary or magnetopause, one in the neutral sheet of the geomagnetic tail (the surface that separates the two lobes of the tail), and a current system around the Earth ('Ring Current') flowing in the equatorial (minimum B) surface. During geomagnetic storms and substorms, substantial changes occur in these systems, in addition to the appearance of field-aligned currents flowing out of and into the lower ionosphere.

To conduct a study of trapped particle motion in the outer magnetosphere, simplified external field models had to be devised (e.g. Mead, 1964; Olson, 1969). In the Appendix A of TN1 we review the Mead-William (1965) model; in Appendix B of TN1 the Olson-Pfitzer (1974) model; in Appendix C of TN1 the Mead-Fairfield model; in Appendix D of TN1 the Tsyganenko and Usmanov (1982) model whose latest update has been published by Tsyganenko (1989). The latter most elaborate analytical model representation of the magnetosphere field is based on the largest amount of IMP and HEOS experimental data. The input parameters of this TU model simulate the effect of solar wind conditions and geomagnetic activity on the external current systems.

We restrict this discussion to a region of the magnetosphere in which the effects of magnetotail currents and of the diurnal and seasonal variation of the tilt of the geomagnetic axis with respect to the Earth-Sun line are small. Under these conditions we can still use the system of geomagnetic or eccentric dipole coordinates. Olson's (1969) calculations show that, to some degree, the whole magnetopause current system is 'locked' to the Earth's dipole; 'gliding' around on that surface so as to maintain its two vortices (the neutral points) at nearly the same angular position with respect to the magnetic axis. The result is, indeed, that diurnal and seasonal dipole tilt effects are small within, say 5-6 Earth radii.

The 'first order' effects of the external current systems are (1) a uniform field compression, (2) a non-uniform compression of the dayside magnetosphere and a non-uniform expansion of the nightside. More explicitly, the ring current alone produces, in first approximation, a uniform field expansion inside its action radius; the magnetopause current produces both a uniform compression everywhere and the non-uniform day-night compression-expansion.

(i) Uniform field compression or expansion.

A uniformly compressed or expanded dipole field derives from a scalar potential

$$V = R_E \left[G_1^o \left(\frac{R_E}{r}\right)^2 \cos\theta + b_1 \frac{r}{R_E} \cos\theta \right] \qquad (2.81)$$

(Since no confusion with geographic coordinates is possible in this section, and since geomagnetic and eccentric dipole coordinates practically coincide for $r > 3\text{-}4\ R_E$, we drop the asterisk from our eccentric dipole coordinates). b_1 is a coefficient that physically represents the intensity of the uniform field. The resulting field on the equatorial surface is, of course, azimuthally symmetric

$$B_o = B_E \left(\frac{R_E}{r_o}\right)^3 \left[1 - \frac{b_1}{B_E} \left(\frac{r_o}{R_E}\right)^3 \right] \qquad (2.82)$$

B_E is equal to $-G_1^o(>0)$. Notice that $b_1<0$ leads to a negative component B_θ (i.e. to a northward directed field on the equatorial plane), of the same direction as that of the main dipole. $b_1<0$ thus represents a compression, $b_1>0$ an expansion of the dipole field.

Drift contours of equatorial particles are circles,

and there is no shell splitting. However, McIlwain's L value does not represent the exact distance from the magnetic centre to the drift contour anymore. In fact, the radius of a constant-B circle is now

$$r_o = R_E\, L \left(1 - \frac{b_1 L^3}{3B_E} \right) \qquad (2.83)$$

where L is related to B_o by eq.(2.75). If the uniform field perturbation is due to a ring current, b_1 is positive (and equal to the Dst index) and represents a field expansion inside the current radius.

An important effect to analyze is that of a time variation of b_1 (for instance, the decay of ring current intensity). Let us assume that this variation occurs on a time scale long enough to be compared to a drift period. I and B_m will no longer be conserved and one must turn to the conservation of the adiabatic invariants.

Instead of the rather unfamiliar quantity Φ in eq.(2.52), Roederer (1970) redefines a 'truly invariant' pair of coordinates L^* and B^*_m that can be used even when slow time variations are present . Roederer (1970) defines the new L^* as the radial distance (in R_E) to the equatorial trace of that shell on which a given particle would be found, if all non-dipole perturbations of the trapping field are slowly (adiabatically) turned off. Notice that, according to this definition, the L^* value of a given particle remains constant, no matter what happens to the magnetic field, provided it happens adiabatically (conservation of all three invariants). Since in this 'reference' dipole field there is a simple relation between L^* and the third invariant Φ, which is conserved throughout the above adiabatic transformation, we have for the new 'truly invariant' L^*

$$L^* = \frac{2\pi B_E R_E^2}{|\Phi|} \qquad (2.84)$$

This quantity should not be confused with McIlwain's L value; it is identical to the latter only in a pure, static dipole field. In general, L^* will depend on the initial coordinates of a particle (e.g., equatorial crossing and pitch angle). The new 'reference mirror field' B_m^* is the field intensity at which the particle would mirror after the non-dipole terms have been turned off. Its determination is not staightforward. Its value must be determined by means of conservation of the invariant, K, and finding the solution of

$$K = R_E \, L^* \, (B^*_m)^{\frac{1}{2}} \, Y[(1 - B_E/(L^{*3} B^*_m))^{\frac{1}{2}}] \qquad (2.85)$$

The energy or momentum of a particle will also have changed in this transformation, and so will the directional flux of a particle distribution according to Liouville's theorem.

The flux invariant of a near-equatorial particle injected into a uniformly compressed (or expanded) field at a point r_{oi} is given by

$$|\Phi| = \frac{2\pi B_E R_E^3}{r_{oi}} \left[1 + \frac{1}{2} \frac{b_1}{B_E} \left(\frac{r_{oi}}{R_E} \right)^3 \right] \qquad (2.86)$$

This expression is independent of the initial pitch angle in the case of a uniformly compressed field. Hence, according to eq.(2.84)

$$L^* = \frac{r_{oi}}{R_E}\left[\,1 - \frac{1}{2}\,\frac{b_1}{B_E}\left(\frac{r_{oi}}{R_E}\right)^3\,\right] \qquad (2.87)$$

For B_m^* one obtains

$$B_m^* = \frac{B_E}{L^{*3}(1 - \cos^2\alpha_{oi})} \qquad (2.88)$$

Mapping an experimentally determined near-equatorial particle in B_m^*, L^* coordinates should lead to a representation that is independent of slow (adiabatic) time variations of the uniform b_1, i.e. independent of slow ring-current variations (true only for near equatorial particles trapped inside the radius of ring current). Notice, that indeed, L^* is equal to McIlwain's dipole L value r_{oi}/R_E when the compression or expansion is turned off (b_1=0).

ii) Magnetopause current effects.

The magnetopause current system imposes a day-night asymmetry to the magnetospheric field. For this reason it is more convenient to describe the field in a coordinate system that, although it still has the θ=0 axis oriented along the magnetic axis, has the reference meridian locked to a fixed local time (rather than to a fixed point on the rotating Earth). Let us define the θ=0 meridian as the magnetic meridian that contains the Earth-antisun line (local midnight).

A first-order description of the magnetospheric field potential (Mead, 1964) is given by

$$V(r,\theta,\phi) = R_E \left[G_1^{o} \left(\frac{R_E}{r}\right)^2 \cos\theta + b_1 \frac{r}{R_E} \cos\theta + \tfrac{1}{2} b_2 \left(\frac{r}{R_E}\right)^2 \sin 2\theta \cos\phi \right] \qquad (2.89)$$

G_1^{o} (<0) is the first coefficient in Table 2.7 and b_1 and b_2 are two coefficients that govern uniform compression (b_1<0) and day-night asymmetry (b_2>0), respectively. They depend in a specified manner on the stand-off distance, R_s (distance to the subsolar point of the magnetopause in Earth radii). A set that fits experimental field measurements reasonable well near the geomagnetic equator for r<7 R_E is (values in nT)

$$b_1 = -25 \left(\frac{10}{R_s}\right)^3 \qquad (2.90)$$

$$b_2 = 2.1 \left(\frac{10}{R_s}\right)^4 \qquad (2.91)$$

Notice the strong dependence with R_s. R_s=10 corresponds to a 'normal' state of the magnetosphere.

The magnetic field intensity B_o on the equatorial plane, derived from the above potential is

$$B_o = B_E \left(\frac{R_E}{r_o}\right)^3 \left[1 - \frac{b_1}{B_E} \left(\frac{r_o}{R_E}\right)^3 - \frac{b_2}{B_E} \left(\frac{r_o}{R_E}\right)^4 \cos\phi_o \right] \qquad (2.92)$$

The equatorial trace of the drift shell generated by a particle injected at point r_{oi}, ϕ_{oi} with a pitch-angle cosine μ_{oi} (μ_{oi}^2<<1)

$$r_o = r_{oi} - \frac{R_E}{3}\frac{b_2}{B_E}\left(\frac{r_{oi}}{R_E}\right)^3 \left(1 - \frac{43}{18}\mu_{oi}^2\right)(\cos\phi_o - \cos\phi_{oi}) \qquad (2.93)$$

Let us first analyze this expression for the case of equatorial particles ($\mu_{oi}=0$). In that case, equation (2.93) represents constant-B contours. The drift contours of equatorial particles are eccentric circles that have their closest approach to the Earth on the night-side; their eccentricity increases rapidly with radial distance and with magnetospheric compression.

Finally, it has been found by Roederer and Schulz (1969) that for $R_S=10$, the quantity $\partial^2 B/\partial s^2$ goes through zero at the noon meridian at $r_o=6.9\ R_E$ becoming negative beyond. This critical distance increases and approaches the magnetospheric boundary, as one moves away from the noon meridian toward dawn or dusk. This obviously means that beyond a certain distance on the dayside, the $\theta=\pi/2$ plane is no longer a minimum-B surface. In that region, field lines attain their minimum B-value at two points situated at a certain finite latitude on both sides of the $\theta=\pi/2$ plane. Again, since the field approximation used here starts breaking down at these distances, more realistic field models must be used to explore the actual geometry of these 'minimum-B pockets' (Antonova and Shabansky, 1968, Roederer, 1969).

For a particle injected at midnight ($\phi_{oi}=0$) with $\mu_{oi}\neq 0$, the maximum radial deviation from a $\mu_{oi}=0$ orbit occurs at noon ($\phi_o=0$) and is given by

$$\Delta ro = ro(\mu_{oi}\neq 0) - ro(\mu_{oi}=0) = \frac{43}{27} R_E \frac{b^2}{B_E} \left(\frac{r_{oi}}{R_E}\right)^3 \mu_{oi}^2 \qquad (2.94)$$

This is a positive quantity, which means that if the pitch angle decreases at the midnight point (μ_{oi} increases), particle shells will reach out farther on the dayside. For a particle injected at noon ($\phi_{oi}=\pi$), the situation at midnight is reversed; when the pitch angle decreases at noon, the shell is displaced inward (toward the Earth) at midnight.

The effects of shell splitting in the external magnetic field have been analyzed extensively by Roederer (1967), Stern (1968), Fälthammar and Walt (1969), Roederer and Schulz (1969), Kosik (1971), Schulz (1972), Luhman and Schulz (1979), Bass et al. (1986).

iii) Slow time variations of the external field.

The expansion parameters b_1 and b_2 depend on the stand-off distance, R_S. This parameter may vary considerably with time. There are essentially two types of variations : (1) decreases of R_S caused by an 'erosion' of dayside boundary field lines that are carried into the geomagnetic tail by interaction with a southward-directed interplanetary magnetic field; (2) decreases (or increases) of R_S caused by changes in solar-wind dynamic pressure. The latter may lead to substantial changes of the magnetospheric field and, hence, to time variations of trapped particle shells. One may again use the set of coordinates L^*, B_m^* to obtain truly invariant labels of trapped particles.

In the absence of diffusion, sources and losses, particle flux mapping in this B_m^* - L^* space would lead to

a stationary representation. Of course, particle energy and directional flux must be accordingly transformed to ensure conservation of M and K.

Even for a static field configuration, L^* and B_m^* are useful invariant particle coordinates. To show this, one can analyze the B_m^*, L^* coordinates of trapped particles sampled by a directional detector on board a synchronous orbit satellite (r_{oi}/R_E=6.6=const). Roederer (1970) field the Mead-Williams model (Williams and Mead, 1965), and computed L^* and B_m^* numerically. Figure (2.21) shows the portions of B_m^*, L^* space that are scanned by such a detector, for different local times and different pitch angles.

First, notice in Figure 2.21 that, for pitch angles near 50°, the local-time dependence is very small, pointing to axisymmetric shells. For any other arbitrary but fixed pitch angle, notice the particular way the detector scans the invariant B_m^*, L^* space. This will lead to a local-time variation of the directional particle flux at synchronous orbit. Assuming that the particle-flux distribution in the invariant $B^*_m - L^*$ space decreases in intensity with both B_m and L^*, it is easy to make predictions on the local-time variation of the pitch-angle distribution. In particular, equatorial (α_o = 90°) particles will have a maximum flux at noon and a minimum flux at midnight. This diurnal variation will decrease in amplitude for α_o < 90° and will practically disappear for α_o ≈ 45-50° particles. For smaller pitch angles its phase will reverse : maximum fluxes will be attained at midnight. The over-all result is a pitch-angle distribution that changes from a single-peaked form at noon (with a maximum at 90°) to a double-peaked 'butterfly-type' form at midnight (with a secondary minimum at 90°). All this has been verified experimentally (e.g. Stevens et al., 1970; Pfitzer et al. 1969).

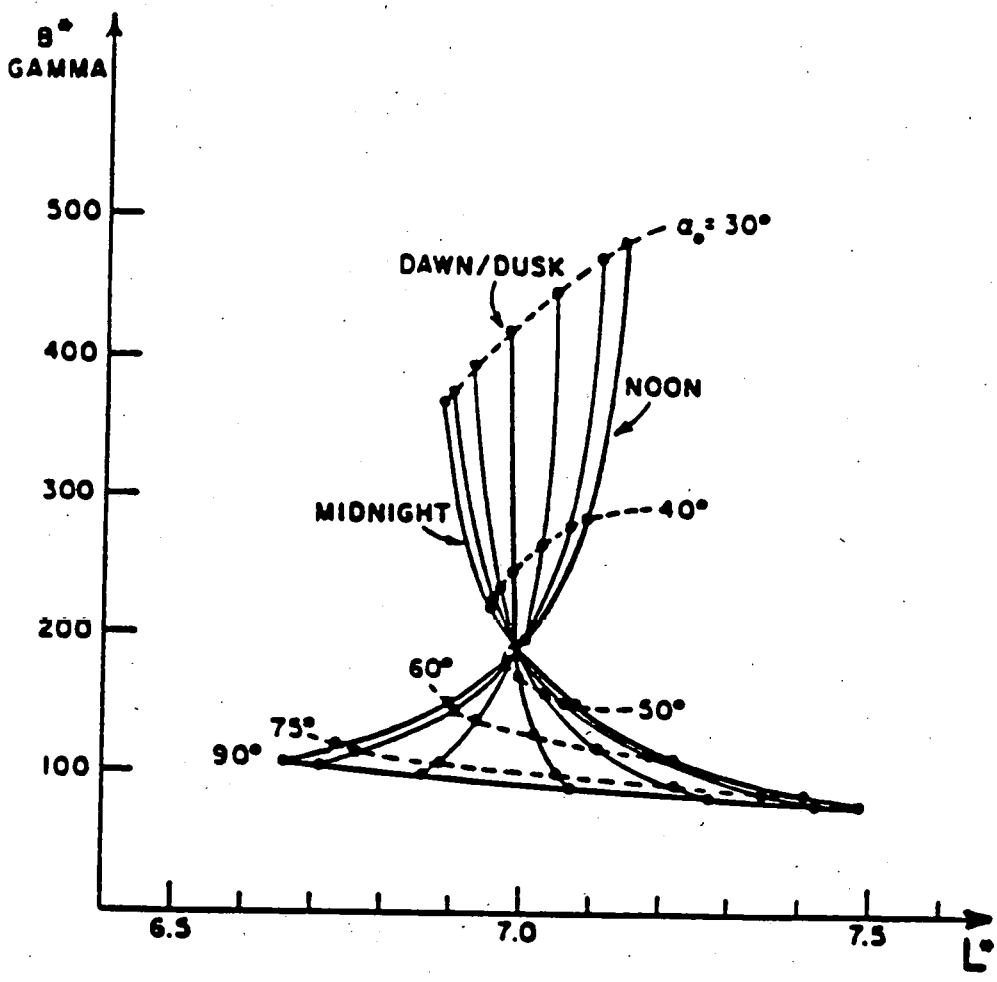

Fig.2-21. Coordinates in invariant B^*-L^* space of particles registred with a directional detector in geosynchronous orbit (after Roederer, 1972)

For an increased magnetospheric compression (smaller R_S), the whole diagram of Figure 2.21 shifts toward higher L^* values and spreads out in L^* coverage. Still, all constant local-time curves cross each other for nearly the same pitch-angle range (45 - 50°). For a compressed magnetosphere, directional particle fluxes at the synchronous orbit will thus be generally lower, but their local-time variations will be amplified. The usefulness of generalized L*,B* coordinates like those discussed above is clear and indisputable. There are, however, practical problems in applying this concept to map trapped radiation fluxes (i) the first is how to compute L* in the case of more realistic magnetic field models like that of Olson and Pfitzer (1976) or of Tsyganenko (1989) (ii) the second difficulty will arise when each group of experimentalists will adjust its magnetic field model (i.e. parameters like b_1 and b_2 in the Mead model) in a manner which may fit their own magnetic field measurements at a given time, and in a given region of space; indeed their model parameters will most likely be inconsistent with the fit made by other groups of experimentalists. There is indeed a danger of more confusion than greater unification.

Considerable reference is made in this section to the reviews of Roederer (1972) as well as to the monographs of Schulz and Lanzerotti (1974). Material from these documents was used liberally in preparing this final report.

2.3 MODELS OF TRAPPED RADIATION FLUXES

A comprehensive description of the distribution of omnidirectional fluxes of trapped protons and electrons, given respectively by the NASA AP8 ad AE8 models, has been presented in Chapter 4 of TREND's TECHNICAL NOTE 1. No one else than Jim Vette, the father of these models, could have presented a better description and overview of the modelling efforts undertaken by NASA at NSSDC/WDC-A-R&S since the 60's. An interesting historical review of the development of the series of NSSDC models has been given in section 4.4 of TN 1. It would be too long to repeat all this within this final report. We will only recall here the main features of the AP8 (for the proton environment) and AE8 (for the electron environment).

2.3.1 The AP8 model

This model was issued in December 1976 (Sawyer and Vette, 1976). It resulted from the analysis of 34 instruments that partially covered the time period from July 1958 to June 1970. It is a static model except for the solar cycle dependence afforded by the incorporation of AZUR data and the work of a number of investigators who studied the processes involved in producing the effect. This solar cycle effect is too small to warrant trying to describe changes on a year basis unless work like that of Blanchard and Hess (1964) or others would be revisited. Otherwise it is a static model.

Time variations that have been observed are pointed out in the document but it was not possible to incorporate these into the model. In that regard efforts are needed in the future to study these effects in more depth. This is a recommendation made by TREND.

The incorporation of the model into a one large numerical matrix has been convenient from a use standpoint now that computer memories are large enough. However, some of the feel for the data has been removed. Local time effects were not studied since only the trapped particles with energies below 10 MeV reach the regions beyond 3 R_E, where protons show local time effects. TREND made the recommendation to pursue this study of local time effect in future modelling efforts.

The production of differential forms (in pitch angle and energy)are possible and a matrix for unidirectional flux was made during the production of AP8. The differential forms do not have the same validity as the basic model; the numerical derivatives taken may produce some peculiar bumps, since the models were not built in a way that insures smooth derivatives.

2.3.2 The AE8 model

The AE-8 model was issued in its computer form around 1980. The model is a synthesis of three previously issued models and the incorporation of new data. The new data were incorporated to improve the model in several respects. The energy spectrum in the outer zone above 2 MeV was found to be low relative to the ATS 6 and the Azur data. Using the data from all four experiments, the whole distribution above 2 MeV was changed. The B dependence is given by the function G (Singley and Vette, 1972a), which is normalized to 1 at the magnetic equator, where

$$G(B/B_o,L) = (B/B_o)^{-M} \{[B_C/B_o - B/B_o]/[B_C/B_o - 1]\}^{M+1/2}$$

Note that B_C (B cutoff) is the value where the omnidirectional flux goes to zero. The atmospheric cutoff for AE-8 models is strictly empirical since there are many effects that result in particles being lost into the atmosphere. AE-4 had a low altitude cutoff that was based

on the atmosphere and had been conservatively chosen where B_C occured when h_{max} = 200 km. The parameter h_{max} is the maximum altitude that the particle reaches in drifting around the Earth for fixed B,L.

Thus for AE-8

$$B_C/B_o = \begin{cases} 0.7000(L/R_e)^{3.4206} ; & 1.2R_e<L<3.0R_e \\ 1.4589(L/R_e)^{3.0495} ; & L<3.1R_e \end{cases}$$

The AE-8 model has an inner zone with energies ranging from 0.04-4.0 MeV and an outer zone with electron energies from 0.04-7.0 MeV. If the highly energetic electrons observed by Baker et al.(1986) at the geostationary orbit are probably from Jupiter, they should not be trapped and should then be treated in a similar fashion to that used for solar protons.

The solar cycle changes are the same as the previous models used to construct AE-8. The L coverage is 1.2 to 11 R_e. The basic product that was distributed by NSSDC is the matrix of omnidirectional integral flux as a function of energy, B/B_o, and L.

The local time dependence has been averaged out in this matrix form, since most satellites would average out the effect with time in orbit. Adding a new variable to the matrix would increase its dimensions by a factor of 5, which places a burden on the storage capacities of users, particularly those using personal computers. The model remains quasi-static.

2.3.3 Ill use of environmental models,errors and inaccurracies.

Like any other model in geophysics the AP8 and AE8 models have their limitations, but it must be admitted that no other space agency has yet produced any trapped environmental model which is better than those of NSSDC. A number of critiques against these models have been formulated and published in the recent years. These critiques have been summarized in Chapter 1 of this report and will not be repeated again.

Some papers indicate that the fluxes observed at low altitude with recent spacecraft like DMSP are factors of 2 or 6 smaller than those predicted by the NASA models. There can be several reasons for these differences. First, one may argue that the old data sets used to build the models are in error or incorrect. This blame for systematic errors in the measurements would than go to the community of PI's. In addition to wrong calibrations, instruments failures, there could be contamination of proton flux measurements by high Z particles. This latter effect could have polluted the AP8 model. Other data including the S^3 data from Fritz could for instance be studied to improve this situation.

Systematic errors in the model are not tractible to identify. Those data sets with problems stand out clearly in disagreement with the overall body of data. The clarification as to the cause of those problems may never be done. The OV1-19 electron data shown in fig 2-22 as well as other measurements and AE-8 model predictions, caused concern and confusion for several years before a resolution was at hand. But, even if we admit that there are a few data sets wich lack the expected high quality and reliability, it is unlikely that the average flux values of

the NASA models obtained by averaging many sets of data can be drastically in error because for these particular reasons.

Assuming, therefore that most of the old data sets (as well as the new DMSP, LANL, IUE data sets) are correctly calibrated, and, that they have been analysed in a consistent way by all the different PI's groups, the observed difference between the recent observations and the model predictions can result either

(1) from a true secular or solar cycle change in the population of trapped particles between the 60-70's and the more recent epoch; indeed the 'magnetospheric weather (or climate)' might have changed since the time the first data sets used to build these models were taken; or

(2) from the spurious 'secular variation' effect described above due to an ill-use of the NASA modls and resulting in unrealistic values for the predicted radiation doses; indeed, the over pessimistic predictiond could partly be due to an improper choice of epoch for the IGRF field used when B-L coordinates are determined for the new data sets,(i.e. BLTIME not taken equal to 1960; see discussion below); or

(3) from statistical fluctuations around the average values given in the AE8 and AP8 models.

This latter possibility induces the question of the need for standard deviations of the omnidirectional fluxes not provided with AE8 nor AP8 originally. Although these statistics where given in earlier NASA models like AE4, TREND recommends to provide to the future users of UNIRAD, updated values of the standard deviations for the logarithm of the omnidirectional fluxes at all energy and at all pairs of B-L values. Not only the average of the logarithm

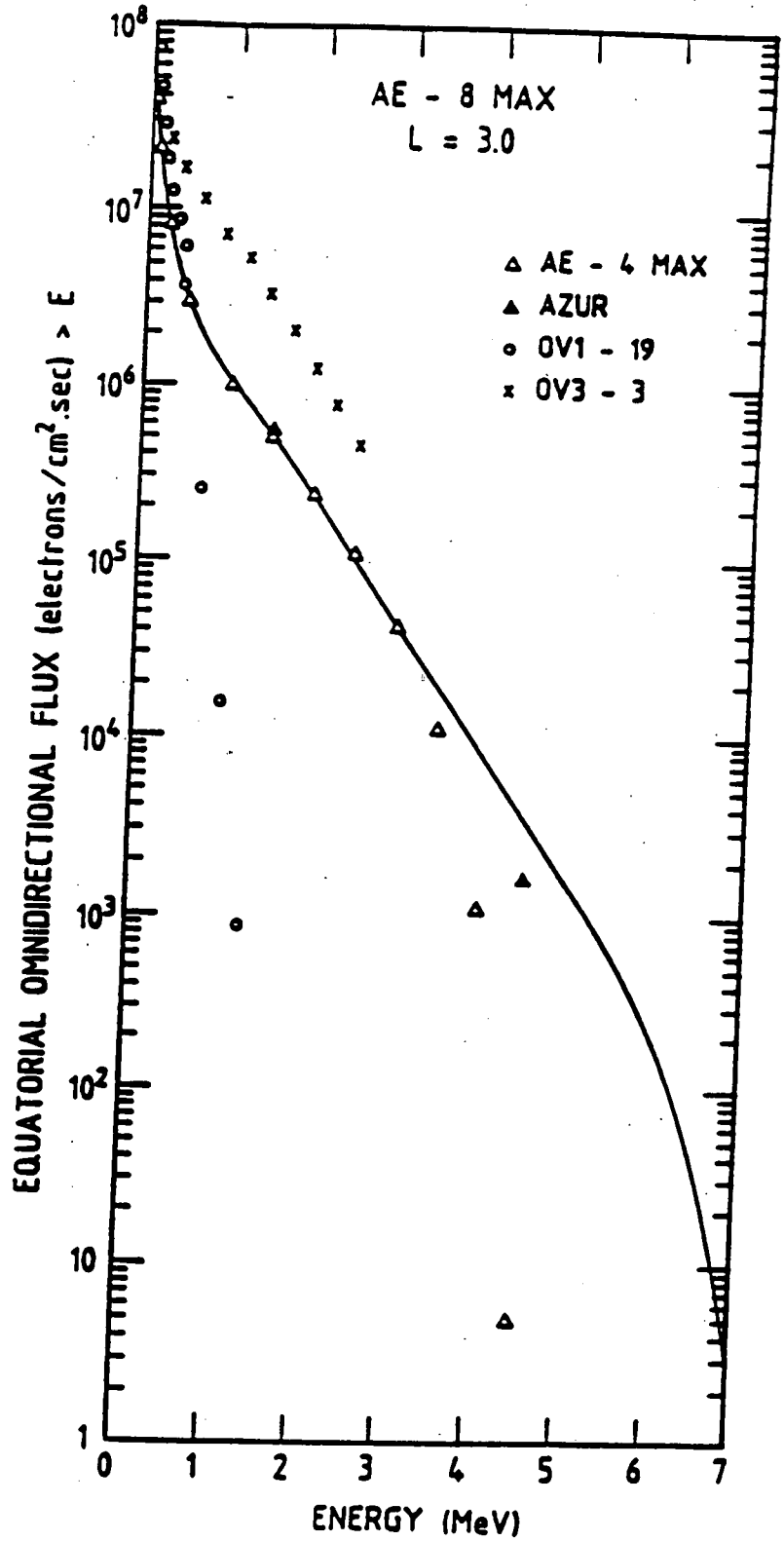

Fig.2-22. Comparison of AE8 and data at L=3.0.

of the omnidirectional flux should be given but the value of the standard deviation should also be given in new models.

TREND recommends also that future trapped radiations fluxes for the regions close to geosynchronous orbit and beyond be built with a proper magnetic field model including the external magnetic field components. It is also argued by TREND that the local time coordinate should be st9ored as an independent variable in the data sets. Although it is expected that with a proper external magnetic field model to compute B-L coordinates the local time dependence will disappear, there will remain a residual LT effect for several reasons; shell splitting is one mentionned above; another reason is that the external magnetic field model used for B-L the mapping is not necessarily realistic for the data sets analysed. Therefore, in order to identify these residual LT effects the new data and new environmental models should possibly be organized as a function of LT also.

2.4 OUTLINE OF TRENDS CONTRIBUTIONS TO MODEL EVOLUTIONS

In the previous sections a description of the geomagnetic and radiation environment has been presented in order 'to set the stage'. A series of definitions and concepts in this area have been introduced with reference to chapters and paragraphs in TREND's TECHNICAL NOTES where more details are given.

In this final part of Chapter 2 we wish to summarize the main contributions and new ideas proposed by TREND during this study in the area of Earth's radiation modelling. Critiques of existing models are also recalled in a constructive manner. Alternative solutions have been identified and evaluated. The software requirements and developments of these new and alternative ideas will then be presented in Chapter 3.

TREND has suggested new solutions and answered a number of critical questions and issues: e.g.

- What is the precise definition of McIlwain L-parameter? Indeed, the very meaning of L is often misunderstood and misused outside the specialized modelling community!

- Is there a simpler algorithm to compute McIlwain L-parameter?

- What is the meaning and usefulness of alternative generalized L^*-parameters (i.e. 'truly invariant' field line coordinates and Euler's constants)

- Can B-L coordinates still be used at high altitudes where drift shell splitting becomes important i.e. at and beyond geostationnary orbit? How to accomodate for local time variations in trapped radiation at high altitudes?

- Should an external magnetic field model be added to determine B and L at high altitude? Which model to suggest? What are the limitations of such an improvement in modelling the geomagnetic field and in obtaining the associated B-L coordinates?

- How to cope with atmospheric cut-off? What kind of coordinate should be used instead of B and/or L at low altitude where atmospheric effects are important?

- What are the reasons of the spurious secular increase of the low altitude fluxes of trapped particles, when the epoch of geomagnetic field models is extended to the year 2000? How to resolve this issue, which was first emphasized by McCormack (1986)?

- How to cope with the short term but large amplitude variability of outer zone relatistic electrons fluxes? What are the standard deviations of fluxes observed at and below geosynchronous orbit?

- What are the alternative models for prediction of solar flare events? Which model(s) should be implemented in future UNIRAD software?

- What are future requirements for future generations of trapped radiation models?

Let us now consider these different questions one by one and summarize the answers proposed by TREND.

2.4.1 What is the preciese definition of McIlwain L-parameter? How is it calculated?

It is not unusual to see in magnetospheric plasma physics paper : "...let us consider the geomagnetic field line characterized by McIlwain's parameter L = 6 or L'...".

However, this is an incorrect statement since according to its original definition McIlwain's parameter L does not identify a geomagnetic fiels line, but L and B identify a 'drift shell' where B_m is the magnetic field intencity at the mirror point location.

It may be pointed out here, that in McIlwain's original derivation of F, the value B_E (magnetic field intensity at the Earth equation) was assigned the value of 0.311653 Gauss; this value corresponds also to the magnetic dipole moment M at Epoch 1960 in the GSFC interim magnetic field model of Jensen and Cain (1962).

To conclude this section, we wish to emphasize that it is essential to realize that L does not correspond to the actual equatorial distance of the geomagnetic field line as it is sometimes assumed. It is only for a pure dipole that L is equal to this equatorial distance and may be used to characterize a whole magnetic field line. However, for a non-dipole field the whole magnetic field line cannot easily be characterized by a single L-parameter. Indeed, each point along any non-dipole field line is characterized by a different pair of B_m and I values i.e. a different pair of B_m and L values. However, it has been shown by McIlwain (1961) that the values of L for all points along geomagnetic lines computed from a standard IGRF field model, varies by less than 1 % in the inner magnetosphere. As a consequence one should be cautious not to say : "...let us consider the geomagnetic field line characterized by McIlwain's parameter L = 6 or L'...".

2.4.2 Is Hilton's algorithm simpler to compute McIlwain's L-parameter?

Hilton (1971) has found a simpler numerical algorithm to compute L for given values of B_m and I (see above).

This procedure formulated by Hilton is therefore more

straightforward. The error obtained by using Hilton's approximation to determine McIlwain's L-parameter is less than 0.01%.

It is shown in TN1 that the algorithm proposed by Hilton (1971) 'does the same job' as that proposed almost 10 years before by McIlwain (1961), except that the former is simpler to use and to code in FORTRAN. This is the only reason why TREND has recommended to change the method of calculation of L in UNIRAD and to implement Hilton's formula instead of McIlwain's former algorithm.

2.4.3 Should the value of the magnetic moment be changed in the programs for transforming geodetic coordinates to B-L?

It has been argued that it might be more reasonable to compute McIlwain's L-parameter using the value of B_E (or M) from the best available field model for the corresponding Epoch of the measurements (Schulz and Lanzerotti, 1974, p 24). The reason for such a claim was to take into account the secular decrease in the Earth's dipole magnetic moment, M. As a consequence of the secular decrease of B_E and M, the equatorial radii of alldrift shells decrease slightly as a consequence of the conservation of the third adiabatic invariant. Some theoreticians have become sensitive to this issue, and have searched for 'truly invariant' shell parameters like the generalized L^* parameter introduced by Roederer (1970).

The alternative procedure to compute L with BE changing from one Epoch to another, instead of being fixed to 0.311653 Gauss, appears to have more practical disadvantages than it has advantages. In fact, McIlwain (1989,personal communication) has shown that over a period of 25 years the secular change produces a variation of 0.8% in L. This is a small difference compared to other uncertainties associated to any choice of a particular B-

field model or associated to the errors of flux measurements themselve.

Therefore, we share the opinion that changing the value of B_E in the algorithm defining L from one set of data to the other would lead to more confusion than it would resolve problems. Changing B_E would be alike to constantly change the unit of length of a ruler to measure distances at different Epochs! This can certainly be done as long as each PI explicitely informs the community as to which value of B_E he has used to compute the B,L coordinates ; but since an L-parameter should only be regarded as one of the 'LABEL' (or a coordinate) to identify a geographical point or a drift shell, it is reasonable to keep using the same value of B_E all the time. This is a recommendation of TREND.

2.4.4 What is the meaning and use of an alternative generalized L*-parameter?

It can be shown that in the case of a pure dipole magnetic field, the third adiabatic invariant (i.e. the magnetic flux encompased by a drift shell) is related to the value of McIlwain's L-paramater by

$$\Phi = \frac{2\ p\ RE^2 B_E}{L} \qquad (2.95)$$

The inverse relation has been used by Roederer (1970) to assign to each trapped particle a 'truely' invariant L^*-parameter, which characterizes not only a drift shell but the magnetic field lines forming this shell. While McIlwain's L determines (with B_m) a segment of a magnetic field line, the L^*-parameter can be used to identify the magnetic field line as a whole. In other words L^* is the same for each point along a given geomagnetic field line, while this is not the case for McIlwain's L-parameter.

This generalized invariant L*-parameter, looks more satisfactory and appealing to some theoreticians, indeed it is derived from the third adiabatic invariant Φ. When the geomagnetic field moment,(or B_E) experience slow secular changes it is expected that the drift shell shrinks or expands accordingly, and, that L* varies in phase, such that the flux invariant Φ is conserved.

This would be correct provided that all the geomagnetic field variations have characteristic time constants which are much longer than the time period required for the trapped particles to drift around the Earth (i.e. 1500 seconds for a 1 MeV proton or electron). It is not often the case that the geomagnetic field is inactive -unperturbed- for time exceeding 35 minutes, and that this adiabaticity condition is really met. It is therefore illusory to except than Φ remains constant over times comparable to those corresponding to the secular variations of the geomagnetic field i.e. 2000 years (Schulz and Paulikas, 1972). Of course, this limits terribly the usefulness of a 'truely invariant L^*-parameter'.

Furthermore, the actual lifetime of trapped protons and electrons limited by collisions and wave-particle interaction is much smaller than 2000 years, i.e. the characteristic time corresponding to the secular geomagnetic field variation. This has been demonstrated by the decay time of the energetic electrons injected in the region between L = 1.75 and 2 by the Starfish nuclear explosion.

Although an expression of L^* can be obtained for a pure dipole or for a uniformly compressed dipole magnetic field (see Roederer, 1970), however for more realistic geomagnetic field models (e.g., the IGRF or Tsyganenko's external magnetic field model) the calculation of a generalized L^*-parameter is currently beyond grasp. Therefore, it appears that the usage of such a generalized

L^*-parameter is not likely to supersede that of McIlwain's L-parameter.

The same remarks apply of course also to the Euler potentials, which are also interesting theoretical concepts. Northrop (1963) and Stern (1976) have introduced Euler potentials (α and β) as alternative magnetic coordinates. They use a and b as parameters (or coordinates) to label magnetic field lines. These parameters are of course constant all along a magnetic field. This is what makes their conceptual interest and appeal. Furthermore, from the point of view of classical mechanics the (α, β) coordinates are canonical. Finally, Stern (1987) has shown how 'stretch transformations' can be applied to Euler potentials to describe distorted dipole magnetic field lines.

But since these Euler potentials are difficult and cumbersome to calculate in the case of non-dipole magnetic field distributions, these curvilinear coordinates have never been used in practice to represent geomagnetic field lines corresponding to a multipole harmonic expansion like that given by the IGRF, nor for any complex external magnetic field like that of Tsyganenko (1989).

Based on these pragmatic considerations TREND recommends to continue using McIlwain's L-parameter instead of any generalized L^*-parameter, or Euler's potentials for the multipolar geomagnetic field description.

2.4.5 What are the reasons for the spurious secular increases of low altitude fluxes of trapped particles, when the epoch of the geomagnetic field model is extended to the year 2000? How to resolve this issue which was first highlighted by McCormack (1986)?

The solution to this problem was suggested by TREND. Indeed, it was found that a residual secular variation is a consequence of the change of the higher order multipoles

as a function of epoch. It is TREND who draw the attention on the fact that not only the dipole terms (i.e. the value of M) should be considered, but also the higher order terms and their secular variations.

In this respect the quadrupole terms correspond to an eccentric displacement of the main dipole from the center of the Earth which is currently of the order of 500 km (see fig. 2-14). This distance increases at a rate of 2-3 km/year, or 60-90 km in 30 years of time. This implies that the drift shells are shifting deeper into the atmosphere in the region of the South Atlantic Anomaly. This secular displacement of the magnetic dipole center with respect to the atmosphere by more than one density scale height in 30 years contributes a significant fraction of the residual dose variation illustrated by the lower curves in fig 2-14. This has been pointed out by TREND. Indeed, when the secular variation of the quadrupole terms are also cancelled the predicted secular variation of the dose is reduced again; a.s.o. with the octopole and higher order terms.

It should also be pointed out the magnetic dipole center experiences also a westward drift. This westward drift, combined with the change of the magnetic dipole tilt angle, explains the observed westward drift of the South Atlantic Magnetic Anomaly (SAMA or SAA).

This exercise has lead TREND to the following conclusions and practical recommendations concerning the utilisation of geomagnetic field models at different epoch. The epoch for the geomagnetic field given by BLTIME in the UNIRAD input-file should be set equal to the epoch of the geomagnetic field model used to build the trapped radiation model; e.g. Jenssen and Cain's geomagnetic field model corresponding to the epoch 1960 has consistently been used to build AE8 and AP8 flux models. Consequently, dose calculations for any future period of time should be based

on the Jensen and Cain's magnetic field model with BLTIME=1960, when the NASA flux models AE8 and AP8 are employed for the prediction.

On the other hand when the UNIRAD software is employed to organize new flux measurements in B-L space with the aim to build a new flux model, the obvious choice for BLTIME will be the actual epoch when the flux observations have been taken in the magnetosphere, let us say: 1986 for LANL data.

When this new environmental model produced with IGRF-85 for BLTIME=1986, is employed for predicting the radiation doses expected during a mission to be flown in the year 2000, the BLTIME variable which determines the epoch in the geomagnetic field model in SHELLG, or in BLXTRA, should not be taken equal to 2000 (as done before, and, as done to obtain the results illustrated in fig. 2-14); but BLTIME=1986 should then be the right setting in BLXTRA.

2.4.6 How to accomodate for local time variations at high altitudes?

When a directional detector measures a particle flux at right angle with respect to the local magnetic field direction, it measures particles which mirror at the location where this measurement is made. The drift shell of these particles is uniquely determined by the values of B and L provided that the magnetic field model used to compute B and L is 'appropriate'. According to the conservation of the first and second adiabatic invariants, and, as a result of Liouville's theorem, this same detector would measure the same flux at other longitudes and/or local time provided that B and L are identical, and that the pitch angle is also equal to 90 °.

But to be 'appropriate' a magnetic field model must

properly describe the local time variation of this field which is very significant at large radial distances due to all magnetospheric current systems.
If the model magnetic field comprises only the internal geomagnetic field components (as in the former version of the UNIRAD software package), it is obvious that the values of B and L will not correspond to the actual drift shell of mirroring particles. As a consequence of the actual local time dependence of the magnetic field , the particle flux measurements will be local time dependent, when they are mapped with these uncorrect B-L coordinates. To remove this undesirable local time dependence from these flux measurements, there is no better solution than to include a proper model taking into account the local time dependence of the external magnetic field component.

The inclusion of such an external magnetic field in the UNIRAD software package was therefore recommended by TREND. It was not only recommended in TREND's TECHNICAL NOTE 1, but it has been implemented in the BLXTRA software program replacing the former SHELLG one. The software requirements and description of BLXTRA have been presented in TN 2 and 5. They will be recalled in Chapter 3 of this final report.

2.4.7 Which 'appropiate' model can be recommended to describe the external magnetic field component due to magnetospheric currents?

In TREND's TECHNICAL NOTE 1 we have reviewed most current empirical models which have been developed by different authors to describe the field perturbations produced by the ring current, by the Chapman-Ferraro currents at the magnetopause, by the magnetotail current systems... There are many of such models on the shelf. All have advantages and limitations.

MEAD-FAIRFIELD (1975) model is one of the oldest and

easiest to implement. It has been used very often and is based on a large range of measurements scattered between 4 and 17 RE for the period of 1966-72. The tilt angle of the magnetic dipole can be changed and there are different versions depending on the level of geomagnetic activity. TREND recommended to implement this model as an option in BLXTRA.

The 1987 and 1989 versions of TSYGANENKO's models are based on an broad set of observations distributed in the magnetosphere ranging down to 2 RE and up far into the magnetotail. The different current systems taken into account in Tsyganenko's models depend also on the tilt angle of the Earth's dipole with respect to the Sun-Earth direction. In Tsyganenko's 1989 version there are 6 different models corresponding to 6 different ranges of Kp, Bartels geomagnetic index. This model is not only one of the most sophisticated one now available, but it simulates rather well the observed local time variations of the equatorial magnetic field distribution near geostationnary orbit.

Because of the poor coverage in the ring current region, it seems, however, to be less reliable in the inner magnetosphere. But at these smaller radial distances the components of the internal magnetic field dominate anyway over the small external field contribution. This makes the errors of Tsyganenko's external field relatively modest in the inner magnetosphere were some like to disclaimed it.

Therefore, despite these limitations TREND recommended to implement TSYGANENKO's external magnetic field models as an alternative (default) option in addition to the Mead-Fairfield model. Both the 1987 version and the 1989 version have been implemented by TREND as explained in the next chapter, and, in TREND's TECHNICAL NOTE 5.

2.4.8 Can B and L coordinates still be used at high altitudes where drift shell splitting becomes an important factor to cope with?

It should be emphazised that shell spitting does not exist in dipolar magnetic field and in general for any multipole component which is azimuthaly symmetric. But since the contribution of odd multipole terms is small and vanishes rapidly at large radial distances, the main origin of shell splitting in the outer magnetosphere comes from the external magnetic field which is azimuthally asymmetric as a consequence of its local time dependence.

Particles measured with pitch angles smaller larger than 90° do not drift on shells characterized by values of B and L corresponding to the point of measurement, but their mirror point is located at a lower altitude along the same magnetic field line. Therefore, when unidirectional flux measurements are available one needs to determine the actual position of the mirror point corresponding to each particular pitch angle α. This can be easily done by tracing (by numerical integration) the magnetic field line from the point of measurement down to the mirror point where the magnetic field intensity is equal to

$$B' = \frac{B}{\sin^2 \alpha}$$

Once the geodetic coordinates of the actual mirror point are known, it will be easy to follow the normal procedure to determine L' using the BLXTRA program.This is the procedure that TREND that recommends to analyse the directional flux measurements of IUE in the future.

It must be pointed out that for omnidirectional measurements particles at all pitch angles enter the detector. As a matter of consequence particles drifting on a wide range of different drift shells are measured at

once. These different drift shells are characterized by L values which are nearly the same (at least in the inner magnetosphere where the magnetic field lines are closely dipolar) and by values of B which are varying over a wide range in any case.

The success of B-L coordinates comes from the fact that they organise very well omnidirectional fluxes in the inner magnetosphere where L has nearly the same value for all points along a given magnetic field line, and, where shell splitting is relatively unimportant. But in the outer magnetosphere, where magnetic field lines become less dipolar like, and where shell splitting takes place, the usefullness of the B and L coordinates has been questioned for mapping omnidirectional fluxes.

Although TREND recognized this problem, it recommends to continue with B and L, until a better solution will be found. For directional flux measurements with good angular resolution there is not so much of a problem than for omnidirectional flux measurements, as indicated above. Unfortunately, the view angles of directional detectors are often quite large, therefore the pitch angle resolution is rather poor in many cases. Consequently, the range of mirror point altitudes corresponding to the wide range of pitch angles is anyway rather broad; the corresponding values of B′ and L′ coordinates of these mirror points are spread over a range of finite extent .

2.4.9 How to cope with the atmospheric cut-off? What kind of coordinate system should be used instead of B and L at lowt altitudes where the atmospheric effects are importanot?

This question has already been introduced above. A

full chapter was devoted to this question in TN 1. TREND has pointed out that the atmospheric density plays a comparatively more important role than the geomagnetic field on the distribution of trapped particles at low altitudes i.e. at the inner edge of the radiation zone. This has also been demonstrated and confirmed by Pfitzer (1990) who suggests to use the local atmospheric density instead of B or B/Bo to map omnidirectional fluxes between 150 km and 1000-2000 km altitude.

But instead of the atmospheric density at the altitude of the measurement, TREND has suggested to introduce a new 'averaged height' parameter. Indeed to account for the global effect of the atmosphere it is necessary to integrate the density over the trajectory of the particle or of its guiding center. The reason is that the altitude of mirror points varies with longitude from 100 km up to 1500 km in certain cases . For comparison it should be pointed out that the density scale height is about 50-70 km in the thermosphere.

A direct numerical integration of the trajectory of particles as C.STORMER did it more than 80 years ago for cosmic ray particle, would be too demanding in CPU time. To avoid such a time consuming calculation of atmospheric averaged over a drift shell, Hassitt (1964) has developed an elaborate and interesting method which is outlined in sect 1.3.3.2 of TREND's TECHNICAL NOTE 2. The FORTRAN code of HASSITT has been unearthed by C.E.McIlwain at UCSD/CASS (La Jolla), where it was developed more than 25 years ago by one of his post doc. TREND is very thankful to C.E.McIlwain for providing to TREND this software package . This code has been implemented at the IASB (Brussels) were it has been tested, and where it is now waiting for further developments and resources.

This program calculates first a drift shell averaged atmospheric density, then it determines a corresponding

'height' using a simple standard atmospheric model with exponentially decreasing densities.At McIlwain's suggestion TREND has called this: the Hassitt shell height (H_S). The definition of H_S is then: the altitude where the density in the standard (conventional and simple) atmosphere model is equal to the actual average density that the guiding center of a trapped particle sees when it drifts along its B-L-shell. TREND recommends the use of this new coordinate instead of Pfitzer's local atmospheric density, and in any case instead of B or B/B_O.

The original version of the Hassitt code is based on the Jensen and Cain (1960) 48 terms expansion of the geomagnetic field. This old field model and the primitive atmospheric model used 25 years ago by Hassitt need to be updated. The software needs also to be optimized to reduce the rather long CPU time of the original code. The lack of resources prevented us to develop and optimize this code any further within the framework of this contract. But it is hoped to find new support to carry out this work later on in collaboration with C.E.McIlwain.

2.4.10 What are the alternative models for prediction of solar flare events? Which model(s) should be implemented in future UNIRAD software?

The question of fluence due to solar proton events has been raised already above as well as in Chapter 6 of TREND's TECHNICAL NOTE 1. There are two alternative models available. The first due to King (1974) is already old and based on one solar cycle worth of data (i.e.cycle 20 which is now known to be less representative of the current one). The second and more recent model is based on data collected during for three solar cycles, and is due to Feynman et al. (1988).

King's model is a well referenced standard. Despite its limitations due to the smallness of the data sample, it

is likely to remain the standard model that most users may wish to employ for a while. This is the reason TREND recommends to leave this early model as an option in future UNIRAD softwares.

The results from Feynman's probabilistic model which is based on the wider sample of observations and on simpler basic assumptions (e.g. the absence of 'Anomalously Large' events; all solar proton events, even the largest one are considered as 'Ordinary' events). This is one of the decisive reasons to incorporate this new model into the new UNIRAD software as the default option.

This closes the outline of the TREND's evaluations of existing models; the major recommendations suggested by TREND concerning future models have also been presented here. We are now ready for chapter 3 where software and data requirements and developments will be explained.

3. SOFTWARE & DATA REQUIREMENTS & DEVELOPMENT

Based on the model description and evaluation given in TN1 and on model formalism and software requirements outlined in TN2, we present here the new software tools which have been developed to analyse the selected set of satellite data. All available data relevant to this study have been presented and catalogued in TN3 and will first be recalled below. The rationale for selection of the two sets of data (LANL and IUE) which have been analysed by TREND as part of this contract will also be given below as well as the analysis plan.

3.1 Data available and selection criteria

Based on Table 3-1 from the 'ESA statement of Work', NSSDC and NGDC catalogues of spacecraft and particle experiments, as well as other compilations more specific to satellite instrument descriptions, a comprehensive listing of energetic electron and proton data have been identified by TREND. Technical Note 3 contains a catalogue characterizing data with respect to species, energy range, spatial, directional and temporal coverage.

The presentation of the new catalogue has been made as user friendly as possible. Full details as to why particular formats were adopted are given in TN3.

The satellite instrumentation with respect to reliability and accuracy has also be given for each of the entries in TN3. The Laboratory address and name of the PI for these instruments is also provided.

Spacecraft	Instrument	PI
ATS-1	ASC	Paulikas
ATS-5	UCSD	McIllwain
ATS-6	U. Minn.	Winckler
	NASA	Konradi
	MDAC	Masley
	ASC	Paulikas
SCATHA	SC3	Reagan
	SC5	Hardy
DMSP-F7	SSJ*	Gussenhoven
DMSP-F1	SSJ*	Blake
GEOS	S321	Korth
IMP	NOAA	Williams
	U. Md.	Gloeckler
	JHU/APL	Krimigis
	U. Ch.	Simpson
	Caltech	Stone
Los Alamos		
76-059A		Higbie
77-007A		Higbie
79-053		
SMS/GOES	SEM	Sauer
TIROS	SEM	
NOAA	SEM	
ISEE-1		Williams
ISEE-2		Keppler
ISIS-2		McDiarmid
S3-2		Fennell
S3-3		Vampola
		Yates
NTS		

Table 3-1 List of spacecraft missions with energetic particle detectors (from ESA statement of work, 1988).

Orbit Parameters	Spacecraft/Instrument Acronym	Electron Energies	Proton Energies	Time Coverage
Hi Elliptical i = 29 ha/p = 138000/281	ISEE1&2/L-GM	> 45 keV	> 600 keV	11/77 - 10/87
	ISEE1&2/EAP	8 - 200 keV 30 - 200 keV	8-200, 30-200 200 - 300 keV	11/77 - 10/87
	ISEE1/EEAP	0.02 - 1 MeV	0.02 - 1.2 MeV	11/77 - 8/79
	ISEE2/EEAP	20 - 300 keV 0.02 - 1.2 MeV	0.02 - 2 MeV	11/77 + 7 years
	ISEE1/LECR	75 - 1300 keV	66, 130 keV	11/77 - 10/87
Hi Elliptical i = 0 ha/p = 51000/5550	CCE/MEPA		0.01 - 1 MeV	8/84 - p?
	CCE/CHEM		1 - 300 keV	8/84 - p?
i = 29 ha/p = 113000/550	IRM/SICA	35 - 220 keV	10 - 300 keV	8/84 - p?
~Circular/580 i = 98	STPP78-1/GEE	0.04 - 2.5 MeV		3/79 - 2/80 ?
~Circular/850 i = 102	NOAA/SEM	>30,100,300 keV > 6 MeV	> 80 keV	10/78 - p
~Circular/840 i = 99	DMSP/SRD	> 1 & 2.5 MeV	>20,35,51,75 MeV	11/83 - 7/88
Synchronous i = 29 ha/p = 45000/26600	IUE/PFM	> 1 MeV		11/80 - p
Synchronous i = 8 ha/p = 43200/27600	STP P78-2/RSPD	0.05 - 1 MeV	0.05 - 7 MeV	3/79 - 5/80
	STP P78-2/PD		17 - 717 keV, 0.7 - 3.3 MeV	3/79 - 5/80
	STP P78-2/CPD	0 - 81 keV	0 - 81 keV	3/79 - 5/80
	STP P78-2/HEPD	0.3 - 2.1 MeV	1 - 100 MeV	3/79 - 5/80
Geostationary i < 1.9	LANL/CPA	30 - 300 keV 0.2 - 2 MeV	145 - 560 keV 0.4 - 140 MeV	7/76 - p
	LANL/SEE	3-5, 5-7, 7-10, 10-15 MEV		6/79 - p
i < 0.3	GOES/EPD	> 2 MeV		9/80 - p
i < 1.9	GMS/SEM	> 2 MeV	1 - 500 MeV	8/81 - p
i = 0	MTSAT P2/LOE	30 - 300 keV		6/88 - p

Table 3-2 Summary of data available and their characteristics.

A comprehensive summary table of data available and relevant to test the environmental models is given in Table 3-2. This table contains on the left orbit type information and provides one with an initial indication as to where a particular spacecraft was located i.e. if the orbit was geosynchronous, polar high latitude, low latitude circular, elliptical or whatever. Next we see the spacecraft name and with it an acronym representing the instrument from which relevant data is available. In the next columns are listed the energy range and detector threshold information for each instrument.

These data show up strengths and weaknesses in the existing coverage of the earth's radiation environment. For example, in the 5-15 MeV range for protons, which are known to produce significant damage to spacecraft borne solar cells, energy coverage is essentially non existent. GMS and STP 78-2 are in the wrong area of space to monitor these particles. CRRES will fill this gap later on. The region from atmospheric cut-off to geosynchronous orbit will be covered by appropriate CRRES monitoring. Meanwhile, although DMSP provide coverage of protons > 20 MeV, these data are truncated in B-L space and there is no coverage of protons with energy >75 MeV.

It is notable that the natural electron population in the inner zone has never been determined well since remenants of the Starfish fission experiment were present up until about 1970 when monitoring instruments were flown. Thus, as noted in Technical Note 2 it would be very interesting to compare DMSP data with inner zone AE8 with a view to investigating the long term behaviour of sources and the processes of atmospheric loss.

At the present time the Geostationary Region is well covered by LANL and TREND has improved the standard deviation model from AE-4 using these data and the 1989 magnetic field model of Tsyganenko.

The role of very energetic electrons in producing deep dielectric charging and system break down is presently not well understood and the behaviour of electrons with energies greater than a few MeV is currently of interest. The SEE instrument on LANL could provide the data necessary to carry out this study.

Almost all of the trapped radiation measurements from 1958 through early 1970 have already been used in producing some 8 proton and 8 electron models. The TN3 catalogue then excludes these measurements. Further, not all the available data accumulated since then, have been included. The criteria for inclusion are :

Species. In the trapped radiation environment electrons and protons are so dominant that higher Z trapped particles experiments are not included.

Energies. Since s/c charging is outside the scope of TREND, plasma data have been excluded. There, working criteria of including only energies > 40-50 KeV for both electrons and protons were used (this eliminates most electrostatic analysers, mass analysers, etc.). There are a number of instruments which span across these thresholds and these are included in the relevant ranges.

Proton detectors which orbited within the trapping region but had energy thresholds too high to measure the ambient particles were also excluded. These are the solar proton monitors.

Categories. Having laid the ground rules, the spacecraft with their payload instruments included in the study were broken up into two categories: research or development spacecraft investigations, and, operational spacecraft including the well known GOES, NOAA, LANL series etc.

Instruments. TREND then set about accumulating information relevant to the individual spacecraft, to the instruments acquiring data within our constraints for acceptance and to existing data set descriptions. In this TREND drew heavily on information in the catalogues of NSSDC and NGDC. However, as a result of activities within TREND, much more detailed information than has been already pusblished concerning many instruments and data sets has become available and this expanded material replaces the data center entries in the catalogue of TN3 which is summarized in Table 3-2.

The suite of satellites indentified in TN3 occupy four types of orbits: (a) highly elliptical, near equatorial, (b) low-altitude, near polar, (c) high-altitude, nearly geosynchronous, and (d) geostationary.

AMPTE/CCE, AMPTE/IRM, and ISEE 1 & 2 are in class (a), while DMSP 5D-2/F7, NOAA 6 - 10, ISIS 2, and STP P78-1 are the ones in class (b). Class (c) contains IUE and SCATHA. The largest class, of course, is (d) containing 7 DoD satellites carrying the Los Alamos National Laboratory (LANL) detectors, the 3 GMS series, the 7 GOES series, and Meteosat 3, which is carrying the low-energy electron portion of the LANL instrument.

3.2 Description of the data selected for analysis, and selection rationale.

As a result of the limited ressources available to TREND, only two sets of data have been analysed in some details using the new software tools designed and built by TREND. The data analysis and data processing considered in this study have been based on the Los Alamos National Laboratory (LANL) electrons measurements, and secondly on the electron measurements obtained from a "minimally

intrusive" particle monitor added to the astronomical payload of the International Ultraviolet Explorer (IUE).

There are several criteria which determined TREND to concentrate on satellite data from the high altitude region more than from the low altitude one. First of all as a result of the model evaluation and software requirements in TREND's TECHNICAL NOTE 1 and 2, it was concluded that the traditional B-L coordinates must be replaced by a new coordinate system (like the Hassitt's shell height) to map adequately the trapped radiation fluxes between 150 and 1000-2000 km altitude. Indeed, at these altitudes the atmospheric density determines the flux of the Earth's radiation environment more significantly than the geomagnetic field distribution.

Despite all the interest such a study extension would have offered for future ESA mission in low-altitude orbit (e.g. Columbus, Hermes), TREND decided to focus its data analysis and data processing efforts on LANL and IUE data which are respectively near geostationnary missions and highly altitude missions on a GTO type of orbit. Indeed, these types of mission orbits are often choosen for astronomical satellites, communication and meteorological spacecraft.

There was an additional reason to prefer high altitude data instead of low-altitude ones in the present case: indeed, the new programme BLXTR was build by TREND to accomodate for the local time dependent deformation of the geomagnetic gield by magnetospheric currents. It was obvious that the best test repository for this new software was by using data from the outer part of the magnetosphere, and not from the region closer to the Earth where the effect of magnetospheric currents is negligible.

LANL provides geostationary data, whereas the IUE satellite is on high elliptical orbit with a period of 24 hours. These orbits are appropriate to study B-L space for

L between 3 and 8. The instruments on board cover an energy range which is adequate to improve the existing AE-8 model in that region of space. In both cases the data cover a long period of time of many years, allowing to identify possible solar cycle effects, long time averages and reliable standard deviations of the particle fluxes measured. The local time coverage is also complete for these two sets of data. The easy and quick availability of these data from NSSDC was another reason for TREND to select these two data sets instead of any other which needed clearance and heavy preprocessing or reformating. Indeed, the duration of this contract was only 15 months. With the limited resources available, excessive time delays to acquire data had to be avoided.

The ISEE 1 data of Don Williams has been undergoing analysis by E. Daly and C. Tranquille at ESTEC/WMA for more than a year and data from a similar instrument on ISEE 2 will soon be brought into their analysis.

There are other also interesting data sets available, possibly for post-TREND studies : e.g. the DMSP data which are collected on a near polar orbit at low altitude (see TN2 Ch.4)

The SSJ* instrument of DMSP/F7 and B-L coverage has energy ranges which would offer be a valuable complement to the results obtained by TREND with the LANL and IUE data sets. But as indicated in chapter 2, mapping of the radiation environment at low altitudes (150km-2000km) requires a novel approach and a new coordinate system: e.g. the Hassitt shell height, which is a parameter determined by the density distribution in the upper atmosphere. Since, this new coordinate system needs serious software developments and optimisation which were not amenable within the time span of this contract, the low altitude DMSP measurements, have been given a lower priority by TREND, despite their relevance in testing the validity of

existing models at low altitudes.

For similar reasons,(i.e. limited resources and the limited validity of B-L coordinates at low altitudes) TREND did not attack the updating of the proton AP-8 model. Indeed, such an undertaking needs much more time and extended efforts to develop additional software tools, to acquire and process additional data sets.

The LANL and IUE data will now be presented in somewhat more detail.

3.3 Los Alamos National Laboratory (LANL) geostationary charged particle analysers(CPA)

3.3.1 The LANL instruments

This instrument has been flown on seven DoD geostationary satellites and the low energy part on Meteosat P2. The DoD satellites were 1976-059A, 1977-007A, 1979-053A, 1981-025A, 1982-019A, 1984-037A, and 1984-129A (USA 7). Following the third launch, there were two active satellites with the third acting as a backup. Since these satellites were moved in longitude during their lifetime (Baker et al. 1981, 1982 and Cayton et al. 1989) only the expected parking positions are given here. They are 35°, 70°, 135°, 155°, and 290° W.

The CPA consists of separate electron and proton systems. The electron detectors are designated LoE and HiE. LoE consists of a fan of five separate detector-collimator units mounted at 0°, ± 30°, and ± 60° relative to the spacecraft (s/c) equatorial plane. The s/c rotate with a 10-s period about an axis that points toward the center of the Earth. Thus complete (over the unit sphere), continuous pitch-angle measurements of electron distributions are made by LoE every 10 s for essentially all magnetic field orientations. The s/c latitude extent of

each LoE field of view is 30° and the geometric factor is 3.6E-03 cm^2-sr and there are six energy channels: 30-300, 45-300, 65-300, 95-300, 140-300, 200-300 keV. The basic CPA sampling rate is 8 ms so that each energy channel of each sensor is sampled 40 times per spin period.

The HiE consists of a single detector-collimator unit that is pointed outward along the Earth-satellite radius vector. The conical collimator has a half-angle cone of 4° giving the system a geometric factor of 1.8E-02 cm^2-sr. There are six energy channels: 0.2-2, 0.3-2,0.4-2, 0.6-2, 0.9-2, 1.4-2 MeV. Only a relatively narrow portion of the unit sphere is sampled as the s/c rotates. However, for normal (approximately dipolar magnetic orientations) nearly all pitch angles will be sampled. For tail-like magnetic configurations HiE samples a very small range of pitch angles.

This data set consists of hourly averages of the energy channels of all the CPA instruments as well as the daily averages; these daily averages are based on estimators and so constitute some type of a model. This averaging then converts the fluxes into isotropic directional fluxes so that the pitch angle information is lost.

The data set starts in January 1979. Their Synoptic Data Set covers the period July 1976 to January 1979. Dr. Thomas E. Cayton is the LANL contact now that Dr. Paul Higbie, the original PI, is no longer associated with the activity. Based on discussions with Tom Cayton the data sets through 1983 are available for TREND and NSSDC was given access to these five files (one for each of the LANL satellites, 1976-059A, 1977-007A, 1981-025A, 1982-019A, and 1984-037A) for transfer over SPAN. A VAX standard "backup" tape was produced. The tape also contains a FORTRAN routine to read and print any portion of the files. The routine identifies each field in the logical record and gives the

representation and the physical units of them.

3.3.2 The LANL data sets

From this data set TREND used the 12 electron channels, which are available as hourly averages in 24 local time (LT) bins. Except for the identification of the appropriate bins for performing longer term averages. The LT is the useful variable both for binning and for graphical display. To prepare for the analysis, i.e., construct the production software, the following processing was done. The electron data as received represents isotropic directional flux. Thus the inputs must be multiplied by 4π to be a more physically meaningful quantity, the omnidirectional flux, denoted by $J(E_i\text{-}E_{ui}, LT, \phi)$ with units of electrons/cm^2-s within the energy band $E_i\text{-}E_{ui}$, where

$$E_{ui} = \begin{cases} 0.3 \text{ MeV}; & i = 1,6 \\ 2.0 \text{ MeV}; & i = 7,12 \end{cases}$$

The longitude, ϕ, is used here, not to infer a dependency, but to serve as an identifier between the different LANL spacecraft (really different parking ϕ's). Because of the nature of the satellites, (i.e., geostationary), it is much more efficient to defer the assignment of physically meaningful position coordinates to the analysis phase. For purposes of requirements, it is convenient to consider this quantity as a 5-index array. Thus J(i,j,k,l,m) will be used where

i	=	channel index, 1,12, i.e. defines the energy band,etc.
j	=	LT index, 1,24.
k	=	day of month index, 1,28,29,30,31.

l = month index, 1,M, where M can be as large as needed

m = parking longitude index, 1,6 or so.

With this notation the following quantities have been be produced:

$$J_k(i,j,l,m) = \frac{1}{N(i,j,l,m)} \sum_{k}^{N} [J(i,j,k,l,m)] \qquad (1)$$

the sample monthly average ; N(i,j,l,m) is the number of measurements for the (i,j,l,m) bin.

$$J_j(i,k,l,m) = \frac{1}{N(i,k,l,m)} \sum_{j}^{N} [J(i,j,k,l,m)] \qquad (2)$$

the sample daily average which corresponds to a daily local time average;

$$J_{jk}(i,l,m) = \frac{1}{N(i,l,m)} \sum_{j}^{N} [J_k(i,j,l,m)] \qquad (3)$$

the sample monthly and local time averages.

$$\Phi(i,j,k,l,m) = \frac{J(i,j,k,l,m)}{J_j(i,k,l,m)} \qquad (4)$$

is an empirical normalized local time variation function.

The LANL data sets also have the standard deviation accompanying each local time bin flux, which will be denoted here as S(i,j,k,l,m). This quantity is a standard deviation of flux measurements observed during one hour UT periods i.e. also LT periods. It is not directly useful in the planned study, but the quantity

$$SL(i,j,k,l,m) = \frac{S(i,j,k,l,m)}{J(i,j,k,l,m)} \qquad (5)$$

is approximately equal to the standard deviation of both the lnJ and logJ over the hourly periods of time;

$$SL(i,j,l,m) = \frac{1}{N(i,j,l,m)-1} \sum_{k}^{N} [J(i,j,k,l,m)-J_k(i,j,l,m)]^2 \qquad (6)$$

is the standard deviation (sigma for short) of the monthly sample used to create (1) above.

File name	Identificator	Nb of records	Size	Longitude(s)	Time coverage
LANL1.DAT	1976-059	16 421	11 442 blocks	290° E 325° E	03/01/79 - 27/06/83
LANL2.DAT	1977-007	31 911	22 081 blocks	70° E	03/01/79 - 30/06/83
LANL3.DAT	1979-053	21 550	15 070 blocks	225° E	22/06/79 - 25/05/85
LANL4.DAT	1981-025	27 840	19 194 blocks	225° E 290° E 70° E	27/03/81 - 30/03/85
LANL5.DAT	1982-019	42 308	40 204 blocks	325° E 290° E	21/03/82 - 27/07/87
LANL6.DAT	1984-037	31 629	21 773 blocks	70° E 225° E	24/04/84 - 31/10/88

Table 3-3 LANL data sets available for this study.

3.3.3 LANL data processing

The LANL data sets from 1979 to 1988 are available on six files names LANLn.DAT with n=1,6.

Table 3-3 summaries LANL data available to TREND. The number of records is the number of valid records whereas the size refers to the total number of records (valid and invalid). The longitudes are determined from the universal time and local time (available within each record).

The detailed description of the LANL data records is given in chap. 4 of TN4, and will not be repeated here.

After reading and validation of the records, the longitude of the satellite is calculated from the Universal time and local time. Daily average flux have been calculated from the local time data using eq.(2) . Similarly monthly and yearly averages have been determined (from eqs.1 and 3) . Similar averages of the logarithm of the fluxes are also computed as explained in TN4, indeed the individual flux measurement follow generally a log-normal distribution.

Standard deviations associated with all these averages have also been determined using eq. (6). Various graphical plots of these averages and standard deviations have been generated. A few examples will be presented in the next chapter.

Omnidirectional electrons integral spectra are fitted with two exponential energy distributions (Cayton et al., 1989)

$$J(>E) = A \exp(-E/E_a) + C \exp(-E/E_c) \qquad (7)$$

where A, and C are constants, E_a and E_c are exponential

gradients and E the lower energy limit.

The differential flux is then given by

$$J(E)=(A/E_a)\ \exp(-E/E_a)+(C/E_c)\exp(-E/E_c) \qquad (8)$$

The parameters A,C,E_a, and E_c,are determined by the least square method using the 12 electron energy channels available. The procedure is described in TN4.

The data have also been fitted to a power law

$$J(>E) = A\ E^{-C} \qquad (9)$$

where A and C are again ajustable constants determined by the least square technique. The LANL data fit the power law less well than the exponential law.

The B-L coordinates of the LANL positions are calculated using the new software BLXTRA described in TN5. Since one of the objectives of this study is to determine the amplitude and phase of the local time variation of trapped electrons near geostationary orbit, the B-L coordinates are first determined using a magnetic field model which is not local time dependent (i.e. the IGRF model corresponding to the epoch of the measurements). In this case all measurements are characterized by nearly the same value of B-L. Indeed the satellites is fixed within the IGRF distribution used to model the geomagnetic field. In a second step, new B-L coordinates are computed with BLXTRA but with a magnetic field model which depends on local time and on the level of geomagnetic activity Kp. (i.e., the same IGRF model as above; Tsyganenko's external magnetic field: T89). In this second case the geostationary satellite changes position with respect to the B-L drift shells.

The first approach is called the 'conventional approach' ; the second one is the approach with an external

field model. In chapter 4 the results of both approaches are compared with each other and with AE8 model predictions.

In the first case (i.e. the conventional approach) once all B-L values are available a grid of points is determined in B-L space.

-four B bins [0.00102,0.00106],[0.00106,0.0011] [0.0011,0.0014],[0.0014,0.0018].
-five L bins [6.5,6.6],[6.6,6.7],[6.7,6.8] [6,8,6.9] and [6.9,7]

The omnidirectional fluxes for each B-L bin, and for each local time bin are then averaged; this is repeated for each energy threshold.

The observed local time variations are then compared to those of the AE4 models which are described analytically by the formula

$$\Phi_T(E,L,\phi) = K_T(E,L)\ 10^{C_T(E,L)\cos(\pi/12)(\phi-\Omega_T(E,J))} \quad (10)$$

where:

- T denotes the epoch dependence,
- E is the energy level,
- L is the McIlwain shell parameter,
- ϕ is the local time,
- $\Omega_T(E,L)$ is the phase (constant and taken equal to 11 in AE4 model),
- $K_T(E,L)$ and CT(E,L) are dimensionless parameters (amplitudes of the LT variation)

- $K_T(E,L)$ is a normalisation factor such that,

$$\frac{1}{24} \int_0^{24} \Phi_T(E,L,\phi)\,d\phi = 1 \qquad (11)$$

Physically, K_T represents the normalized amplitude of local time variation of flux levels. In AE8-AE4 models, it is linked to the integral flux $J_T(>E,B,L,\Phi)$ by the formula

$$J_T(>E,B,L,\phi) = N_T(>E,L)\ \Phi_T(E,L,\phi)\ G(B,L) \qquad (12)$$

where :

- J_T is the time average omnidirectional flux above energy E,
- B is the magnetic field strength,
- N_T is the spectral function (described in section 4.4.5 of TN1),
- G is the model B-dependence. (described in section 4.5.2 of TN1 and in section 2 of this final report)

LANL data are used to update coefficients C_T, K_T, and Ω_T for the geostationary orbit at epochs T covered by LANL satellites (that is, 1979 to 1988) keeping the same analytical expression for Φ_T but including a B dependence for these 3 coefficients.

The values of the coefficients C,K, and Ω are determined by a least square technique, and stored on file. Their values determines the local time variation which will be discussed in chapter 4.

Assuming the logarithm of the electron flux is

normally distributed at all points of observation in space, a standard deviation can be computed and compared to those from the earlier model AE4.

The details of this calculation are presented in TN4. The standard deviation is provided for each B-L bin, ϕ-bin, and energy threshold E : $\sigma(>E,B,L,\phi)$. Provided the statistical distribution of fluxes is log-normal, the value of r can be used to compute the probability distribution. The result will also be discussed in chapter 4.

In order to preserve compatibility with AE8MIN/MAX, the new values for the flux obtained from the LANL observations are stored in block data file called TREM-G.FOR. The internal organisation of AE8MIN/MAX models is also used for TREM-G. This new acronym stands for : Trapped Radiation Environmental Model for Geostationary orbit.

The same procedure is followed to determine the alternative model TREM-GX. The X in the acronym means that an eXternal magnetic field model (T89) has now been used in BLXTRA to determine B-L coordinates.

Since Tsyganenko's model depends on the value of the geomagnetic index Kp, the transformation from geodetic coordinates to B-L coordinates will depend on K_p. All observations have been binned into 4 intervals of K_p :

$$K_p<2^+, \quad 2^+\leq K_p<3^+, \quad 3^+\leq K_p<5^+, \quad 5^+\leq K_p$$

These four geomagnetic activity levels correspond to quiet, mean, strong activity and magnetic storm conditions. Wider ranges of B and L values are now covered as a result of the local time dependence of the magnetic field distribution and the K_p dependence. The B-L grid is now divided in

- eight B-bins [0.00094,0.00098],[0,00098,0.00102]
  [0.00102,0.00106],[0.00106,0.0011]
  [0.0011,0.000114],[0.00114,0.00118]
  [0.00118,0.00122] and [0.00122,0.00126]

- eight L bins [6.6,6.75],[6.75,7],[7,7.25],
  [7.25,7.5],[7.5,7.75],
  [7.75,8],[8,8.25],[8.25,8.5]

The integral electron spectra J_T (>E,B,L,K_p) for each B-L bin, are also given for 4 K_p intervals instead of 24 local time intervals. Similarly, the standard deviation σ(>E,B,L,K_p) is now a function of K_p, the local time dependence being averaged out. This is a reasonable procedure, since introducing an appropriate external magnetic field should cancel or at least reduce the local time variation of the flux J_T (>E,B,L,K_p).

The objective of this analysis is to build new trapped electron flux tables for the geostationary region of B-L space. The model matrix is stored in block data files named TREMGXn.FOR, where n refers to the number of the four K_p ranges considered above. The results obtained are displayed and discussed in chapter 4.

3.4 The IUE particle flux monitor (PFM)

3.4.1 The IUE instrument

These data have been supplied to TREND by NSSDC on a demand basis on tape that contains the orbit elements, the attitude of the spacecraft roll and pitch axes in the geocentric equatorial inertial (GEI) coordinate system [given as Euler angles], the median voltage reading from the instrument count ratemeter for intervals of about 5-

minutes, and the number of voltage readings that were made during each interval. The PFM is comprised of a lithium-drifted silicon detector, a 16° half-angle collimator with the opening covered by a 0.357-g/cm^2 Al absorber, pulse discriminator, associated electronics, a logarithmic count ratemeter, and overall shielding of 2.31 g/cm^2 except for the collimator opening. The electron threshold energy is 1.0 MeV and the proton threshold is 15 MeV.

IUE is in a 24-hr elliptical orbit at an inclination of 31.6°. The apogee altitude is 42,413 km and the perigee height is 29,155 km. These parameters have varied somewhat over the lifetime of the satellite.

Data have been collected in digital form since Nov. 6, 1980 and continue to be deposited in NSSDC by the IUE project at the present time. The tapes are 9-track, 1600-bpi, EBCDIC, and multifiled. Each tape contains approximately 15 files.

3.4.2 IUE Data processing

A program (IUESYS) developed by Vette and Abdul Doyle in 1981 is capable of handling this data set but some modifications had to be made.

Since the IUE data provides a measure of the directional flux > 1.0 MeV off the magnetic equator in the 20 - 40° range, the position tagging to physically meaningful coordinates cannot be postponed until the analysis phase. Since IUE only generates one data point every 5 minutes. The only requirement that takes some new logic, is to trace the total field line from the position of the satellite to the position of the miror point corresponding to the pitch angle i.e. the angle between the direction of the particle detector with respect to the magnetic field direction.

There are fourty-three IUE data files at present in the possession of TREND and these cover the period November 6th 1980 to March 27th 1981. ESTEC has independently received additional data files covering nearly 10 years of operation. The files in EBCDIC format have been converted to ASCII format prior to using them. The characteristics of the IUE files are given below.

From the 43 IUE files provided to TREND we have built 25 'sorted' IUE files, each being characterised by a set of constant orbital elements. Indeed, after examining IUE data, it has been observed that different files had the same orbital elements whereas in the same file one finds occasionally several times the same set of orbital elements. The format of these files is the same as the original ones; only the list of records is different.

As IUE files do not provide the position of the satellite at start and stop times, an orbit generator had to be used to relate date and time to the geographical spacecraft position. The SAPRE module is utilised for this purpose.

For each IUE file, we read the (constant) orbital element and the starting date/time and create the associated SAPRE namelist file. Then, SAPRE generates an output file containing the geodetic coordinates of the points of data observations. This file is used as input by program IUESYS.

The main objective of processing these data prior to their analysis is to bring the data set to the same level as the LANL data. This process was done at Los Alamos National Laboratory before the LANL data were made available to TREND via NSSDC. In brief, the processing tapes of IUE observations starts from the raw data. Also involved are transformation matrices to obtain e.g. geographic coordinates and solar magnetic coordinates.

The preprocessing program provides the following variables, which do not contain B,L nor the pitch-angle information.

YEAR	- year, (integer)
T	- Starting date/time of the logical record, (decimal days)
DT	- Time increment, (decimal minutes)
FLUX	- Directional flux of electrons with energies larger than 1 MeV, (electrons/cm^2-s-sr)
NQUAL	- Quality index, number of samples for median.
GLA(K,1)	- GEO x-component of detector, look angle unit vector.
GLA(K,2)	- GEO y-component of detector, look angle unit vector.
GLA(K,3)	- GEO z-component of detector, look angle unit vector.
GLA(K,1)	- GEO s/c radial distance, (km).
GEOP(K,2)	- GEO s/c latitude, (degrees).
GEOP(K,3)	- GEO s/c east longitude, (degrees).
GLT	- GEO local time or s/c, (hours).
ISLEW	- The slew flag.

The contents of these processed IUE files allows to plot :

- the omnidirectional flux versus local time assuming an isotropic flux (multiplication of variable FLUX by 4π),

- the cumulative distribution of the log flux, that is the probability to exceed a given flux treshold.

Some of these plots will be shown and discussed in chapter 4.

For each record B and L are then computed with and without external magnetic field. In both cases, we use program BLXTRA with IGRF-85 internal field model (with BLTIME = Year of the IUE data measurements) and Tsyganenko-89 external field model. For each record, the value of K_p is read in the K_p file.

The following four tasks have been accomplished :

- determination of the B-L coverage of IUE satellite with B and L computed with IGRF-85 only,

- determination of the B-L coverage of IUE satellite with B and L computed with IGRF-85 and Tsyganenko-89

- mapping of flux in B-L coordinates with B and L computed with IGRF-85 only,

- mapping of flux data in B-L coordinates with B and L computed with IGRF-85 and Tsyganenko-89.

The graphics tools used are based on the MATRA graphics library GRAPHLIB. Results are described in chapter 4.

This processing of IUE data assumes that the pitch angle distribution of the particle is isotropic: i.e. that the omnidirectional flux can be obtained from the unidirectional flux by multiplying the latter by 4π . Although this procedure is rather questionable, it leads at least to an order of magnitude evaluatation of the actual

omnidirectional fluxes along the IUE orbit. As indicated in TN2 (chapter 4), since the particles entering the detector have in general a pitch angle not equal to 90° (i.e. corresponding to a miror point) a program had to be developed to compute the geodetic coordinates of the actual miror point associated with this pitch angle. This programme is currently under development at IASB but it still needs some work and testing before it can be implemented in IUESYS.

Once these coordinates are known the geomagnetic B-L coordinates can be determined using the BLXTRA programme which will be described in the following section.

3.4 Software tools developed by TREND

In order to analyse the LANL and IUE data a number of software tools have been developed by TREND. Some of these tools are specific to the analysis of LANL and IUE data and will not become part of the UNIRAD software package. But in addition to these programs, TREND has also developed new software packages which have been implemented in the new version of UNIRAD delivered to ESTEC as part of the present contract.

Fig. 3-1 shows a block diagram of the architecture of the UNIRAD software TREND has been concerned with. (see also fig 1-1)

A - The UNIRAD software package contains a suite of programs which computes the geocentric coordinates of a predetermined number of points along the orbit of a satellite. These coordinates are outputs of a program called SAPRE. Although, it was not part of the tasks for the present contract, additional features have been implemented in SAPRE to make it more userfriendly for occasional users of UNIRAD. These improvements have been explained in TN5 and summarized in Appendix B.

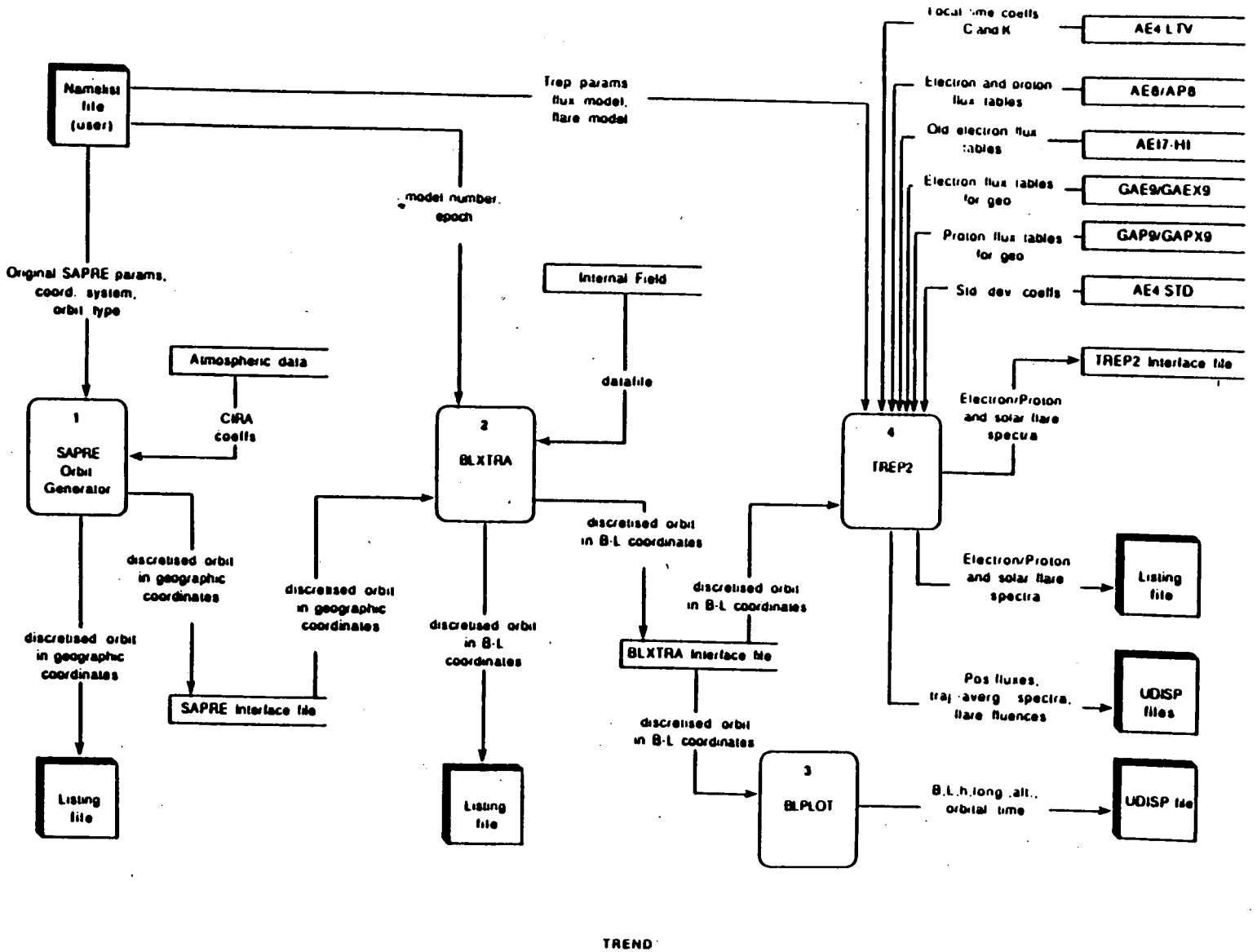

Fig.3-1. Architectural design of UNIRAD software showing the links between the orbit generator program (SAPRE), the B-L transformation program (SHELLG and now BLXTRA) and the radiation flux/fluence program (TREP).

B - The UNIRAD software package contains a second chain of programs and subroutines which transforms the geocentric coordinates into magnetic B-L coordinates by using optional geomagnetic field models. This chain of programs is called SHELLG in the earlier version of UNIRAD; in the new version it is called BLXTRA. It uses one of the 13 optional internal geomagnetic field models implemented in a datafile. The list of optional internal magnetic field models is given below with their ID number (MODEL : a parameter of $SHELL in the NAMELIST file UNIRNML).

MODEL	J	K	DATE	NAME
1	0	0	1960.0	HENDRICK&CAIN 99-TERM GSFC 9/65
2	0	0	1960.0	CAIN ET AL. 120-TERM GSFC 12/66
3	0	0	1960.0	CAIN&LANGEL 143-TERM POGO 10/68
4	0	0	1960.0	CAIN&SWEENEY 120-TERM POGO 8/69
5	1	1	1960.0	JENSEN&CAIN (1962)
6	1	0	1965.0	LEATON MALIN EVANS 80-TERM 1965
7	0	0	1970.0	HURWITZ US C&GS 168-TERM 1970
8	0	0	1975.0	IGRF 1975.0 80-TERM
9	0	0	1975.0	BARRACLOUGH ET AL. 120-TERM 1975
10	0	0	1975.0	AWC 168-TERM 1975
11	0	0	1980.0	IGRF 1980.0 120-TERM
12	0	0	1982.0	GSFC 11/87 MODEL AT EPOCH 1982
13	0	0	1985.0	IGRF85 120-TERM

The value of J indicates wether or not a spheric Earth is used for this specific model. When J≠0 geocentric coordinates are used; when J = 0 the program transforms first geodetic coordinates into geocentric ones. The values of K tells the program wether Gauss-normalized coefficients (K ≠ 0) or Schmit coefficients (K = 0) are used for the Harmonic expansion of the internal magnetic field model.

TREND has added to the list of models already available in SHELL G, the models number 5, 12 and 13. The last one is the latest version of the International Geomagnetic Reference Model (IGRF) corresponding to epoch 1985.0; it is produced by a Working Group 1 of IAGA's division I. The model 5 of Jensen and Cain (1962) was used to built the well known AE8 and AP8 trapped radiation models. Although these models are given for a certain epoch (eg. 1960.0 for MODEEL=5), the secular extrapolation for a latter epoch (BLTIME : a parameter given in $SHELL of the NAMELIST in the file UNIRNML) is automatically computed by the program BLXTRA when BLTIME differs from the epoch corresponding to the B-field model. Indeed, the secular time variations of the harmonic expansion coefficients are also stored in the datafile containing all internal B-field models.

No local time dependent external magnetic field model was available in SHELLG. It has been a major and important task for TREND to design, implement and test a new software package which includes now four different optional external magnetic field models which are local time dependent. The choice of the external magnetic field model is determined by the parameter OUTER given by $SHELL namelist in UNIRNML:

OUTER = 1 corresponds to the Mead-Fairfield (1975) model which has often been used in early studies of the magnetospheric field configuration ;

OUTER = 2 corresponds to the short version of Tsyganenko's model published in 1987;

OUTER = 3 corresponds to the long version of Tsyganenko's (1987) external field;

OUTER = 4 corresponds to Tsyganenko's latest published external magnetic field. These external field models of Tsyganenko (1987,1989) are described in appendix D.

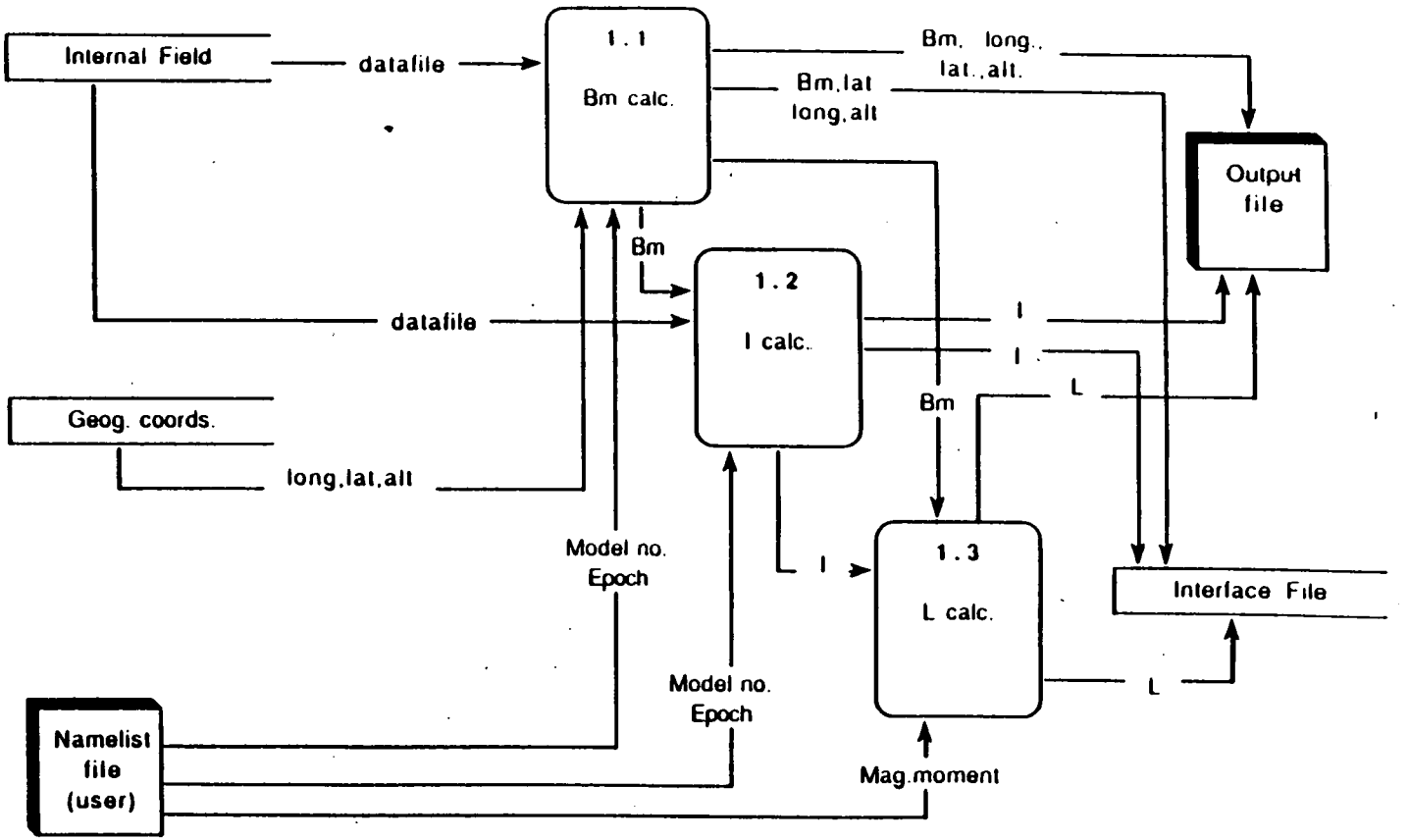

Coordinate conversion

Fig.3-2. Architectural design of BLXTRA program used to transform geocentric coordinates into magnetic B-L coordinates (general overview)

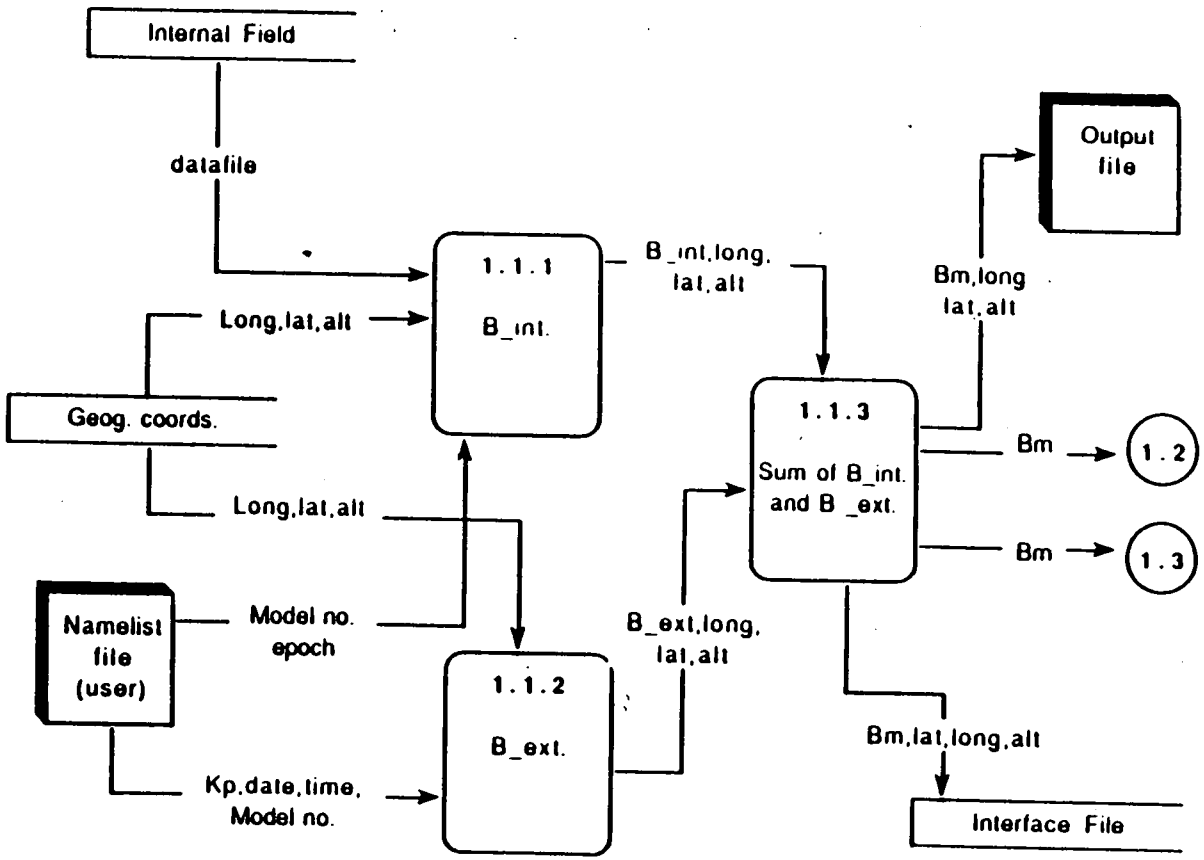

Fig.3-3. Architectural design of part 1.1 of BLXTRA, calculating the total magnetic field as the sum of an internal (B int) and external (B ext) magnetic field components.

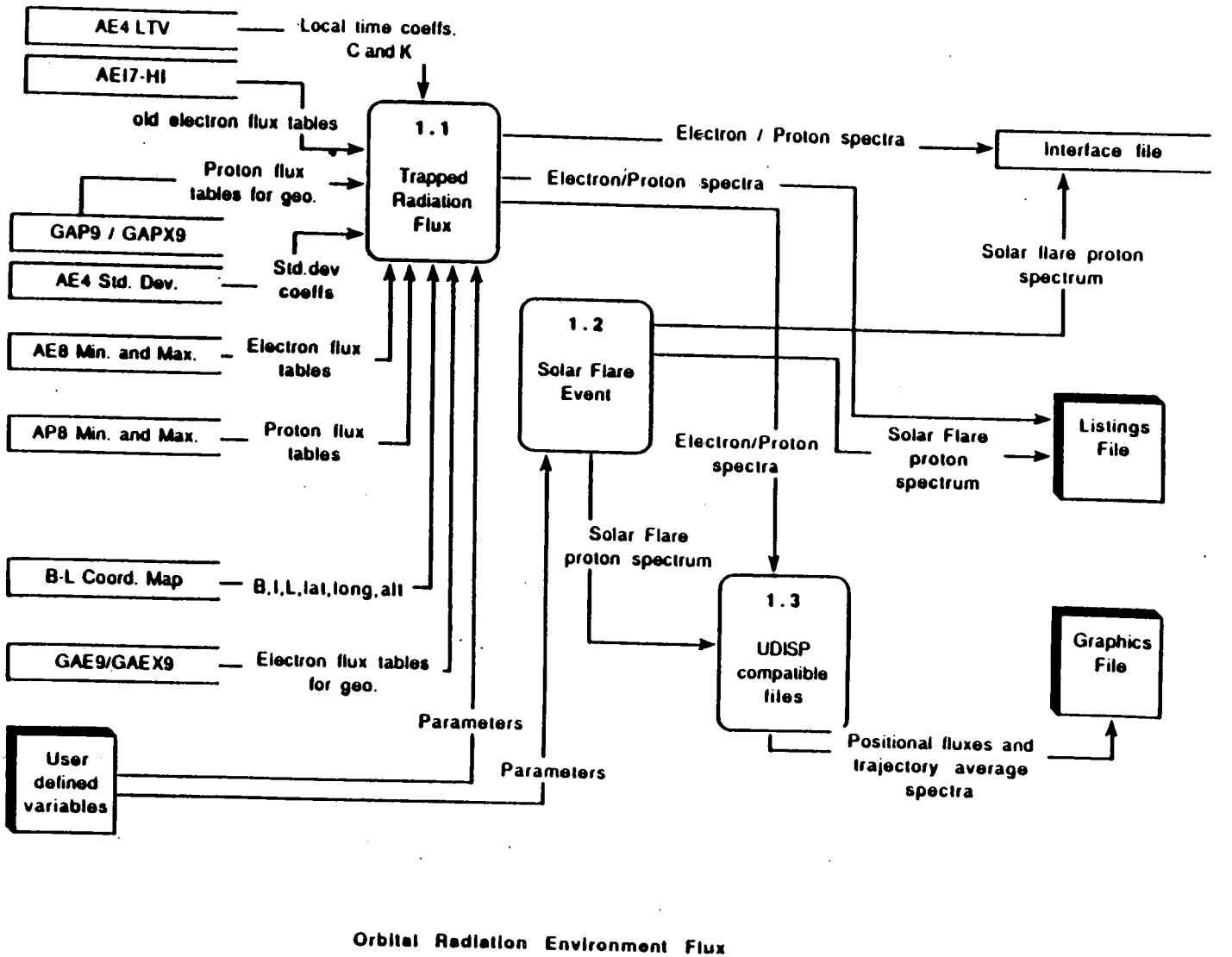

Fig.3-4. Architectural design of TREP (general overview)

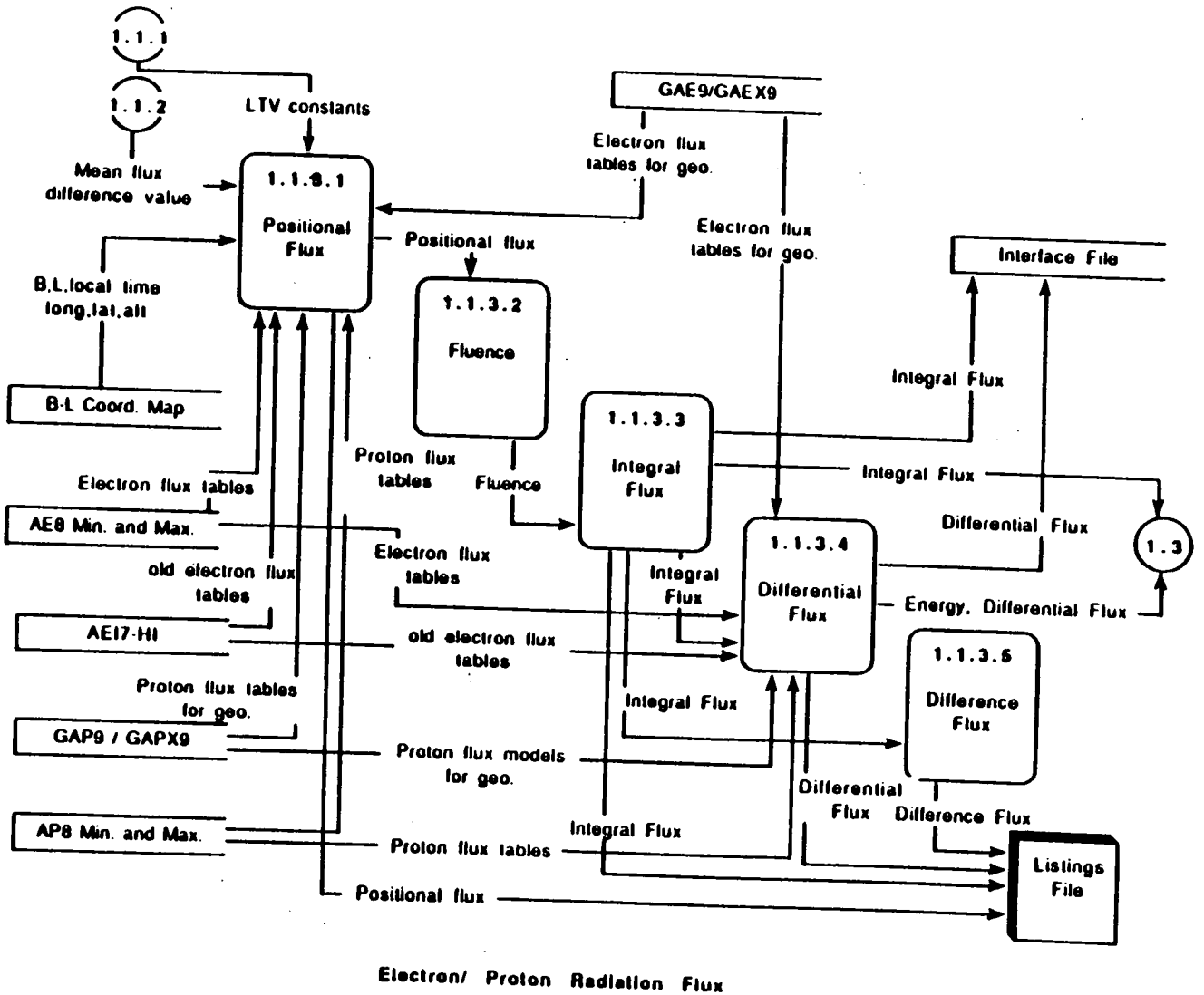

Fig.3-5. Architectural design of Electron and Proton flux calculation in TREP.

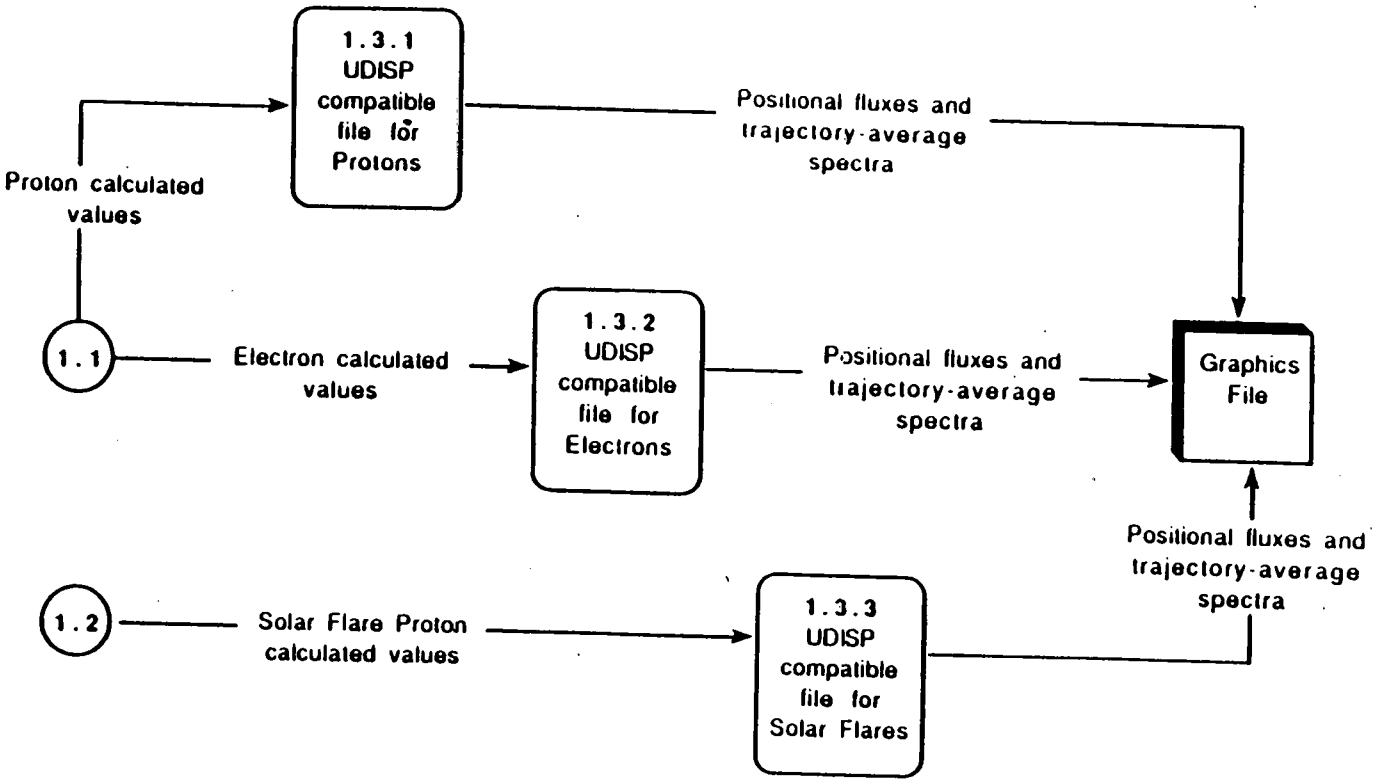

Fig.3-6. Architectural design of UDISP compatible files to determine trajectory-average energy spectra.

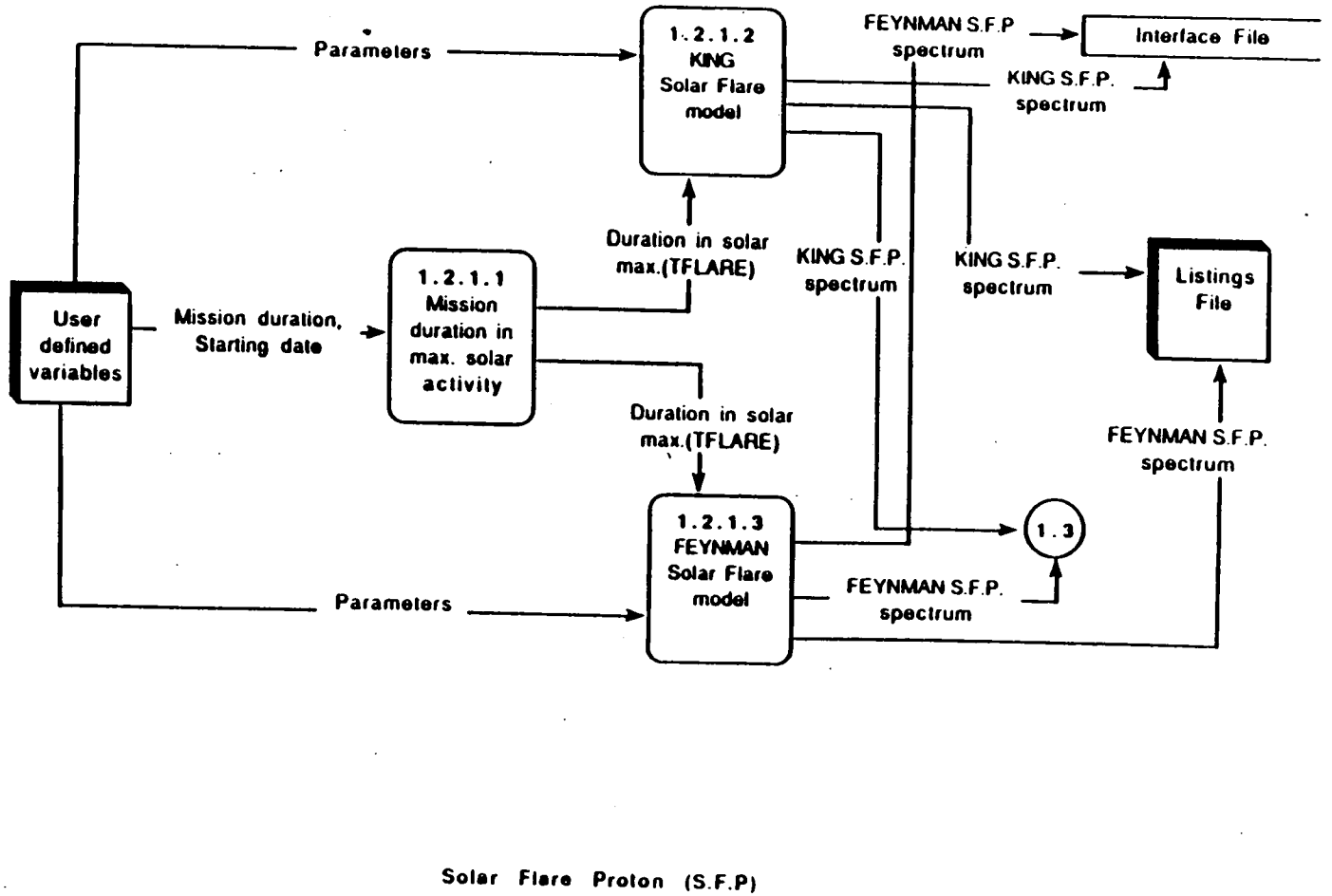

Fig.3-7. Architectural design for the calculation of solar flare proton spectra.

The new software package replacing SHELLG in UNIRAD, is now called BLXTRA. Figs.3-2 and 3-3 shows the architectural design of BLXTRA. BLXTRA is described in TN5 and in Appendix D. It was delivered to ESTEC as a documented FORTRAN source programs. The comparison of results obtained with BLXTRA and SHELLG are presented in TN5 and will be summarised in Chapter 5.

C - The UNIRAD software package contains a third chain of programs called TREP whose overall architectural design is shown by fig.3-4.

(1) This complex of programs calculates the omnidirectional flux of trapped electrons and trapped protons, using optional models like AE8 (for the trapped electron flux distribution) and AP8 (for the proton flux distribution) for each pair of B-L coordinates determined as output of SHELLG, and now BLXTRA. The trapped radiation models are stored in matrix form for a grid of B-L coordinates. Interpolation methods are used to calculate the fluxes at the intermediate B-L pair of values.

The fluxes are given both in differential form and integral form i.e. either for unit energy interval, J(E), and, for energies above an energy threshold, J(>E). Fig. 3-5 shows the architectural design for this part of TREP.

(2) The TREP chain of programs calculates also the fluence for these omnidirectional fluxes and orbital average flux values. (see fig. 3-6 for the architectural design of this part of TREP).

(3) The fluences corresponding to the trapped protons, are added to the contribution due to the solar flare protons. The Feynman et al.'s model described in TN1 and in chapter 2 has been implemented, as the default option, in this part of the TREP software TREND. The original solar proton fluence model by King, which was the only choice in

the earlier version of TREP, has been left as an option for the user of UNIRAD.

Fig.3-7 gives the architectural design for that new part of TREP. The detailed description of these changes are given in TN5. A comparison of the numerical results obtained by both models is also presented in TN5 and will be summarised in chapter 5.

The input parameters for the new version of Trep are given in the namelist section $TREP of UNIRNML file. The definition of these inputparameters and their deefault values are described in Appendix D. The B-L coordinates stored in SHELLOUTI are additional inputs for TREP.

The different outputs of TREP are listed in a report file TREPOUTP as well as in an interface file TREPOUTI. This latter file is used downstream to compute the radiation doses with other additional programs (eg. SHIELDOSE).

Examples of input parameters for 4 typical satellites orbits are given in TN5. The listings of the output files generated by TREP (and other programs of the UNIRAD chain, are also given in TN5 which constitutes the software user manual provided by TREND.

3.6 Software utility subroutines developed by TREND

A series of new utility subroutines have been developed by TREND and added to UNIRAD as part of this contract. They are called in SAPRE, BLXTRA or in TREP programs.

A- The following routines have been added; they are called directly by the main program.

- INIORB: initialisation of constants and commons,

- JD1950 (IYEAR,IMONTH,IDAY,IHRS,IMIN,ISEC,AMJD): computation of the modified Julian time AMJD as a function of date (IYEAR,IMONTH,IDAY) and time (IMIN,SEC,AMJD),

- GREMEQ (AMJD): function returning the sideral time as a function of the modified Julian date AMJD.

These routines are called by the main program of the orbit generator SAPRE. They are described in more details in TN5.

B- The external magnetic field components are computed by the subroutine BEXT which calls the subroutine TSY89. This subroutine computes the GSM components of the magnetic field produced by the magnetospheric current system. It corresponds to Tsyganenko's empirical magnetic field model version published in 1989 which is K_p dependent. It is based on the widest data base ever used to construct an external field model. There are 6 different series of model coefficients which correspond to 6 different ranges of K_p values (see Appendix D). The Earth's dipole tilt angle is another input argument which is however set equal to the zero, i.e. the daily averaged of this angle.

Constant L-contours calculated with and without Tsyganenko's external field are shown in chapter 4. At geostationary orbit a maximum difference of the order of 20% is obtained for L.

C- The optional solar flare proton model of Feynman et al. has been implemented in TREP. The input and output arguments are similar and compatible with those of King's model subroutine already available in TREP The duration of a mission in years during the active part of the solar cycle (TFLARE), and a confidence level, expressed in %

(FLPROB), as well as N values of proton energies E are the inputs (as in King's model). E is expressed in MeV.

P=1-FLPROB/100 is the probability that the fluence does not exceed the calculated fluence during the time length of the mission. The outputs are the fluences (FLUEFL) calculated for each energy level E. The units are protons/cm^2

The program FEYNL used to compute the Probability, P, as a function of the solar proton fluence, F, is based on a numerical method originaly proposed by Feynman et al.. The numerical values of P=P(FLUEFL;TFLARE) for different values of TFLARE were found to be the same as those published by Feynman et al.(1988). These results are discussed in chapter 4.

These values are stored as matrix elements which are used in TREP to calculate by interpolation the value of FLUEFL for any input value of TFLARE and P or FLPROB.

4. DATA ANALYSIS & MODELLING RESULTS

4.1 Results obtained with Feynman et al.'s model.

The FEYNFL subroutines computes the probability FLPROB that a given fluence 10^f is not exceeded during a mission which would last τ years during the active period of the solar cycle (τ = TFLARE). This probability depends on the energy threshold E (in MeV) as well as on the values of τ and f.

The numerical method is based on a Monte Carlo technique which involves the generation of N random numbers. The value of N is large (up to 10^5); this implies that the calculation is very time consuming and cannot be performed directly for each point along the satellite orbit with this subroutine FEYNFL. Therefore, the calculation of FLPROB is performed once for a variety of values of τ, f and for two values of E : 10 MeV and 30 MeV. Conversely, the value of f can be determined for a given value of FLPROB. These values are then stored in matrix form which is then used in TREP by interpolation to determine the value of f or 10f for given value of E, τ, and FLPROB. Table 4-1 shows the values 10^f (in p/cm^2) for τ = 2 years, for E = 10 and 30 MeV, and for two values of the FLPROB : 80% and 95%. The four last columns give the results obtained by TREND for different values of N. The results given by Feynman et al. (1989) are also shown in the fourth's column. It can be seen that the results obtained with the FEYNFL program is consistent with that of Feynman et al. The third column gives the results obtained for the same input conditions with the model of King (1974) for similar conditions.

E (MeV)	FLPROB (%)	King	Feynman	MATRA N=100	1000	10000	100000
10	80	1.3 E10	2.5 E10	2.28 E10	2.48 E10	2.35 E10	2.33 E10
10	95	4.0 E10	7.7 E10	1.12 E11	8.18 E10	7.89 E10	7.83 E09
30	80	4.9 E09	5.0 E09	5.99 E10	4.86 E09	4.80 E09	4.73 E09
30	95	1.7 E10	1.5 E10	2.11 E10	1.50 E10	1.51 E10	1.49 E10

Table 4-1 Comparison of different solar flare proton event models for TFLARE = 2 years.

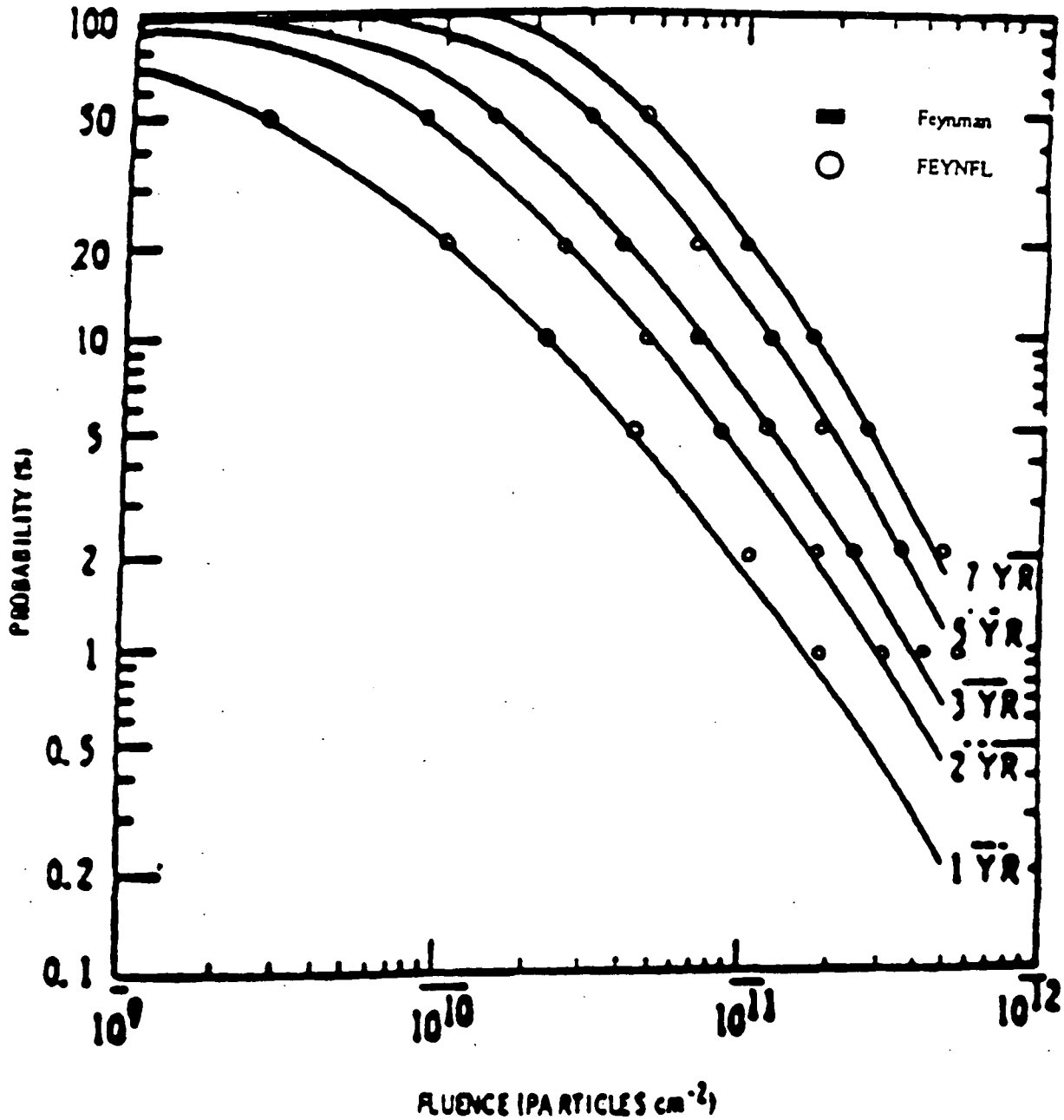

Fig.4-1. Comparison of Feynman et al.'s and TREND's calculation of the fluence of solar flare proton events for 10 MeV.

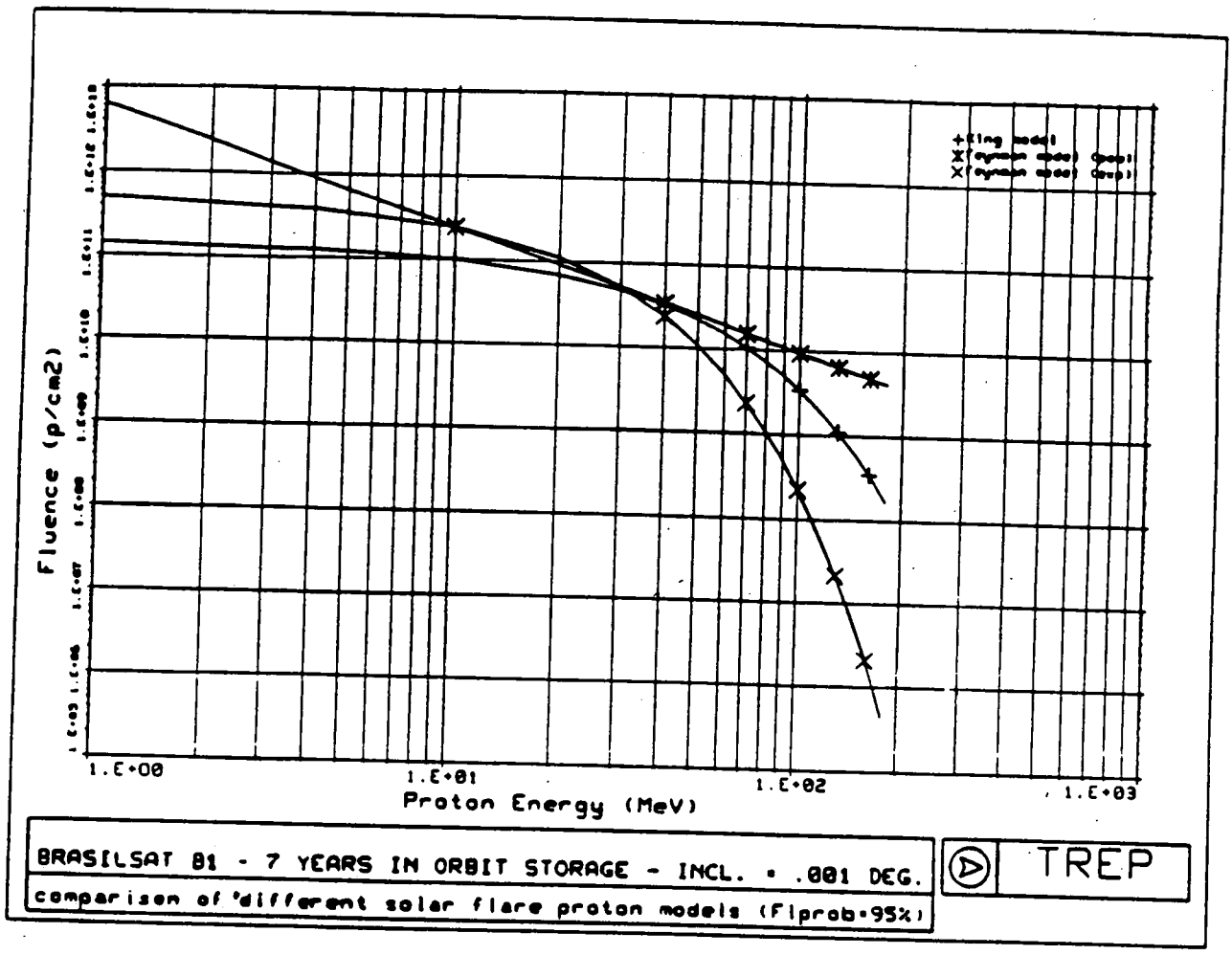

Fig.4-2. Comparison of the fluence spectra obtained from the Feynman et al's model for an exponential fit (X) and power law fit (*), for FLPROB = 95% and τ = 7 years.
The (+)'s give the fluence predicted by King's model.

Note that the CPU time required for calculating one value of the solar proton fluence f for FLPROB = 95% and τ = 2 years is equal to 30 s, 5 min, 45 min, respectively for N = 100, 1000, 10.000 with the FEYNFL. This clearly indicated the need for interpolation tables to be used in TREP instead of a direct calculation with subroutine FEYNFL.

The good agreement between the results obtained by TREND with the FEYNFL subroutine and Feynman et al.'s results is also illustrated in fig.4-1.

In Feynman's statistical study only two energy threshold were selected 10 and 30 MeV. To obtain the fluence at intermediate values of E an energy spectrum has to be assumed. Two different fit functions have been tried: an exponential law, and, a power law. Fig. 4-2 shows the fluence spectrum obtained with an exponential law (X) and with a power law (*) using Feynman et al's model. For comparison the corresponding results obtained with King's model for FLPROB = 95% and a 7 years spacecraft mission is also shown by (+). This figure confirms that the fluence prediction at low energies in King's model is more optimistic (lower values of the fluence) than Feynman et al's model.

However, at higher energies the reverse is true, when Feynman et al.'s observation are fitted with a simple exponential law. The values of $P(\tau, f, E)$ are stored as matrix elements in a file called PSTORE.DAT which is used with a standard interpolation technique to determine in TREP the value of f or 10^f for a given mission length (TFLARE) during the active period of the solar cycle, and for a given energy range or energy threshold.

4.2 B-L coordinates with and without an external magnetic field.

Up to present only internal geomagnetic field models have been used to determine the B-L coordinates of particle mirror points or labels of drift-shells. The 11 models already implemented in UNIRAD/SHELLG did not include the early Jensen and Cain (1962) model (for epoch 1960 ; 48 non-zero coefficients) which was used to construct AE8 and AP8 radiation environment models; it did not contain the most recent IGRF-85 model (epoch 1985 ; 120 coefficients). These two models as well as the GSFC 11/87 model for epoch 1982 (448 coefficients), have been added by TREND to the UNIRAD software package.

When any of these models is used to transform the geocentric position of a geostationary satellite, the B-L coordinates are then constant i.e. independent of universal time (UT) and local time (LT). But the B-L coordinates of geostationary satellite positioned at different geographical longitudes are located somewhere along the curve shown in fig.4-3. The double loop shape of this curve in B-L space is the consequence of the tilt angle of the magnetic dipole and of its eccentric distance with respect to the Earth center (see TN1 and chapter 2 of this report).

The B-L coordinates associated with the flux measurements of LANL geostationary satellites are then independent of UT and LT when B and L are computed with an internal magnetic field only. However, this is no more the case when a local time dependent external magnetic field component is added to the internal geomagnetic field. In this case the values of B-L coordinates of a geostationary

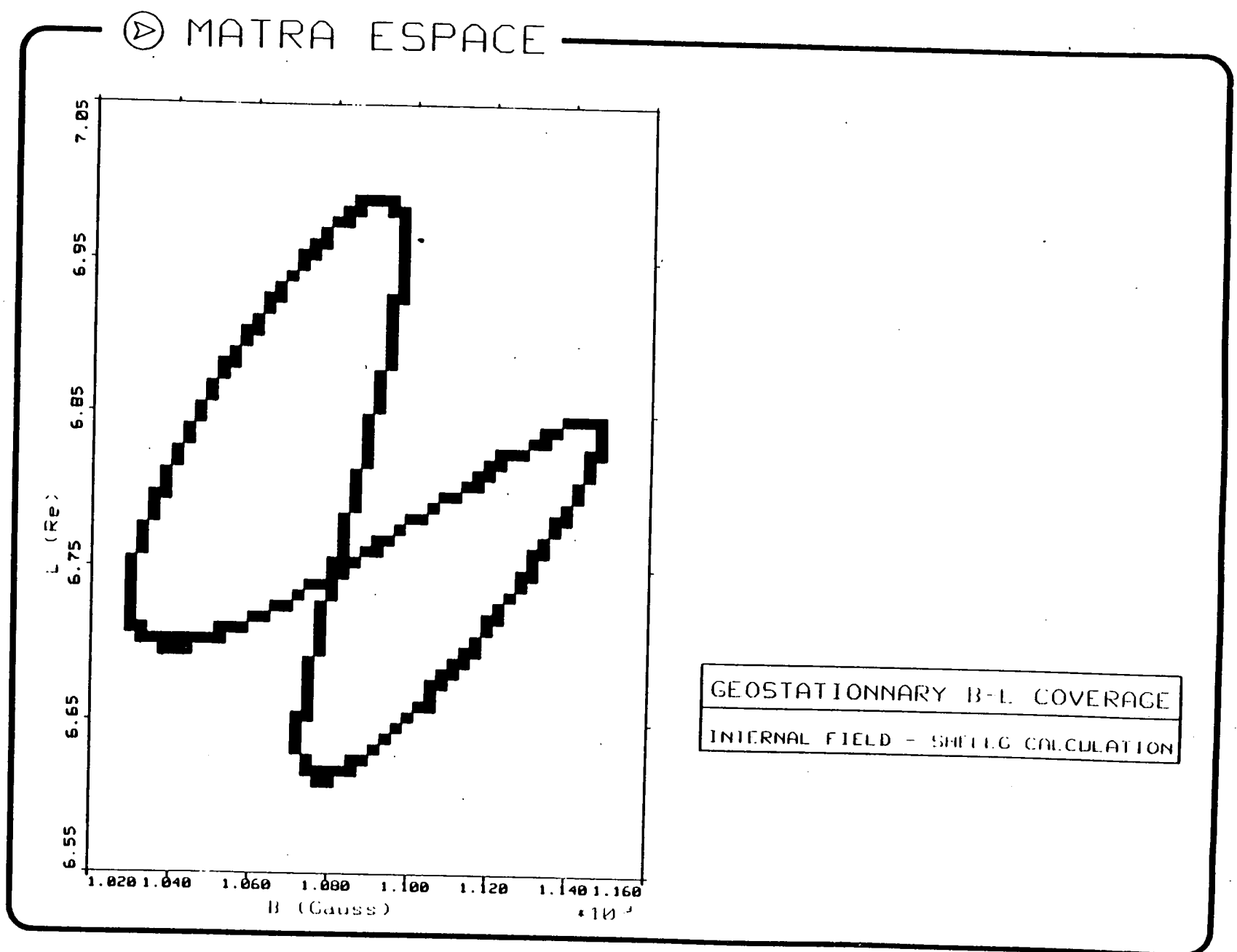

Fig.4-3. B-L coordinates of geostationary satellites located at different geographical longitudes, when the geomagnetic field is approximated by the IGRF-85 model for epoch 1979.

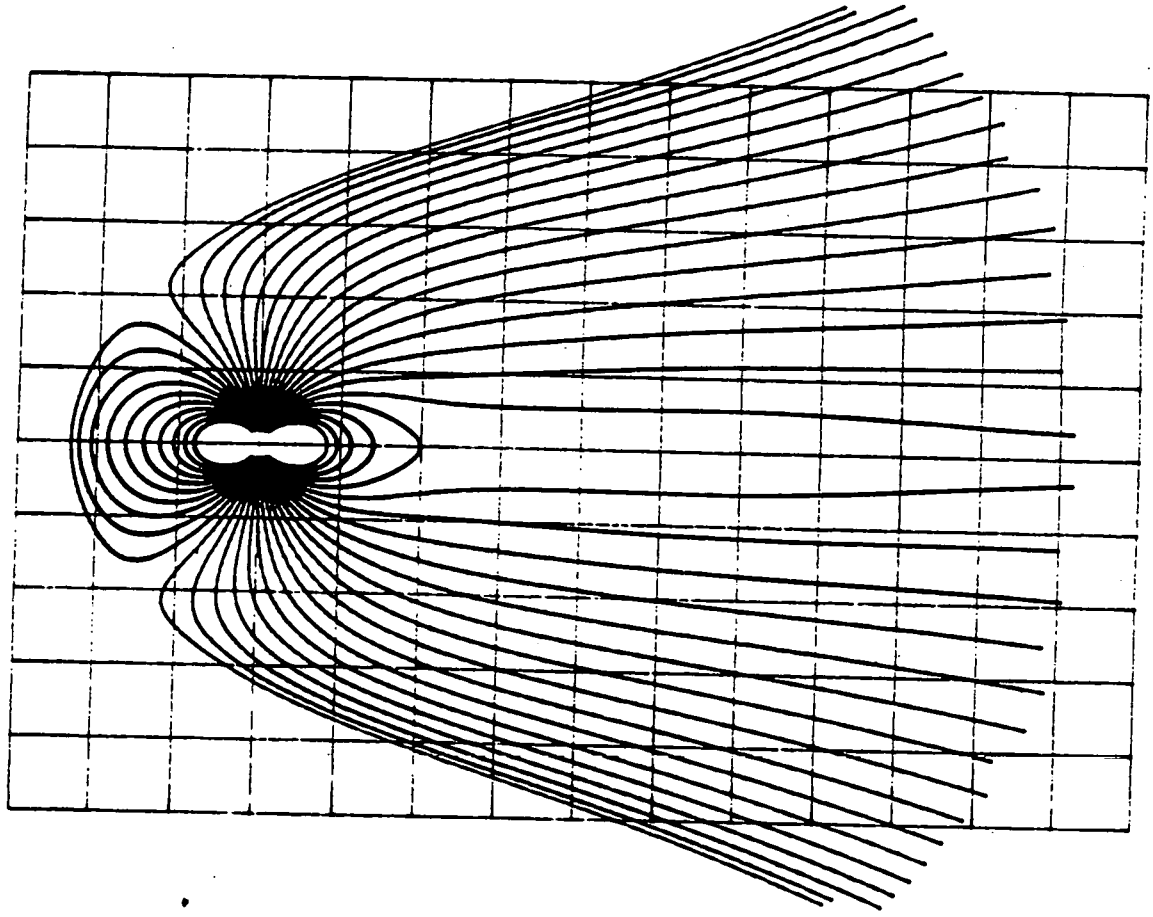

Fig.4-4. Magnetic field line distribution obtained with TSY 89 subroutine for zero tilt angle, and $K_p = 4$. The distortion of magnetic field lines at large distance is quite evident. This implies that the values of L corresponding to a fixed altitude in the midnight local time sector are larger compared to those calculated with an internal field model only. Near noon the values of L are reduced by the addition of an external field. The magnetic field intensity is reduced near midnight, but enhanced near noon local time by the presence of additional magnetospheric currents.

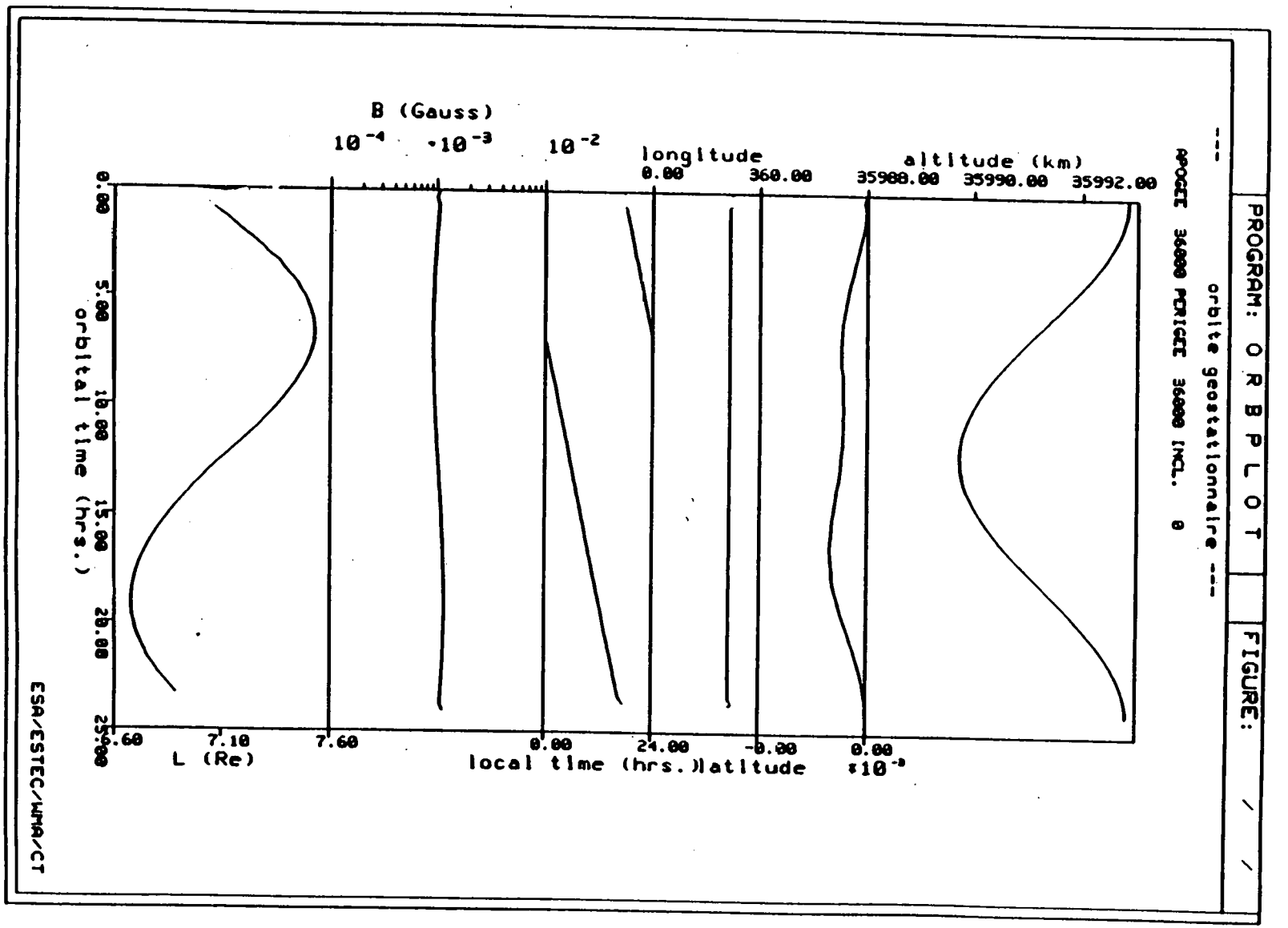

Fig.4-5. B-L coordinates of an equatorial circle coinciding with geostationary orbit.

satellite changes continously with UT and LT. This is a consequence of the day-night asymmetry of magnetospheric currents which produces the observed LT asymmetry of the magnetic field at geostationary orbit (see figs. 4-4 and 4-5). Since this LT asymmetry in the B-field entails a LT asymmetry in (B-L) drift shells (and in addition produces shell splitting) it is essential for mapping radiation environment at large radial distances to include in UNIRAD the best external magnetic field model currently available (see TN1 for a review of different such models).

Despite some of its limitations, the model of Tsyganenko (1989) has been adopted as the default one for UNIRAD. It corresponds to OUTER=4 in the NAMELIST of UNIRAD. It describes in an empirical way the contributions due to

1) the tail current calculated in SM coordinates
2) the ring current calculated in SM coordinates
3) the return current of the tail
4) and the Chapman-Ferraro current both calculated in GSM coordinates.

The coefficients in the equations describing these different contributions depend all on the value of the geomagnetic index K_p which determines, for every tri-hourly period of time, the amplitude of the short term variation of the geomagnetic field.

TREND is of the opinion out that it would have been preferable to parametrize the Ring Current component separately as a function of the D_{st} geomagnetic index instead of Bartels K_p tri-hourly index. TREND also recommends constructing in future external magnetic field models which are directly dependent of solar wind plasma and field parameters instead of K_p. Since such more elaborate models are not yet available except Olson-Pfitzer's dynamical model which goes some way towards those

requirements, the latest version of Tsyganenko models has been adopted by TREND. The equations used are described in Tsyganenko's paper and in TN1. A brief overview of this new model is also provided in appendix E of this report. The subroutine implemented by TREND is called TSY89.

The TREND subroutine TSY89 was tested with respect to the published results and with respect to Tsyganenko's own software. A software package has been received subsequently from Tsyganenko (personal communication 1989). Both codes give the same outputs. TREND's code is just slightly faster on the computer available at IASB than the original version of Tsyganenko (personal communication, D.FONTEYN, 1990).

Fig 4-6a and b show isocontours of the magnetic field intensity at a surface of constant altitude (36,000 km). The latitude and longitude of points forming constant B-lines are superposed on a mercator map of the Earth.

Fig.4-6a corresponds to the case where an internal geomagnetic field model (IGRF85) is used to determine B. Fig.4-6b is obtained for the case when Tsyganenko's model (TSY89) is added to the same internal field model. These figures clearly illustrate the significant effect of the external field on the B-field intensity at large distance.

Fig.4-7a and 7b show in a similar format contours of constant values of L corresponding to all points of the same constant altitude surface (36,000 km). The limit between "open" and "close" magnetic field lines (i.e. where L>20) is strongly local time dependent. It is in the mid-night local time sector that the latitude of the trapping boundary is closest to the equator. Note also that the introduction of an external field lowers considerably the latitude of constant L contours.

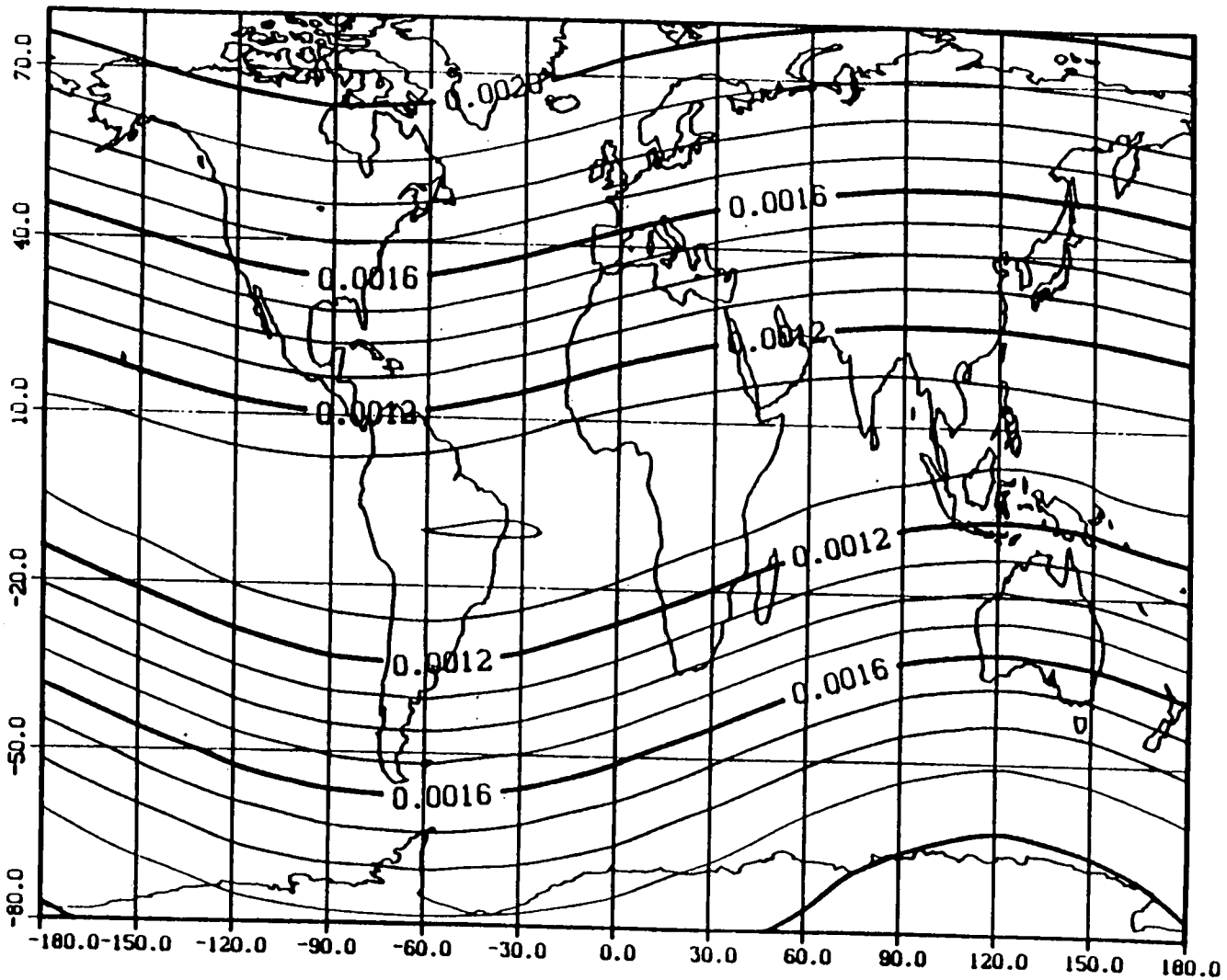

Fig.4-6a Intersection of a sphere of constant altitude (geostationary altitude: 35.677 Km) and surfaces of constant magnetic field intensity (B = 0.0016 gauss; 0.0012 gauss...) when the geomagnetic field is approximated by the internal IGRF-85 model for epoch 1979.

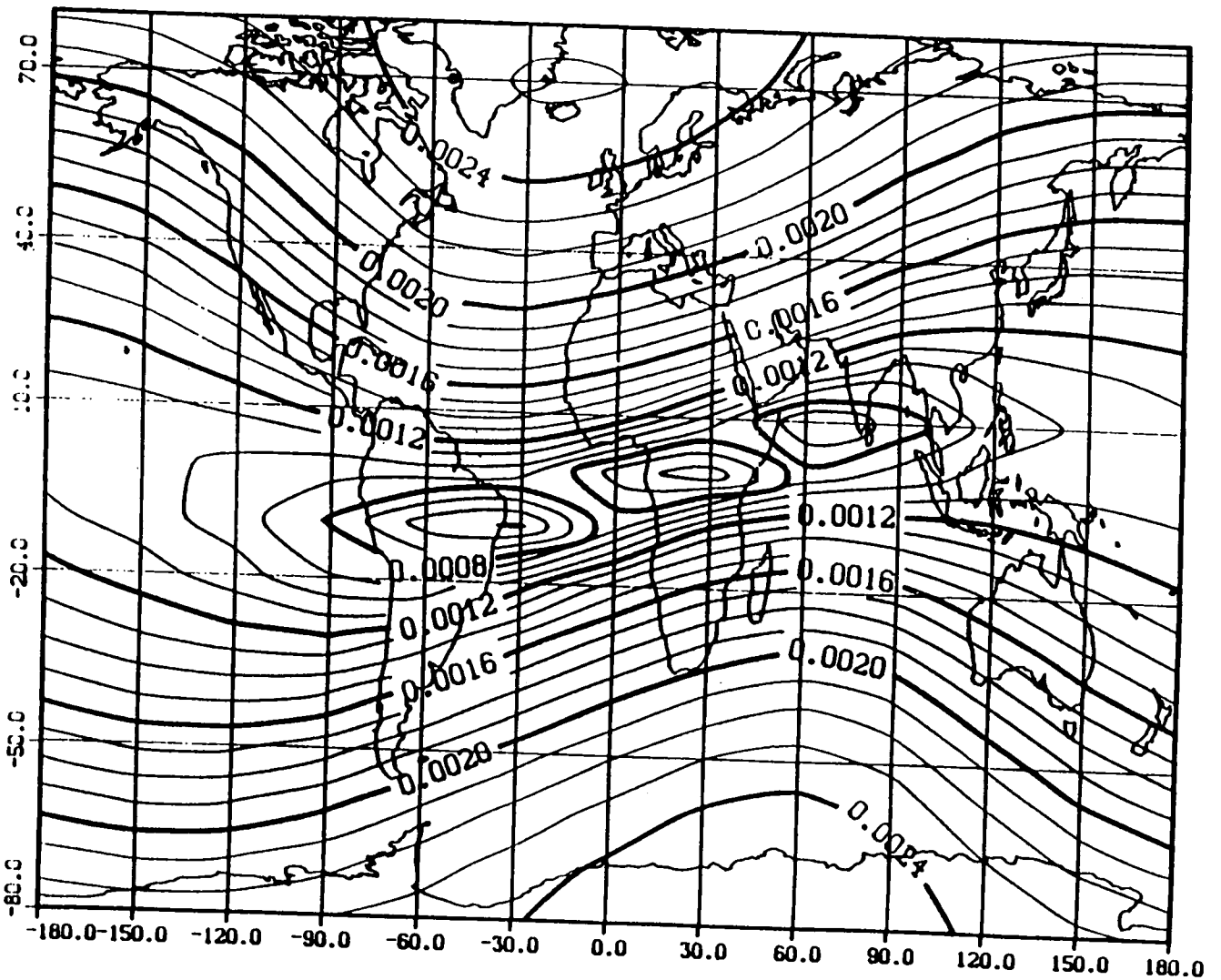

Fig.4-6b Same as fig.4-6a, except that in this case the external magnetic field model of Tsyganenko (1989) has been added to the internal field model IGRF-85.

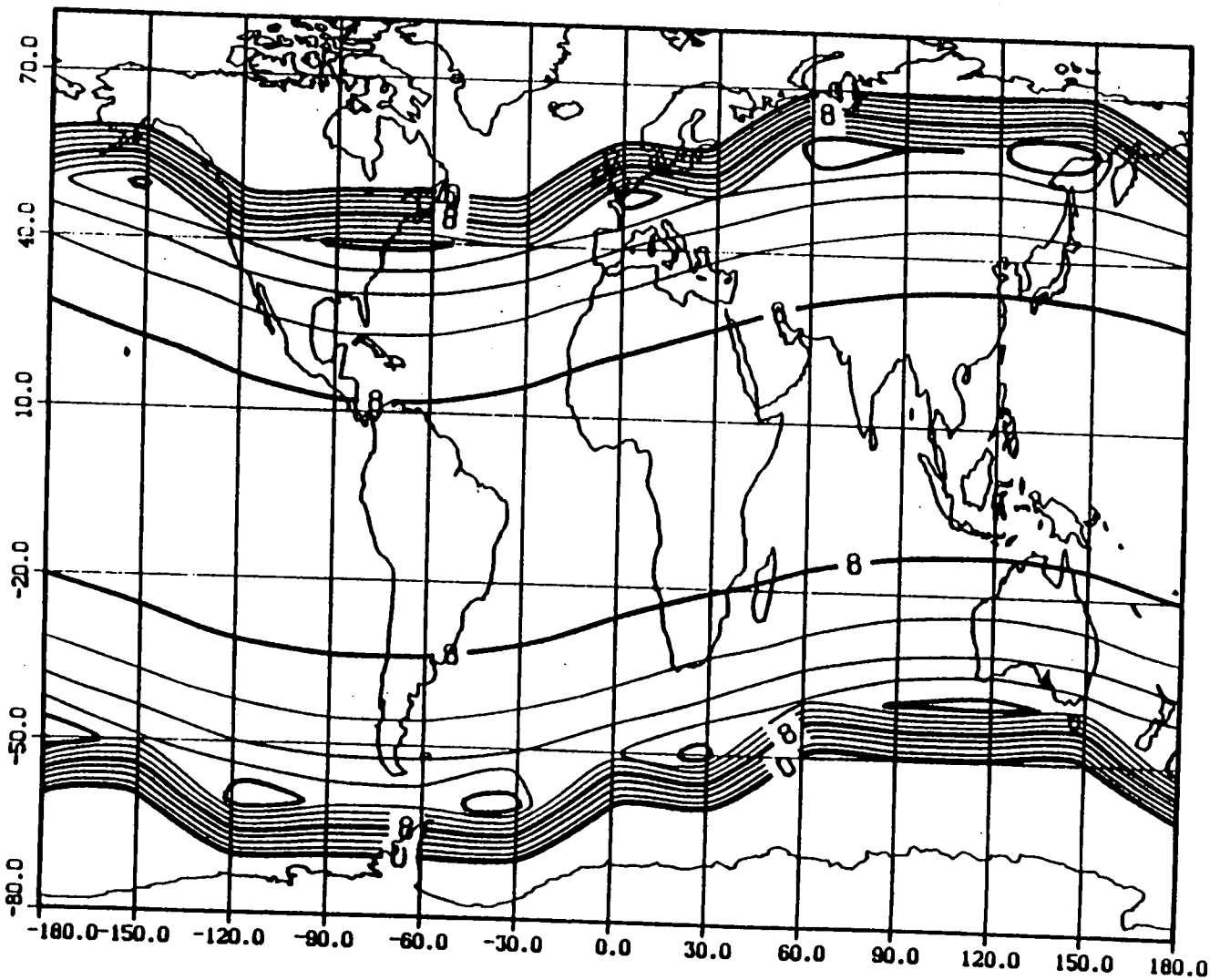

Fig.4-7a Intersection of a sphere of constant altitude (geostationary altitude: 35.677 km) and surfaces of constant L values (L=8,10...), when the geomagnetic field is approximated by the internal IGRF-85 model for epoch 1979.

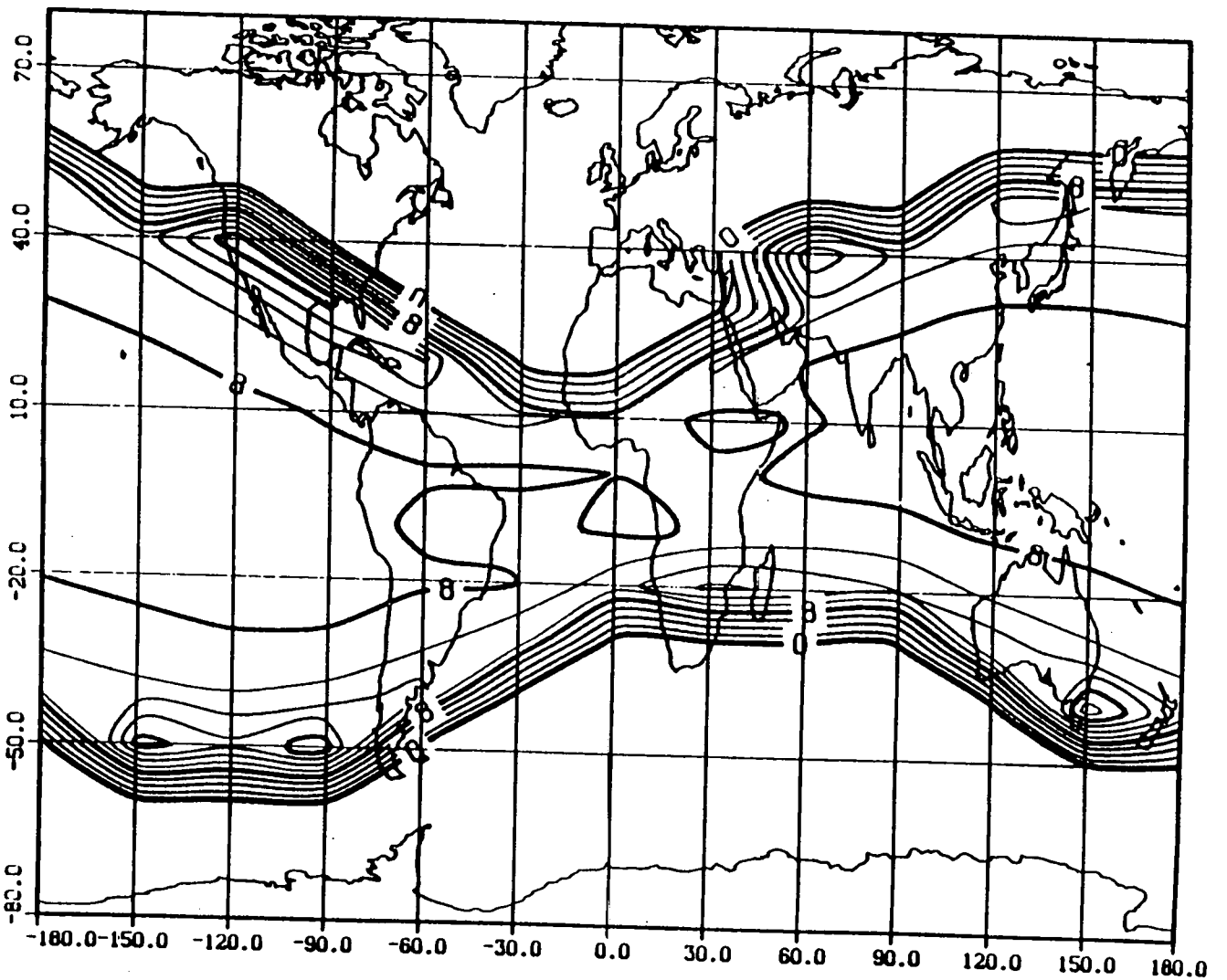

Fig.4-7b Same as fig.4-7a, except that the external field model of Tsyganenko (1989) has been added to the internal field model IGRF-85.

Beyond this trapping boundary the magnetic field lines extend to infinity (at distances larger than 20 R_E); the second adiabatic invariant, I, of particles spiraling along these field lines is not defined; therefore L cannot be defined either. In this region of the magnetosphere, outside the trapping region B-L coordinates are not defined. No valuable alternative to B-L coordinates has been found yet, in this case.

It must be recognized, however, that the flux of trapped particles in the region of open magnetic field lines (and in the quasi-trapping regions) drops to zero and needs not to mapped here. In this region solar flare protons contribute occasionally very large fluxes for short periods of time, and constitute the major hazard for microelectronic device.

It should be pointed out, that the amplitude of LT variation of L for a geostationary satellite is of the order $\Delta L=1$ (i.e. one Earth radius); this remains relatively small ($\Delta L/L$ = 10-15%); furthermore at these larger L values the trapped radiation fluxes in the AE8 model are given at L-intervals of ΔL = 0.5 ! This implies that only two bins in L are concerned by the LT variation resulting from the assymetry of the external magnetic field at geostationary orbit.

4.3 Distribution of LANL positions in B-L space.

Since LANL satellites are geostationary their position in B-L space is a single point when B and L are determined with an internal magnetic field model. This point corresponds to B=1.09 10^{-3} Gauss and L=6.80 for LANL2 (see fig. 4-8a). For the five other LANL satellites located at other fixed longitudes along geostationary orbit the B-L coordinates correspond to five other points of the curve

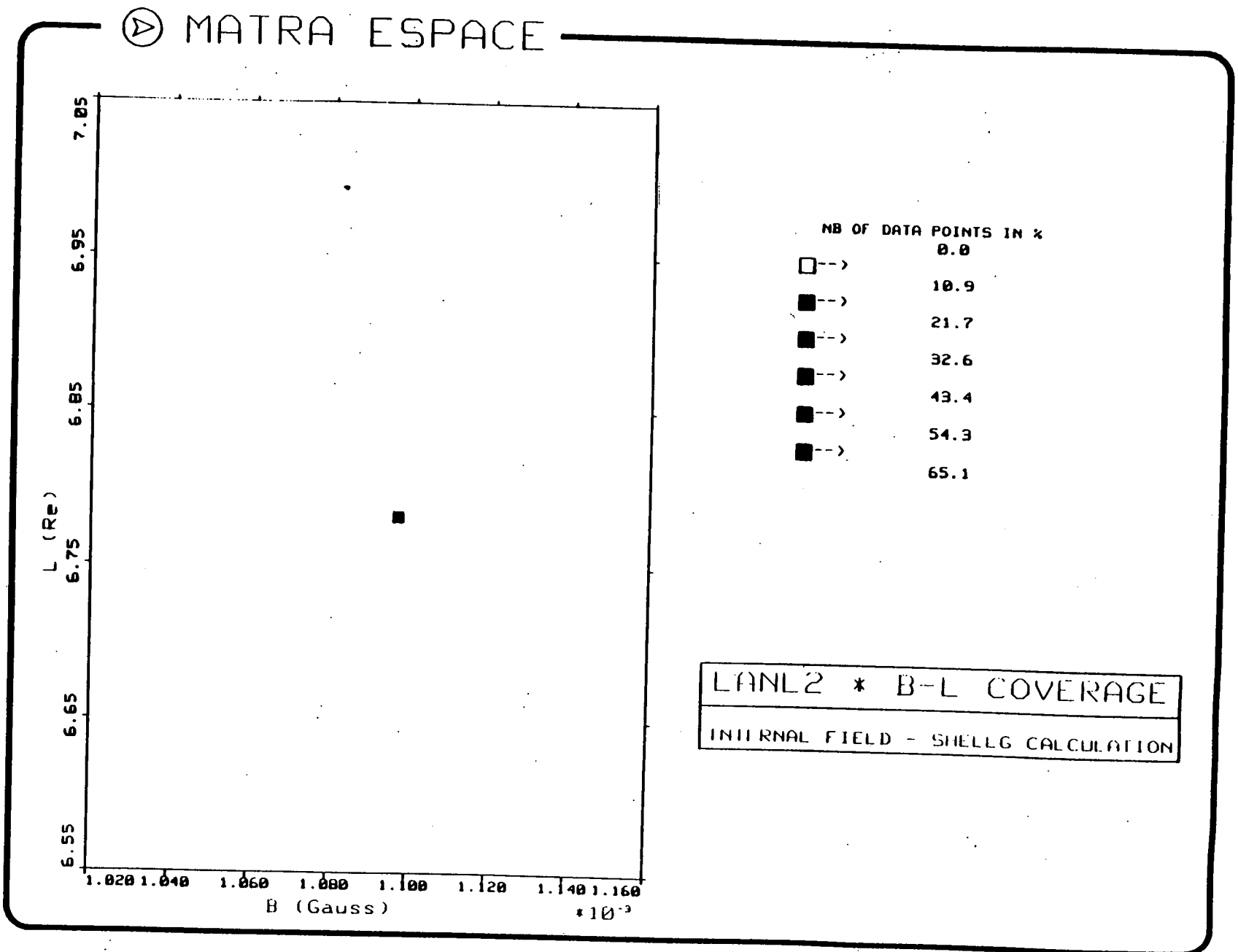

Fig.4-8a Position of the LANL2 data in B-L space when only an internal geomagnetic field model (IGRF) is used.

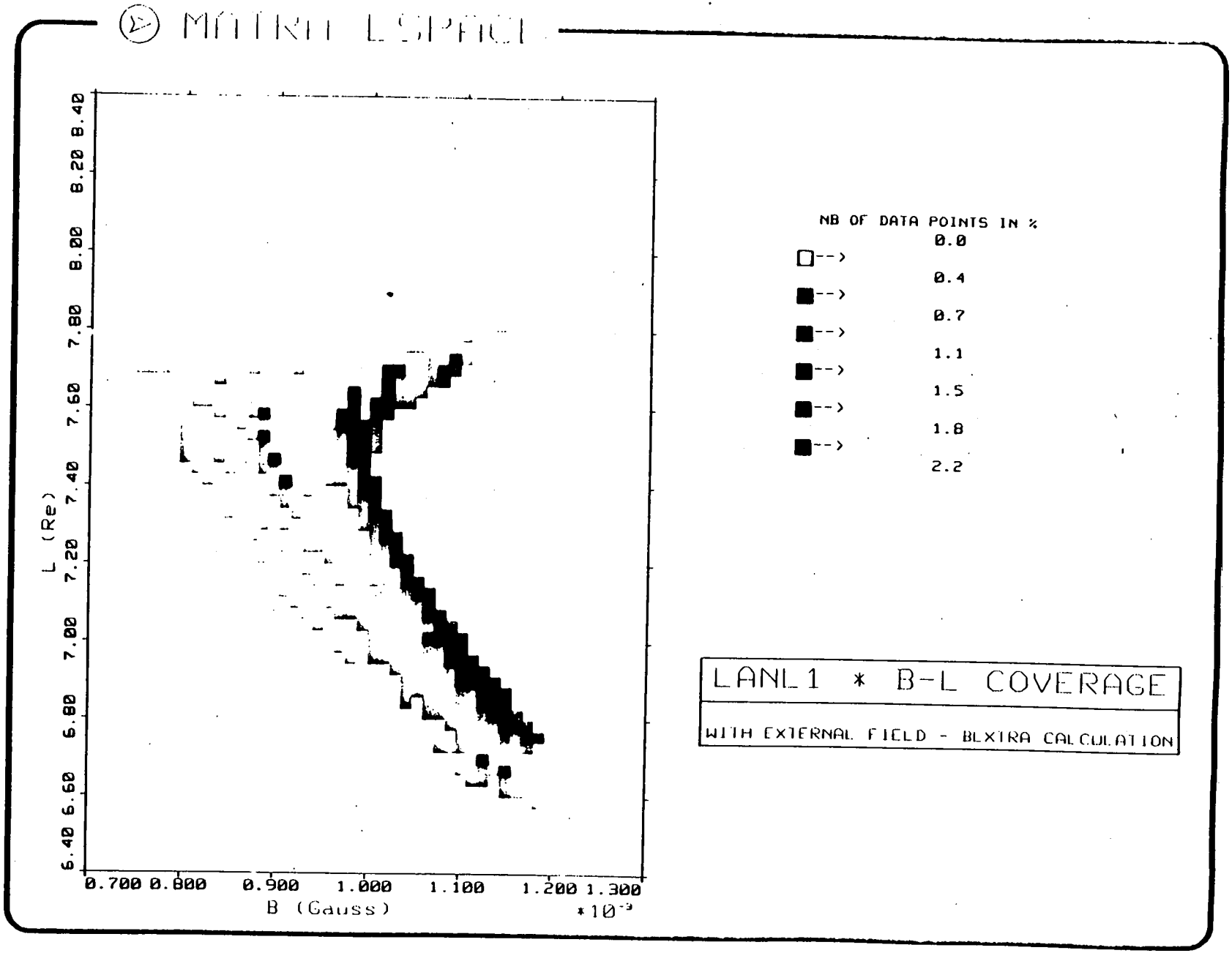

Fig.4-8b Distribution of LANL1 data set in B-L space. The geomagnetic field has been approximated by the K_p- and LT-dependent external field model of Tsyganenko (1989).

shown in fig. 4-3.

When Tsyganenko's external magnetic field is introduced to recalculate B and L at each instant of time, the position of the satellite moves along a closed curve which is fixed in B-L space provided that the external field is constant in time: i.e. when the geomagnetic index K_p does not change. However, in reality the value of K_p changes almost every three hour of UT, consequently the orbit of LANL satellites is not a closed curve, but the positions of the satellites wander in a random manner within extended areas of B-L space. This area is shown in fig. 4-8b for LANL1. The different grey shading shows the relative number of data (in %) available in each small bin of B-L space.

This figure clearly illustrates how the LT variation of the external magnetic field and furthermore its dependence on geomagnetic activity (K_p - index) scatters the positions of a geostationary satellite like LANL1 into a range of B-L bins around the single point corresponding to its position calculated with SHELLG, the former software of UNIRAD.

4.4 Distribution of LANL electron flux measurements.

A brief description of the LANL data has been given in the previous chapter; a more detailed account can be found in TN2 and TN5.

Daily electron omnidirectional flux measurements from LALN1 are given in fig. 4-9a, b, c as a function of time (days of year 1979). In these figures only data concentrated in a given bin of B-L space are diplayed : $0.001065 < B < 0.001085$; $6.95 < L < 7.05$. The three different figures correspond to three different energy

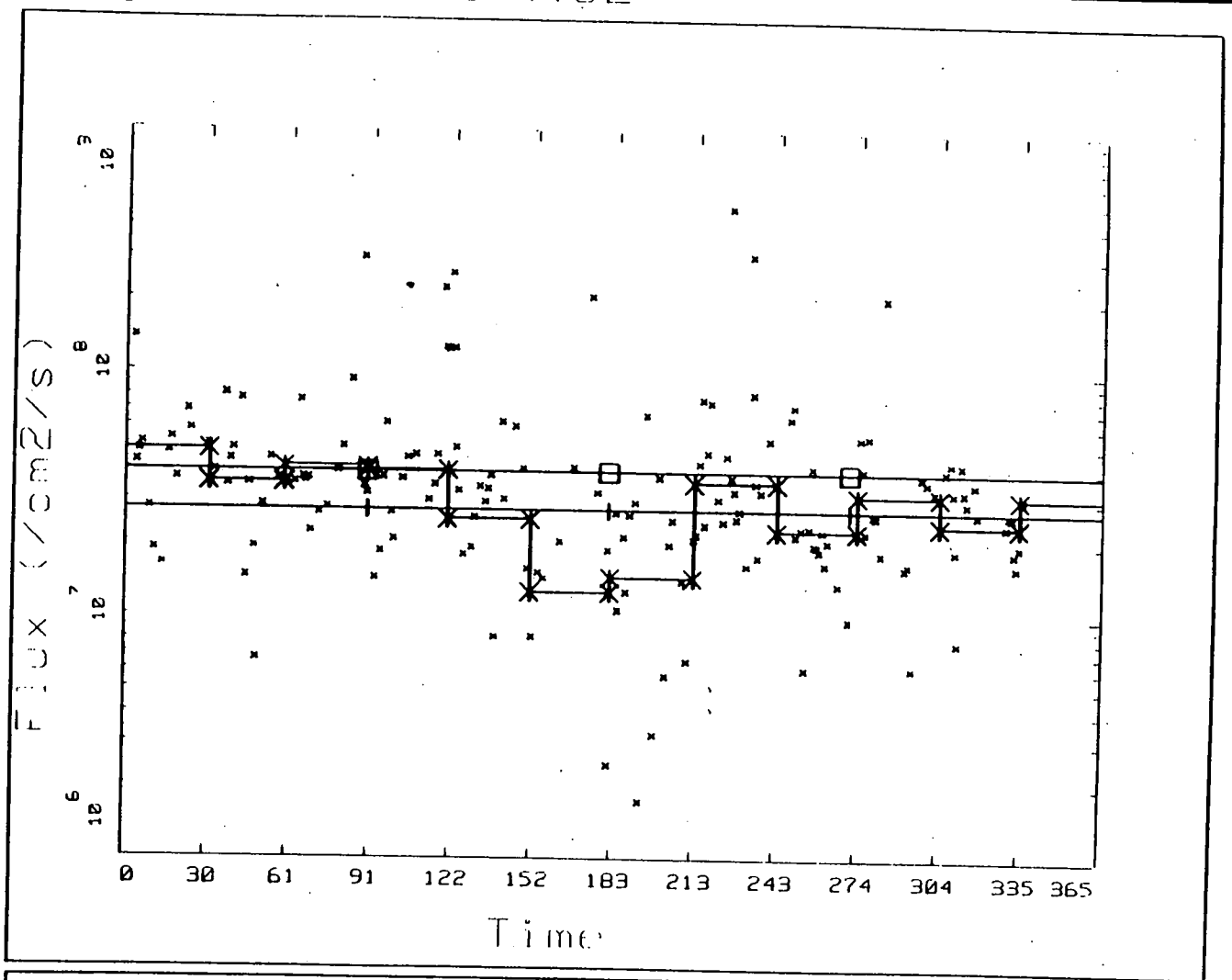

Fig.4-9b LANL1 omnidirectional electron flux measurements as a function of time (days of year 1979). Only data concentrated in a small bin of B-L space are plotted. All data correspond to electrons with energies larger than 100 keV.

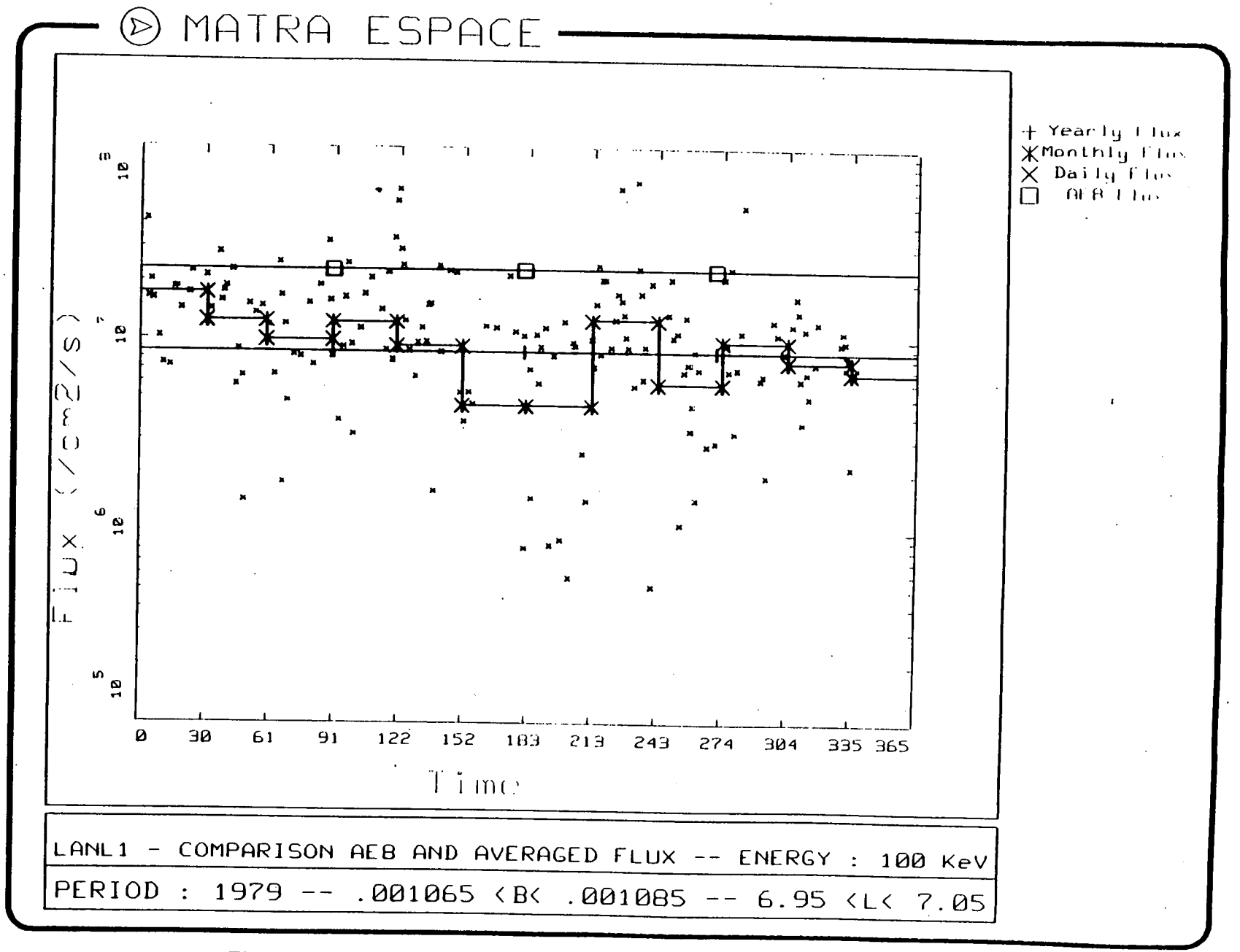

Fig.4-9a LANL1 omnidirectional electron flux measurements as a function of time (days of year 1979). Only data concentrated in a small bin of B-L space are plotted. All data correspond to electrons with

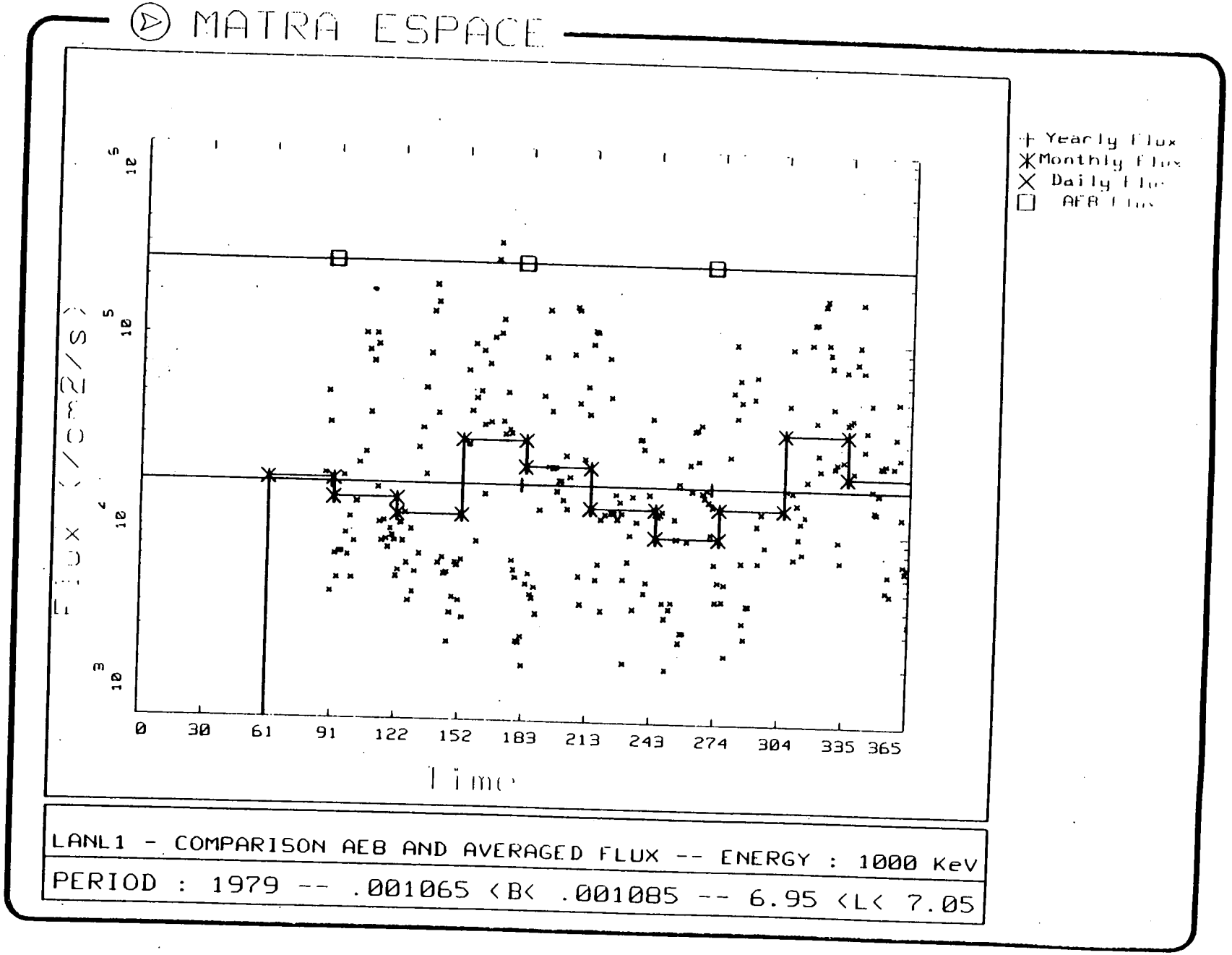

Fig.4-9c LANL1 omnidirectional electron flux measurements as a function of time (days of year 1979). Only data concentrated in a small bin of B-L space are plotted. All data correspond to electrons with energies larger than 1 MeV.

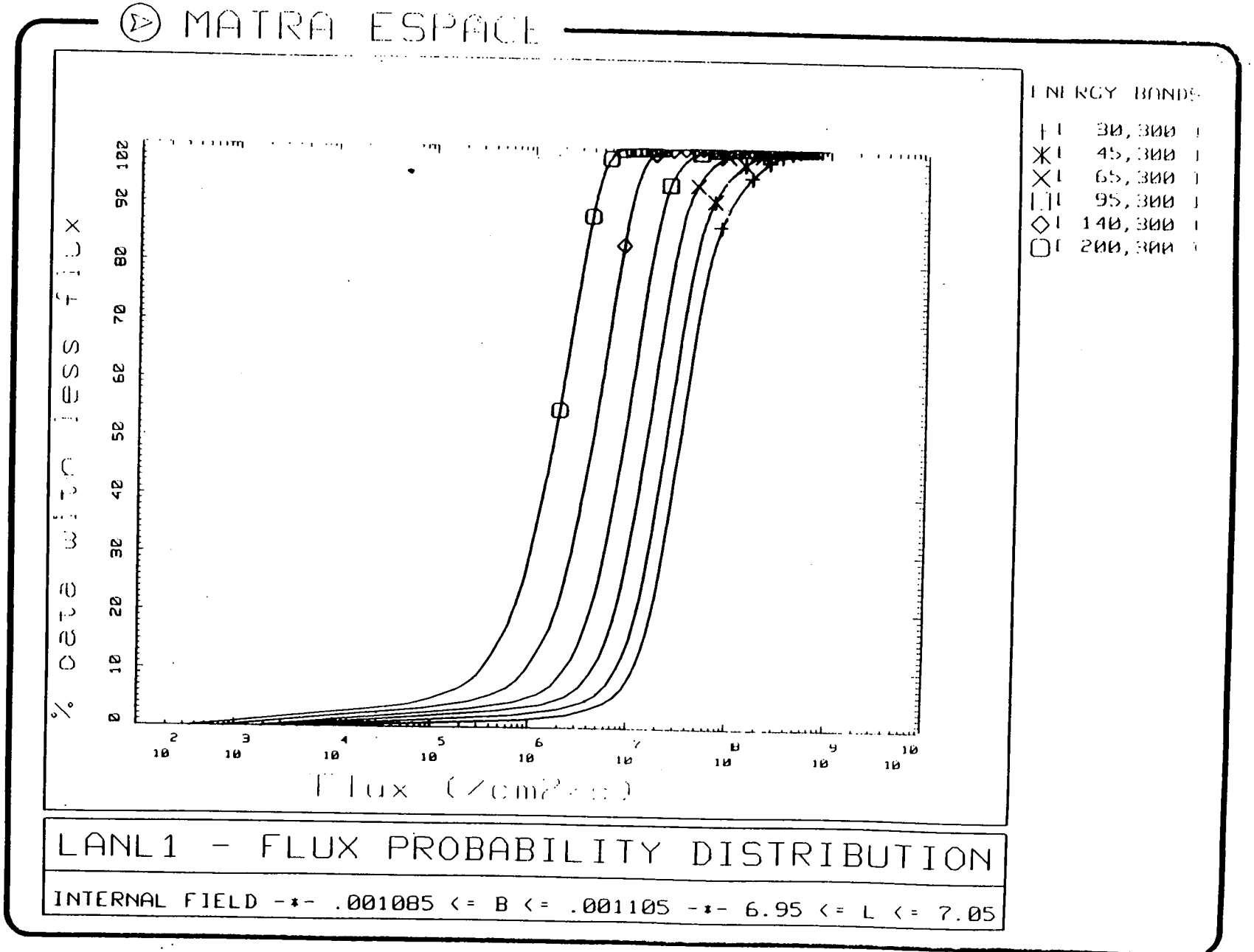

Fig.4-10a Cumulative distribution of LANL1 data with flux values (in selected energy bands) smaller than the numbers given in abscissa

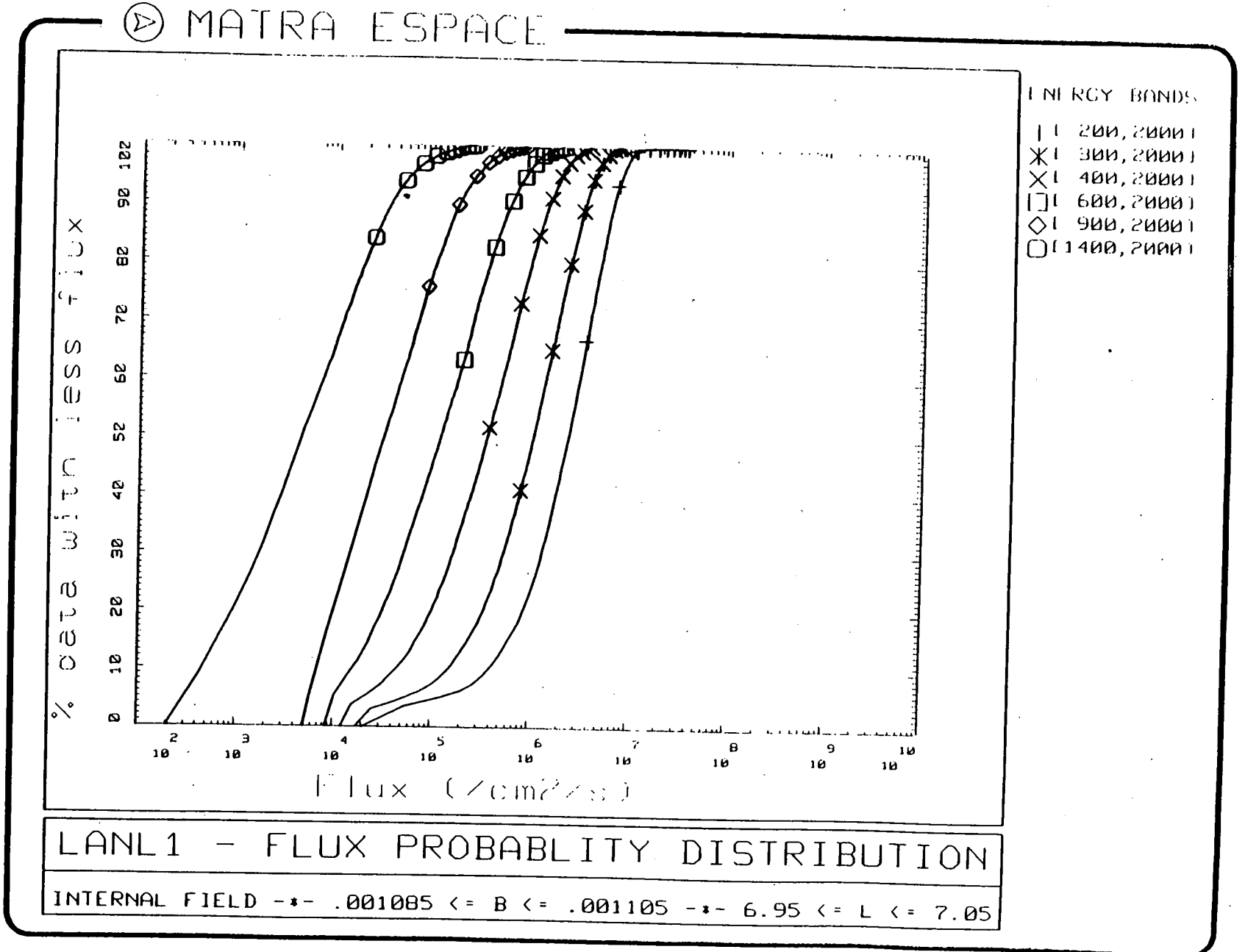

Fig.4-10b Same as fig.4-9, but for higher energy bands.

thresholds : 30 keV, 100 keV and 1 MeV. Yearly and monthly averages are given, as well as the values predicted by the AE8 model in that same bin of B-L space and for the same energy thresholds.

It can be seen that the AE8 model predictions are generally higher than the observed yearly averages for all energies. The tendency for pessimistic prediction (i.e. too high radiation fluxes) increases with the energy threshold. For E < 30 keV, 100 keV an 1 MeV, the yearly averages of LANL1 are respectively a factor of 1.5, 2.6 and 10 smaller than the corresponding AE8 values.

Similar results are obtained for other bins in B-L space, and for the other LANL data sets. These results support earlier data comparison with AE8 model predictions.

The monthly averages of LANL1 omnidirectional flux are also displayed in fig. 4-9a ,b and c. Despite the large dispersion of the daily flux values, a seasonal variation can be seen in the monthly averages. The same seasonal variations are observed in all B-L bins. However, the seasonal variation of low and medium energy electron (> 30 keV and > 100 keV) differs from that of the relativistic electrons (> 1 MeV). At low and medium energies the monthly means are a factor 3-4 smaller during the summer than at the time of solstices. On the contrary for the high energy electrons (>1 MeV) the summer values are a factor 3-4 larger than the solstice values. TREND has not investigated the origin of these seasonal variations. A more detailed study of these different electron populations with respect to the tilt angle of the Earth magnetic field and various geomagnetic activity indices (K_p and D_{st}) would be necessary to draw definitive conclusions concerning the origin of these seasonal variations.

It can also be seen from figs 4-9a ,b and c that the daily electron fluxes are scattered over a wide range of values (1 or 2 orders of magnitudes). This fact is well

known from previous observations of trapped electrons at geostationary orbit. More about the statistics of the LANL data is shown in following figures.

Let us now concentrate on all measurements made in the bin : $0.001045 < B < 0.001065$ Gauss and $6.85 < L < 6.95$.

Figs.4-10a and 4-10b give the cumulative distributions (in %) of the relative number of flux measurements whose value is smaller than x (:the abscissa in these figures). Fig. 4-10a shows this distribution for fluxes of electrons in selected energy intervals (30-300 keV... 200-300 keV). In fig. 4-10b the flux above different energy thresholds are considered (i.e. E>200; >1400 keV).

There are no flux measurements with values smaller than 10^2 cm^{-2} s^{-1} (instrumental limitation). On the other hand 100% of the flux measurements (i.e. all of them) have values smaller than 10^8 cm^{-2} s^{-1}. From these distributions it is possible to test wether the observed fluxes satisfy a log-normal statistical distribution or not.

4.5 Energy spectra deduced from LANL electron flux measurements.

The (X) in Fig. 4-11 shows the observed electron fluxes per cm^2 per second and per unit energy internal (keV), when all the LANL1 data available for all B and L are averaged. This differential energy spectrum has been fitted by the sum of two exponential functions (see TN4, and chapter 3 of this report). The lowest solid line is the best fit obtained by a least square technique. The free parameters A,C,E_a and E_c of this fit function have been determined by TREND, and can be used to determine a new model.

Once these constants are known it is easy to

calculate the integral spectrum using the expression given in chapter 3 (see also TN4). The upper curve in fig.4-11 marked (+) shows the mean integral flux, J(>E) in cm^{-2} s^{-1}, averaged over all LANL1 electron measurements.

Fig. 4-12 has the same format as the previous figure but it shows only the integral spectrum (not the differential spectrum) averaged over a subset of LANL1 data. This subset is obtained by taking only those measurements for which $0.001085 < B < 0.001105$ Gauss and $6.95 < L < 7.05$. The lower curve is the best fit obtained by the least square technique applied to the log of observed flux values. The upper curve, marked (*), corresponds to the sum of the mean value of F and the calculated standard deviation (σ_F). This value of $F + \sigma_F$ is a maximum value that is not likely to be exceeded (at the probability level of 75%).

It can be seen that the double exponential function fits remarkably well the measurements over a wide range of energies : from 30 to 2.000 keV. The flux values vary by 5 order of magnitudes over this range of energy. No attempt is made by TREND to explain the origin of the two populations of electrons which form this composite energy spectrum. Furthermore, it has been found that the energy spectrum is harder for large K_p values.

The large value of the standard deviation results from the large amplitude variations observed as a function of time beyond L = 4 in the magnetosphere. These variations are attributed to adiabatic as well as non-adiabatic acceleration processes which were first pointed out by McIlwain (1963). The source of these electrons as well as their loss mechanisms are not yet satisfactory modelled. In this respect TREND wishes to recommend that renewed efforts should be encouraged and supported by national laboratories and space agencies, to study these basic physical mechanisms.

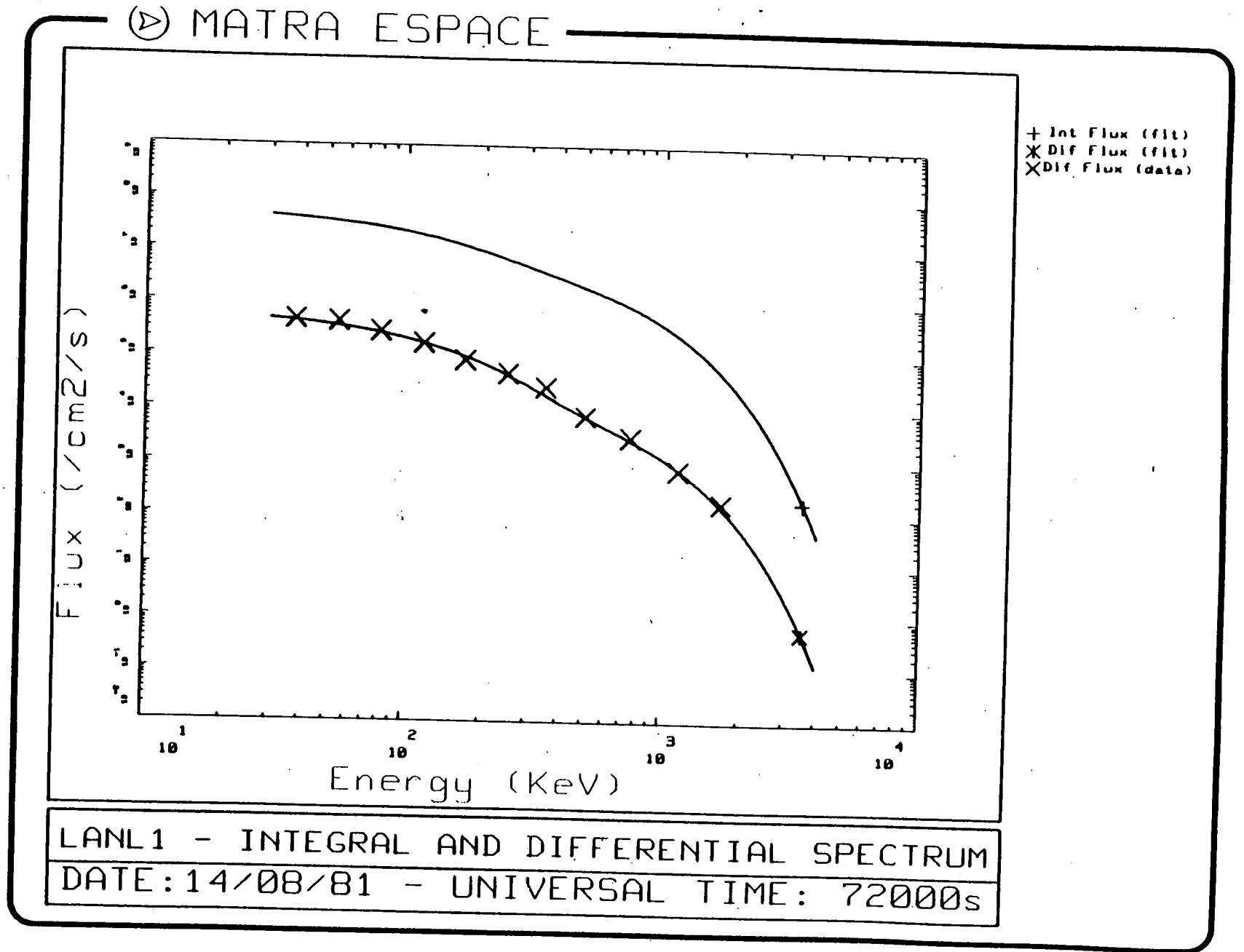

Fig.4-11. Average differential energy spectrum for all LANL1 data set (X). The solid line (lower curve) corresponds to a best fit obtained with a double exponential function.
Units for the differential spectrum are $cm^{-2}\ s^{-1}keV^{-1}$. The upper curve corresponds to the integral flux spectrum J(>E) in units of $cm^{-2}\ s^{-1}$.

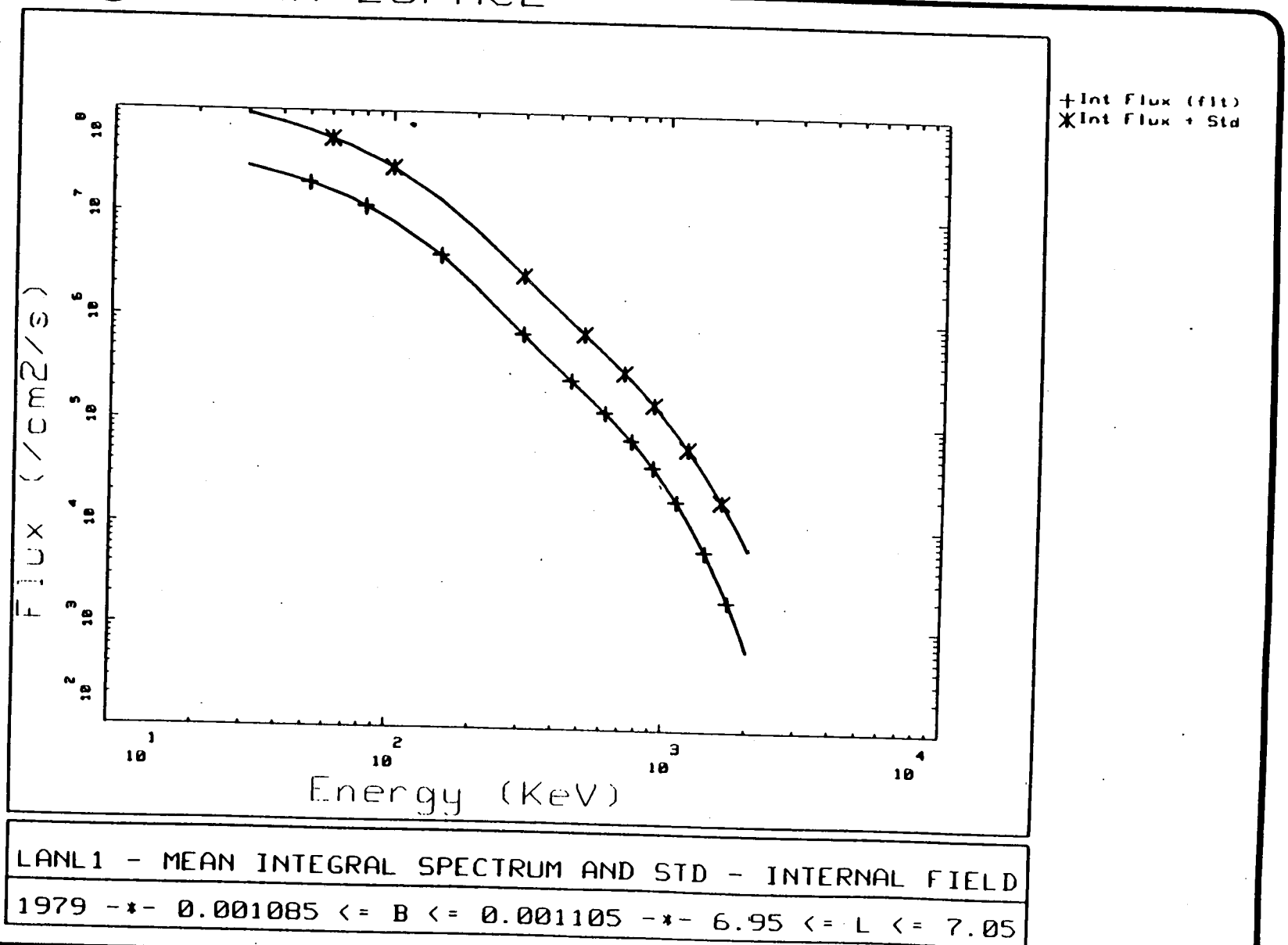

Fig.4-12.Average integral spectrum (data +; and double exponential fit) of LANL1 data. The upper curve and data points (*) correspond to

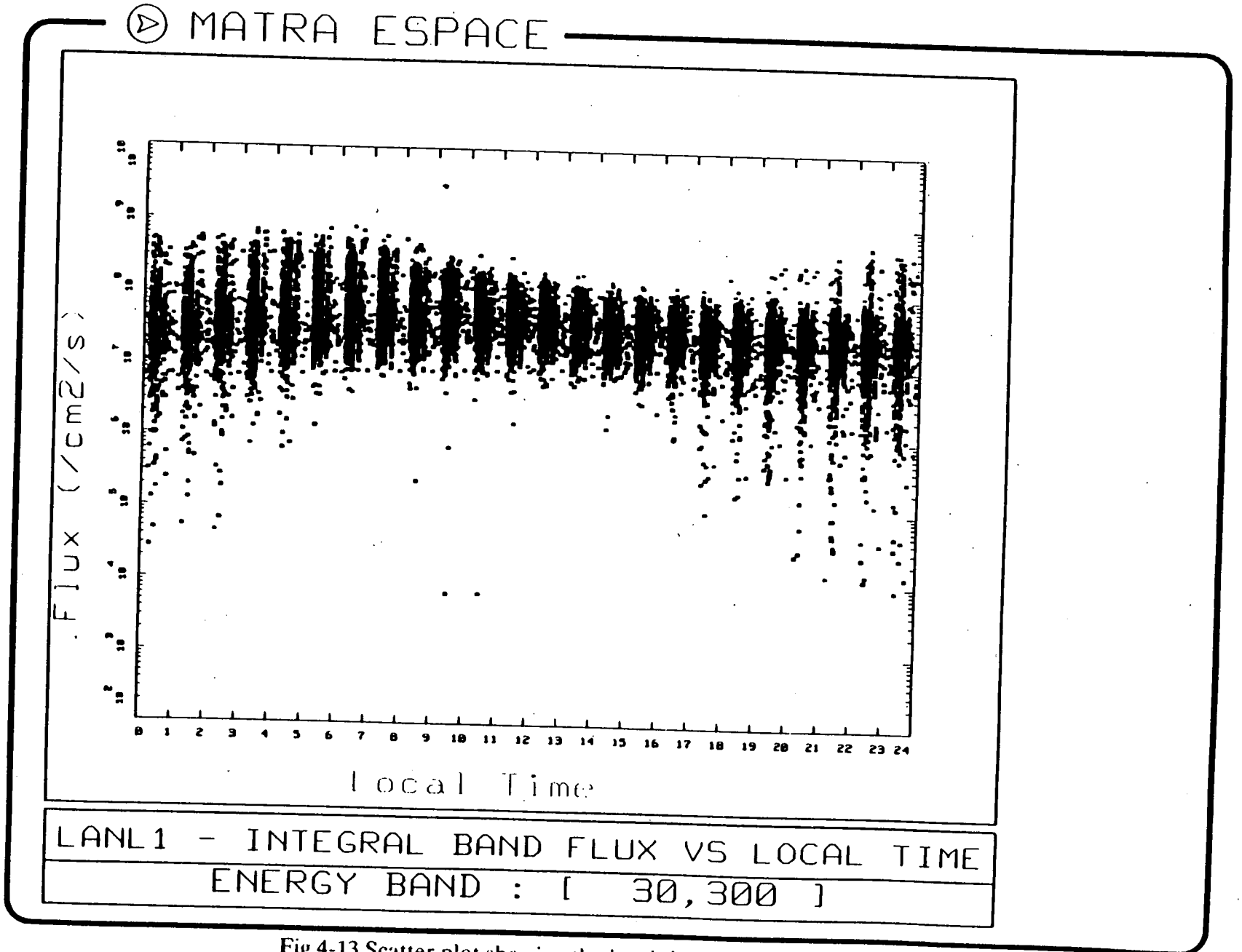

Fig.4-13.Scatter plot showing the local time distribution of all LANL1 flux measurements in the energy interval 30-300 keV.

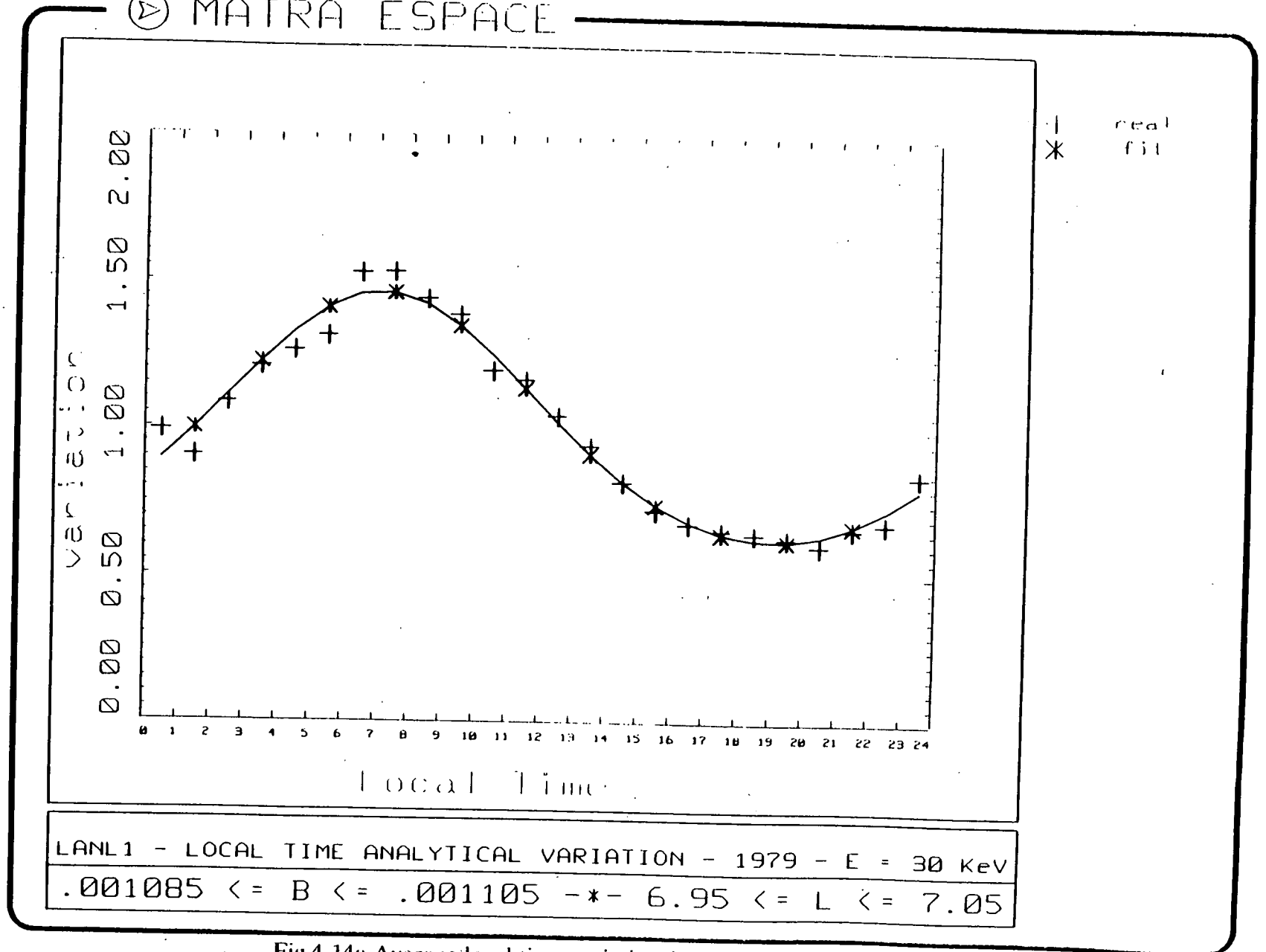

Fig.4-14a Average local time variation for LANL1 integral fluxes values for energies above 30 keV. The solid line and * symbols correspond to a best fit of the average fl...

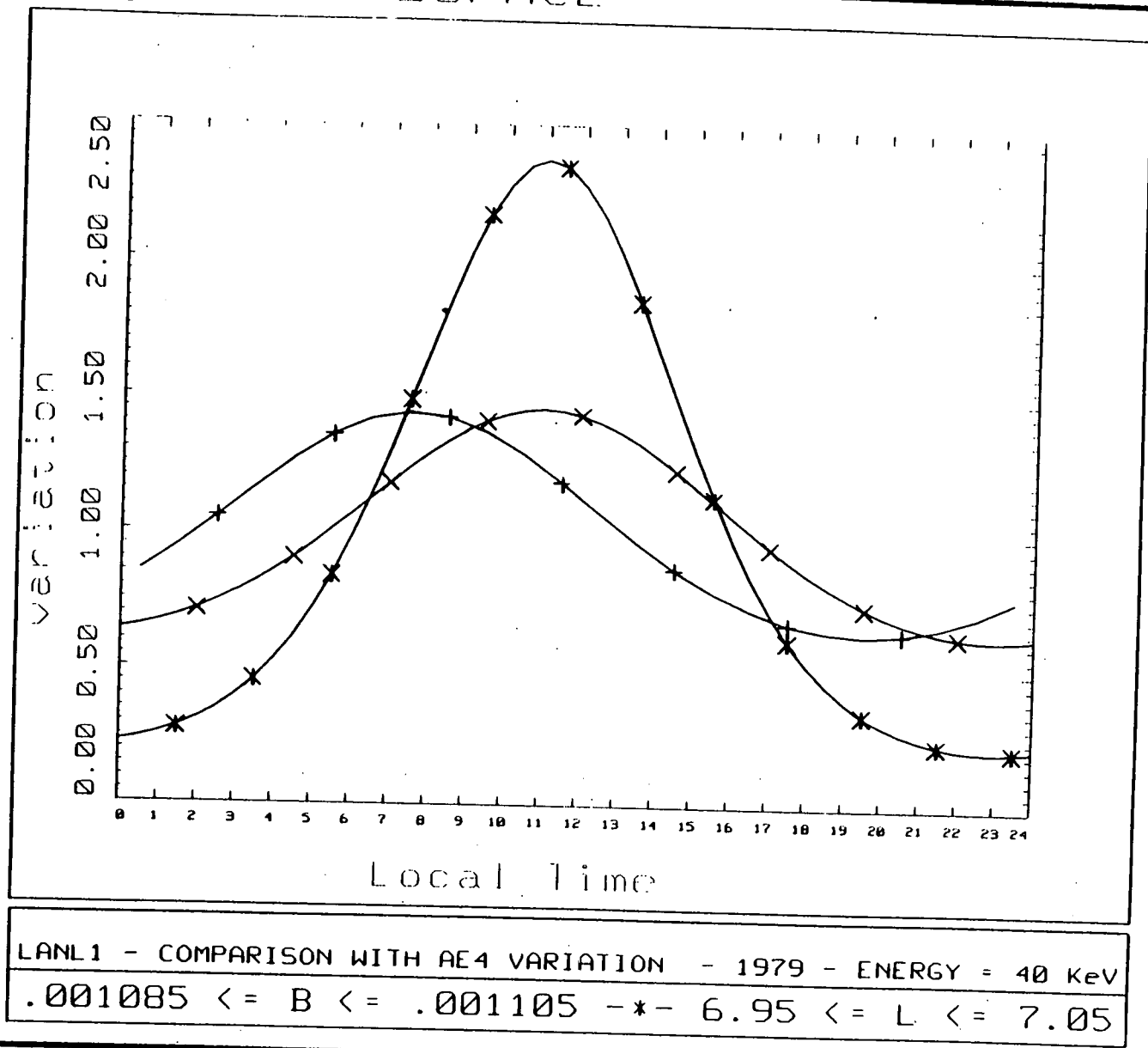

Fig.4-14b Average time variation for LANL1 integral flux for energies above 40 keV are shown by (+). The corresponding curves for the AE4-1964 and AE4-1967 models are also shown for comparison.

Indeed, the eventual goal of modelling efforts should be to build physical models instead of empirical ones. But to build a physical model of trapped electrons in a given energy range, the source and sinks of these electrons need to be well understood and modelled. This remains to be done in the future. Unfortunately, since late 1960's there is a characteric void of interest for such basic studies, except recently by Baker and colleagues and within the CRRES team of investigators. TREND recommends that a new generation of modellers attack these unsolved issues i.e. the origins and sinks of energetic electrons; TREND recommends also that future modellers develop physical models and compare them to empirical models like AE8 and those like TREND has been working on.

4.6 Local time variation of LANL electron flux measurements.

Fig.4-13 shows a scatter diagram of all LALN1 electron flux measurements for energies between 30 and 300 keV. It can be seen that at any local time there is a large dispersion of values, up to three orders of magnitudes near 00.00 LT.

When LANL data are sorted according to K_p values, one obtains slightly different scatter plots. When the mean values of log J are computed (this corresponds to calculate a geometrical mean value instead of the arithmetic mean value) for each local time hour a clear local time variation appears in the data.

This is illustrated in fig.4-14a which shows (+ marks) the relative values of all observed fluxes J(>30keV) as a function of LT, for $0.001085 < B < 0.001105$ and $6.95 < L < 7.05$. This LT variation is normalized to unity corresponding to the mean value of the sample considered.

The solid line and * marks determine a best fit to these mean values using the same fit function as used earlier in the AE4 model (see TN4 and chapter 3 of this final report).

Fig 4-14b shows the analytical fit of the local time variation for LANL1 fluxes of electrons where energy is larger than 40 keV. The two other curves correspond to the predictions of AE4-1964(MIN) and AE4-1967(MAX) models.

The parameters K_T, C_T and Ω_T of local time function have been obtained by least square fit. The values deduced with LANL data are very much like those obtained earlier by Vette et al. for the AE4 model. The LT time variation for the mean integral flux of electrons is of the order of 50% of the average value, with a maximum around Ω_T = 11.00 LT and a minimum near midnight. Note however that Ω_T changes from one set of data to the next. In this calculation all LANL1 data have been included. When too small bin sizes are taken the statistics becomes poor in certain local time sectors and a satisfactory LT variation can hardly be deduced with one set of data, only.

4.7 Distribution of electron flux for a constant L-value.

Fig.4-15a shows the scatter plot of J(>E) of all LANL1 data for which 6.95 < L < 7.05. The integral flux is plotted versus B/B_o where $B_o = 0.311563/L^3$, is the equatorial magnetic field intensity associated with L. This scatter plot shows again the large variability of electron flux measurements at large radial distances. The straight line indicates the mean value of J(>E) near the equator where $B = B_o$.

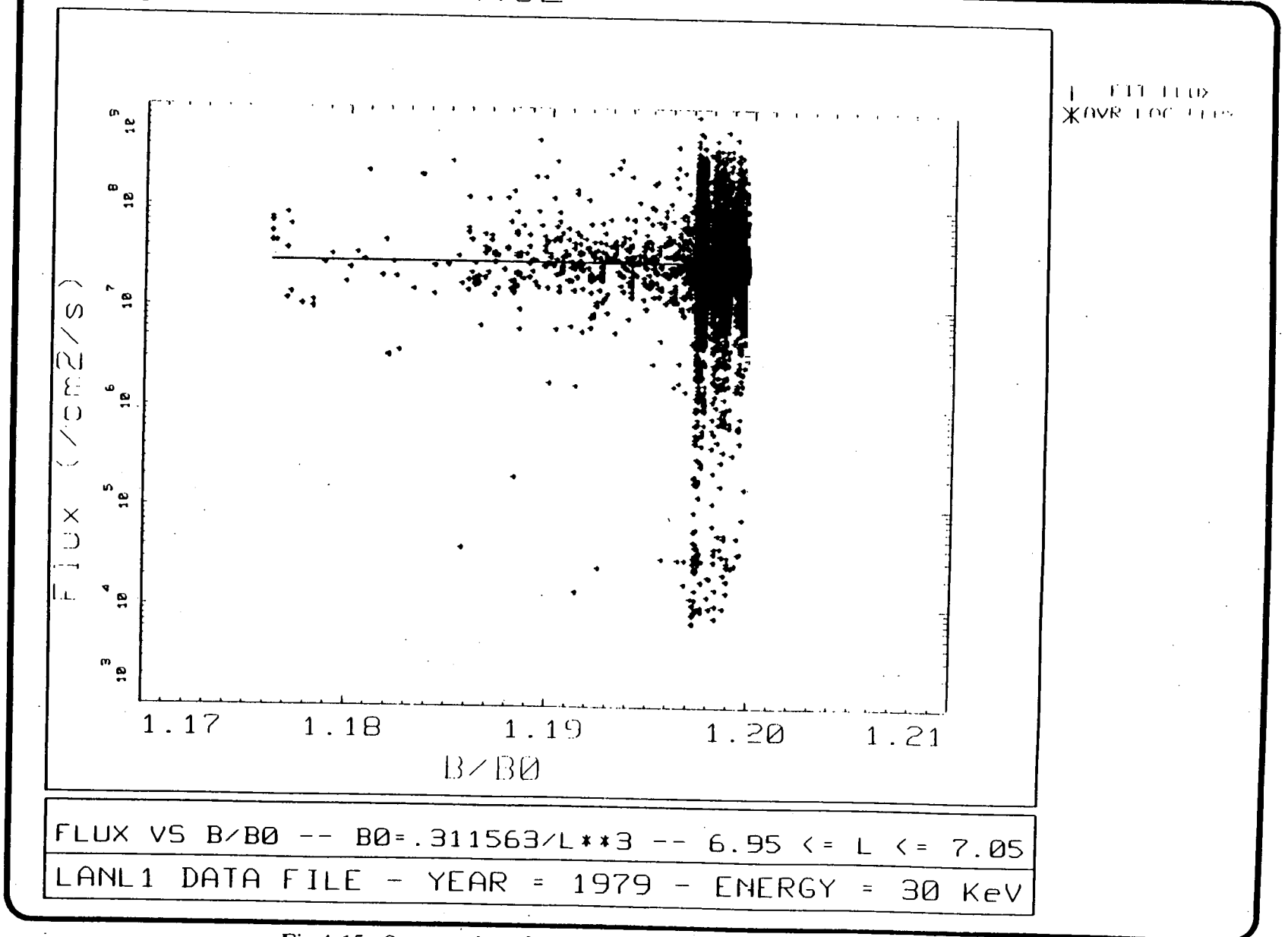

Fig.4-15a Scatter plot of LANL1 integral flux values, J(E>30keV) as a function of B/Bo for a constant L-value (:6.95≤L>7.05). The solid line corresponds to an average value which can be extrapolated for B/Bo=1 corresponding to the magnetic equatorial plane

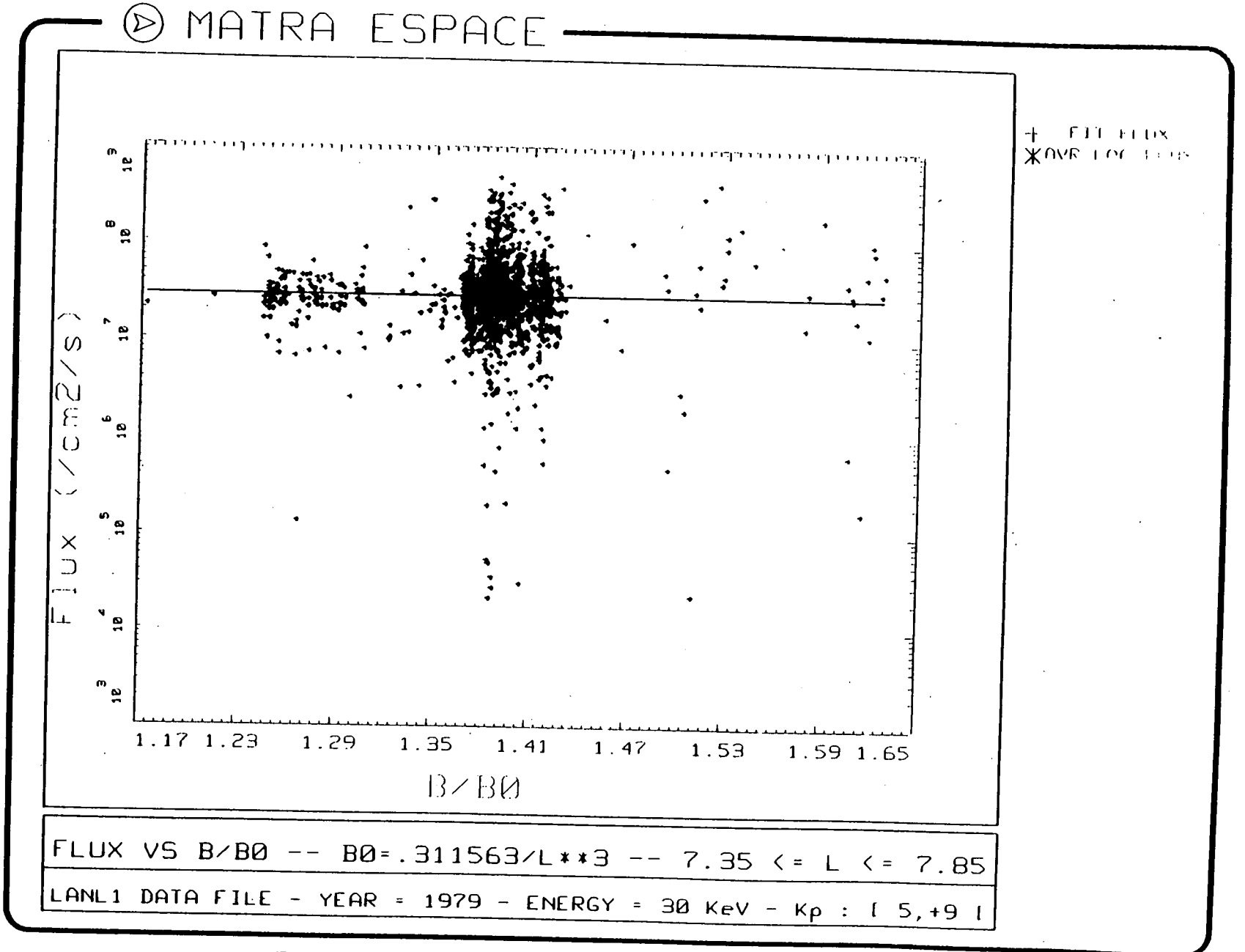

Fig.4-15b Scatter plot of LANL1; similar to fig 4-15a ewcept that in this case only measurements corresponding to high K_p values have been selected

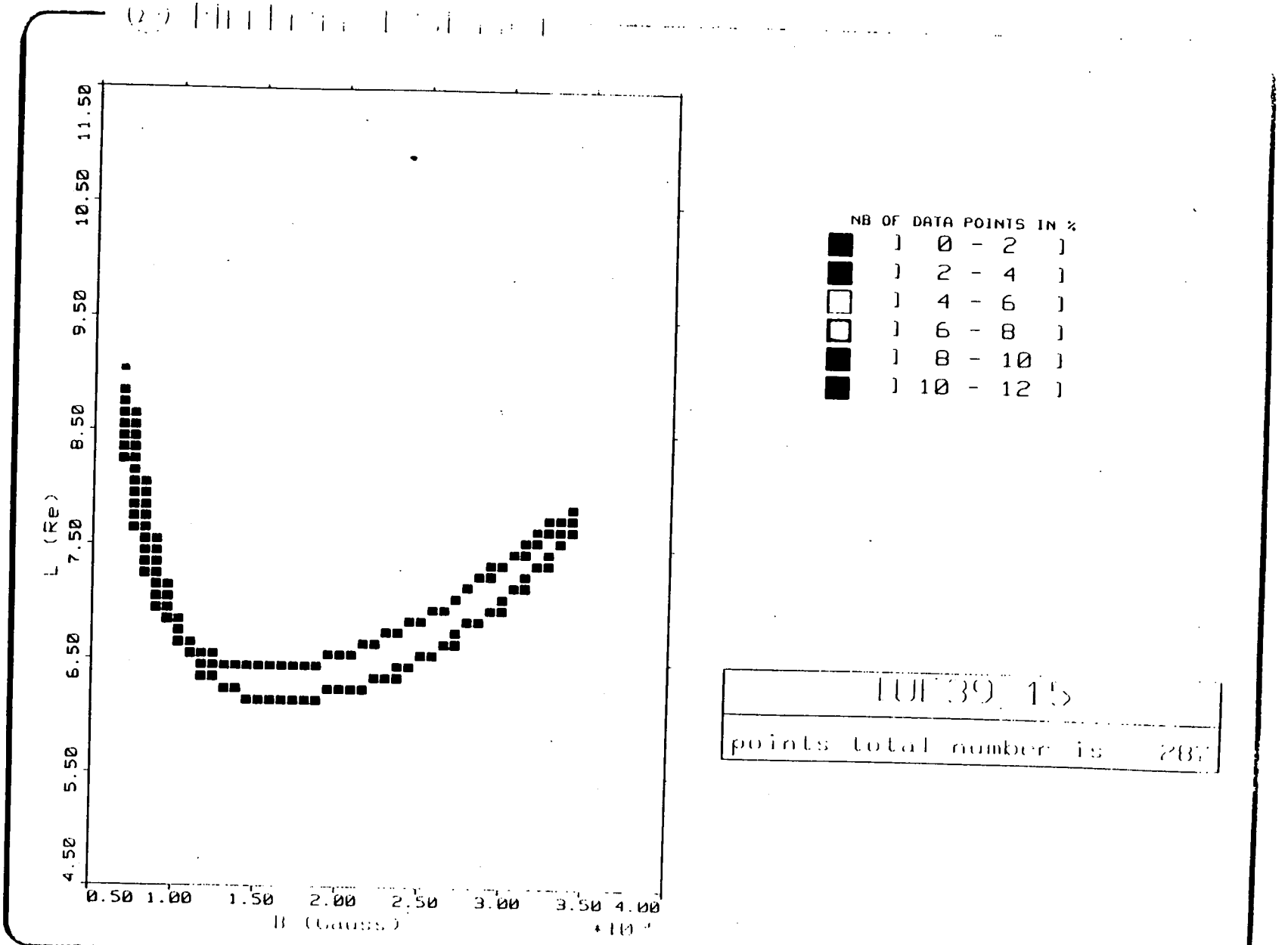

Fig.4-16 Distribution of 287 positions of the IUE satellite along its orbit.

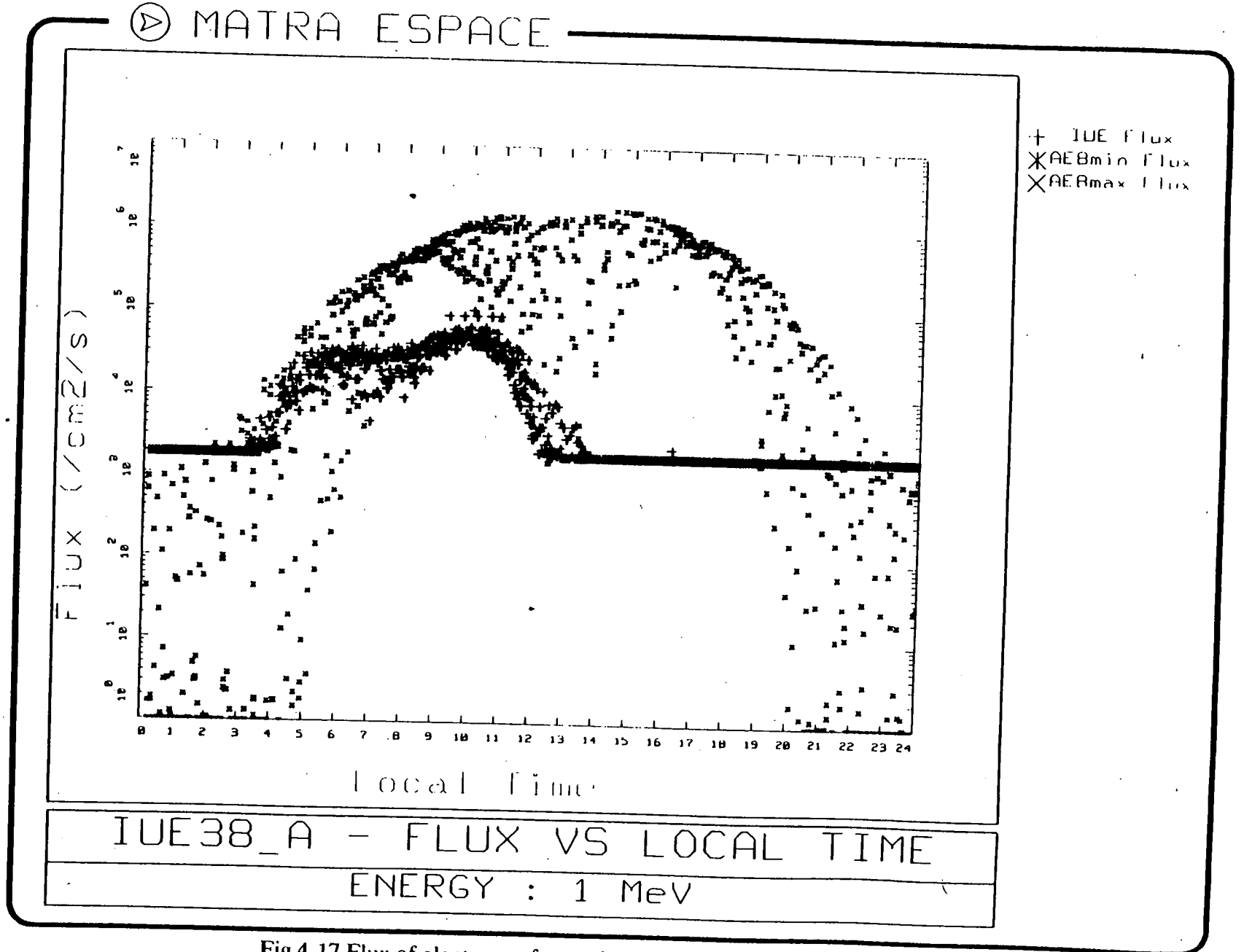

Fig.4-17 Flux of electrons of energies larger than 1 MeV measured along the IUE orbit versus local time (+). For comparison the (x) and (*) give the flux predictions from the A8 min and A8 ...

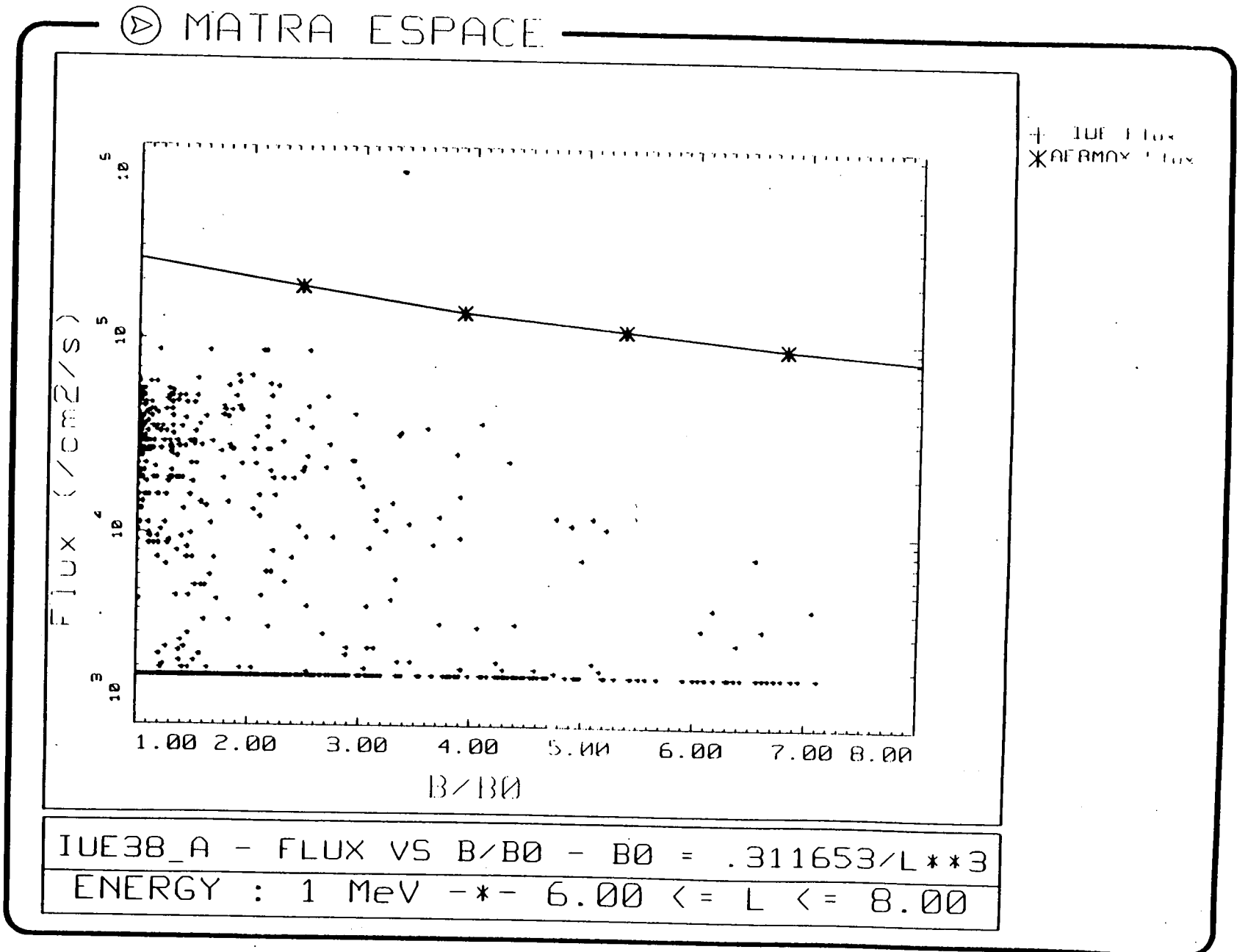

Fig.4-18 Flux of electrons of energies larger than 1 MeV measured along the IUE orbit for $6<L<7$, as a function of B/B_0. For comparison the predicted values from the AE8 max model are given by (*)

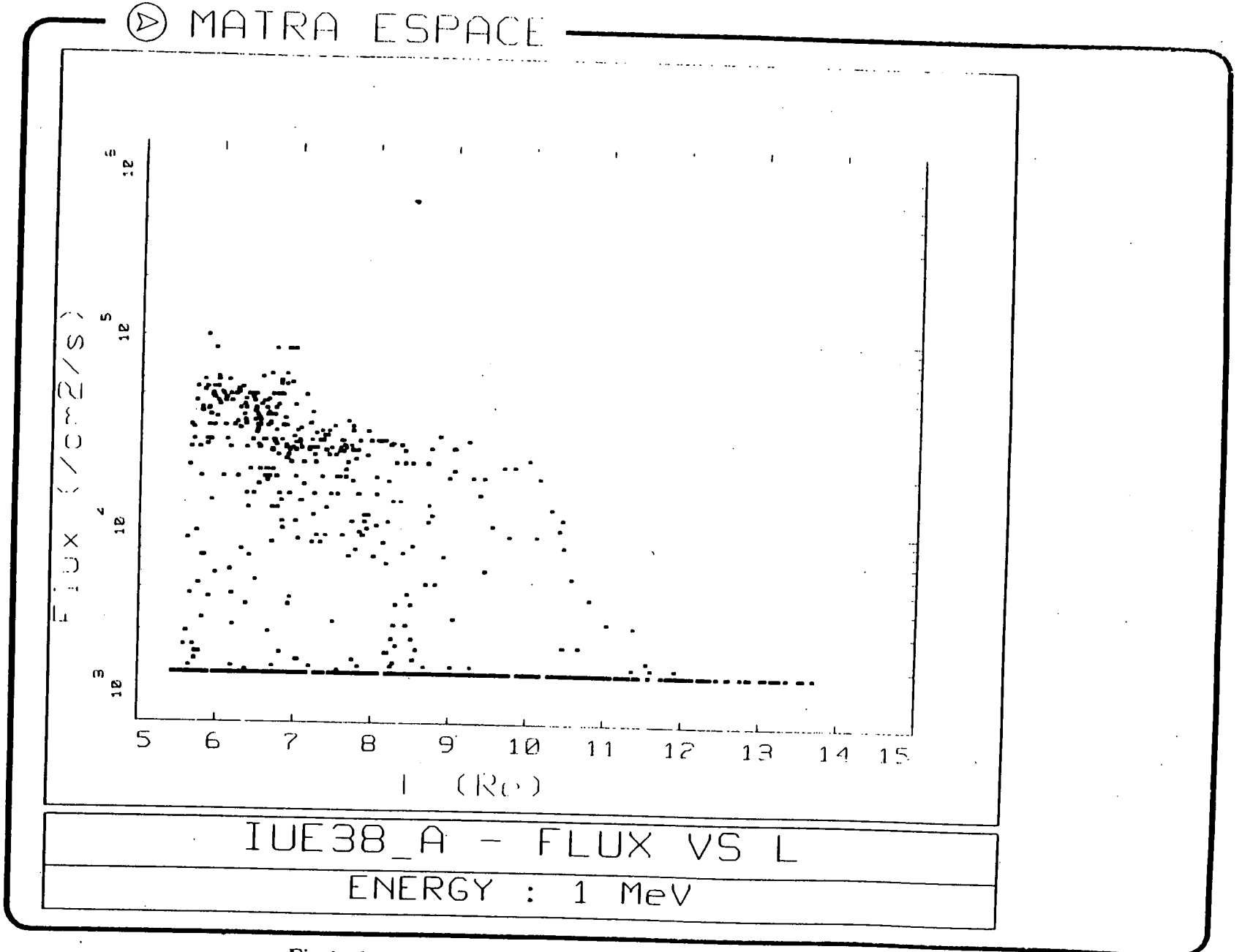

Fig.4-19 Flux of electrons of energies > 1 MeV as a function of L..

This mean value can be compared with that given in the AE8 model for $B/B_o = 1$ and for $6.95 < L < 7.05$. Owing to the large standard variations the agreement between the LANL data and the AE8 model is not too bad, although the AE8 are often more pessimistic.

TREND has found a slight increase of this mean value when K_p increases (see fig. 4-15b). However, owing to the large standard deviations this small difference is not of paramount significance.

In this chapter we have shown the results obtained with the LANL1 data set collected during the year 1979. The results for the 5 other LANL data confirm the conclusions outlined above.

4.8 Results from IUE data.

With IUE a much wider range of B-L space is covered than with the geostationary LANL satellites. Indeed IUE is on a 24 h elliptical orbit with apogee at 42,413 km perigee at 29,155 km, and an inclination of 31°6, variable over its lifetime.

Fig. 4-16 shows the distribution of IUE positions along its orbit. It can be seen that L varies between 6 and 9 while B changes from $0.5\ 10^{-3}$ to $3.5\ 10^{-3}$ Gauss.

The electron flux for $E > 1$ MeV is shown in fig. 4-17 by (+) as a function of local time along one complete orbit of IUE. The maximum fluxes are reached between 05:00 and 10:00. The fluxes corresponding to the same B-L are also given by (X) and by (*) respectively for the A8 min and A8 max models. It can be seen that the NASA model predictions are most of the time much higher than the IUE measurements.

Fig. 4-18 shows the distribution of IUE electron

fluxes for constant L-values (ranging between 6 and 7) as a function of B/B_o.

For comparison the NASA AE8 max model predictions are given by (*) and by the curve in the upper part of this figure. The much larger predicted flux confirm that the conclusions of earlier studies which showed that NASA models are generally somewhat pessimistic.

Fig. 4-19 shows the distribution of > 1MeV electron fluxes along the orbit of IUE versus L. The gradual decrease of the flux as a function of L can be seen. The large scatter in the measured fluxes is also clearly evidenced in this figure as well as in all previous ones.

As indicated in chapter 3 and TN2 and TN4, IUE electron flux measurements are directional ones i.e. the pitch angle of particles is not equal to 90° as it would be for particles mirroring in the vicinity of the position of the satellite. Therefore the mirror point of all these particles is located at a lower altitude along the field. A new version of BLXTRA has lately been implemented by TREND to determine the geocentric coordinates of this mirror point when the pitch angle at the point of measurement is known.

Indeed, from the equation

$$B_m = B_1 / \sin^2\alpha_1$$

the magnetic field intensity B_m at the mirror point is determined when α_1 and B_1 are known either from a direct measurement of B_1 (the magnetic field at the point of measurement when magnetometer data are available) or from a B-field model, and the direction of the IUE particle detector view angle. Once the geocentric coordinates of mirror point where $B=B_m$ are determined by numerical integration of the magnetic field line equations, the B-L coordinates of that miror point can be determined using

the standard numerical method described in chapter 2 and in TN1.

Although this new version of BLXTRA now exists and has been tested, it is not described in TN4, nor has it yet been used to reexamine and organize the IUE in a more appropriate manner. Indeed, the IUE electron fluxes have so far been mapped in B-L coordinates corresponding to the points of measurements, but not to the actual miror points. The directional fluxes measured by IUE have been converted to omnidirectional ones by multiplying the measured values by the geometric factor 4π. Although this procedure is a standard procedure, it is not an ideal one. Indeed, with directional flux measurements and assumed (or measured pitch angle distributions) one can obtain a much more consistent B-L mapping for the IUE electron fluxes, than those displayed in figures 4-16, to 4-19. Unfortunately, the new implementation of BLXTRA was not completed before the term of the TREND contract. Therefore, the IUE data presented here have not yet been analysed with this new BLXTRA version which commputes B-L coordinates of particles whose pitch angle α_1 is not necessarily equal to 90°.

As a consequence, the mapping of IUE electron fluxes in this alternative B-L space is a task that remains to be achieved in the future.

It can be mentioned already that this alternative and more appropriate procedure should reduce the large scatter of data points seen in figs. 4-18 and 4-19. Indeed, the directional flux measurements at small pitch angle α_1, which have low values because of the loss cone effect, will be removed from the B-L bins corresponding to the satellite positions . As a matter of consequence the low flux values in fig. 4-18 and 4-19 will be removed or shifted in regions of BL space corresponding to lower altitudes (i.e. where the radiation fluxes are smaller).

In any case TREND recommends that the exploitation of the IUE data, and of the other data sets identified in TN3 be pursued or undertaken to extend the coverage in B-L space beyond the narrow region which has been sampled with LANL satellites.

5. FLIGHT MEASUREMENT REQUIREMENTS

5.1 Introduction

With the exception of galactic cosmic rays (GCR) the only types of particles that are important from the point of view of radiation hazards are the energetic electrons and protons trapped in the Van Allen Belts. These particles provide a hostile environment for space systems.

Electrical charging which occurs as a result of hot plasma (20 keV magnetospheric electrons) can produce surface discharges that result in spurious operation or damage to the spacecraft. Energetic electrons of 0.5-1.5 MeV embed within dielectrics, producing potentials in excess of the breakdown potential of the material, again resulting in discharges damaging sensitive components. Radiation dose effects, which are observed at all altitudes, limit the operational life of microcircuits, and solar cells. They cause single event upset (SEU), latch up (LU), which produce spurious signals, and are a nuissance for the operation of all sensitive microelectronic devices which are onboard. In certain cases these particles constitute and additional heat input to low-temperature systems, especially those with passive radiators designed to operate at temperatures under 100 K. For ultra-low-temperature infra-red red sensors, such as those of IRAS, a transient additional heat load of 5 W/m^2 due to energetic particle population, must be considered in the design of the thermal management system; this could be a major constrain in the spacecraft design. For manned missions the radiation flux in space is a major element in planning orbits and extra-vehicular activies of the astronauts.

It is true that too optimistic models for the radiation dose would be fatal to certain sensitive devices, to man, as well to the mission operation. While too

pessimistic radiation models would lead to design spacecraft too heavily shielded, too heavy, and too costly.

All this indicates how serious it is to have a continous monitoring of the radiation environment and to obtain a comprehensive mapping for the omnidirectional fluxes of energetic electrons and ions which are trapped in the geomagnetic field.

In this chapter we resume the main ideas and conclusions contained in TREND's TECHNICAL NOTE 6. It will be split into three main sections :

Where is there need for additional or new data?

What are the future flight opportunities for incorporating radiation monitoring detectors?

What is a 'minimally intrusive' detector to achieve cost effective monitoring?

5.2 Spatial regions of importance for the space radiation environment

The present knowledge has been derived mainly from the data obtaned during the first twelve years of the space age along with the theoretical analytical, and modelling efforts associated with them. It should be pointed out that the first area of dicovery and scientific effort in space involved energetic paticles. The instruments were readily available out of nuclear physics, high-energy physics, and balloon borne/rocket borne cosmic-ray work. It took nearly a decade to develop instruments for other areas, such as plasma, astronmy, and earth resources where the main thrust has been for the past two decades

5.2.1 Knowledge of galactic cosmic rays

The basic work in GCR in the energy range of interest for TREND is largely complete. The energy spectrum, composition and solar cycle modulation have been studied for more han 60 years by ground-based, balloon, rocket, and satellite instruments. The omnidirectional flux of GCR (> 100 MeV/nucleon) is about 4 particles/cm^2-s at solar minimum, and 2 particles/cm^2-s at solar maximum. More details are given in TN6.

The knowledge gained from this work is adequate for all foreeable spacecraft engineering work. This is why the study of GCR has not been included in the work packages of TREND.

5.2.2 Knowledge of solar protons

These particles have been monitored nearly continuously since the launch of IMP 4 in May 1967. Of course earlier satellites also measured them on a research basis. Ground based observations go back to 1956. Recently a model has appeared that incorporates data that covers the 1956-1985 period containing most all of the 19th, 20th, and 21st solar cycles. These particles appear on a random event basis when looked at from a predictive aspect. There were 140 solar proton events in this period, which resulted in a total fluence of 1.06×10^{11} protons > 10 MeV and 2.8×10^{10} protons> 30 MeV. Converting these numbers into skin dose one obtains 55 and 6.2 krads, respectively. The average flux is about 118 and 31.1 p/cm^2-s, respectively.

Except for man and films these numbers are tolerable even for solar cells on a 10-year mission. Within an 11-year solar cycle there are seven years in which proton events are most likely and four years when the events are

less likely and produce lower fluence events. The difference in yearly fluences between these two periods is about a factor of 25-50. By starting with a zeroth index year centered at solar maximum and running from year +6 down through -4, the active proton event years are -2 thru +4 and the less active ones are -4,-3,+5, and +6. Although the GCR do not contain protons of such low energies, their integral flux above such thresholds produce fluences which exceed those of the less active years for E > 30 MeV and are comparable for E > 10 MeV.

The observation of these particles far out in the solar system by Pioneer 10 and 11 and Voyager 1 and 2 spacecraft have provided further understanding of the propagation process so that flux levels measured in the vicinity of the Earth can provide some estimates for the outer reaches of the solar system.

The events can be treated much like terrestrial weather in that enough is known about the behaviour of the solar atmosphere that crude short term predictions of the order of a week can be made. In addition, large active regions live longer than a solar rotation (27 days) so that monthly predictions also have some credibility. However, these only benefit short manned missions. Most unmanned missions extend for 5 years or longer. Consequently, there are other models which can be made with the wealth of data.

Although monitoring by high altitude geocentric spacecraft is fast disappearing (IMP 8 is likely to be the last), there is monitoring on the NOAA series of polar weather satellites that cover the energy range from 16 - 850 MeV with a number of channels. These satellites spend about 40% of the time in the interplanetary medium over the polar cap. The present set of instruments provide coverage back to October 1978. In addition, the geostationary meteorological staellite series, GOES and GMS, have high energy proton detectors for covering the range 0.6 - 500

MeV in 7 channels. This set of instruments provides coverage back to September 1980.

Consequently, the outlook is good for continuing coverage of these types of particles and, as the low altitude weather instruments move to the Polar Platform, it is expected that the monitoring detectors will also be flown there. The LANL satellites also monitor solar protons in the 0.4-140 MeV band and this set of instruments started operating in July 1976.

In the case of solar protons there has been and will be a wealth of data. The modelling for these has not been very active. From the doses they deliver, it seems clear that SEUs are the major concern relative to spacecraft now that devices have 10 krad or higher hardness. Of course manned flights at higher latitudes and 'soft' electronics or detectors are still quite vulnerable to solar protons.

5.2.3 Knowledge of trapped protons

This element of the radiation environment is in much poorer shape than that of the two previously discussed. Part of the problem is the difficulty in obtaining coverage with a single satellite, and another is the complexity of understanding the source and loss mechanisms in quantitative detail. The AP-8 model, which covers all energies above 0.1 MeV, used essentially all of the proton observations made by non-Soviet satellites. This covered the time period July 1958 - June 1970 but with many time gaps. There were 29 experiments flown on 24 different spacecraft and a total of 90 energy channels were available from this assembly of data. Even with this, the low altitude regions were never sampled simultaneously by two satellites and the equatorial region 3-4 Re was only sampled by Explorer 26.

There are protons of at least 500 MeV trapped in the

magnetosphere. Once protons get too energetic, their gyroradius gets too large for trapping to occur; this sets the upper energy limit. The most energetic protons peak around 1.4 Re. By the time the energy drops to 40 MeV the peak has moved to 1.5 Re. This trend continues so that 5 MeV protons peak at 1.8 Re. The outer boundary also has the same trend. 400 MeV protons reach the background flux at 2.1 Re, 50 MeV do at 2. Re, and 10 MeV reach to 3.7 Re. At any given L shell the energy spectrum hardens as one goes away from the equator. The more energetic protons have a flatter equatorial pitch angle distribution than lower energy ones. The peak fluxes are quite high relative to anything discussed so far. For example, electrons with threshold energies of 30, 15, and 10 MeV have peak fluxes of $4x10^4$, $1.1x10^4$, $4x10^6$ which means skin dose rates of about 32, 152, 760 rads/hr or 0.28, 1, 3, 6.6 Mrad/yr.

The sources are believed to be cosmic-ray albedo neutron decay (CRAND) protons for the highest energy protons down to about 10 MeV and from the solar wind through the geomagnetic tail, with inward radial diffusion producing acceleration from the solar wind energy (~ 1 KeV) to that observed. There is some difficulty getting enough acceleration to achieve the right energies. The CRAND source has been studied extensively and detailed calculations have been made, but the energetic protons that exist are larger by about a factor of 20 than the calculation predicts.

There is somewhat better agreement with the loss of protons to the atmosphere. However, there remain significant problems. The secular changes of the magnetic field possibly produce an addition source that decreases with increasing altitude.

At any rate there is no reliable way to extrapolate the existing AP-8 model to low altitude to correct for the problem of having increasing fluxes as one extrapolates to

later times. The dosimeter results from manned flight missions show no increases in the doses except for the known solar cycle effect. Thus the combination of the source and loss terms plus the transport/acceleration produced by the changing field all seem to cancel at the inner boundary, but what is the underlying process and what do things look like at higher altitude?

The DMSP/F7 data covering the time period from November 1983 - July 1988 show about a 6-7% increase over this time period, which is probably a solar cycle effect, since the period concerned coincides primarily with the interval when the density of the atmosphere is decreasing at low altitude. These data are becoming available for modellers soon but no plans are known for undertaking a proton study. The energies covered are > 20, > 35, >51, and > 75 MeV. The limited equatorial coverage is the same as the NOAA series discussed below.

In reviewing the outputs from TN3 it was noted that there are no mesurements of protons in the energy region for solar cell damage. Nor are any being planned that TREND is aware of except for the CRRES satellite. This spacecraft will touch all the bases and one hopes it will have,a long and successful life. Fortunately, in its near equatorial orbit with detectors that measure pitch angles all the particles on the field line will be sampled twice per period. There is not a CRRES follow-on planned, so the long term outlook is rather bleak. Maybe the outputs of CRRES will have to satisfy environment users in many regions of phase space for the next twenty years.

At energies > 15 MeV, the NOAA Space Environment Monitor (SEM) has two sets of detectors, MEPED and HEPAD, which have proton channels. The first covers the ranges 16-80, and 80-215 MeV and the latter covers the interval 370-850 MeV in three ranges plus > 850 MeV.

The MEPED detectors are three separate "omni"

detectors commonly used to measure the omnidirectional flux. These should be straightforward to use. The HEPAD is a counter telescope with a 24# half angle conical field of view. It is not clear at this time if the pitch angle of the measured particle can be ascertained. If not, the data from this instrument for trapped proton analysis may be difficult to interpret. The MEPED data may provide a way to perform a systematic relook at protons in important energy bands for spacecraft engineering. Six satellites in this TIROS-N series have been launched starting in October 1978; there are three more in this series. The MEPED data set should be used for modelling purposes and could be compared with the DMSP/F7 data. Unfortunately, equatorial coverage is missing but CRRES can fill in this gap.

5.2.4 Knowledge of trapped electrons

These particles are found throughout the magnetosphere depending on the lower energy limit. Even if one chooses 500 keV as suggested earlier, the flux cutoff is around 10.5 Re but islands (in a sea of no flux) can be seen in the tail. Since the atmosphere is the cause of the low altitude boundary, this boundary is similar to that of the protons. However, the electrons are lost to the atmosphere through pitch angle scattering instead of by dT/dx. This causes one to see a longitudinal dependence in the these fluxes. This is known as the windshield wiper effect and results from the electrons drifting through the South Atlantic Anomaly (SAA). As the low altitude electrons encounter the atmosphere drifting from west to east, they are scattered out of the radiation belt. This hole is then filled on the eastern side where scattering is still occurring and this brings new particles down from higher altitudes. After the electrons clear this region, there is little scattering on the rest of the drift path until the SAA is again approached.

From this inner boundary the electrons have two main

peaking regions. The first is around 1.6 Re for 1 and 2 MeV electrons, with the 500-KeV ones peaking at 1.7 Re. One should point out that there have never been good measurements of natural electrons in the inner zone. Throughout the period from July 1962 until late 1969, the Starfish injected electrons dominated this region. Peak fluxes here are about 10^6 for 1-MeV electrons, which means a skin dose rate of 120 rad/hour which is equivalent to the 15 MeV proton skin dose. However, the important thing here is the response of solar cells and the 1 MeV equivalent ratio for protons to electrons is 1.2×10^3 . In addition, the electron spectrum is such that the proportion of particles that can penetrate into most spacecraft is small relative to protons. The bottom line is that inner zone electrons are not a problem - but only because the energetic protons are more of a problem.

The slot region lies between 2-3 Re and this shows a dip in the electron fluxes; one may recall that the protons showed no such behaviour. The higher the energy the deeper the dip. At 500 KeV the dip is less than a factor of two while at 2 MeV the dip is more than a factor of 100. The region below 2 Re shows hardly any time variations now that the Starfish residue has decayed.

The slot region has considerable time variations but nothing like these existing farther out. Only a few of the many injection events from the tail, as seen at the geostationary position, are seen in the slot. However, because the number is small, these events determine the long term average flux and as with small number statistics, the averages are highly variable. Yearly averages differ by up to a factor of 10.

The electron lifetimes in the energy range of interest are lower in the slot than on either side of it. In fact one has to get near the geostationary position before the lifetimes are as low. The presence of VLF noise

and other wave disturbances are believed to be the cause for this decay. Flux levels are low enough on average not to be a problem and in general it is the most benign region until one gets past 7 Re. One can see factors of 30-100 changes in the flux but the structure change is slower than in the heart of the outer belt. The higher energy electrons have a longer life so that for injection events that reach the slot, the spectrum gets harder with time.

Starting around 3.3 Re one finds the maximum of the long term (~ 9-12 months) 7-MeV flux. Then as one goes to a lower energy this maximum moves farther out. For solar maximum conditions the peak of the 500-KeV particles is at 4.75 Re while in solar minimum it is found around 5.1 Re. The general effect is that the solar minimum peak flux is invariant but the inner side of the peak grows during maximum conditions and pushes the observed maximum inward and to a slightly higher value. This is a fine detail that is difficult to see with all of the time variations that are present.

Solar max peak fluxes are $3.5x10_6$, $5x10^5$, $4.5x10^3$ at 1, 2, 4 MeV while solar min peaks are $3x10^6$, $3.5x10^5$, $4.5x10^3$ at 1, 2, 4 MeV while solar min peaks are $3x10^6$, $3.5x10^5$, $2.2x10^3$. Thus, the relative change increases with energy. Comparing with the inner zone peak at 1 MeV, one sees there is about three times the flux in the outer zone. This ratio rises rapidly above 2 MeV, being about 100 at 3 MeV. The inner zone has no 4 MeV electrons any more while the outer zone has them up to at least 7 MeV, possibly to 15.

The time variations in this 3.3-5 Re region show large injection events with the flux rising abruptly by as much as a factor of 1000. Then there is a period of exponential decay until this is interrupted by another injection type of rise. The decay times at 4 and 5 Re are nearly the same but, at 5 Re, one sees about three times the number of

injections. This pattern continues as one moves higher, except the decay times become less. When one looks at the geostationary region, the exponential decay pattern is essentially gone and the time structure can be characterized by many injection events of varying size (rarely exceeding a factor of 100) that appear as jagged top rectangular waves. As one moves on to greater distances the pattern looks more chaotic and there are periods where there is no discernible flux.

At geostationary orbit there is no solar cycle effect so the average fluxes are essentially constant. The flux levels at 1, 2, 4 MeV are 4.5×10^5, 3.5×10^4, 5×10^2. The skin dose rate is 54, 4.2, 0.06 rads/hr or 471, 36, 0,52 krads/yr and the 1-MeV equivalent electron fluence is about 1.4×10^{13}. This is more benign than the trapped energetic proton region, but the environment here is still a factor to consider. There is no compelling evidence that the very energetic electrons seen by the LANL satellites are trapped. If one considers that the Jovian electrons have access to the geostationary region without attenuation then eqn (6) indicates that these electrons would start to dominate the trapped spectrum somewhere around 5 MeV. Except for the LANL SEE experiment there have been no good electron measurements > 3.9 MeV at geostationary orbit. According to TREND information from LANL, the experimenters are still sorting out the energy calibration on this detector system, so the data are not yet available to modellers.

As in the case of solar protons, the geostationary region is well covered for electrons except with respect to the particles cited directly above. The LANL Charged Particle Analyzer measures electrons between 0.2 - 2 MeV in 6 bands. A lower energy system measures 6 other bands between 30-300 KeV. Their combined time coverage is from July 1976 to the present. The GOES/GMS series of geostationary meteorological satellites carry detectors

that measure electrons > 2 MeV, while Meteosat P2 carries the low energy LANL system. It is expected that the geostationary meteorological satellites will continue to carry similar monitors for the foreseeable future. Hopefully, higher energy electron channels can be added to provide a comparsion with the LANL SEE data and shed more light on the deep dielectric discharge problem. The whole region from 3-7 Re should be considered as a region of danger.

There is a tremendous amount of data available in the geostationary region that covers all energy ranges of interest. Additionally, much of it is easy so use. The main things needed to be done are model the time variations using global knowledge; study the cause of the local time behaviour (mostly from the external field), and analyze variances of the log of the flux in more detail than the previous work.

For the regions beyond geostationary, one should first mention the synchronous satellites, SCATHA (officially STP P78-2) and IUE. These satellites were in similar orbits with a period very close to 24 hours. The perigee was ~ 27.000 km and the apogee was ~44.000 km. SCATHA had an inclination of 7.9° , IUE was about 31° . IUE was launched in January 1978 and SCATHA in January 1979.

The main goal of SCATHA was to study spacecraft charging and as such it covered a full complement of energetic electron detectors. One covered the 0.05-1 MeV range in 16 channels and the other covered the 0.6-5 MeV range in 4 bands. The L shells from 5.4 to 8.6 were sampled within the magnetic latitude range from 0-18.8°. Although the satellite was operated for at least 6 years most of the data that has been processed only covers the period from March 79 - May 1980.

IUE is an astronomy satellite but a Particle Flux Monitor (PFM) was placed on board to indicate the electron

flux near perigee so that the maximum exposure time that could be taken with the camera would be known. The PFM is a solid state detector with a 16° half angle conical field of view. It is a threshold detector; the pitch angle can be determined since the satellite is three axis oriented. The instrument is still producing data. The spatial coverage is similar to SCATHA except that the magnetic latitude range goes to about 42° and the L value goes to about 14°. However, the intensity threshold is equivalent to about 10^4 electrons/cm^2-s so coverage past L=10 or 11 is rare.

The synchronous region described above is an ideal one for study in conjunction with the geostationary satellite to understand drift shell splitting and the effects of external magnetic fields. TREND has made a start on such a study.

Complementing this, to round out the story over the whole flux tube, are the electron detectors on DMSP/F7 and the NOAA series. DMSP has > 1 and > 2.5 MeV channels while the NOAAs cover >30, >100, >300 keV as well as lower energies that are not of interest here. As mentioned earlier the NOAA series has three more to be launched and continuation on a new series is hoped for. Unfortunaly, the DMSP series does not fly energetic particle detectors very often.

Finally, the distant reaches of the magnetosphere are not covered well in the energy range of interest. Beyond 8 Re there is usually not enough flux to cause any radiation damage problems but certainly background counting rates for some missions can be a problem. In the past 12 years only the ISEE and AMPTE (CCE and IRM) spacecraft have traversed this region with appropriate instruments. ISEE 1 and 2 lasted nearly 10 years and their termination was re-entry not a radiation problem. ESA has been processing the ISEE 1 electron data in the 22-1200 KeV range in 8 channels for

application to their space-based astronomy missions that will use synchronous orbits with apogees in the 12-20 Re range. It is unlikely that the future particles and fields spacecraft will carry energetic particles detectors.

Since the boundaries of the magnetosphere are so variable at these distances and much of the flux seen is related to solar events, a more logical solution than trying to model such a region would be to fly a simple particle detector system appropriate for operational needs in the same manner that IUE did. The solar Maximum Mission did the same thing to sense the SAA so that the large X- and gamma-ray detectors would turn off appropriately so as not to suffer degrading saturation effects.

In summary, in respect of looking towards the future, there seems to be good coverage of the energetic particle environment in the polar weather orbit and in the geostationary orbit from both meteorological and other operational missions. The polar orbits provide sampling at the foot of all the magnetospheric field lines but the electron coverage does not go to high enough energies (i.e. 7 MeV).

These satellites also provide reasonable coverage of the trapped energetic protons except for the important 5-15 MeV range for solar cells, where there is a lack, except for GOES data from 2 to 430 MeV. There has been nothing in the past 10 years (really more like 20) relative to electrons in the remainder of the magnetosphere. This includes the slot, the outer zone (except near geostationary) and the far reaches of the cavity past 7 Re.

5.3 ESA's future missions and flight measurements requirements

In the Appendix of TREND's TECHNICAL NOTE 6 background informations on measurements, and missions are presented with a comprehensive list of recent and future satellite missions. Based on these inputs, we outline in this section the requirements TREND has identified for future ESA missions.

5.3.1 What are the radiation problems for space missions?

In the introduction to this chapter it has already been noted that electrostatic charging of spacecraft surfaces, deep-dielectric charging due to energetic charged particles are major problems for satellites.

Astronomical measurements are sometimes hampered by such detrimental effects (e.g. on HIPPARCOS). Detectors flown on astronomy satellites are very sensitive to the damage caused by the ambient trapped particles as well as secondary particles reducing the efficency of these detectors and shortening their lifetimes.

It has not normally been the practice in the past to monitor radiation background levels. This has lead to lack of knowledge for planning later missions and performing analysis of data. Past missions have relied on environment models which have been shown are weak in some respects.

In addition to the detrimental effects on the spacecraft material, equipment and instrumentation, energetic electrons and ions pose important problems for manned missions as well. Safeguarding astronauts from adverse biological radiation effects inflicts stringent requirements on the length of manned mission, and on orbit selection and the planning of EVAs (Extra Vehicular Activities). For occupations involving radiation hazards,

(e.g. nuclear reactor enginnering, radiology..), The U.S Environmental Protection Agency guidelines set the acceptance dose rate limit at 5.000 mrem/year over the natural background experienced at the surface of Earth (60-160 mrem/year). This implies a careful planing of all manned especially when EVA are required.

There are also important uncertainties in the effects of cosmic rays. A further important element of the environment is the biological effects and SEU from energetic protons undergoing nuclear reactions within the body or within components.

An accurate prediction of the radiation dose expected during any (manned or unmanned) mission requires therefore reliable trapped radiation models. Indeed, too optimistic model predictions must be avoided for obvious reasons, while over-pessimistic ones lead to unnecessary, heavy and costly shielding or costly alternative orbits.

In this respect it has been shown by Gussenhoven et al. (1987), Vampola (1989) and others that the average fluxes given by current models, like AE8, are in certain instances misleading. Although AE8 remains a basic reference model describing the energetic electron environment, it is poorly suited to evaluate radiation effects on high altitude eccentric orbits where external magnetic fields are predominant, as well as at low altitudes where atmospheric cut off and secular variations of the geomagnetic field are important (see TECHNICAL NOTES 1&2).

Evaluation of the extreme values or standard deviations of the high altitude fluxes are needed in addition to the average values. The AE8 model provides average omnidirectional fluxes for electron energies ranging from 40 KeV to 7 MeV. Fluxes at the upper energy limit are mainly extrapolated from lower energy data. Extrapolation from lower altitude data is often used to

provide values up to 11 Earth radii.

TREND has investigated the geostationary orbit for the outer zone electrons by adding confidence levels and standard deviations for the predicted fluxes in the vicinity of geostationary orbit; the geomagnetic activity dependence, as well as local time dependence (similar to that existing in AE4) have been investigated.

These new evaluations have been useful to check the earlier models. However, like all previous radiation environmental models, the results are static and take no ac count of the many dynamic processes which occur in the magnetosphere over periods as short as days and even hours. But, as emphasized in TECHNICAL NOTE 2,(Chapter 6), more detailed dynamical models can only be built into the framework of long term modelling efforts backed up by continued multi-satellite observations of particles of high energy, in all regions of the magnetosphere.

In the following section we outline a strategy to achieve this goal within the framework of future European space activities.

5.3.2 How to manage these problems?

As indicated above, there is need for the European space community to devote some effort towards improving the radiation environmental models beyond the point where TREND has carried this effort already. Such a long-term effort could be envisaged in parallel with that of other Space Agencies. The CRRES mission dedicated to the study of the radiation belt environment is a good example of such an effort undertaken in the US.

Although, CRRES detectors cover a wide range of particle energies, and a wide range of B- and L-values, there are regions of space which will not be visited by

this spacecraft. Sampling the environment with a single spacecraft will always be limited in B-L space. Simultaneous and multi-point observations are necessary to obtain the required time and spatial coverage. The more synoptic observations will become available for the future modellers, the more detailed and reliable will the new generation models become.

These are good reasons for all space agencies, including ESA, to consider now the incorporation in a number of their future missions, of "minimally intrusive", mission-specific radiation environment monitoring. It is worth pointing out here that such "minimally intrusive" monitors had been added (at the last minute !) to the payload of the astronomical satellite IUE (International Ultraviolet Explorer); these unsophisticated particle detectors monitor continously since 1978, the trapped particle radiation background. They are still in operation and provide already over one solar cycle worth of data. These data are useful indicators for evaluating the background noise spoiling the UV telescope measurements; but they happen also to constitute a most valuable and inexpensive data bank of directional flux measurements for trapped electrons over a whole solar cycle. These data have been analysed by TREND for the purpose of evaluating the AE8 trapped radiation model. It has been demonstrated in TECHNICAL NOTE 5 that these directional electron flux measurements collected by an astronomical satellite (i.e. not a magnetospheric satellite) can be usefully exploited to improve existing trapped radiation models.

Dependable and cost effective background monitors (like those of IUE) or radiation monitors should be incorporated not only in manned missions, (like Space Sation / Columbus) or geostationary environment monitors (ERS), but also in most scientific missions (like ISO, LYMAN, and possibly REGATTA, and the Polar-Platform), in application satellites (Polar Earth Resources,

Communications, and Meteorological satellites), or in TDP missions.

The addition of radiation monitors to any such satellite allows its operation to be optimised. Furthermore, provided there are built-in alert procedures triggered on board by such radiation detectors, these simple devices could be very valuable to protect vulnerable instruments of the payload.

Note also that such radiation detectors on a particular mission yield data (average fluxes, maximum flux or fluence, integral values, standard deviations ...) which are directly useable in planing follow-on missions on similar orbits (for instance had the EXOSAT X-ray astronomy satellite carried a radiation monitor, it would have made planning of the follow-on X-ray mission XMM much easier).

In order to be more specific we present a list of future flight opportunities where planners should be encouraged to fly dedicated monitors to understand and model the Earth's radiation environment

The modelling of climate or weather systems rely on data collected all over the surface of the Earth at the same time, at different locations; why should it not be the same in the case of modelling the radiation environment in outer space?

In order to be more specific TREND has presented in TECHNICAL NOTE 6 a list of future flight opportunities which are becoming available and should be encouraged to carry dedicated monitors to get more comprehensive models of the Earth' radiation environment. These opportunities are discussed there in some details. In the following section we only will mention a few of them fro illustration.

5.3.3 Future missions: radiation concerns and possible monitoring?

Monitoring the Earth's radiation environment should not only be carried and aboard magnetospheric missions like CRRES. Indeed, the science objectives of such missions are not necessarily compatible with environment modelling & monitoring. Magnetospheric satellites are usually dedicated to investigate specific plasma phenomena occuring in the magnetosphere; in recent missions these scientific objectives had little to do with monitoring the Van Allen radiation Belts which, these days is an out of fashion activity for space physicists. This is the case for CLUSTER whose main scientific objective is to study the bow shock and magnetopause boundary layers.

Therefore, it would be inefficient to leave the role of monitoring the Earth's radiation environment to magnetospheric scientists and to the missions they are proposing. There are other SCIENCE missions as well, MANNED missions, APPLICATIONS missions, and missions belonging to the Technological Demonstration Programme (TDP) which are ideal carriers of radiation detectors.

5.3.3.1 Science missions

Science payloads become more and more sophisticated, employing new technology for their sensors,microprocessors, mass memories, and basic components. In general, these become more radiation sensitive, so it is imperative to remain aware of the radiation environment and its effect on space flight payloads.

IUE, the International Ultraviolet Explorer, is an astronomical mission (as already mentioned above); it carried very simply built small background monitors which contributed significantly (since 26 January-1978 for more than one solar cycle), to knowledge of both the radiation

environment and its background.

IUE consists of a three-axis stabilised platform supporting a 45 cm telescope with UV spectrographs in the Cassegrain focus. The purpose of this project is to supply a common user facility for ultraviolet spectrophotometry to the worldwide astronomical community. IUE is a joint venture between ESA, NASA, and the British SERC. The satellite is in a geosynchronous orbit with an apogee of 45,000 km and a perigee of 26,000 km. Normal spacecraft telemetry data are continously transmitted.

There are two reasons for astronomical missions to get far away from Earth. One is to escape from being occulted frequently by the Earth, and the other is to avoid the radiation belts because of the background signals the energetic particles can generate.

IUE data have been used by TREND to evaluate existing models of the outer zone trapped electrons (see TECHNICAL NOTE 5).

HIPPARCOS, another astronomical mission dedicated to the precise positional measurement of some 100.000 selected stars, did not unfortunately have a radiation monitor, .

It could have done with such a particle detector since its optical astronomy payload is susceptible to radiation-induced background. This is especially true now that HIPPARCOS is in a near-GTO orbit instead of operating at GEO where it was originally planned to be. In Geostationary Transfer Orbit (GTO), the radiation background is continously variable. Large amounts of important environmental data could have been acquired had HIPPARCOS carried a "minimally intrusive" radiation monitor like that of IUE. This would have been useful, also if it had been sucessfully injected into geostationary orbit where it would still have experienced the radiation background.

EXOSAT European X-ray Observatory Satellite), is also an astronomical spacecraft, operational from May 1983 to April 1983. During that time it made 1780 observations in the X-ray band studying most important astronomical X-sources.

EXOSAT was in a highly-elliptical, highly-inclined orbit and experienced mainly cosmic-ray background. To avoid radiation damage in the radiation belts the instruments were always switched off below 70,000 km altitude. Little analysis went into deciding this switch-off altitude, except that it was perceived to be 'safe'... If, however, it had had a monitor, with possibly an automatic switch-off for a critical radiation flux threshold, it would have operated to much lower altitudes and collected longer time series of useful data. Moreover, engineers would have acquired data to allow possible identification of cheaper orbits, since the apogee altitude strongly drives mission costs and limits payload.

EXOSAT is another example where "minimally intrusive" radiation detectors would have been of great benefit for astronomers, future mission planners and environment modellers alike.

XMM, the High-Throughput X-ray Spectroscopy Mission, is aimed at making a major step forward in astrophysics . This long-duration observatory facility has an anticipated lifetime of ten years.

The scientific objectives of XXM require a powerful imaging instrument with the largest possible collecting area for high-quality spectral measurements on faint sources and fast, low- and medium-resolution spectroscopy on the brighter objects. Major elements of the instrumentation are a set of grazing-incidence X-ray optics and CCD detectors. XMM's 24-hours, 71.000 km-apogee elliptical orbit of around 53 degree inclination means that it passes through the Earth's radiation belts on every

orbit and performs its observations outside them.

With apogee (~12 Re) near 53° latitude one can expect to be relatively free of energetic particles but the local time of the apogee and the argument of the perigee change through the mission . Consequently, there will be long periods when one can expect to encounter some substantial fluxes of electrons up to 500 KeV. The background produced by particles might cause some problems or confusion, particularly for the study of time fluctuations in the astronomical sources. The proton fluxes encountered around perigee give rise to important degradation of CCD detectors.

In all likelihood the XMM payload will have some radiation monitor. It would be highly beneficial, if such well-defined radiation monitors could indeed be flown for the whole mission (almost one whole solar cycle).

ISO (Infrared Space Observatory) is a follow-on of the succesful Infrared Astronomical Satellite IRAS. It is also an astronomical observatory facility, built upon the results and the experience gained from IRAS. ISO should be launched in 1993 into a 24-hour, 71,000 km-apogee elliptical orbit of around 7 degree inclination.

This orbit will stay within the trapping or pseudo trapping region all the time, so the electron bursts will be more frequent and larger than for XMM. It may prove useful to install an electron monitor so that all instruments would register when the flux of electrons is large enough to cause problems. Above these levels, either flags could be set in the data stream, or selected instruments could be turned off automatically. ISO does not plant to carry a radiation monitor. This is a real lost opportunity for the experimenters who need to operate the instruments outside the Radiation Belts, and who will have to analyse the data of ISO facing the problems of radiation background; this is also a lost opportunity for the next

generation of experimenters and mission planners.

TREND recommends that the ISO project examine the feasibility of including "minimally intrusive" particle detectors late in the programme, if there are spare budgets in mass, power and telecommunication. In this respect the sucessful experience of IUE could be taken as a representative case study.

FIRST, the sub-millimeter spectroscopy mission, will explore the 50 micron to 1 mm region of the electromagnetic spectrum of astronomical objects. It will also be launched in an ISO or XMM-type orbit (24 hour or 48 hour period). Therefore, it will pass through the Van Allen Belts every day. Its heterodyne detectors are not sensitive to the Earth's radiation environment, but other detectors and electronic parts of the payload are.

Consequently, for the reason emphasized already above, TREND recommends that "minimally intrusive" radiation monitors be added to that payload.

QUASAT is a mission to operate an orbiting radio telescope in conjunction with a worldwide, Very-Long-Baseline-Interferometry (VLBI) network of ground based radio-telescopes. The QUASAT mission has chosen a high perigee geostationary transfer orbit (GTO) which avoids the core of the energetic protons but still encounters many of them, including the peak fluxes for the 5-15 MeV range, which is the most damaging to solar arrays. QUASAT has been an ESA phase-A study; although it was not selected it may be reconsidered and it is believed the Soviet Union is already planning such a mission.

LYMAN, is a phase-A study which was not selected, but which may also be reconsidered in some form. Like IUE, its scientific objective is to study astronomical objects in the ultra-violet spectrum range with detectors very sensitive to energetic electrons and ions trapped in the

geomagnetic field. Its detectors are sensitive to primary and secondary radiation of quite low energy and so outer parts of the magnetosphere are important. LYMAN is again a HEO mission like that planed for XMM or ISO. We would make the same recommendations as above for this mission.

GRASP, was a phase-A study which was not selected. A mission to study Gamma-ray astronomy from HEO like the orbit of XMM or ISO. INTEGRAL is the name of a new ESA gamma-ray assesment study. The detectors of INTEGRAL would be very sensitive to the instantenous background of trapped particles, but also to the delayed emissions from activated material after the spacecraft passes through the proton belt. TREND again recommends to include radiation monitors in such a potential payload with feedbacks to protect sensitive instrumentation when the level of radiation exceeds a certain threshold. It would be a inexpensive way to gain vital data on environmentally induced activation.

For GRASP/INTEGRAL activation during the passage through the energetic proton region is unavoidable. Short lived products will decay during the ascent to apogee. Long term decays become a background that must be accounted for; even GCR can produce such activation. It may be useful to monitor the protons for this mission so that one can obtain a better estimate of the proton fluence than can be obtained from the old radiation models.

CLUSTER, is a fleet of four similar spacecraft to study plasma structures in three dimensions. The near-polar orbits of these space vehicles will have a perigee of 4 Re and an apogee up to 22 RE, i.e., well within the solar wind beyond the magnetopause and the magnetospheric bow shock. Six month later the satellite system will swing through the magnetotail and plasma sheet.

Although in a relatively benign radiation environment, except as always during solar proton events, CLUSTER has generally light shielding and sensitive components,

including transputers. This is because down-link limits mean that much processing has to be done on-board. Radiation housekeeping would obviously be prudent to monitor device health!

SPACE-STATION Payloads. Astronomy, geophysical as well as biology payloads which are sensitive to corpuscular radiation are envisaged to be flown on SS, both external or internal to the Space-Sation/Columbus Attached Laboratory. Although, this facility will be used primarily for payloads and experiments in material science, fluid physics and life sciences, important investigations on nuclear disintegrations 'stars' resulting from energetic trapped protons interactions can also be considered; these nuclear interactions lead to single-event upsets in electronic devices and to (still uncertain) radiobiological effects.

Since the module axis of Space Station Freedom and of the attached Columbus module will be closely parallel to the direction of their orbital velocity, the East-West asymmetry of the flux of inner zone protons could easily be observed and studied from this orbit. Note that ESA's module end will be located on the West end of the Space Station structure; this means that it should, in principle, be exposed to the highest trapped proton and cosmic ray energetic ion fluxes. Secular variation of the low altitude distribution of inner radiation belt protons can also be studied as part of a Columbus long-term environmental programme.

These effects are strong candidates for study by the US and European scientific communities. In parallel or in collaboration with the NASA Neutral Environment with Plasma Interactions Monitoring System (NEW PIMS) for Space Station Freedom (SSF), ESA is considering to develop a Columbus-PIMS (C-PIMS) package to provide significant contributions to monitoring of the SSF environment. A radiation monitor is strongly recommended for such a system.

In the meanwhile, it is proposed that a C-PIMS package be deployed from the Scientific Airlock and that a PIMS prototype be carried on Spacelab Pallet or a Hitchhiker structure, to include the radiation monitor for preliminary evaluation of the E-W asymetry, SAA variations and STARS.

COLUMBUS POLAR PLATFORM. Although the Columbus polar platform, the third element of the COLUMBUS DEVELOPMENT PROGRAMME, is mainly driven by its prime customer, the Earth-observation community, it will accomodate various Solar-Terrestrial Physics (CSTP) experiments including a Particle and Field Package (PAFP) with an electron spectrometer in the energy range of 10-600 keV. This package will be very useful to study the low altitude (500 km) radiation environment in the region of the South Atlantic Anomaly (SAA). NOAA proposes the Space Environment Monitor (SEM) for the ESA polar platform.

Space Station Freedom (SSF) payloads cover a wide range of disciplines; probably biology and astronomy interests are the most sensitive to radiation. The most important data in this orbit are stars, the highly ionizing secondary products produced by energetic protons and GCR. Nuclear emulsions, plastic track, and solid state detectors with pulse height analyzers are used to study these interactions. One cannot avoid SEUs from these stars and the rate is quite dependent on the payload mass and composition. Monitoring is clearly necessary.

Planetary and interplanetary missions are straightforwa33rd as concerns radiation. The solar proton environment is now well known and not extremely severe. Thus, Huygens, Rosetta, and Vesta, require no further comment; SOHO and Ulysses both carry instruments to measure solar protons to which CCDs are sensitive. Note that Jupiter and Saturn have very severe radiation environments. So missions such as Cassini-Huygens to these planets have to face internal charging, radiation damage, interference

and SEU.

5.3.3.2 Manned missions

Manned missions are confined to low altitude orbits to avoid the energetic protons, while both science and applications payloads cover a broader range of geospace.

The radiation exposure limits for man and the effects of highly ionizing particles, both secondary and primary, remain uncertain. Thus, there will be a continuing study of radiation biology as one moves more into extended periods in space. Such a continuing study has as a necessary input, a continuous and reliable record of the environment.

The Soviets have had a number of particle detectors associated with their Mir Station. For biology experiments and for the cosmonauts these measurements will most likely be done routinely on SSF by specialized instruments, as opposed to radiation monitoring.

Certainly, the east-west effect, in which protons coming from the west are more intense than from the east requires special orientation of the detectors. In principles this effect can be estimated from present models but their accuracy in this region was never good because of the steep gradients and lack of measurements with suitable instruments.

In addition, the secular change in the magnetic field even though small, produce a considerable change in the geometry of the SAA and the the protons distribution near their inner boundary.

Consequently, there is no reliable quantitative description of the east-west effect. Since the Columbus attached laboratory records directly protons coming from the west, modern measurements of these particles seems

mandatory. The effective boundary of the SAA has also shifted with the secular change of the field (the geometry) and no measurements exist at present to define this.

SPACE STATION/COLUMBUS and HERMES. The environment where the European Space Shuttle Hermes, the Columbus Attached Laboratory, and the man-tended Free-Flying Laboratory will orbit, is unique in respect to the radiation hazard to man (low-level, high energy, nuclear interactions).

It has been shown in TECHNICAL NOTE 1 that in this region the classical B-L coordinate systems used to model the Inner Zone Radiation Flux is the least reliable, (i) because of the atmospheric cut-off not properly described in this coordinate system, and (ii) because of the secular variation of the Geomagnetic Field. In TECHNICAL NOTE 2 it has been shown that there is an urgent need to reexamine the mapping of the low-altitude Earth's radiation environment with a new altitude like coordinate like the Hassitt shell height.

Standardized monitors on-board these manned vehicles would obviously provide an invaluable and unparalleled data bank for the next generation of mission planners and modellers of the low-altitude Earth's radiation environment. Such monitors would help solve some of the problems in planning and deciding on Extra Vehicular Activities for the astronauts.

This is why TREND strongly recommends also to add standardized "minimally intrusive" monitors on-board all manned missions.

5.3.3.3 Application missions

POLAR EARTH RESOURCES.

Future Earth resources programmes of ESA are planned

to be on polar orbits. Electronics, high performance microprocessors , high capacity memories, CCDs which will be used in future missions are radiation sensitive devices whose environment requires constant monitoring.

The first ESA Remote Sensing Satellite (ERS-1) will fly in the familiar polar orbit that is well known relative to the radiation environment. The Columbus polar platform will also occupy this region later with the American and, later, the Japanese version. The need for the continuation of radiation monitoring was addressed already. It would seem natural that ESA should participate in that monitoring.

The Columbus free-flying laboratory and other co-orbiting platforms will traverse space in the same region as the Space Station Freedom and so the remarks of the previous subsections apply here.

COMMUNICATIONS.

The Data Relay Satellite, PSDE-SAT-2 communication technology project have increased the requirement for on-board signal processing. Also under consideration are navigation satellites and high-latitude communication satellites which will be at lower altitudes than GEO or in inclined elliptical orbits. As a consequence, these spacecraft will be exposed to very much higher radiation levels: a radiation monitor would be necessary in these orbits for the reasons already given above.

There have been dosimeters with particle identification flown on several of the 12-hour US DOD navigation satellites but very little of that data is available. Depending on the exact orbits, these satellites might pass through the high energy electron region in the outer belt. This is important for studies of deep dielectric charging and constitutes a severe environment for payloads.

METEOROLOGY.

Meteosat data have experienced problems with disruption, probably due to deep-dielectric charging. An on-board instrument like the LANL LoE detector for electrons should be on future Meteosat missions as it was on METEOSAT-3, under responsability of MSSL.

TECHNOLOGY DEMONSTRATION PAYLOADS.

Given the aims and objectives of the Technology Demonstration Programme (TDP), a radiation environment monitor fits very well in the program and should be encouraged. This would provide basic environment data, flight-test a developed monitor for application on many of the above missions, and provide engineering data if flown alongside radiation effects experiments such as components, solar cells or charging.

Small-Sats, Spacelab, Small Payloads-Of-Opportunity on Communication Satellites, ERS and Meteorological satellites will be availabe from time to time. If TDP leads to development of a unit which is available and minimally intrusive, it could be put on board at short notice. Environment monitoring, by its very nature, needs to be carried out on frequent flights in a variety of orbits over a long time span.

It may be of interest to mention here that inexpensive and cost-effective small satellites have been built by among others, the University of Surrey. This group has launched small spacecraft launched into polar, sun-synchronous, low Earth orbit by NASA in 1981 and 1984 (UoSAT-1&2) and by ARIANE-ASAP in 1990. Such a 'standard' inexpensive small satellite bus can be used for a variety of mission payloads, including specific studies of the Earth's radiation environment.

5.3.3.4 Inter agency cooperation and stimulation

US MISSIONS.

GOES-NEXT, Polar Platform, PHIDE AN SSF, CRRES are other ideal carriers for monitoring the Earth's radiation environment. CRRES is a major mission in this respect,and , there are opportunities to cooperate in the data analysis and modelling efforts. As far as we know there is no follow-on for CRRES which is the US mission specially equiped to the study of the Earth's radiation environment.

ESA could consider a dedicated mission. It would fit with ESA's declared aim of autonomy in space, and the implication that this has to develop abilities to independently pursue areas of applied research such as environmental monitoring. Unfortunately, there is currently no ESA program that could support the cost for such a dedicated mission.

A CRRES follow-on type of mission could possibly be part of the Technology Demonstration Programme, TDP, and/or of the preparatory programmes of ESA.

Monitoring the Radiation Environment within the framework of these programmes should be coordinated and analysed with those from other scientific and application missions of ESA, and of other Space Agencies.

5.3.4 What is a "minimally intrusive" system?

In the previous sections we suggested to have on future mission spacecraft "minimally intrusive" radiation monitors. A minimally intrusive system is one which is light (~1 kg; definitely less than 2 kg), consumes low power (~1 Watt; definitely less than 2 W), and needs low bit rate (less than 100 bps). It should be easy to mount and with very few interface problems including data system and telemetry interfaces.

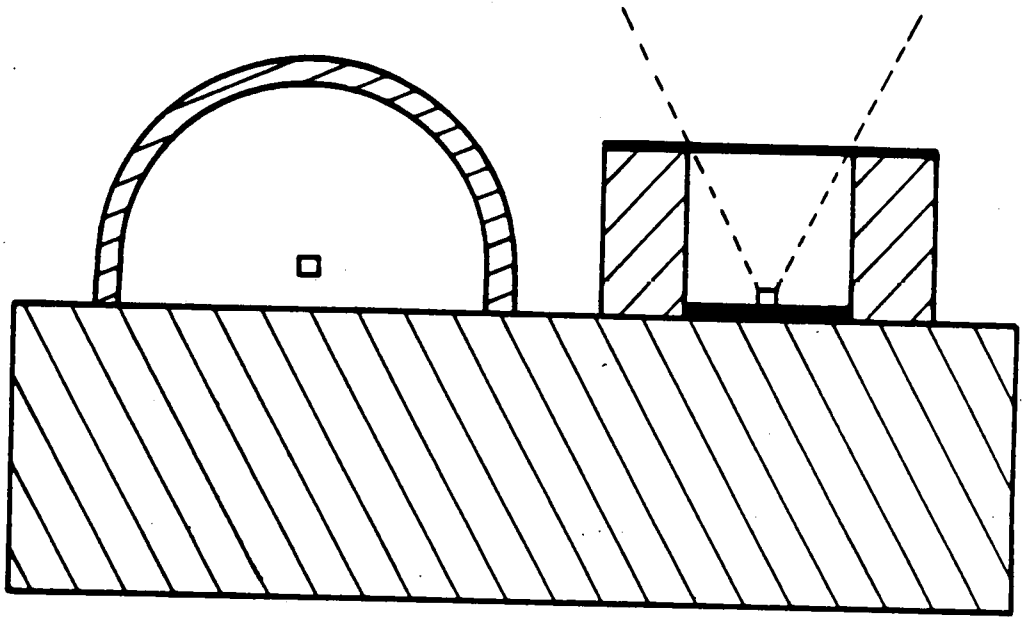

Fig.5-1 Geometry of bafles for omnidirectional detector (hemispherical bafle, on the left) and directional detector (cylindrical bafle, on the right hand side).

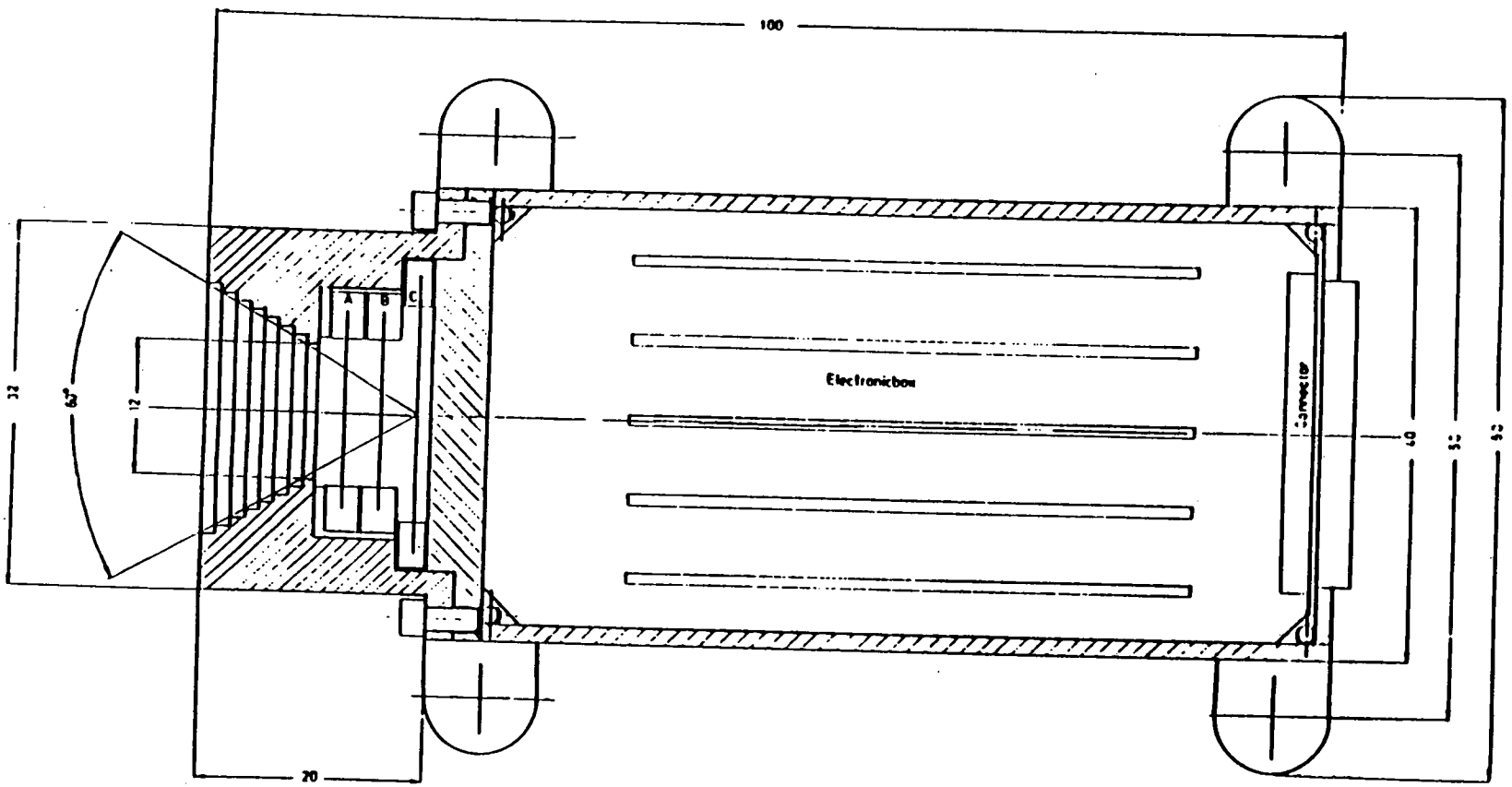

Fig.5-2. Cross-section of a directional particle telescope built by Space Technology Ireland Ltd. (McKenna-Lawlor et al. 1981, 1987, 1990).

In certain instances omnidirectional flux measurements are sufficient while in other case a directional monitor can be prefered. Fig. 5.1 illustrates how, with different baffle design, both types of detectors can be constructed most simply. The hemisphere dome geometry (on the left) returns omnidirectional measurements, while the cylindrical baffle on the right gives directional ones useful for pitch angle sampling. With hemispherical domes, magnetometer and spacecraft attitude is not needed. One may also consider either single or double silicon detectors with preamps, pulse-height analysis and discrimination.

Electrons as well as protons of different energies should be measured. Note that not too high energies several tens of MeV should be required to avoid sophisticated methods.

By using solid state detectors one avoids the high voltage problems of arcing, pump out, etc. and the weight of the detector is minimal. The system is made omnidirectional with hemispherical domes so that magnetometers and attitudes are not needed. With the use of just two discriminators a single integral electron channel and a single proton band measurement are possible with each detector. To obtain good energy coverage, four detectors have been used on several occasions, e.g. ATS 1, ATS 6, DMSP/F1, DMSP/F7. For the last two a pulse height analyzer was used to determine the dose in the detector as well as to provide single channel information for each particle. Such systems have covered the range of electrons from 0.3-10 MeV and protons from 5-100 MeV. Stars are readily identified by even higher discriminator levels. Thus, the important range of particles identified earlier can be covered quite nicely.

New technology may permit other ways of doing the above, but the important characteristics will be the same. Thresholds can be changed easily by dome thickness and

discriminator triggering level. Certainly one should also be prepared for more sophisticated opportunities, but one must realize that more lead time would then be required. For an opportunity on the Technology Demonstration Program (TDP) one could use a pulse height analyzer with the above system and have a good spectrometer for all the important heavily ionizing particles. Such a measurement fits in with the aims and objectives of TDP and would provide a good flight test for such an instrument.

Example of such units are the DMSP/F7 dosimeter and its forerunner flown on DMSP/F1. The IUE PFM was a similar instrument except there were two major differences; the project needed it at the last minute (about 3 weeks before launch) and it was a directional detector. In earlier times it was possible to build very small piggyback satellites (~2-5 kg) with fundamental particle detectors. In that case the satellite hitched a ride instead of an experiment. Examples are ERS 12,13,17,18,27, which all traversed the radiation belts from 300 km to 18 R_e. (Note: the ERS name was first used for this US satellite series in the '60s).

In TREND's TECHNICAL NOTE 6 a few examples of "minimally intrusive" monitors have also been given (see for instance Fig.5-2). Their descriptions will not be repeated here. There are different types of detectors : Energetic particle detectors, Space "dosimeters" (counting dosimeters), RADFETS (integrated dosimeters, the new Radiation Monitor developed in the Technology Demonstration Program.

5.4 How to use future radiation data to update Earth's radiation environment models and produce new ones?

Of course it is not just enough to build monitors for future European and possibly US and Japanese spacecraft, and to transmit their data to ground. Indeed, once these data are stored on tapes at the mission data centers they should be used for updating and renewing the earth's radiation models. However, after collection, there is often not enough manpower, available to examine such large amounts of new data, or to make use of them for updating radiation environmental models; most experimentalists are by then already busy constructing the next instrument for the next space project.

Furthemore, ESA does not effectively support multi-disciplinary scientists to analyse data which have become available. For the time being, there is not a concerted strategy to cross-fertilize data obtained during different missions, nor to make the best use of all the efforts put into particular missions by individual scientists and consortia of experimentalists.

The lack of interest in cross-correlating and cross-fertilizing data from different missions and using them to develop more reliable environment models does not come only from lack of encouragement and financial support by the Space Agencies for this sort of multi-disciplinary activity, it results also partially from the lack of coordination between Science Departments and Application Departments or Directorates. Perhaps more importantly, it results from the lack of interest of space scientists themselves for such 'tasks' which are unfortunately considered by some people as being of minor interest for 'their Science'. It is noteable that in the US, many institutes encourage the exploitation of space acquired

data for applied purposes (NOAA/SEL, NSSDC, AFGL, Aerosp.Corp.)

It is true that modelling the Van Allen Trapped Radiation Belts, or predicting the fluence of solar proton events for the next solar cycle has become a less exciting scientific endeavour than investigating 'reconnection or Flux Transfer Events'; but for future scientific, applications, manned and commercial spacecraft design it is important to obtain more precise and more reliable models of the Earth's radiation environment since these models have a direct impact on the shielding, weight and cost of future missions transportation systems.

Note that not only the radiation environment should be modelled on a continuing, reliable and concerted basis by the different Space Agencies, but also neutral atmospheric and ionospheric models, as well as model distributions of natural and artificial debris in orbit around the Earth, should be developed.

The long-term format of the European effort needs to be established. Some continuing funding is obviously a prerequisite. Coordination with national and/or private efforts (if such ever exist) would be obviously benificial.

5.5 Recommendations for future flights and modelling efforts.

ESA has declared its aim of autonomy in space. This implies that it is willing to pursue the updating and extension of knowledge of the space environment. Consequently, it seems appropriate to make some recommendations relative to the energetic particle environment. It should be clear at this point that our knowledge has been eroding for a decade or two in some facets of this field. It is important to understand what is lacking (as has been pointed out above) and how to be

effective in filling the gaps. The latter topic is treated next.

It is doubtful that there will be a follow-on to CRRES for many years, so dedicated missions for radiation studies are highly unlikely. The way in which radiation monitoring has proceeded in recent years has been in two directions. The first is quite visible in this report. It is part of an ongoing program as exemplified by the NOAA, GOES, GMS, LANL satellites; the rationale : it is part of space weather. The second way is to have a monitoring flight unit that is minimally intrusive; this means it should be light (1Kg), low power (1Watt), with a large geometric factor (>0.8cm^2/ster), the capability to monitor ions and electrons with a high temporal and spatial resolution ,easy to mount with very few interface problems, including data system and telemetry interfaces.

Where besides TDP should such a monitor be flown ? Certainly the 71,000 km apogee astronomy orbit would be useful and the outputs could be of operational use to the mission, as pointed out previously. To cover the geostationary orbit METEOSAT would be preferable to the communication satellites because of the operational environment but, in either case, the emphasis should be on high energy electrons.

The ERS and Polar Platform provide access to the polar weather orbit; however, it is recognized that this orbit is quite well monitored now. Monitoring the LEO environment is important to obtain updated models in view of secular variations, to monitor the E-W assymetry and to ensure astronaut exposures are controlled. SEU due to protons are also a concern.

In short, it is recommended that ESA establish a radiation environment programme that is practical, useful to its aspirations, and pertinent to the extension of our knowledge of the radiation environment and its effect on

space systems. Such a long term programme would of course require first collecting Earth's radiation environment data simultaneously, in all region of space, over extended period of time with "minimally intrusive" systems. A second step would be to stimulate in the European scientific and "applied science" communities coordinated activity to deal with the special data analysis and modelling tasks.

6. CONCLUSIONS & RECOMMENDATIONS

The significant conclusions and results reached by the TREND team over these 15 months, should be useful for future developments in this area. Recommendations have been made all along this study. They are detailed in the six TECHNICAL NOTES which have been produced under this ESA contract.

But before summarizing the results and recommendations of the five previous chapters of the present FINAL REPORT, it may be suitable to re-emphasize the usefulness and benefits of having updated and comprehensive models for the Earth radiation environment. It is then appropriate to compare the situation before and after this study. The recommendations for the future will be given in the last section.

6.1 Why there is a need for environment radiation data and updated models

The detrimental effects of hard corpuscular radiation is not limited to engineering technical aspects e.g. component radiation damage, crew health, degradation of solar cells, damages due to electric discharges, ... It interferes and spoils also the measurements taken by scientific instruments in orbit around the Earth. Astronomical measurements programmes are hampered by such detrimentral effects (e.g. HIPPARCOS, IUE). Indeed, detectors flown on most astronomy satellites are very sensitive to the noise caused by the ambient trapped particles. Primary particles as well as secondary particles reduce the efficiency of these detectors and shorten their life.

But in addition to the detrimental effects on the

spacecraft material, equipment and instrumentation, the bombardment of energetic electrons and ions poses critical problems for manned missions as well. Safeguarding astronauts from adverse biological radiation effects inflicts stringent requirements on the length of manned missions, on the orbit selection and planning of extravehicular activities.

A factor of two (or more) uncertainty in the average value of the omnidirectional fluxes of trapped electrons and protons has therefore important consequences on the design of the spacecraft or/and on the overall mission operation, including the selection of orbits. Too optimistic flux models would be a disaster for obvious reasons. Over-pessimistic or too conservative models are leading to unnecessary heavy shielding of the spacecraft, or costly alternative orbits.

Furthermore new models need additional functionalities (e.g. directional flux, statistics, temporal evolution, dependence on atmospheric density). Accurate prediction models for the radiation dose is therefore mandatory. But this requires reliable and constantly updated models of the trapped particle environment both at low altitudes and at high altitudes beyond geostationary orbit. Collecting synoptic environmental data with "minimally intrusive" detectors is, like in meteorology and climatology, the safest way to go in space. It would help the astronomers to plan the orbits and operation of their satellites and sensitive instruments. It would help the engineers to have more reliable dose predictions for scientific and commercial satellites. It would certainly benefit the astronauts to know with greater confidence what is the dose of radiation they likely are going to be irradiated with.

All this leads to the conclusion that there is need for studies like the present one, and that this first effort from the european community has to be encouraged and

continued in the future.

6.1 The situation defore and after TREND

The present knowledge about the Earth's radiation environment has been derived mainly from the data obtained during twelve years of the space era along with the theoretical, analytical and modelling effort associated with them. It should be pointed out that the first area of discovery and scientific effort in space involved energetic particles. The instruments were readily available out of nuclear physics, high-energy physics, and balloon borne/rocket borne cosmic-ray work. It took nearly a decade to develop instruments for other areas, such as plasma, astronomy, and earth resources where the main thrust has been for the past two decades.

Unlike the Earth's radiation models, geomagnetic field models are updaded almost every five years by IAGA Division V. The latest update is IGRF-85. TREND implemented this new IGRF-85 model as well as its secular variation.

TREND implemented also the Jensen and Cain (1962) geomagnetic field model for epoch 1960, which was missing in the former UNIRAD software. It is precisely the Jensen and Cain B-Field model which has been used to build the whole series of NASA trapped radiation models, including AE8 and AP8. It was interesting to have also this model available in UNIRAD since TREND came to the conclusion that the magnetic field model used for predictions must be the same as that used to build the trapped particle model.

Furthermore, TREND pointed out that, in order to avoid spurious secular evolution in radiation dose prediction, it is essential to use the same magnetic field model as that which was used to build a particular model for omnidirectional particle fluxes. To predict the radiation dose for a space mission planned in the year 2000, it was

common practice to use the geomagnetic field model corresponding to the year 2000 while the AE8 and AP8 radiation models employed were built with a geomagnetic field corresponding to an epoch in the 60's. It has been shown during this study that this is a wrong method of calculation, and, that it should definitely be abandonned in future simulations. Therefore TREND recommends to use the same epoch for the geomagnetic field than for the radiation models used to make dose prediction calculation in the future.

It was also suggested that the spurious secular variation in radiation doses pointed out by McCormack (1986), would disappear by replacing in McIlwain's algorithm the standard value for the magnetic moment, 0.311653 Gauss R_E^3, by the actual magnetic moment M at the epoch of time for which the prediction is to be made. As a result of the present study, TREND advises the user community not to adopt such a practice. Indeed, this would not resolve the embarassing secular variation mentioned above, because of the secular variation of the higher order moments in the geomagnetic field models. On the contrary, such a non standard practice would bring in even more confusion than there is already in this community about the true meaning and understanding of the B-L coordinate system.

The calculation of McIlwain's L shell coordinate from the values of B and I, the geometric field invariant, was based on the orginal algorithm introduced by McIlwain (1961). Since Hilton (1971) published a simpler algorithm to obtain the same result, but in a more immediate manner, TREND has implemented the more recent Hilton's method in UNIRAD.

There has been (and still remains) a dream of theoreticians to identify a generalized L^* parameter which would be 'truely invariant' (constant) along a given

magnetic field line; indeed, McIlwain's L-parameter is not strictly the same for all mirror points along a given magnetic field line. Having investigated a quantitative formulation of this idea, TREND has concluded that this dream is beyond grasp. The reason is the high degree of complexity of the IGRF and external magnetic field models used in practice. The mathematical expressions for L^* or for the canonical Euler potentials characterizing a whole field line are untractable and difficult to determined for the 120 terms of the IGRF and sophisticated external magnetic field models, although, some new avenues have been discussed by J.I. Vette during TREND's progress meetings.

The UNIRAD software did not include any external magnetic field model which is local time dependent. Recognizing the need for such an external magnetic field component to calculate proper values of the B-L coordinates at large radial distances, TREND has implemented in UNIRAD four alternative external field options including the most recent model of Tsyganenko (1989). Tsyganenko's model depends on the level of geomagnetic activity which is determined by the value of the Kp-index. Therefore, after TREND's study the user of UNIRAD will have the option to select an external magnetic field model and to input the value of an additional free parameter corresponding to the value of Kp.

The righteousness of B-L coordinates for low altitude mapping had never been seriously questioned. As part of this study TREND has pointed out that between 150 km and 1500 km altitude, the atmospheric density distribution must necessarily to be taken into account in modelling the trapped radiation fluxes. For these low altitudes TREND has suggested to replace B or B/Bo by a mean atmospheric density value which is an average over the drift shell of the particle. The Hassitt shell height has been proposed by TREND as an appropriate new coordinate depending both on the geomagnetic field distribution, and, on the actual

atmospheric density distribution; the latter is a complex function of altitude, latitude, local time, season, solar and geomagnetic activity. Because of the lack of man-power TREND has not updated, nor optimized the original programme designed at UCSD (La Jolla) by Hassitt (1965), and, kindly provided to TREND by Carl McIlwain. But other alternatives new coordinate system have also been discussed in TECHNICAL NOTE 2.

The UNIRAD user had only to rely on the NASA solar proton events model introduced sixteen years ago by King (1974). TREND has implemented model which is based on solar proton events observations extending over three solar cycles instead of one. This new solar flare proton model is due to Feynman et al. (1989). Since the NASA model will still remain a reference for some time, it is possible to access it as an option in UNIRAD.

The NASA models AE8 and AP8 are the only trapped radiation environment models available to UNIRAD users. During the TREND study new electron flux tables have been built using LANL omnidirectional measurements made at geostationary orbit. These tables are called TREM-G and TREM-GX where TREM stands for 'Trapped Radiation Environment Model'; G for 'near Geostationary region'; X means that it has been determined with Tsyganenko's eXternal magnetic field model. These tables can be used with additional data, to build a new model similar to AE8.

The TREM-G table contains local time averaged integral fluxes. TREM-GX is Kp dependent; four different Kp ranges have been selected. Besides the average integral and differential energy spectra usually given by standard software packages, TREND has updated the standard deviations of these omnidirectional fluxes as a function of electron energy.

The results of LANL and IUE analysis have been used to obtain new statistical and local time models. Interesting

results have been obtained by TREND from the intercomparison of AE8 model predictions with TREM-G. Furthermore, the comparison of model predictions with and without the external magnetic field model (i.e. TREM-G versus TREM-GX) has also been a significant new contribution of TREND.

Comparison between the predictions made with Feynman et al.'s model and those obtained with King's approach have been made, and constitute an original contribution of TREND to this field of investigation.

Comprehensive catalogues of experiments which have commected fluxes of particles in the range of energy of interest for designing trapped radiation models are given in TECHNICAL NOTE 3. Future experiments which could contribute to future modeling efforts have been identified also in TECHNICAL NOTE 6. Based on these catalogues of data, regions of space and domains of energy where more data are needed have been outlined. There are many data already available, like IUE measurements, which await to be used for the purpose of designing new, more complete and elaborated models.

This is a summary of most significant contributions that have been made by TREND within the rather short time span of 15 months. All these achievements could not have been accomplished without important investments in manpower and computer time made by MATRA-ESPACE, by JIV Assoc., by STI, and by IASB.

There are many possible extensions of TREND's work. Below, we are presenting recommendations for such future extensions, and, more generally,for Earth radiation environment modelling efforts to be undertaken or pursued by ESA or any other space agency.

6.3 Recommendations for the future

In the course of this study TREND has formulated a number of recommendations for future developments in the area of Earth's radiation environment modelling. These recommendations have been presented in the various chapters of TREND's TECHNICAL NOTES.

TREND recommends to pursue the data analysis of LANL and IUE data beyond the stage where TREND's resource sustained it. There are several other data sets which are available to extend these modelling efforts and extend the B-L coverage of TREM-G and TREM-GX. The DMSP data now being deposited at NSSDC, is another interesting set of energetic electron and proton flux measurements which has been considered by TREND, but which could not been handled within the time limits of this present contract. TREND recommends strongly the exploitation of these valuable DMSP data for the purpose of improving the reliability of low altitude radiation environment models.

How can this be achieved? Computer algorithms would have to be constructed and tested to calculate the new coordinates to be used as alternatives to B and L, for any point along LEO satellites. A database including the flux measurements as a function of energy and azimuthal angles (when available) would be stored in a database with the coordinates (including the traditional B-L ones) as well as universal time. To determine the new coordinates (like the Hassitt shell height, or other coordinates discussed in TECHNICAL NOTE 2) an atmospheric model (like MSIS-86) would be necessary. This atmospheric density model varies with universal time, depending on solar and geomagnetic activity. Averaging of measured fluxes in energy bins, azimuthal angles bins, for different values of solar and geomagnetic activity indices, must be performed as a function of the new alternative coordinate system. The statistical standard deviations corresponding to these bins

will also be computed as it has been done in TREND's analysis of LANL and IUE data. Local time and longitudinal dependence of these fluxes would be stored in multidimensional matrix arrays. As for AP8 and AE8 interpolation methods can eventually be used to determine the predicted flux value at any point in space and for any given energy range.

Development of updated and new models has to be encouraged. This can be a multi-agency activity. There are many complementary directions to go in this respect. As already emphasized above, one first most urgent improvement would be to develop a new model for the low altitude region between 150 and 1500 km height, taking into account the atmospheric density distribution. In this respect TREND has recommended in TN2 the 'Hassitt shell height' as a new coordinate to map the lower altitude region of the Van Allen belts but other alternatives should also be investigated..

Since the outer magnetic field distribution is directly dependent on the solar wind parameters, TREND recommended in TN1 to develop new external magnetic field models which are dependent on these solar wind parameters. Furthermore, in addition to the K_p geomagnetic index, TREND recommend to develop future external magnetic models ring current contribution depends on the Dst geomagnetic index and not on K_p.

Since the number of solar proton events taken into account in the stastistical analysis of King (1964) and even of Feynman et al.(1989) is relatively limited, TREND recommends that the prediction of both models should be tested using forthcoming data from the current solar cycle.

A series of recommendations dealing with radiation environment monitoring have been recalled already in the previous chapter of this FINAL REPORT. They can be summarized in the following words:

- Propose a follow-up of CRRES mission dedicated to study the energetic particles injected or trapped in the geomagnetic field.

- Use the opportunity of future science missions (astronomical and magnetospheric missions) to monitor the energetic particle populations in the inner and outer magnetosphere.

- Use the opportunity of manned missions to collect data at the lower edge of the inner radiation belt.

- Use the opportunity of TDP, or small satellites to monitor radiation in space as frequently as possible to obtain, as in Meteorology, Climatology, or Oceanography, the best coverage in time and space of the Earth radiation environment.

To organise these various measurement surveys, standardized "minimally intrusive" detectors should be used on these different mission opportunities. Minimally intrusive particle monitors have been described in TN6 as well as in chapter 5 of this FINAL REPORT.

To analyse the synoptic data sets which would be collected for over one solar cycle, the different space agencies including ESA, should stimulate and support multi-disciplinary groups or teams to update and improve Earth's radiation models. Specialized laboratory departments and World Data Centers should also promote this kind of application.

Development of space environment models must be considered as long term tasks by specialized teams of scientists and programmers. In chapter 6 of TN2 Jim Vette, TREND's consultant who has gained considerable experience and know-how in this field over a 26-year period has

outlined a possible progression for longterm developments in the area of model formalism. This strawman evolution, which is given in Appendix A, starts with the simplified trapped radiation models currently available after TREND study, and extends in the far future when highly sophisticated dynamic models will be designed, similar to those now available in Meteorology and Oceanography or Earth Resources.

But before that final goal is reached much more synoptic observations must be collected. Serious and concerted incentive must be given to the space radiation modelling community, like that given to the climat modelling community during the recent years. The needs are similar and the returns are directly cost effective.

APPENDIX A : OUTLINE FOR FUTURE LONGTERM DEVELOPMENTS

A.1. Introduction

Development of space environmental models must be considered as long term continuing tasks by specialized teams of scientists and programmers; such teams might exist at space research institutes and /or World Data Centers. These models need constant updating and improvment by permanent personnel who has gained experience in modelling and accumulated specialized know-how in this field. On an even larger scale one can look at the modelling of the Earth's weather as a real ongoing example. Over the 15-month TREND study it was impossible to develop completely a new trapped radiation or solar proton model. REND has achieved improvements of existing models and software programs.

Designing fully new model structures is however undamental long term undertaking that is beyond the resource and time limits of TREND. However, we consider it important to outline such a long term effort for energetic space radiation model development. The aim of this chapter is precisely to provide such a perspective. An outline of a possible progression of a model formalism is given below in sections A.2 to A.9. In order to make the outline somewhat realistic strawman choices are given to realize a model; the rationale for these choices is not provided. Clearly such choices would require study of data and theory. Consequently these strawman choices should be taken in the proper conte .. The format for each section will be

a. A short descriptive title of the model with a short name (Model XY-Z) included

b. A listing/discussion of the physical processes/effects included

c. A listing of the physical processes/effects that are excluded

d. Physical parameters that are needed

e. Recommended choices of physical parameters with the rationale

f. Supporting models that are needed

g. Recommended choices of models with the rationale

h. Useful/Valid range of the model

i. Software requirements to support the model

j. Identification of existing and available software

k. Software to be developed

A.2. Static Simplified Adiabatic Trapped Radiation Model (Model TR-A)

a. see : A.2. above

b. Adiabatic motion of electrons and protons, static perturbed dipole geomagnetic field

c. Source and loss terms, transport/acceleration, electric fields, time varying magnetic fields, L shell splitting, solar wind effects, local time effects, east-west effect, pseudo-trapping regions

d. Spatial position of data points or test points [r(t)], observed or supporting model magnetic

coordinates, particle fluxes (and pitch angles if directional fluxes are used)

e. Canonical forms : r in geographic polar coordinates, magnetic coordinates B and I, 'invariant' coordinates B/B_o and L* (Roederer's L) and the particle data as fluxes differential in angle and in energy

f. Internal geomagnetic field at epoch of model i.e., without secular changes), a dipole function for determining L, a baseline trapped radiation model to build on

g. Jensen and Cain geomagnetic field model with epoch 1960, the Hilton dipole function using a magnetic moment of 0.311653 Gauss, AE8 and AP8 converted to the canonical form

h. Spatial region within altitudes above about 1000 km and L values below 3 R_e. Energy ranges between 0.04 - 5 MeV for electrons and 0.1 - 400 MeV for protons

i. Orbit generation programs with drag and gravitational effects, magnetic field, I, L, and L* computational programs, flux conversion programs to convert to and from omnidirectional, unidirectional, and other flux forms, and programs to store and retrieve the flux as a function of equatorial pitch angle, L, and energy

j. UNIRAD contains all the software except that given in k. below

k. Hilton's algorithm integrated into UNIRAD, flux conversion programs from NSSDC or new set developed for TREND, interface routines for UNIRAD to work with unidirectional flux as the canonical form, and L* computational programs

A.3. Secular Adiabatic Trapped Radiation Model Model TR-B)

a. see: A.3 above

b. Adiabatic motion with secular acceleration, perturbed dipole magnetic field with secular changes, simple source and loss mechanisms based on boundary conditions and particle conservation within the bounded volume (a particle continuity equation) and L shell splitting

c. Realistic source and loss terms, transport/ acceleration except for secular acceleration, electric fields, magnetic fields with sources external to the Earth, local time effects, solar wind effects, east-west effects, pseudo-trapping regions

d. Spatial position of data points or tests points [r(t)], observed or supporting model magnetic coordinates, invariant coordinates [only 2 are independent], particle fluxes and kinematics in 'adiabatic invariant flux' form

e. Canonical forms:r in geographic polar coordinates, magnetic coordinates B and I, 'invariant' coordinates K and L* (Kaufman's K and $L^* = 2\pi\ [.311653]/\Phi$, P (momentum) and α (pitch angle) for the dynamical variables, particle density differential in angle and momentum for the flux form

f. Internal geomagnetic field model with secular change, model for determining the drift shell of the particle, a baseline trapped radiation model to build on

g. IGRF geomagnetic field models, Pennington's perturbed dipole model to find the drift shell, AE8 and AP8 converted to the canonical form

h. Same region as A.2h

i. Same as A.2i with the addition of Pennington's algorithms, and a program to change from energy to momentum (relativistically) and convert fluxes to density

j. Assuming A.2k. has been added to UNIRAD then remainder given in A.3k

k. Programs to effect requirements in A.3i

A.4. Advanced Model TR-B with Slowly Varying External Magnetic Fields Added (Model TR-C)

a. see: A.4. above

b. Adiabatic motion with secular acceleration, perturbed dipole magnetic field with secular changes, external magnetic fields with slow changes (3rd invariant is conserved), local time effects, solar wind effects, pseudo-trapping regions, simple source and loss mechanisms based on boundary conditions and conservation, and L shell splitting

c. Realistic source and loss terms, transport/ acceleration except for acceleration conserving the 3rd invariant, electric fields, magnetic fields with time changes that would break the invariants, east-west effects

d. Spatial position of data points or test points [r(t)], observed or supporting model solar magnetic coordinates, invariant coordinates, particle fluxes and kinematics, 'adiabatic invariant flux' form

e. Canonical forms:r in polar geographic and solar magnetic coordinates depending on regions, magnetic coordinates B and I, 'invariant' coordinates K and L*, P (momentum), α (pitch angle), and phase angle around field line (δ) for the dynamical variables, particle density differential in angle (including phase) and momentum for the flux form

f. Internal geomagnetic field model with secular change, external model that accounts for ring current, tail current and boundary currents as well as the dipole tilt, model (method) for determining the drift shell of the particle in the total magnetic field, a baseline trapped radiation model to build on

g. IGRF geomagnetic field models, Tsyganenko (1987 and 1989) model, extend Pennington's perturbed dipole model to higher order, develop new model to obtain drift shells, AE8 and AP8 converted to the canonical form using AE8 local time function for electrons

h. Spatial region within altitudes above about 1000 km and below the boundaries of the magnetosphere. Energy ranges the same as AE8 and AP8

i. Same as A.3i with the addition of software to effect the Tsyganenko model in UNIRAD, coordinate transformation routines to handle geomagnetic, geographic, solar magnetic, and solar magnetospheric coordinate systems, software to determine drift surfaces, routines to handle an additional variable in both the coordinate and the kinetic parts of particle phase space

j. & k. See i

A.5. Advanced Model TR-C with Atmospheric Source and Loss Terms (Model TR-D)

a. see: A.5 above

b. Adiabatic motion with secular acceleration, perturbed dipole magnetic field with secular changes, external magnetic fields with slow changes (3rd invariant is conserved), local time effects, solar wind effects, pseudo-trapping regions, simple source and loss mechanisms based on boundary conditions and particle continuity equation and L shell splitting, atmospheric source and loss terms, east-west effect

c. Realistic source and loss terms for outer zone particles, transport/acceleration except for acceleration conserving the 3rd invariant, electric fields, magnetic fields with time changes that would break the invariants

d. Spatial position of data points or test points [r(t)],effective atmospheric height, observed or supporting model solar magnetic coordinates, invariant coordinates, particle fluxes and kinematics, 'adiabatic invariant flux' form

e. Canonical forms:r in polar geographic and solar magnetic coordinates depending on regions, magnetic coordinates B and I with atmospheric height variable added, 'invariant' coordinates K and L* with an atmospheric height variable similar to Hassitt's shell height based on average density but taking into account the gyro motion of protons (H'), P, α, δ for the dynamical variables, particle density differential in P, α, δ

f. Internal geomagnetic field model with secular change, external model that accounts for ring current and boundary currents as well the dipole tilt, model (method) for determining the drift shell of the particle in the total magnetic field, a baseline trapped radiation model to build on, atmospheric model(s) for densities and composition, model (method) to compute motion of charge particles without adiabatic approximation (e.g., direction integration of equations of motion via Stoermer approach), atmospheric source model

g. IGRF geomagnetic field models, Tsyganenko (1987 and 1989) model, extend Pennington's perturbed dipole model to higher order, develop new model to obtain drift shells, AE8 and AP8 converted to the canonical form using AE8 local time function for electrons, latest CIRA model CRAND model adjusted by strength parameter to match observations

h. Spatial region within altitudes above about 150 km and below the boundaries of the magnetosphere, Energy ranges the same as AE8 and AP8

i. Same as A.4i with the addition of software to compute trajectories of charge particles in magnetic fields numerically, software to interface UNIRAD to CIRA/MSIS, programs to determine H' for both electrons and protons, software to perform CRAND calculations to determine both proton and electron source terms

j. & k. See i above

A.6. Dynamical Model with Diffusion, Electromagnetic Environment, and Tail Sources (Model TR-E)

a. see: A.6 above

b. Adiabatic motion, non-adiabatic motion, pitch angle diffusion, magnetic and electric diffusion with breaking of 2nd and 3rd invariants, wave particle interactions and flux limiting, internal and external magnetic fields with realistic time variations, magnetospheric electric fields, local time effects, solar wind effects, pseudo-trapping regions, shell splitting, realistic source terms from the atmosphere and injection from the geotail under various magnetic activity conditions

c. Only very special situations

d. Spatial position of data points or test points [r(t)] effective atmospheric height, observed or supporting model solar magnetic coordinates, invariant coordinates, particle fluxes and kinematics, 'adiabatic invariant flux' form, diffusion coefficients, wave particle interaction parameters, and other TBD parameters

e. Canonical forms : TBD

f. Internal geomagnetic field model with secular

change, external model that accounts for ring current, tail current and boundary currents as well the dipole tilt, model (method) for determining the drift shell of the particle in the total magnetic field, a baseline trapped radiation model to build on, atmospheric model(s) for densities and composition, model (method) to compute motion of charge particles without adiabatic approximation (e.g., direction integration of equations of motion via Stoermer approach), atmospheric source model, electromagnetic power spectra density model for the magnetosphere, geotail injection model, diffusion models, wave particle interaction models, othep models TBD

g. TBD

h. same as A.5h with extensions to lower energy

888 j., & k. TBD

A.7. Solar Proton Model Based on Feynman et al. (Model SP-A)

a. see: A.7 above

b. Solar flare proton acceleration and propagation from Sun to Earth as observed over three solar cycles, cutoffs in TREP, mission oriented probabilistic fluences

c. Basic understanding of flare acceleration and propagation processes, realistic cutoffs based on model external geomagnetic fields, categorizing of individual events and their spectra

d. Event integrated fluence above kinematic thresholds, event times,

e. Briggs logarithm of fluences above proton energies of 10 and 30 MeV, event times in decimal solar cycle years,

f. Statistical model for the distribution of fluence, model for the probability of event occurrence, and geomagnetic field model for cutoffs

g. Normal distribution for the log of the fluence, F, with parameters μ for mean and σ for standard deviation; Poisson distribution for event occurrence with parameter w for the mean number of events per solar cycle year, geomagnetic fields in TREP for cutoffs

H. - K; TBD

A.8. Advanced Model SP-A with Categorized Events Model SP-B)

a. see: A.8 above

b. Solar flare proton acceleration and propagation from Sun to Earth as observed over three solar cycles, cutoffs in TREP, mission oriented probabilistic fluences, categorized events with spectra

c. Basic understanding of flare acceleration and propagation processes, realistic cutoffs based on model external geomagnetic fields

d. Event integrated fluence above kinematic thresholds, event times, event categories and spectra

e. Briggs logarithm of fluence above proton energies of 10 and 30 MeV, event times in decimal solar cycle years, 6 categories of events based on high, medium, and low fluence and on hard and soft spectra; each category to be characterized by the fluence, spectral parameters (e.g., power law index) and probability of occurrence

f. Statistical model for the distribution of fluence, model for the probability of event occurrence, and geomagnetic fields in TREP for

cutoffs

g. Normal distribution for the log of the fluence, F, with parameters μ for mean and σ for standard deviation; Poisson distribution for event occurrence with parameter w for the mean number of event, spectral parameters for categorized events geomagnetic fields in TREP for cutoffs

h. - k. TBD

A-9 Model SP-B with more realistic cutoffs (model SP-C)

APPENDIX B : SAPRE - THE ORBIT GENERATOR

B.1 PURPOSE.

Program SAPRE is an orbit gnerator. Trajectory osculatory orbital elements are computed using either a numerical Runge-Kutta integration method or a KOZAI parameter update analytical method.

The numerical orbit generator which can be used for low altitude orbits, geostationary orbits and highly eccentric orbits, takes Earth oblateness, Sun and Moon gravitational attraction, air drag (CIRA atmospheric model) and solar radiation into account.

The KOZAI analytical orbit generator is used for low altitude orbits only. In addition to air drag and solar radiation pressure it takes into account the same perturbations as Runge Kutta method.

The eccentric anomaly is the independent variable. Osculatory elements are computed at constant equidistant eccentric anomaly steps. SAPRE produces output (orbital positions with time) together with an interface file used by program SHELLG.

B.2 INPUTS.

SAPRE takes input from the two namelist sections $TEXT (common to all program) and $SAPRE in the UNIRNML file.

We give below the description of the relevant $SAPRE namelist parameters. They can also be found in the ESABASE Reference Manual.

Parameter	Explanation and default value
OEYEAR	Orbit epoch year (year - 1900) - default value : 0
OEMONTH	Orbit epoch month - default value : 0
OEDAY	Orbit epoch day - default value : 0
OEHOURS	Orbit epoch hours - default value : 0
OEMIN	Orbit epoch minutes - default value : 0
OESEC	Orbit epoch secondes - default value : 0

Parameter	Explanation and default value
ORBTYP	Orbit type (character*3) - 'GEO' for a geostationary orbit, 'HEL' for an heliosynchronous orbit and 'GEN' for a general orbit - default value: 'GEN'.
IAE	Flag for the use of semi major axis/eccentricity instead of perigee/apogee - (0: we input perigee/apogee, 1: we input semi major axis/eccentricity) - default value: 0
IG50	Flag for the choice of the coordinates system - (0: Greenwich, 1: Gamma 50) - default value: 1
HPER	Altitude of perigee of orbit (in km above the mean Earth's surface - Earth radius = 6378.144 km) - default value : 0.
HAPO	Altitude of apogee of orbit (in km above the mean Earth's surface - Earth radius = 6378.144 km) - default value : 0.
INCL	Orbital inclination (in decimal degrees) - default value : 1.D-2
ARGPER	Argument of perigee (in decimal degrees) - default value : 0.
RAAN	Righ ascension for the ascending node (in decimal degrees) - default value : 0.
SOLTIM	Local solar time (in hours) - only used for heliosynchronous orbit - default value: 0.
TRANO	True anomaly (in decimal degrees) - default value: 0.
OELONG	East longitude (in decimal degrees) - only used for geostationary orbit - default value: 0.
ORBITS	number of orbits to be generated - default value: 1
STEP	Eccentric anomaly step (in decimal degrees) - for Runge-Kutta generator only - default value: 2.
DT1	Time step for output (in seconds) - used if altitude is less than DH2 km - default value: 240. seconds
PRINT	Flag for writing the ephemerides to a report file - 0 : printing of each ephemerides step and no orbital element, 1: printing each 60^{th} step (beginning with the first one) with orbital elements) - default value: 1

B.3 OUTPUTS.

The output from SAPRE consists of two files : an interface file and a report file.

The interface file contains the orbital trajectory data to be used by BLXTRA (or other programs within ESABASE). The file is divided into orbital arcs, and each orbital arc is subvided into one or more orbital points. Each orbital point consists on ten values which are :

- the date/time in modified Julian days,
- the longitude (in degrees),
- the latitude (in degrees),
- the altitude (in degrees),
- the satellite coordinates in the geocentric inertial reference frame (in km).

The report file is a printable file containing the input data, the orbit parameters and, if requested, the summary tables.

Parameter	Explanation and default value
ORBNUM	Number of orbits - default value: 1
EPDUR	Duration of the trajectory calculation (in days) - if 0 or omitted, the program will look for a value for ORBITS - default value: 0.
WIBAIR	Air drag parameter (only used for orbit altitude smaller than 700 km) - default value: 0.
WIBSPR	Solar radiation pressure parameter - for Runge-Kutta generator only - default value: 0.
SUN	Flag to include gravitational perturbations from Sun - for Runge-Kutta generator only - default value: 0
MOON	Flag to include gravitational perturbations from Moon - for Runge-Kutta generator only - default value: 0
KZONAL	Integer number of zonal harmonic gravity coefficients (0 to 9) - for the Runge-Kutta generator only - if KZONAL and KTESS are less than or equal to 1, the oblatness of the Earth is ignored - default value : 6
KTESS	Integer number of tesseral harmonic gravity coefficients (0 to 4) - for the Runge-Kutta generator only. If KZONAL and KTESS are less than or equal to 1, the oblatness of the Earth is ignored - default value: 3
NCIRA	CIRA atmosphere density model number (0 to 11) - must be entered if WIBAIR is not 0 - default value: 5
TAPE	Selects whether an interface file is generated for SHELLG (0: do not generate interface file, 1: generate an interface file) - default value: 1
OGEN	Choice of the orbit generator (0: the program assumes that results are available from a previous run, 1 : the Runge-Kutta generator is used, 2 : if EPHMR is not 0, the KOZAI generator is used) - default value: 1

EPHMR	Selects the KOZAI generator (0: no ephemerides are output, 1: the world map coordinates and geocentric inertial ephemerides are sent to the report file, 2: ephemerides are calculated and printed) - default value: 2
IBUG	Used for debugging purpose only (0: do not generate extra output, 1: generate extra output) - default value: 0
RUN	Integer run number - default value: 1
PP(1)	Bow-shock parboloid constant - default value: 22.164
PP(2)	Bow-shock parboloid constant - default value: 15.
XP(1)	Bow-shock parboloid constant - default value: 15.25
XP(2)	Bow-shock parboloid constant - default value: 10.
DT2	Time step for output (in seconds) - used if altitude lies between DH2 km and DH3 km - default value: 10^7 seconds
DT3	Time step for output (in seconds) - used if altitude is larger than or equal to DH3 km - default value: 10^7 seconds
DH2	Select DT1 if height is less than DH2 (in km) - default value: 10^7 km
DH3	Select DT2 if height is less than DH3 (in km) - default value: 10^7 km
SEYEAR	Orbit start year - default value: -1.
SEMONT	Orbit start month - default value: -1
SEDAY	Orbit start day - default value: -1
SEHOUR	Orbit start hours - default value: -1
SEMIN	Orbit start minutes - default value: -1
SESEC	Orbit start seconds - default value: -1

APPENDIX C : BLXTRA - COORDINATE TRANSFORMATION

C.1 PURPOSE

The program BLXTRA converts positions given in longitude (degree), lattitude (degree) and height (km) into B-L coordinates system using an internal geomagnetic field model and optionally an external field model. B denotes the magnitude of the geomagnetic field at a given point (in Gauss) and L is the McIllwain's shell parameter (dimensionless).

The most useful internal geomagnetic field models are the IGRF'80 and '85 models (International Geophysical Reference Field) corresponding respectively to MODEL=11 and 13; the Jensen and Cain for epoch 1960 which was used to built the NASA trapped radiation models, corresponds to model=5. The most recent external field model is the Tsyganenko'89 one (OUTER=4).

For each set of coordinates generated by SAPRE, BLXTRA reads the $SAPRE namelist section to obtain orbit start time, apogee, perigee and inclination.

If desired, an orbit parameter plotting facility (program ORBPLOT) produces a plot of altitude, latitude, longitude, magnetic field magnitude B and magnetic shell parameter L versus local time. Program ORBPLOT reads the SHELLG interface file. A print file can also be produced.

The origin of the new name BLXTRA comes from : BL coordinates computed with an eXternal magnetic field.

C.2 INPUTS

Some of the input parameters are given in the namelist sections $TEXT (title), $SHELL (selection of geomagnetic model, maximum orbital time, print options, Kp range,etc...), the geocentric coordinates are taken from the interface output by SAPRE (start time, longitude, latitude, altitude).

The description of the $SHELL namelist parameters is given below.

Parameter	Explanation and default value
MODEL	Geomagnetic field model number (among others; 5: IGRF75, 9: IGRF80, 11: Barraclough'75) - default value : 11
MMOFLG	Flag for the choice of the geomagnetic dipole moment (0: the standard value .311653 is used, 1: it is computed with the first 3 sets of terms of the field model) - default value: 1
BLTIME	Time (in decimal years) to which the field coefficients are to be updated (1900 ≤ BLTIME ≤ 2000) - default value: 1970 - Warning: the use of BLTIME larger than 1970 is not recommended due to the secular variations of B.
OUTER	Flag for the choice of the external magnetic field model (1: Mead-Fairfield, 2: Tsyganeneko-87 short version, 3: Tsyganenko-87 long version, 4: Tsyganenko-89) - default value: 4
VALUE_KP	Value of the geomagnetic activity index K_p (range [0, 9]) - default value: 2
CUTOFF	Maximum orbit time (in hours) for which B and L conversion has to be performed. Orbit time is defined 0.0 hours with the start of each trajectory - default value : 9999. hours
PRINTC	Flag for printing (0: every line, > 0: every 60^{th} beginning with the first one) - default value: 1
IPLOT	Flag for the activation of the orbit parameter plotting facility (0: no activation, 1: activation) - default value : 1
DEBUG	Debug output control parameter (0: no additional printout, > 0: some additional printout are produced) - default value: 0

C.3 OUTPUTS

The output of BLXTRA are

B the magnetic field intensity (in Gauss) at given position

L the McIllwain's parameter corresponding to the magnetic shell passing at this given position

These outputs and the geocentric coordinates are stored in a report file SHELLOUTP.DAT as well as in an interface file SHELLOUTI.DAT which is used later on by the program TREP.

APPENDIX D : TREP - TERRESTRIAL RADIATION ENVIRONMENT PROGRAM

D.1 PURPOSE

The program TREP calculates orbital radiation environment fluxes for arbitrary spacecraft orbit trajectory. It uses the detail of the trajectory in B-L coordinates for accessing particles fluxes. It computes solar proton event probabilities and fluences. Fluxes as a function of time and trajectory average spectra together with solar flare fluence spectra, tacking into account geomegnetic shielding.

D.2 METHOD

The program TREP accesses the standard NSSDC model of the trapped proton environments at each orbital point contained in the input file. Each orbital location is defined in terms of geomagnetic B-L coordinates (generated by BLXTRA) because flux models are organised according to B-L-E coordinates. Fluence spectra are accumulated and orbit-average flux spectra are produced. King's model or Feynman et al's model is used to generate solar flare proton spectra, depending of the flight time and user-defined probability not to be exceeded. The number of flares can be input by the user.

The user can specify a more exact energy dependent treatment of geomagnetic shielding which includes consideration on the arrival direction of a proton.

Local time variation of outer radiation zone electron environment is also considered, based on the old AE4 local time models for epoch 1964 (solar min) and 1967 (solar max). The standard deviation of the fluxes can also be obtained as an output.

The NSSDC electron (proton) environment models are AE8MAX/MIN (AP8MAX/MIN).

D.3 INPUTS

The input parameters are given in the *TEXT and $TREP namelist sections of UNIRNML.DAT file. The description of the $TREP namelist parameters is given below.

Parameter	Explanation and default value
TREMOD	Flag for the choice of the trapped radiation electron model (1: AE8, 2: AE17-HI, 3: TREM-G - default value: 1
SOLACT	Solar activity 'MAX' or 'MIN' - default value : 'MAX'
PERIOD	Orbit period (in hours). If PERIOD=0 or absent, PERIOD is computed from IAPG and IPRG - default value : 0.
ELEEN (30)	Electron spectral energies required (in MeV) - default values: .04, .1, .2, .3, .4, .5, .6, .7, .8, 1., 1.25, 1.5, 1.75, 2., 2.25, 2.5, 2.75, 3., 3.25, 3.5, 3.75, 4., 4.25, 4.5, 4.75, 5., 5.5, 6., 6.5, 7.
PROEN (30)	Proton spectral energies required (in MeV) - default values: .1, .5, 1., 2., 3., 4., 5., 6., 8., 10., 12., 15., 17., 20., 25., 30., 35., 40., 45., 50., 60., 70., 80., 90., 100., 125., 150., 175., 200., 300.
ENERFL (30)	Solar flare proton spectral energies required (in MeV) - default values: from 10. MeV to 300. MeV, step 10 MeV.

ETHP(2)	Proton energy thresholds for time prints and plots (in MeV) - default values: 1. MeV, 10. MeV
ETHE(2)	Electron energy thresholds for time prints and plots (in MeV) - default values: 0.1 MeV, 1. MeV
FLUXTH	Threshold flux for flux-free time table (in $cm^{-2}.sec^{-1}$) - default value: 1.
ILTV	Local time variation flag (0: local time variations are included on the electron model, > 1: trapped and solar flare protons are not considered) - default value: 0
ISIG	Statistical model flag. (Electron fluxes are modified according to an extension of the AE4 statistical model of Singley and Vette). ISIG takes values -2, -1, 0, 1, 2 corresponding to the number of standard deviations to be applied to the log fluxes - default value: 0
FLAMOD	Flare model (1: King's model, 2: Feynman's model) - default value: 2
TFLARE	Mission duration (in years) - default value: 1.
FLPROB	Probability that protons fluence will be exceeded (in percentage) - default value: 90 %
NAL	Number of anomalously large solar flares (King's model of the August 1972 event) to be included. It allows the user to manually define the number of occuring flares - only used with King's model - default value: 0
NOR	Number of ordinary solar flares (according to King's ordinary flare model) to be included. It allows the user to manually define the number of occuring flares. If NOR is input as, or predicted to be 1, and if the probability level is larger than or equal to 90 %,then a worst-case ordinary flare spectrum is produced - only used in King's model - default value: 0
IFLATT	Flare particle attenuation flag. If IFLATT=0 or omitted, the Stassinopoulos-King model of flare attenuation through geomagnetic shielding is used (perfect shielding at L <5 Re, none at L $>$ 5 Re). If IFLATT$>$0, a model considering proton arrival from non-vertical directions troughout the L range is used. Although more rigorous, the differences are not normally large after orbit-averaging - apply to both King and Feynman's model - default value: 0
KPRINT	Print flag. Print every KPRINT points on time print - default value: 60
IPLOT	Produce plot if positive - default value: 1
INTERF	Produce interface file if positive - default value: 1
IBUG	Produce extra debug output if positive - default value: 0

Since the default values are normally the most appropriate values, only a minimum number of these parameters are required from the user. Addiotinal inputs for TREP are stored in the interface file SHELLOUT.DAT. It contains the B-L coordinates of points along the trajectory of a spacecraft.

D.4 OUTPUTS

The outputs of TREP (integral flux, differential fluxes of electrons and protons, fluences) are reported in the file TREPOUTP.DAT, as well as in the interface file TREPOUTI.DAT, for use downstream by the SHIELDOSE program.

APPENDIX E : THE TSYGANENKO MAGNETIC FIELD MODELS

One of the most recent series of magnetic field model taking into account the Ring Current, the magnetopause currents, and the plasmasheet currents is the model of Tsyganenko and Usmanov (1982) often called the TU model followed by two more recent versions by Tsyganenko (1987,1989).

There are elaborate analytical models for the outer magnetospheric region based an a large amount of IMP and HEOS magnetic field measurements (12,616 and 6,000 B-field averages from IMP and HEOS, respectively). The updated and improved versions published by Tsyganenko (1987, 1989), are based on an even wider set of satellite data distributed more evenly in all magnetospheric regions. This new data includes 12,616 points on which the Mead-Fairfield (1975) model was based (IMP observations from 1966 to 1972) for R~4-17 R_E; 6,248 points from HEOS-1 and 2 (1969-1972 for R~6-35 R_E); 11,150 points from data of IMP-A, C, E, F, G and I (1964 - 1973) for x_{GSM}~-66 to -15 R_E; 6,675 points derived from IMP-H and J (1973-1980 for R~2-45 R_E).

The 1989 model version for the B-field contains 26 input parameters by means of an iterative minimization method to fit the model parameters to the experimental data corresponding to different levels of geomagnetic activity. In some respects it resembles the Mead and Fairfield (1975) model which was however less elaborated and suffered of two major shortcomings : (i) the IMP data set used in this later model do not cover the high-latitude distant magnetosphere; (ii) the electric current distributions ($j = \text{rot } B/\mu_o$) deduced from this simple analytical model have only a faint resemblance with those deduced from experimental observations. The Tsyganenko (1987) model does

not have these shortcomings and is considered to be a valid approximation up to distances of 70 R_E in the tail. A 'truncated' model has also been proposed with 20 parameters and applicability limit of 30 R_E. The latest version (1987) of Tsyganenko model is a somewhat different approach to the modeling of the intra magnetospheric current system has been developed which takes into account plasmasheet current sheet wrapping as well as spatial current variations of the current sheet thickness along the Sun-Earth and dawn-dusk durations. A comparison of the (1987) and (1989) versions shows that significant improvement is obtained with the latter model in the distant nightside magnetosphere. The main result is that a significantly more depressed field is obtained in the near magnetotail region for all K_p intervals, the most dramatic changes being observed for the highest level of disturbance. We will outline below the main equations on which the (1987) model of Tsyganenko are based on. We refer the reader to the recent paper by Tsyganenko (1989) for a more detailed account of his latest magnetic field model.

E1. Ring Current Magnetic Field Component

Assuming the ring current has axial symmetry, cylindrical geomagnetic coordinate system (ρ,φ,ζ) are used with the z-axis antiparallel to the Earth's magnetic moment vector. The following distribution of the magnetic vector potential $\mathbf{A}=(0,A_\varphi,0)$:

$$\mathbf{A}\varphi = C\rho \left(\rho^2 + \zeta^2 + 4 \right)^{-3/2} \qquad (E.1)$$

is introduced.

The only difference between (1) and the corresponding expression for the purely dipolar vector potential is an additional term 4 in the brackets, which eliminates the singularity at the origin of coordinates. At large

distances, i.e. for $\rho>>1$ and/or $\zeta>>1$ the vector potential (D.1) corresponds to a dipolar source, whereas at $r=R_E(\rho^2+\zeta^2)^{\frac{1}{2}}<2$ we have a continuous axisymmetric ring-lie current distribution with a characteristic radius of the order of 0.8.

From (D.1) we obtain the magnetic field components

$$B\rho = B_{RC} \frac{12\rho z}{(\rho^2 + \zeta^2 + 4)^{5/2}} \qquad (E.2a)$$

and

$$B\zeta = 4B_{RC} \frac{2\zeta^2 - \rho^2 + 8}{(\rho^2 + \zeta^2 + 4)^{5/2}} \qquad (E.2b)$$

The constant C in eq.(E.1) is determined in terms of the magnitude of the field depression BRC near the Earth and the coordinates are measured in units of RRC :

$$\rho = (x^2_{SM} + y^2_{SM})^{\frac{1}{2}} / R_{RC} \text{ and } \zeta = z_{SM}/R_{RC} \qquad (E.3)$$

The proposed analytical representation of the ring current contribution contains only two parameters RRC and BRC and combines mathematical simplicity with its capability to model the main observed features.

Given a point (x_{GSM}, y_{GSM}, z_{GSM}) in the magnetospheric system GSM the following calculations derive the components of the Ring Current field in the SM coordinate system:

(i) starting from xGSM, yGSM, zGSM and the geodipole tilt, ψ, find the solar magnetic coordinates (z axis along dipole, xz plane contains the Sun's direction)

$$x_{SM} = x_{GSM} \cos \psi - z_{GSM} \sin \psi$$

$$y_{SM} = y_{GSM} \qquad \text{(E.4)}$$

$$z_{SM} = x_{GSM} \sin \psi + z_{GSM} \cos \psi$$

(ii) from (E.3)-(E.4) find B_ρ and B_ζ

(iii) calculated Cartesian solar-magnetic component of $B^{(1)}$

$$B_{xSM} = B_\rho x_{SM}/(\rho R_{RC}),$$

$$B_{ySM} = B_\rho y_{SM}/\rho R_{RC},$$

$$B_{zSM} = B\zeta \qquad \text{(E.5)}$$

(iv) make the final transformation to the GSM system :

$$B^{(1)}x_{GSM} = B_{xSM} \cos \psi - B_{zSM} \sin \psi$$

$$B^{(1)}y_{GSM} = B_{ySM}$$

$$B^{(1)}z_{GSM} = B_{xSM} \sin \psi + B_{zSM} \cos \psi$$

E2. Magnetic field component produced by magnetotail currents

The plasmasheet currents are assumed to be spread over

a layer of half-thickness D in the oz direction, and between $x=x_N$ (inner edge of the plasmasheet) and $x=x_F$ (outer edge of the current slab). A linear current density distribution in the oy direction is assumed to flow between x_N and x_F+x_N in the 1984 model version.

However, in the 1987 paper Tsyganenko uses $x_F=\infty$ and a non-linear variation of the current density I(x) along the tail.

$$I(x) = \frac{c}{2\pi} B_T(x) \qquad (E.6)$$

where the following simple (integrable) function has been assumed for $B_T(x)$

$$B_T(x) = B_o + \frac{B_1}{x - x_1} + \frac{B_2}{(x - x_1)^2} \qquad (E.7)$$

where B_o, B_1 and B_2 are three linear parameters and x1 and x^2 are two non-linear ones. Assuming an infinite extension of the current sheet in the direction $y\to\pm\infty$ and $x\to-\infty$, one gets

$$Bx^{(2)}(x,z) = -\frac{z}{\pi}\int_{-\$}^{xN} B_T(x_o)\,\frac{dx_o}{(x_o - x)^2 + z^2 + D^2} \qquad (E.8)$$

$$Bz^{(2)}(x,z) = \frac{1}{\pi}\int_{-\$}^{xN} B_T(x_o)\,\frac{(x_o - x)\,dx_o}{(x_o - x)^2 + z^2 + D^2} \qquad (E.9)$$

where x_N defines the location of the inner edge of the current sheet.

A return current is introduced in the 1987 model version. The return current system is simulated by a pair of additional current sheets parallel to the central one and located at $z_{GSM}=\pm R_T$ above and below the equatorial plane, where $R_T=30\ R_E$ is taken of the order of asymptotic tail radius. Each sheet carries an eastward current with density $-\frac{1}{2}I(x)$, i.e. minus half of that in the main current sheet.

In order to restrict the current sheet width in the dawn-dusk direction both field components (E.8) and (E.9) are multiplied by an even function f(y) which falls off to zero by $y\to\pm\infty$ with a scale length $\Delta y\sim 15\ R_E$. This bends current flow lines near the inner edge of the sheet, so that a smooth continuous transition occurs in the current flow line distribution from the ring current to the plasma sheet. In the magnetotail cross-section one obtains two closed current loops, which form the well-known theta shaped structure encircling the tail lobes.

A shift in z of the whole central current sheet by $z_S=R_H \sin\psi$ has been introduced to take into account the effects of the geodipole tilt.

As a result, the field component $B_x^{(2)}(x,y,z)$ are given by the following calculations (this tail current model does not contribute to the By component of the total field). Tsyganenko introduces :

$$\varsigma_1 = x_1 - x, \quad \varsigma_2 = x_2 - x, \quad \varsigma_N = x_N - x$$

$$z_r = z - R_H \sin\psi, \quad z_+ = z - R_T, \quad z_- = z + R_T$$

$$\beta(z_r) = (z^2_r + D^2)^{\frac{1}{2}}, \quad \beta_+ = (z_{+2} + D^2)^{\frac{1}{2}},$$

$$\beta_- = (z_{-2} + D^2)^{\frac{1}{2}}$$

$$\gamma_1(b) = \xi_1^2 + \beta^2, \quad \gamma_{1\pm} = \gamma_1(\beta_\pm)$$

$$\gamma_2(b) = \xi_2^2 + \beta^2, \quad \gamma_{2\pm} = \gamma_2(\beta_\pm)$$

$$P_1(\gamma_1, \beta) = \frac{1}{2\gamma_1} \ln \frac{(x_N - x_1)^2}{\xi_N^2 + \beta^2},$$

$$P_2(\gamma_2, \beta_2) = \frac{1}{\gamma_2^2} \ln \frac{(x_N - x_2)^2}{\xi_N^2 + \beta^2}$$

$$P_{1\pm} = P_1(\gamma_{1\pm}, \beta_\pm), \quad P_{2\pm} = P_2(\gamma_{2\pm}, \beta_\pm), \qquad (E.10)$$

Then he finds 1

$$S_o = \beta^{-1}[\pi/2 + \arctan[(\xi_N/\beta)]$$

$$S_1 = P_1 - (\xi_1/\gamma_1)S_o$$

$$S_2 = -\xi_2 P_2 - \frac{1}{(x_N - 2x_2)\gamma_2} + \frac{\xi_2^2 - \beta^2}{\gamma_2^2} S_o$$

$$G_o = \frac{1}{2} \ln \frac{\xi_N^2 + \beta^2}{[(\xi_N^2 + \beta_+^2)(\xi_N^2 + \beta_{-2})]^{\frac{1}{2}}}$$

$$G_1 = \frac{\beta^2}{\gamma_1} S_o + \xi_1 P_1$$

$$G_2 = \frac{\beta^2 - \xi_2^2}{2} P_2 - \frac{2\beta^2\xi_2}{\gamma_2^2} S_o - \frac{\xi_2}{(x_N - x_2)\gamma_2} \qquad (E.11)$$

He also derives quantities $S_{o\pm}$, $S_{1\pm}$, $S_{2\pm}$, $G_{1\pm}$, $G_{2\pm}$, given by (E.11) with substitutions $\beta \to \beta_\pm$, $\gamma_{1,2} \to \gamma_{1,2\pm}$, $P_{1,2} \to P_{1,2\pm}$, $S_o \to S_{o\pm}$. After that he writes down final expressions for the model magnetotail field components

$$Bx^{(2)}(x,y,z) = f(y)\{B_o\,[z,\ S_o - \tfrac{1}{2}(z_+ S_{o+} + z_- S_{o-})] + B_1(z_r\ S_1 - \tfrac{1}{2}(z_+ S_{1+} + z_-\ S_{1-})] + B_2[z_r\ S_2 - \tfrac{1}{2}(z_+\ S_{2+} + z_-\ S_{2-})]\}$$

$$B_y^{(2)} = 0$$

$$B_z^{(2)}(x,y,z) = f(y)\{B_o G_o + B_1\,[G_1 - \tfrac{1}{2}(G_{1+} + G_{1-})] + B_2[G_2 - \tfrac{1}{2}(G_{2+} + G_{2-})]\} \qquad (E.12)$$

where

$$f(y) = \frac{1}{\pi}\,[1 + (y/\Delta y)^2]^{-1} \qquad (E.13)$$

E.3. Magnetopause current and the average magnetic effect of field-aligned currents

Magnetic field from the magnetopause currents has the largest spatial variation scale in comparison with the other sources. This facilitates the choice of fitting functions. In particular, the same power series expansions, as those in the Mead-Fairfield model, can be applied. However, it is impossible to obtain in this case an accurate representation of the observed field distribution at distances beyond x≈10RE due to non-monotonic behaviour of polynomials. For this reason, Tsyganenko and Usmanov (1982) have chosen a polynomials approximation in terms of y, z and $\exp(x/\Delta x)$. The exponential factor of x provides a satisfactory fit to the data both in the dayside magnetosphere and at large distances in the tail region. The Tsyganenko (1987) expansion of the "long version models" can be found in Tsyganenko (1987). We will only reproduce here the "truncated version models" which is quite sufficient for modelling the magnetic field up to geostationary orbit.

The "truncated" models were developed, based on experimental data points with $x_{SM} \geq -25 R_E$. The significantly shorter range of distances allow the following simplifications : (i) the third term in (E.7) is deleted in putting B2=0 and thus eliminating all the terms with the subscript 2 in final expressions (E.10) - (E.12), and for the magnetopause current the following expression are retained :

$$B^{(3)}_x = e^{x/\Delta\omega}[a_1 z \cos\psi + (a_2 + a_3 y^2 + a_4 x z^2) \sin\psi$$

$$B^{(3)}_y = e^{x/\Delta\omega}[b_1 y z \cos\psi + b_2 y + b_3 y^3 + b_4 y z^2]\sin\psi]$$

$$B^{(3)}_z = e^{x/\Delta\omega}[(c_1 + c_2 y^2 + c_3 z^2)\cos\psi + (c_4 z + c_5 z y^2 + c_6 z^3) \sin\psi] \qquad (E.14)$$

The dependence on the Earth's dipole tilt angle, ψ, is included in (E.12) by terms containing sin ψ .
The representation (E.12) contains 20 free parameters given in Table (E.1). Table (E.2) gives similar model coefficients for the Tsyganenko 1989 model version.

Like in the Mead and Fairfield (1975) approach, the coefficient an has not imposed the condition rot B=0 and hence, the expansions (E.14) can in principle account for the magnetic effects from other magnetospheric currents, which for some reasons have not been taken into account for properly in (E.2) and (E.12);in particular, this holds for the field-aligned currents.

E.4. Determination of the free parameters in the Tsyganenko Model

The total magnetic field produced by extraterrestrial sources is obtained by the sum of (E.2), (E.12) and (E.14). A model is defined completely by setting numerical values to the input parameters.

Derivation of independent parameters was carried out by means of an iterative scheme; at each step all the linear coefficients using a least squares procedure are computed and then finding the non-linear parameters by a version of the consecutive descent method, minimizing the r.m.s. deviation of the model field using the experimental data set. Bining the initial data sets, corresponding to different levels of ground geomagnetic activity levels have been carried out in such a way that, on the one hand, a sufficiently detailed resolution in Kp has been achieved. On the other, the number of experimental points in each set is large enough, ensuring that sufficient reliability results.

Results of fitting the "truncated" model parameters to the data sets are listed in Table (E.1); each column corresponds to one of the above K_p values or intervals. The following quantities are given in the columns (from the top): the value of K_p-index, the number of points in the data set (N), the r.m.s. deviation of the model field from the data.

Figures (E.1) and (E.2) show the field line configurations in the "truncated" version of the model, for $K_p=1^-$, 1 and $K_p\geq 5^-$. The main effects of increased disturbance, easily seen in the average model field structure, are the equatorward displacement of dayside polar cusps from latitude $\approx 79°$ up to $73°$ and some stretching of the near-tail field lines.

E.5. Advantages and Limitation of the Tsyganenko Model

The advantages of this elaborate model is that the magnetic field distortions produced by external (magnetosphere) currents simulate fairly well the observations in the outer magnetosphere. Therefore, it is

expected to be a useful B-field model for geosynchronous orbit. The model is analytic and therefore gradients rot B, I and L can easily be computed. Another advantage is that the model is K_p dependent and is a function of the tilt angle ψ of the Earth's dipole.

On the other hand, the large number of free parameters involved can be a disadvantage for the end user who needs a simple model to compute Iand L, or a generalized L* parameter from this model. Too many free parameters are often more confusing than clarifying when data processing has eventually to be achieved.

However, assuming that the set of parameters given in Table (E.1) for different values of K_p are reliable and that they will be confirmed by other independent statistical analysis, in the future, the Tsyganenko (1987 or 1989) models as they stand, could constitute useful packages to map the intensity of trapped radiation near geosynchronous orbit.

A verification (and a possible updating) of this model using independent and additional field observations near geosynchronous orbit would be a useful task to comfort its usefulness and to make it a standard model for future studies of the outer magnetosphere.

K_p	0.0°	1°, 1	1°, 2°	2, 2°	3°, 3, 3°	4°, 4, 4°	≥5°	≥5°
N	2556	3948	4000	3728	4275	1905	862	378
$\langle B_z \rangle$	17.41	21.26	24.46	25.97	30.88	36.03	42.62	44.31
σ	7.63	9.95	11.36	12.17	14.37	15.72	20.18	22.69
a_1	1.126	1.403	1.589	1.699	2.141	2.252	2.773	2.919
a_2	26.66	29.24	31.07	36.28	41.51	39.35	40.95	34.96
a_3	−0.077	−0.0693	−0.06527	−0.07514	−0.1518	−0.04525	0.00667	0.0*
a_4	−0.06102	−0.0864	−0.07447	−0.1448	−0.1857	−0.2062	−0.133	0.0*
b_1	−0.06197	−0.07202	−0.07632	−0.05049	−0.1015	−0.1491	−0.1304	−0.1609
b_2	−2.048	−2.068	−2.413	−2.209	−2.929	−3.059	−5.187	−5.077
b_3	0.00327	0.00286	0.002719	0.000919	0.004584	−0.000183	0.004623	0.0*
b_4	0.008473	0.007438	0.01098	0.0.084	0.01589	0.02614	0.03651	0.0*
c_1	12.72	16.37	16.20	17.38	18.29	15.48	20.0	22.1
c_2	−0.00867	−0.02705	−0.02355	−0.03516	−0.02514	−0.02144	−0.03765	−0.05915
c_3	−0.001953	−0.0281	−0.03475	−0.03886	−0.05927	−0.06608	−0.09066	−0.1051
c_4	−0.3437	−0.6040	−0.4377	−1.169	−1.336	−1.855	0.5838	0.6321
c_5	−0.002903	−0.002256	−0.002169	0.004239	0.00185	0.006199	−0.01462	0.0*
c_6	−0.000999	0.000152	−0.001383	0.000881	0.001066	−0.00013	−0.007189	0.0*
B_0	18.41	20.20	18.70	21.79	21.31	23.91	24.87	28.11
B_1	−270.3	−140.1	−292.6	−162.0	−358.8	−161.0	−186.07	−330.1
B_{RC}	−25.94	−29.65	−35.25	−41.87	−47.91	−51.48	−74.81	−86.82
R_{RC}	5.21	5.62	5.29	5.15	5.13	4.61	4.57	4.00
N_N	−6.20	−5.52	−5.18	−3.62	−3.74	−3.32	−4.03	−3.00*
D	2.29	2.02	2.21	2.35	2.07	1.68	1.70	1.73*
Δy	11.96	14.66	14.03	17.26	17.23	15.22	12.15	12.56
K_{11}	8.315	8.06	7.66	7.61	6.33	6.68	6.87	5.11
Δx	44.22	27.76	17.56	17.99	32.51	0.6765	−1.746	4.0*
	11.15	10.94	10.90	10.74	9.73	8.007	8.9	7.866

Table D.1 Input parameters for the TU-87 model for different geomagnetic activity levels (after Tsyganenko, 1987).

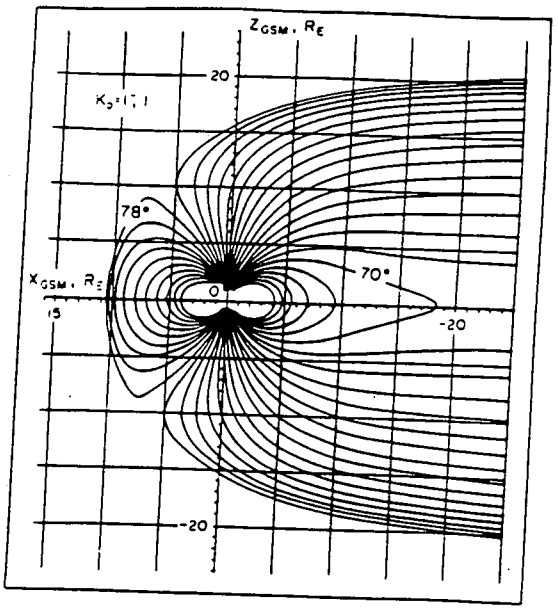

Fig. D.1 Field line pattern in the "truncated" version of TU-87 model, for quiet conditions with $K_p = 1^-$, 1 (after Tsyganenko, 1987)

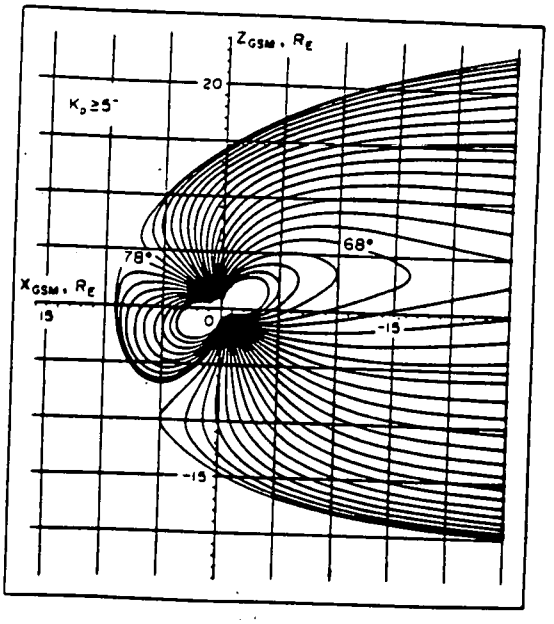

Fig. D.2 Field line pattern in the "truncated" version of TU-87 model, for strongly distrubed conditions with $K_p \geq 5^-$ (after Tsyganenko, 1987).

APPENDIX F : THE FEYNMAN ET AL. MODEL

F.1. Data Base

Data on proton fluences used in this study come from two major sources : observations using riometers, rockets and balloons from 1956 to 1963 and observations taken in space since 1963. The first data set is that used by Yuker (1970) and consists of the events between 1956 and 1962. The validity of this data set has been reviewed by Aarons and Silverman (1962), Malitson and Webber (1962), Fichtel et al. (1962). Following these authors, the fluences reported in this data set are accurate within a factor of two. Furthermore, Fichtel et al. (1962) claim that the accuracy obtained is frequently much better.

Since 1963 instruments have been observing proton fluxes in space. All of the feasible data from satellite observations have been collected and edited for valid solar particle responses (Armstrong et al. , 1983). A nearly time continuous record of daily average fluxes of particles above the thresholds of 10, 30 and 60 Mev has been constructed. The details of the production of this data set are described in Armstrong et al. (1983). These data form the second of the two sets used.

A complete list of all the events used in the data base of the Feynman et al. model can be found in Feynman et al. (1988a). Because solar flares producing protons occur in groups with several flares occurring over a period of days in the same active center (Malitson and Webber, 1962), these grouped events can not be assumed to be occurring independently from one another. Consequently, the distribution of fluences in a data set that considers each of these flares to be a separate event cannot be expected to be a random sample of any underlying parent population.

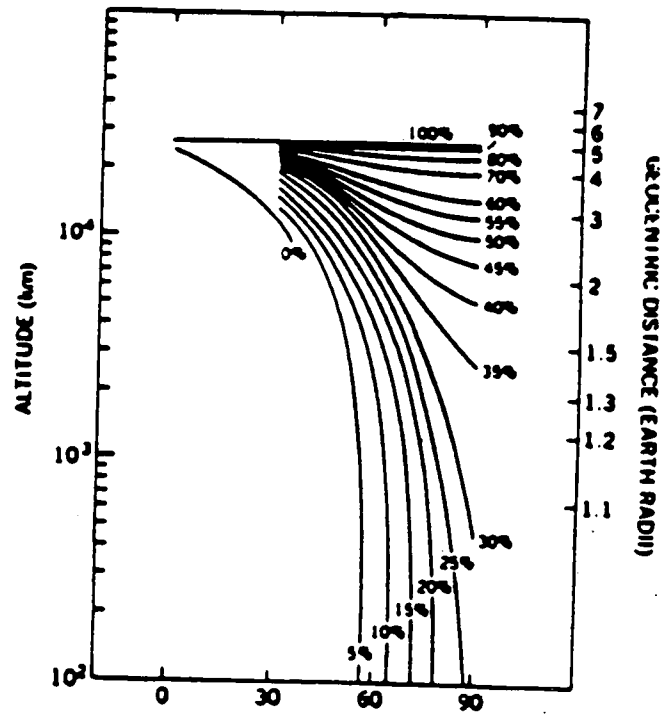

Fig. F.1. : Percentage of interplanetary fluence intercepted by spacecraft in circular geocentric orbits as a function of orbital altitude and inclination (after King, 1974).

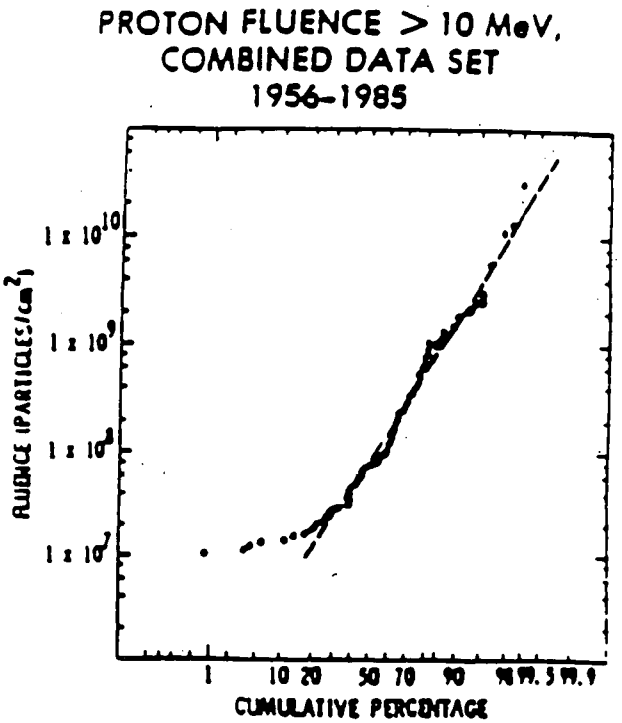

Fig. F.2. : Distribution of fluences for complete data set, 1956 - 1986 for proton energies > 10 MeV. The dashed line is to guide the eye in comparing the data to a straight line (after Feynman et al., 1988a).

Therefore, in the definition of "event fluence", an integration over each group of flares has been made for establishing the data base.

Using the event fluences of the data base, the distribution of fluences has been compared to a log normal distribution. The events were ordered according to the log of the magnitude and fluences were plotted against (i x 100)/(n - 1) where i is the rank value of the events ordered from smallest to largest and n is the total number of events used in the data set. The result for the data set with E> 10 Mev and fluence cut-off at 1 x 10^7 particles cm^{-2} is shown in figure F-2. The graph paper used to plot the results is ruled so that a log normal distribution will appear as a straight line. It can be seen that most of the data lie on a straight line.

However for the lowest fluences shown, the data turn up and the observed fluences become much larger than those expected from any straight line. There are at least 2 contributing effects. First, this turn up is expected whenever a data set is truncated (Yucker, 1972). Second, the log normal distribution is expected to under-estimate the number of events at very low fluences because the number of actual events on the sun increases as fluence decreases (Feynman et al., 1988b) whereas for a log normal distribution the number of events at fluences less than the median fluence decreases as fluence decreases. However, for a data set with a large enough range of fluences the contribution of the low fluence events to the total fluence occurring in time intervals long enough to be of interest to modern space missions is negligible. In this study care was taken to use data sets with a large enough fluence range so that this criterion was satisfied.

Figure F-3 shows the data for the E>30 Mev case. The low fluence cutoff was at 1 x 10^6 particles cm^{-2}. The error bars have been added to two of the pre-1963 events to show

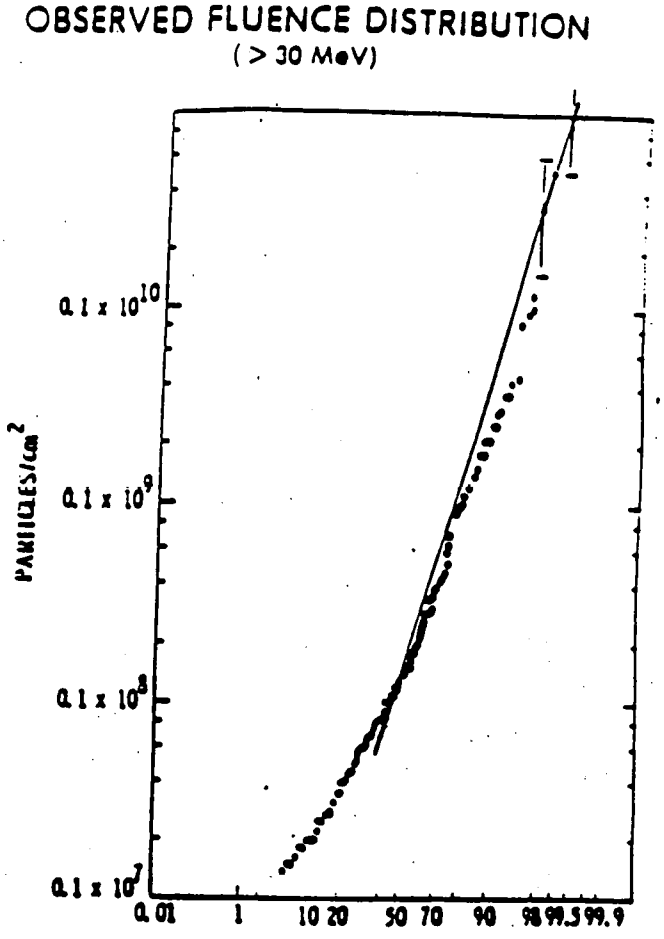

Fig. F.3. : The same as figure F.2 but for proton energies > 30 MeV (after Feynman et al., 1988a).

the effect of a factor of 2 uncertainty in the event fluence.

In figures F-2 and F-3, the distribution of fluences for events having fluences above the median fluences are well fit by a straight line. This is in constrast to King's results (King, 1974) where only the data from cycle 20 were considered. In the Feynman et al. model the 1972 event is not outstanding and in fact is not the event with highest fluence (Nelson, 1982). Instead it is the second highest fluence event.

F.2. Solar Cycle Variation

In the Feynman et al. model, the time of cycle maximum is defined accurately to 0.1 years instead of the usual 1 year accuracy. The "zero years" of the cycles were then defined as 365 day periods centered on the sunspot maximum correct to 0.1 years. The other "years" of the cycle were defined in a corresponding manner, i.e. "years" are not calendar years.

The results of this analysis for the 3 cycles are shown in figure F-4. Notice the clear difference between the 7 years of high fluence and the 4 years of low fluence in each cycle. With only two exceptions, the annual fluences exceeded 108 particles cm^{-2} during the 3 sets of 7 hazardous years cycle -1 and was less than that during the other 3 sets of 4 years cycle -1. This is true even if no major proton events occurred during a hazardous year of a particular cycle. Furthermore, note that the hazardous period is not centered on sunspot maximum but extends from 2 years before maximum to 4 years after maximum.

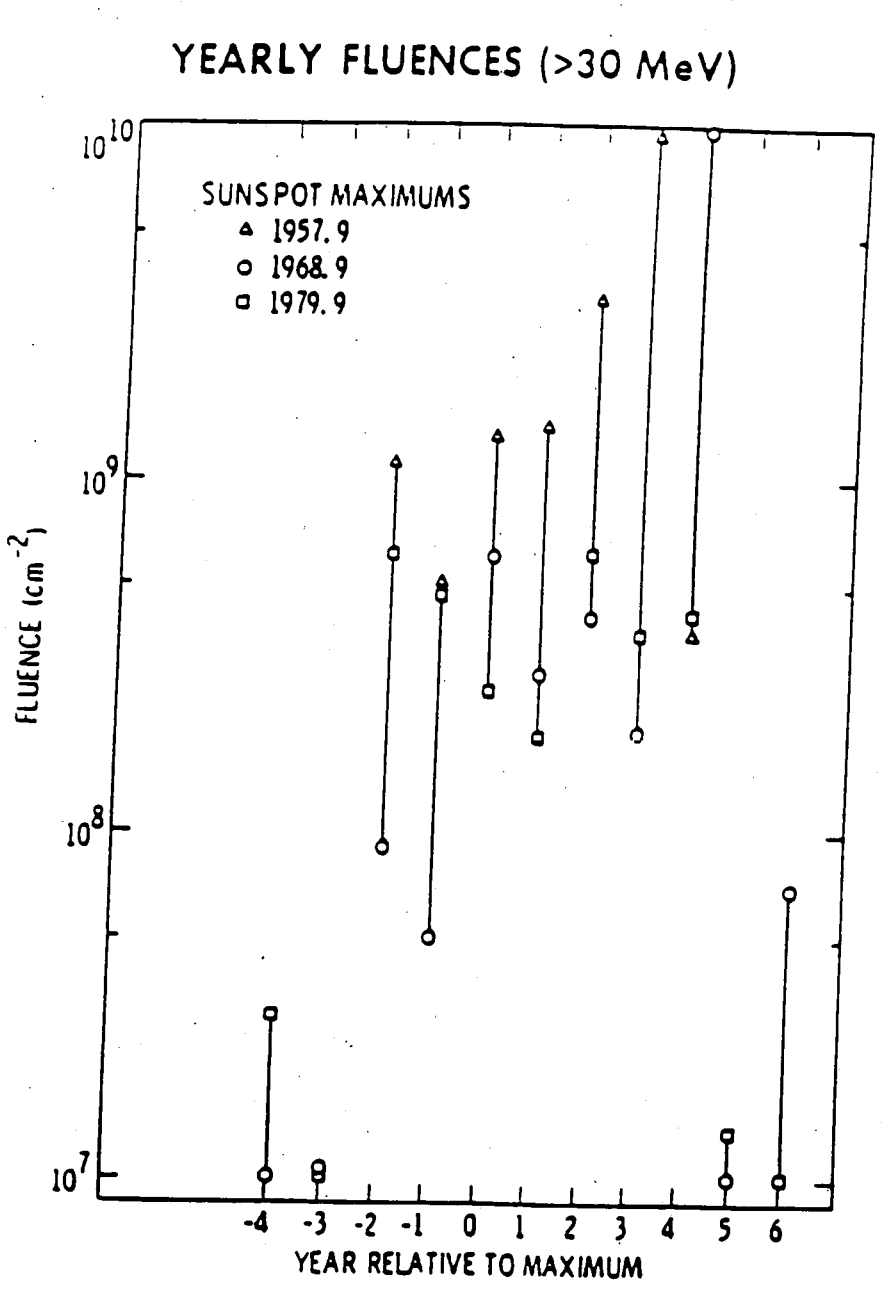

Fig. F.4. : Solar cycle dependence of annual fluences, 1956 - 1986. See text for definition of "years" (after Feynman et al., 1988a).

This clear result has important implications to space missions. In comparing the fluences to be expected during different missions it is very important to take into account the actual launch date, since this result predicts negligible fluences during the 4 minimum years of each cycle. Also notice that the dates of the last three cycle maxima occurred 11 years apart to the 0.1 year, so that with reasonable confidence, the time of the next maximum sould be about 1991.

F.3. Solar Cycle Corrected Proton Fluences

The fluence distribution has been constructed using data from only the 7 hazardous years in each cycle. The few small events that occurred during the 4 year quiet periods have been dropped from the data set.

The hazardous years fluence distribution for protons with E> 10 MeV is shown in Fig.F-5 and that for E > 30 MeV in Fig. F-6. Again there is a turn up of the points at low fluence due to truncation of the data set and the underestimation of the number of small fluence events.

The approach to the problem of the deviation of the data from a straight line is to note that it is only those events with large fluences that influence the total fluence during a year. It is therefore more important to fit the large fluence part of the distribution than the low fluence part. Feynman et al. (1988a) have shown that the straight line fits shown in Figures F-5 and F-6 do not depend crucially on the accuracy of the determination of the fluence from any one event.

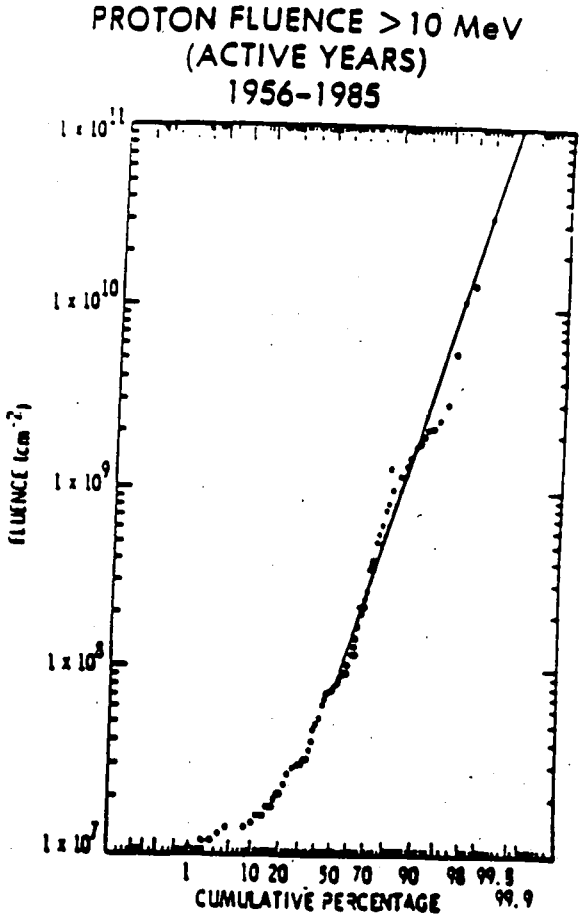

Fig. F.5. : Distribution of fluences for solar cycle active years for proton energies > 10 MeV (after Feynman et al., 1988a).

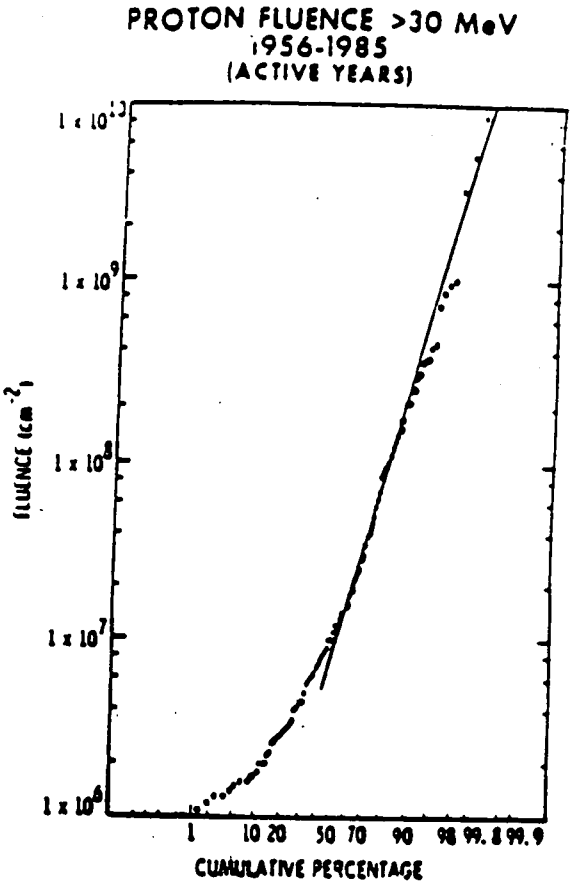

Fig. F.6. : Distribution of fluences for solar cycle active years for proton energies > 30 MeV (after Feynman et al., 1988a).

F.4. Statistical Analysis

Let F be the log-proton fluence. Since the proton fluence is distributed lognormally, then F is distributed normally and its density function is commonly expressed as

$$f(F) = \frac{1}{(2\pi)^{\frac{1}{2}}\sigma} \exp\left[-\frac{1}{2} \left(\frac{F - l}{\sigma}\right)^2 \right] \qquad \text{(F-1)}$$

where r is standard deviation, and l is the mean log fluence.

The probability that during a mission length s the fluence level will exceed fp (a proton fluence threshold) is

$$P(>F, s) = \sum_{n=1}^{\infty} p(n, ws)\ Q(F,n) \qquad \text{(F-2)}$$

where
p(n, ws) is the probability of n event(s) occurring during mission length s if an average of w events occurred per year during the observation period. The probability is assumed to follow a Poisson distribution and is calculated as

$$p(n,ws) = e^{-ws} \frac{(ws)^n}{n!} \qquad \text{(F-3)}$$

This choice of occurrence distribution is somewhat different from that of King who used an extension of the Poisson method introduced by Burrell (Burrell, 1972) to account for the small size of the sample of events available to King. Q(F,n) is the probability that the sum

of all fluences due to n events will exceed 10F.

The values of Q(F,n) were simulated using a Monte Carlo method. The Monte Carlo program utilized two subroutines (Press et al., 1986). One is a random number subroutine which generates random numbers with a uniform distribution in the interval of [0,1]. The other is a subroutine which applies the Box-Muller method (Box and Muller, 1958) of inverse transformation to obtain a Gaussian distribution. The inverse transformed method is discussed in detail in Yost (1985).

The random numbers are assumed to be the inverse function of p(F) which is defined as :

$$p(F) = \int_{-\infty}^{F} \frac{1}{(2\pi)^{\frac{1}{2}}\sigma} \exp\left[-\frac{1}{2}\left(\frac{F^* - 1}{\sigma}\right)^2\right] dF^* \qquad \text{(F-4)}$$

which can be written as

$$p(F) = \int_{-\infty}^{z} \frac{1}{(2\pi)^{\frac{1}{2}}\sigma} \exp\left(-\frac{1}{2} t2\right) dt \qquad \text{(F-5)}$$

where $z = \dfrac{F - 1}{\sigma}$

The values of 1 and r used in equation (F-5) are those obtained from the straight line fit to the log fluence F distribution. The events below the median fluence portion of the distribution were ignored in making the fit. Since the largest fluence events were very important in calculating the total expected fluences, the largest events were given greater weight than the remaining small fluence events in determining the fitted straight line. Generating these random numbers and performing the inverse transformed

calculations on them will result in a set of numbers that are random samples of the fit to the log fluence F distribution.

The actual simulation of Q(F,n) consists basically of two steps. In step one, N sets of random samples from a Gaussian distribution are generated. N is a large number to ensure the randomness (100,000). Each set j is a collection of n random numbers x_i. In step two, each set j is assigned a value of 1 if

$$\sum_{i=1}^{n} (10x^{i\sigma+\mu}) \geq 10^{F} \qquad \text{(F-6)}$$

The ratio of the cumulative numbers of set j with value of 1 over the total numbers of generated sets N is the probability of exceeding fluence fp due to n event(s). This procedure is repeated to determine the value of each Q(F, n) of interest.

Equation (F-1) has been evaluated for various mission lenghts s and the result is shown in Fig. F-7 for an energy threshold > 10 MeV. In this figure all curves approach 100 % asymptotically but the values are so close to 100 % for fluences less than 10^{10} particles and mission lengths of 7 years that the asymptotic nature of the curve may not be obvious. The result for > 30 MeV is shown in Fig. F-8.

F.5. Results and Use of the Model

The Feynman et al. model can be used for the active years of the solar cycle and for various mission lengths. Figures F-7 and F-8 give the probability of exceeding a given fluence level over the life of the mission assuming a constant heliocentric distance of 1 AU. These figures show five mission lengths. In calculating mission length only

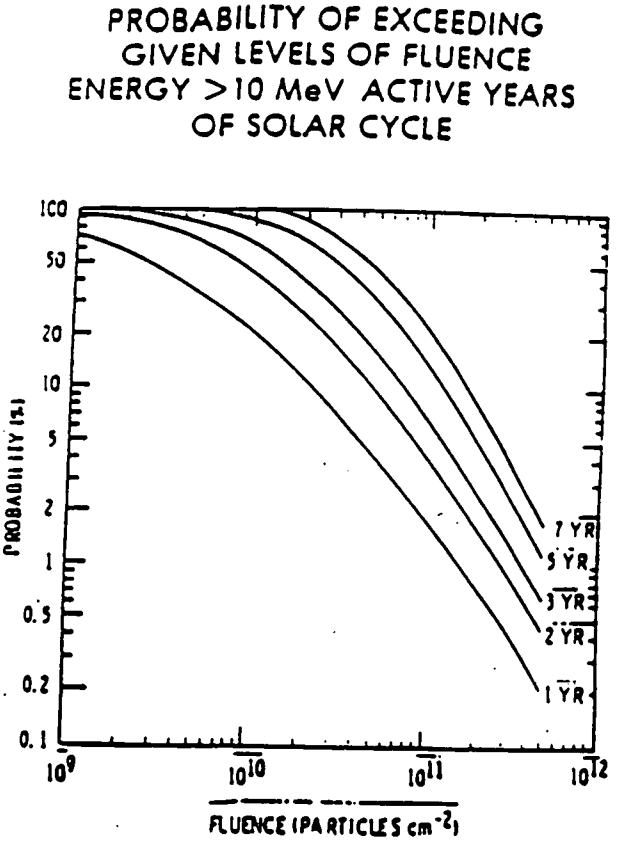

Fig. F.7. : The probability of exceeding selected fluences for different mission lengths for proton energies > 10 MeV. All curves approach 100 % asymptotically (after Feynman et al., 1988a).

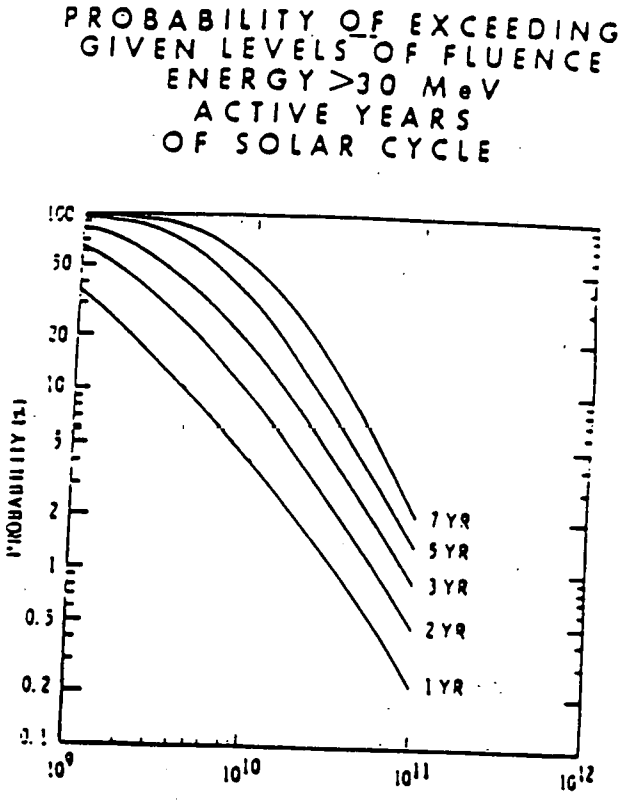

Fig. F.8. : The probability of exceeding selected fluences for different mission lengths for proton energies > 30 MeV (after Feynman et al., 1988a)

the time that the spacecraft spends in interplanetary space during solar cycle active years should be included.

To use figures F-7 and F-8 to estimate mission fluences, find the line in the figure that corresponds to the number of years the mission will be in space during active solar cycle years. Then locate the "confidence level" required, recalling that a confidence level of 95 percent means that only 5 % of missions identical to the one being considered will have fluences larger than that determined for a confidence level of 95 %. That is, the ordinate on the figures gives the probability of exceeding a given level of fluence and that probability plus the confidence level is 100 %. If a mission will be in space during more than one solar cycle the best method for finding the total expected fluence from the figures is to estimate the additional fluence per year from the 7 year fluence curve and add appropriate number of yearly fluences to the 7 year line. Feynman et al. recommend against using the 1 year curve to estimate the additional fluence expected on a long mission because it will overestimate the fluence.

In some applications a small lowering of the confidence level requirement may be acceptable and result in a large enough decrease in estimated fluence to eliminate an otherwise important problem. Fig. F-9 shows the percent of missions exceeding selected fluences for a one year mission at 1 A.U. The "confidence limit" of course is 100 %. Analogous graphs can be constructed for other mission lengths from figures F-7 and F-8.

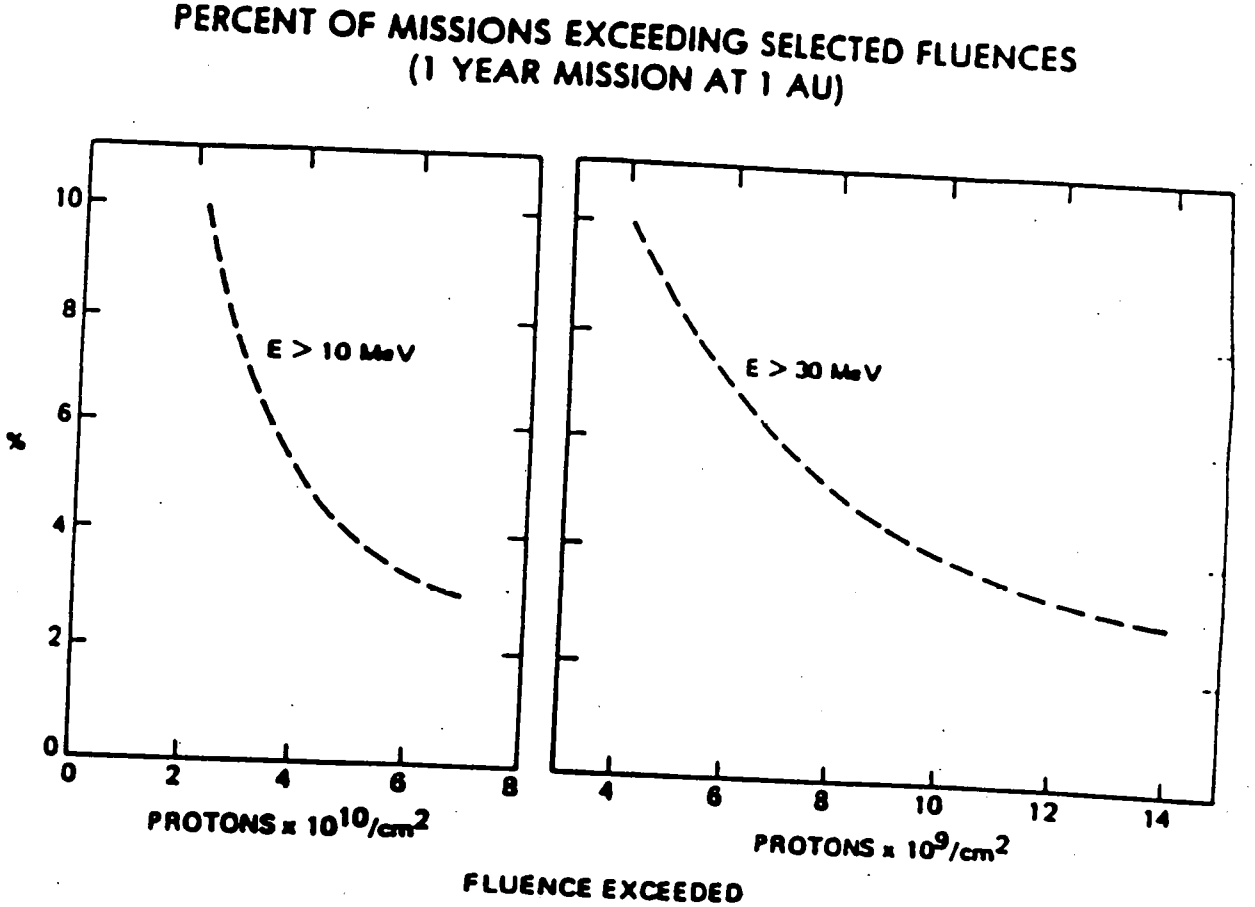

Fig. F.9. : Fluence as a function of "confidence level" for a 1 year mission at 1 A.U. (after Feynman et al., 1988a).

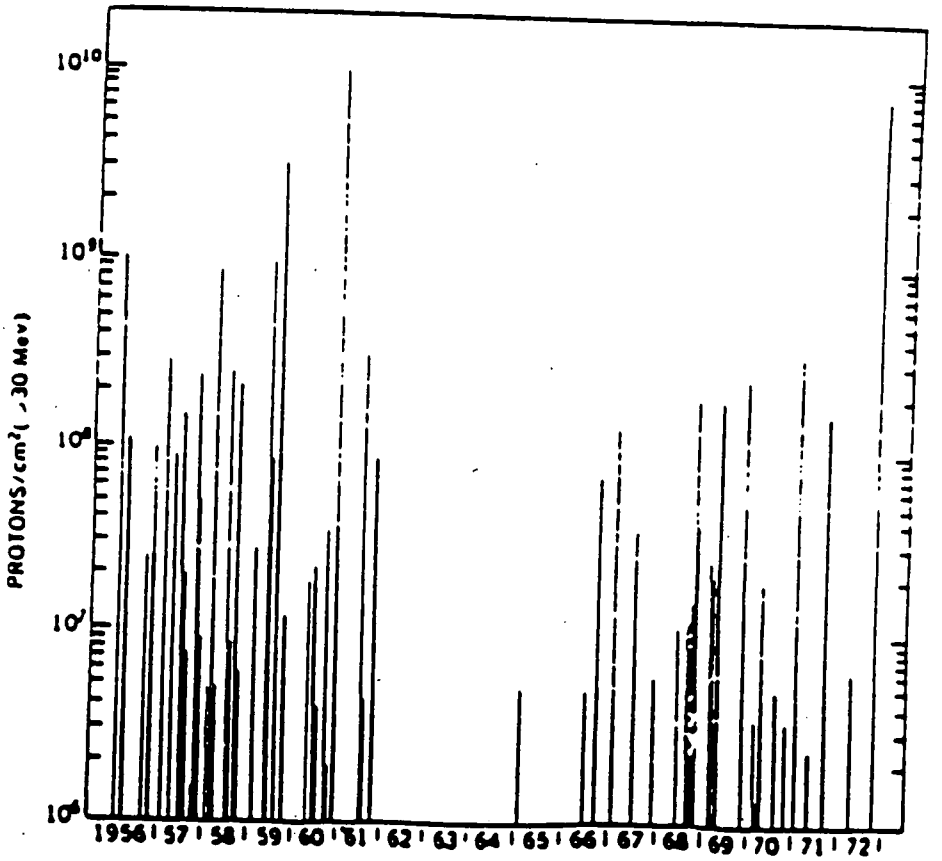

Fig. F.10. : Event-integrated proton fluxes above 30 MeV for the major solar events of the 19th and 20th solar cycles (after King, 1974).

F.6. Discussion

Figure F-10 illustrates the event-integrated fluxes above 30 MeV for the major solar events of the 19th and 20th solar cycles. This figure has been drawn from the data set used by King (1974). From the figure it was realized by King that the fluence during the solar cycle that maximized in 1957 (cycle 19, maximum annual sunspot number 190) was much larger than the fluence during the 20th cycle that had just been completed. Indeed, the major contribution to the 19th cycle fluence was from 4 or 5 major events. In contrast, the fluence during cycle 20 was dominated by a single event with fluence comparable to the major events of cycle 19, the great proton event of August, 1972. This lower fluence during cycle 20 (maximum annual sunspot number 107) was in agreement with the notion that was widely held at the time, i.e. that the number of major solar particles events during a solar cycle was a function of the cycle's maximum sunspot number. Furthermore, the predictions King used for sunspot maximum for cycle 21 indicated that it would resemble or be smaller than cycle 20. With these assumptions about the relation between sunspot number and major proton events and about the intensity of cycle 21 it was very reasonable to ignore the cycle 19 data and to use the cycle 20 data base to make a conservative prediction of cycle 21 fluence and King developed his model using only cycle 20 data. However, neither of these assumptions have proved valid for cycle 21. There were no major proton events (fluence greater than 1×10^9 for E above 30 MeV) at all during cycle 21 despite the fact that the maximum annual sunspot number in cycle 21 was 155, compared to cycle 20's maximum of 107.

Feynman et al. (1988b)have studied the relation of event sizes to the sunspot number and the solar cycle phase. They have found a clear and strong variation of annual integrated flux with solar cycle phase with a 7 year active phase that extends from 2 years before through 4

years after maximum. They have also shown there is almost no relation between the maximum sunspot number in a solar cycle and the solar cycle integrated flux or the annual sunspot numbers and annual integrated flux. On the other hand, Goswami et al. (1988) have found no definitive correlation between cycle-averaged solar flare proton fluxes and peak sunspot numbers.

In producing a new model for the prediction of proton fluences, Feynman et al. (1988a) indicated the importance of reviewing the data set. Because no relation has been observed between cycle amplitude and integrated proton fluence during the last three solar cycles, the predictions of their model do not depend on the expected maximum sunspot number in a cycle. Furthermore, the distinction made by King between "ordinary" events and "anomalously large" events was not required by the data set.

The data set of the Feynman et al. model can be compared to the data set given by King (1974) for 24 events during the same period. The ratios of the fluences given by King to the fluences used by Feynman et al. for both the E > 10 MeV and the E > 30 MeV cases have been calculated (Feynman et al. 1988a). The agreement was generally good. For the E > 10 MeV case, 20 of 24 events had ratios between 1.6 and 0.8 and for the E > 30 MeV case, 18 of 24 events had ratios between 1.3 and 0.4. There was a slightly smaller average slope to the particle spectrum between > 10 MeV and > 30 MeV in the data used by Feynman et al. than in the data used by King.

For the August 1972 event, the event-integrated fluxes given by King for both E > 10 MeV and E >30 MeV are 1.6 times the values used by Feynman et al. However, the uncertainty in the observations is probably of the same order as the differences between the two data sets.

Energy Range	Confidence Level	2 Year Mission Fluences (p cm^{-2}) King	New
>10 MeV	80%	1.3×10^{10}	2.5×10^{1}
>10 MeV	95%	4.0×10^{10}	7.7×10^{1}
>30 MeV	80%	4.9×10^{9}	5×10^{9}
>30 MeV	95%	1.7×10^{10}	1.5×10^{1}

Table F.1. : Expected fluences (p cm^{-2}) for a mission length of 2 years at 1 AU. A comparison between the King values (King) and the Feynman et al. values (New) is made. (after Feynman et al.,1988a).

Fitting Parameters

Parameter	> 10MeV	> 30MeV
w	5.8	7.5
μ_0	7.8×10^7	8.6×10^6
σ	1.125	1.193

Table F.2. : Fitting parameters for the Feynman et al. model (after Feynman et al., 1988a).

In Table F-1 the new expected fluences given by the Feynman et al. model are compared with the King values for a mission length of 2 years at 1 AU. The fluences are unchanged for energies > 30 MeV but the new fluences are about twice the King fluences at energies > 10 MeV. The "confidence levels" should be interpreted as meaning that if 1,000 two year missions were flown consecutively during solar cycle active years then 800 of them (or 950 depending on the chosen "confidence level") would have fluences no larger than the fluences shown in the table.

Furthermore, the long-term averaged solar proton flux of ~ 100 cm^{-2} s^{-1} (E > 10 MeV) over time periods of 1 -10 million year (obtained from lunar sample data), excludes the possibility of the occurrence of a single particle event with proton fluence (E > 10 MeV) larger than 1016 cm-2 within this time scale (Goswami et al, 1988). Therefore, any deviation of solar proton fluxes from the million-year averaged value, over shorter or longer epochs, most probably results from the presence of a large number of particle events with moderately high fluences rather than a single particle event with extremely high fluence.

It is of interest to contrast the solar proton fluences with galactic proton fluences. The galactic proton flux which must be regarded as a quasi-steady-state component of the interplanetary particle environment, has a value of about 1.5 x $10^8/cm^{-2}$ year, independent of energy in the 10 - 100 MeV threshold range. There is a factor of 2 variation over the solar cycle. The galactic proton data points of Figure F-2. (from King, 1974) demonstrate that for a two-year mission, there is a 75 % chance that solar proton fluence (E ≥ 30 MeV) will exceed the galactic fluence, while for a one-month mission, the corresponding figure is only 16 %. At higher proton energy thresholds, these percent figures will decrease. The point is that, in

the limits of short missions and high energies, galactic particle fluence is very important relative to solar particle fluence. Galactic fluxes are also likely to be of prime importance for solar minimum phases.

F.7. Recommandations

The variability observed in solar particle fluences and spectra during the last three solar cycles precludes the possibility of improving the predictability of solar particle activity at present (Goswami et al. 1988) unless the physics of solar flares in terms of energy generation, storage and release is better understood with particular emphasis on their interrelationship with energetic particle emission during flare events.

At the present time, the Feynman et al. model represents the most reliable (in the statistical sense) engineering model designed to be used for the prediction of proton fluences for space mission analysis. We recommend to implement it in the UNIRAD system of ESA.

Furthermore, the determination of solar proton spectra using the data base of Feynman et al. would be a useful task that should be considered in the future.

LIST OF REFERENCES

Aarons ,J. and Silverman,S. Ed., AFCRL Studies of the November 1960 Solar - Terrestrial Events, AFCRL - 62-441, April 1962.

Adams, J.H, Jr., Letaw, J.R. and Smart, D.F.,Cosmic Ray Effects on Microelectronics, Part II:The Geomagnetic Cutoff Effects, NRL Memorandum Report 5099, 1983.

Adams, J.H. Jr., Silberberg, R. and Tsao, C.H., Cosmic Ray Effects on Microelectronics, Part I : The Near-Earth Particle Environment, NRL Memorandum Report 4506, 1981.

Albagli-Hutner, R., Phys. Rev., 55, 614, 1939.

Alpher, R.A., Theoretical Geomagnetic Effects in Cosmic Radiation, J. Geophys. Res., 55, 436-471, 1950.Baker, D.N., J.B. Blake, R.W. Klebesadel, and P.R. Higbie, J. Geophys. Res., 91, 4265, 1986.

Armstrong, T.A., Brungardt, C. and Meyer, J.E., Satellite Observations of Interplanetary and Polar Cap Solar Particle Fluxes from 1963 to the Present. Weather and Climate Responses to Solar Variations, B.M. McCormac, Ed. Colorado - Associated University Press, 1983.

Blake, J.B. and G.A. Paulikas, in Particles and Fields in the Magnetosphere, ed. by B. M. McCormac, D. Reidel Publishing Co., Dordrecht-Holland, p380, 1970.

Box, G.E.P. and Muller M.E., A note on the generation of random normal deviates, Ann. Math. Statist., 29, 610, 1958.

Burrell, M.O., The Risk of Solar Proton Events to Space Missions, Proceedings of the 1971 National Symposium on Natural and Manmade Radiation in Space, edited by E.A. Warman, TMX - 2440,Jan 1972, NASA, pp. 310 - 323 (printed separately as TND - 6379, June 1971, NASA).

Daly, E.J., Effects of Geomagnetic Field Evolution on Predictions of the Earth Radiation Environment at Low Altitudes, ESTEC/W.P.1531, 1989.

Daly, E.J., ESA Journal, 12, 229, 1988.

Daly, E.J., The Evaluation of Space Radiation Environments for ESA Projects, ESA Journal, 12,.229-247, 1988.

Feynman, J, Armstrong, T.P., Doa-Gibner, L. and Silverman, S., Preprint 1988.

Feynman, J., Armstrong, T.P., Dao-Gibner, L. and Silverman, S., Solar Proton Events During Solar Cycles 19, 20 and 21, Solar Physics, 126, 385, 1990.

Feynman, J., Armstrong, T.P., Dao-Gibner, L.V. and Silverman, S., A New Interplanetary Proton Fluence Model, accepted for J. Spacecraft, 1988a.

Fichtel, C.E., Guss, D.E. and Ogilvie, K.W., Details of Individual Solar Particle Events, Chapt. 2 appearing in Solar Proton Manual, 1962.

Fraser-Smith, A.C., Rev. Geophys. 25, 1, 1987.

Goswami, J.N., Mc Guire, R.E., Reedy, R.C., Lal, D. and Jha, R., Solar Flare Protons and Alpha Particles During the Last Three Solar Cycles, J. Geophys. Res., 93, 7195-7205, 1988.

Haerendel, G., in Particles and Fields in the Magnetosphere, ed. by B.M. McCormac, D. Reidel Publishing Co., Dordrecht-Holland, p416, 1970.

McCormac, D. Reidel Publishing Co., Dordrecht-Holland, p416, 1970.

Haffner, J.W.: Radiation and Shielding in Space, 347pp., Academic Press, New York, 1967.

Hassitt, A., J. Geophys. Res., 70, 535, 1965a.

Hassitt, A., J. Geophys. Res., 70, 5385, 1965b.

Heinrich, W. and Spill, A., Geomagnetic Shielding of Cosmic Rays for Different Satellite Orbits, J. Geophys. Res., 84, 4401-4404, 1979.

Hess, W.N. The radiation Belt and Magnetosphere, 548pp., Blaisdell Publishing Company, Waltham, Mass., 1986.

Hilton, H.H., J. Geophys. Res., 76, 6952, 1971.

Hovestadt, D., G. Gloeckler, C.Y.Fan, L.A.Fisk, F.M. Ipavich, B. Klecker, J.J. O'Gallagher, and M. Scholer, Geophys. Res. Letts., 5, 1055, 1978.

IAGA Divisions I Working Group 1, J. Geomagn. Geoelectr., 37, 1157, 1985.

International Geomagnetic Reference Field 1965.0, IAGA Commission 2 Working Group 4, Analysis of the Geomagnetic Field, J. Geophys. Res., 74, 4407-4408, 1969.

Jensen, D.C., and Cain, J.C., an interim magnetic field, J. Geophys. Res., 67, 3568, 1962.

Kasper, J.E., The Earth Simple Shadow Effect on Cosmic Radiation, Nuovo Cimento, 11, Suppl. N^{3}1,1-26, 1956.

King, J.H., National Aeronautics and Space Administration, Special Publication NASA SP-3024 Vol.IV, 1967.

King, J.H., Solar Proton Fluences for 1977 - 1983 Space MIssions, J. Spacecraft, 11, 401 - 408, 1974.

Konradi, A., Hardy, A.C. and Atwell, W., J. Spacecraft, 24, 284, 1987.

Konradi, A., Science, 242, 1283, 1988.

Lemaire, J., Bull. Soc. Royale Sciences Lige, 31, 556, 1962.

Lemaitre, G. and Vallarta, M.S., Phys. Rev., 43, 87, 1933.

Lemaitre, G. and Vallarta, M.S., Phys. Rev., 50, 493, 1936.

Malitson, H.H. and Webber, W.R., A Summary of Solar Cosmic Ray Events, chapt. 1 appearing in Solar Proton Manual, Frank B. McDonald ed., NASA Goddard Space Flight Center, X-611-62-122, Greenbelt, MD, 1962.

McCormack, P.D.: Space: Opportunities for All Peoples. Oxford-New York-Frankfurt, Pergamon Press, IAF/IAA-86-380, 1986.

McIlwain, C.E., Coordinates for mapping the distribution of magnetically trapped particles, J. Geophys. Res., 66, 3681-3691, 1961.

McIlwain, C.E., J. Geophys. Res., 66, 3681, 1961.

McIlwain, C.E., Processes acting upon Outer Zone Electrons, I; Adiabatic Perturbations, unpublished preprint, 1966c.

McIlwain, C.E., Space Sci. Rev., 5, 585, 1966a.

Mead, G.D. and Fairfield, D.H., J. Geophys. Res., 80, 523, 1975.

Mullen E.G. and Gussenhoven, M.S., SCATHA Environmental Atla, AFGL-TR-83-0002, 1983.

Mullen, E.G., Gussenhoven, M.S. and Hardy, D.A., Proceedings of NATO Advanced Study Institute "Terrestrial Space Radiation and its Biological Effects", Corfu, Oct. 1987.

Nelson, W., Applied Life Data Analysis, Wiley, 1982.

Northrop, T.G., The Adiabatic Motion of Charged Particles, Interscience, New York, 1963.

Olson, W.P. and Pfitzer, K.A., A Quantitative Model of the Magnetospheric Magnetic Field, J. Geophys. Res., 79, 3739-3748, 1974.

Olson, W.P. and Pfitzer, K.A., J. Geophys. Res., 79, 3739, 1974.

Pfitzer, K.A., The Effect of Magnetic Field Models on Cosmic Ray Cutoff Calculations.PP. 242-252, in : Olson, W.P. (Ed.), Quantitative.Modeling of Magnetospheric Processes, Geophysical Monograph 21, American Geophys. Union, Washington, D.C., 1979.

Pomerantz, M.A., Cosmic Rays, Van Norstrand Rheinhold, Momentum Books, New-York, 1971.

Press, W.H., Flannery, B.P., Teukolsky, S.A. and Vetterling, W.T., Numerical recipes, Cambridge University Press, p. 192, 1986.

Pruett, R.G., J. Spacecraft, 17, 270, 1980.

Reagan, J.B., Nightingale, R.W., Gaines, E.E., Imhof, W.L. and Stassinopoulos, E.,G., J. Spacecraft Rockets, 18, 83, 1981.

Roberts, C.S., Coordinates for the Study of Particles Trapped in the Earth's Magnetic Field : A Method of Converting from B,L to R, λ Coordi-nates, J. Geophys. Res., 69, 5089-5090, 1964.

Roederer, J.G., J. Geophys. Res., 72, 981, 1967.

Roederer, J.G., Rev. Geophys. Space Phys., 10, 599, 1972.

Roederer, J.G., Rev. Geophys., 7, 77, 1969.

Roederer, J.G.: Dynamics of Geomagnetically Trapped Radiation, 166pp., Springer-Verlag, Berlin, 1970R

Rossi, B. and Olbert, S., Introduction to SpacePhysics, McGraw-Hill Book Company, New-York, 1970.

Rossi, B., Cosmic Rays, McGraw-Hill Book Company,New-York, 1964.

Sawyer, D.M. and J.I. Vette, National Space Science Data Center, NSSDC/WDC-A-R&S 76-06, Dec. 1976.

Schulz, M. and Lanzerotti, L.J. : Particle Diffusion in the Radiation Belt, 215pp., Springer-Verlag, Berlin, 1973.

Schulz, M. and Paulikas, G.A., Bull. Amer. Phys. Soc., Ser. II, 17, 123, 1972b.22, 123, 1972b.

Schulz, M. and Paulikas, G.A., J. Geophys. Res., 77, 744, 1972a.

Schulz, M., J. Geophys. Res., 77, 624, 1972.

Schwartz, M., Penumbra and Simple Shadow Cone of Cosmic Radiation, Nuovo Cimento, Vol. 11, Suppl.N^{3}1, 27-59, 1959.

Shea, M.A. and Smart, D.F., Report N° AFCRL-TR-75-0185, Hanscom, AFB, Mass., 1975.

Shea, M.A., Smart, D.F. and McCracken, K.G.,A Study of Vertically Incident Cosmic-Ray trajectories Using Sixth-Degree Simulations of the Geomagnetic Field, Environ. Res. Paper N^{3}141,AFCRL 65-705, September 1965$_{b}$.

Shea, M.A., Smart, D.F. and McCracken, K.G., A Study of Vertical Cutoff Rigidities Using Sixth Degree Simulations of the Geomagnetic Field,

Shea, M.A., Smart, D.F. and McCracken, K.G., A Study of Vertical Cutoff Rigidities Using Sixth Degree Simulations of the Geomagnetic Field, J. Geophys. Res., 70, 4117-4130, 1965a.

Shea, M.A., Smart, D.F. and McCracken, K.G., A study of Vertically Incident Cosmic-Ray trajectories Using Sixth-Degree Simulations of the Geomagnetic Field, Environ. Res. Paper N° 141, AFCRL 65-705, September 1965b.

Shea, M.A., Smart, D.F. and Mooney, W.R., 13thIntl. Cosmic Ray Conf., 2, 1075, 1973.

Shea, M.A. and Smart, D.F., Report N^{3} AFCRL-TR-75-0185, Hanscom, AFB, Mass., 1975.

Shea, M.A., Smart, D.F. and Mooney, W.R., 13th Intl. Cosmic Ray Conf., 2, 1075, 1973.

Singley, G. W. and J.I. Vette, National Space Science Data Center, NSSDC/WDC-A-R&S 72-06, Aug. 1972a.

Singley, G. W. and J.I. Vette, National Space Science Data Center, NSSDC/WDC-A-R&S 72-13, Dec. 1972b.

Smart, D.F. and Shea, M.A., 15th Intl Cosmic Ray Conf., 11, 256, 1977.

Smart, D.F. and Shea, M.A., A Study of the Effec-tiveness of the McIlwain Coordinates in Estimating Cosmic-Ray Vertical Cutoff Rigidities, J. Geophys.Res., 72, 3447-3454, 1967.

Spjeldvik, W.N., J. Geophys. Res., 82, 2801, 1977.

Stassinopoulos, E.G. and King, J.H., An Empirical Model of Energetic Solar Proton Fluxes with Applications to Earth Orbiting Spacecraft, IEEE Transactions on Aerospace and Electronic Systems, Vol. AES-10, Nø 4, July 1974.

Stern, D.P., J. Geophys. Res., 73, 4373, 1968.

Stern, D.P., J. Geophys. Res., 76, 257, 1971.

Stern, D.P., J. Geophys. Res., 92,4437, 1987.

Stern, D.P., Rev. Geophys. Space Phys., 14, 199, 1976.

Störmer, C., Periodische Elektronenbahnen im Felde eines Elementarmagneten und ihre Anwendung auf Brüches Modellversuche und auf Eschenhagens Elementarwellen des Erdmagnetismus, Z. Astrophys., 1, 237-274, 1930.

Teague, M. J. and J. I. Vette, National Space Science Data Center, NSSDC/WDC-A-R&S 76-04, May 1976.

Teague, M.J. and E.G. Stassinopoulos, GSFC X-Document X-601-72-487, Dec. 1972

Teague, M.J. and J. I. Vette, National Space Science Data Center, NSSDC/WDC-A-R&S 72-10, Nov. 1972.

Teague, M.J. and J. i. Vette, National Space Science Data Center, NSSDC/WDC-A-R&S 74-03, Apr. 1974.

Teague, M.J., J. Stein, and J. I. Vette, National Space Science Data Center NSSDC/WDC-A-R&S 72-11, Nov. 1972.

Teague, M.J., Stein, J. and Vette, J.I., The Use of the Inner Zone Electron Model AE-5 and Associated Computer Programs, preprint NSSDC 72-11, 1972.

Tsyganenko, N.A., Planet. Space Sci., 35, 1347, 1987.

Tsyganenko, N.A., Planet. Space Sci., 37, 5, 1989.

Vampola A.L. and Gorney D.J., Electron energy deposition in the middle atmosphere, J. Geophys. Res. 88, 6267 - 6274, 1983.

Vampola, A.L., Blake, J.B. and Paulikas, G.A., J. Spacecraft Rockets, 14, 690, 1977.

Vette, J. I. and B. Lucero, National Aeronautics and Space Administration, Special Publication NASA SP-3024 Vol. III, 1967.

Vette, J. I., A. B. Lucero, and J.A. Wright, National Aeronautics and Space Administration, Special Publication NASA SP-3024 Vol.II, 1966.

Vette, J. I., in Particles and Fields in the Magnetosphere, ed. by B.M. McCormac, D. Reidel Publishing Co., Dordrecht-Holland, p 305, 1970.

Vette, J. I., National Aeronautics and Space Administration, Special Publication NASA SP-3024 Vol. 1, 1966.

Vette, J.I., Chan, K.W. and Teague, M.J., Problems in Modelling the Earth's Trapped radiation Environment, AFGL-TR-78-0130, 1977.

Walt, M., J. Geophys. Res., 69, 3947, 1964.

Yost, G.P., Lectures on Probability and Statistics,LBL-16993 Rev.84/HENP/3, June 1985.

Yucker, W.R., Solar Cosmic Ray Hazard to Interplanetary and Earth-Orbital Space Travel, in Proceeding of the National Symposium on Natural and Manmade Radiation in Space (Las Vegas, Nevada, March 1-5, 1971), E.A. Warman, Ed. NASA TM-2440, p. 345, 1972.

Yucker, W.R., Statistical Analysis of Solar Cosmic Ray Proton Dose, McDonald Douglas Report MDCG - 0363, June 1970.